Y3.At7:
36/15-2

Reactor Technology

1972
Quarterly
Technical
Progress
Review
Volume 15-2

A publication of the
Office of Information Services
U.S. Atomic Energy Commission
Prepared in Cooperation
with
The American Nuclear Society

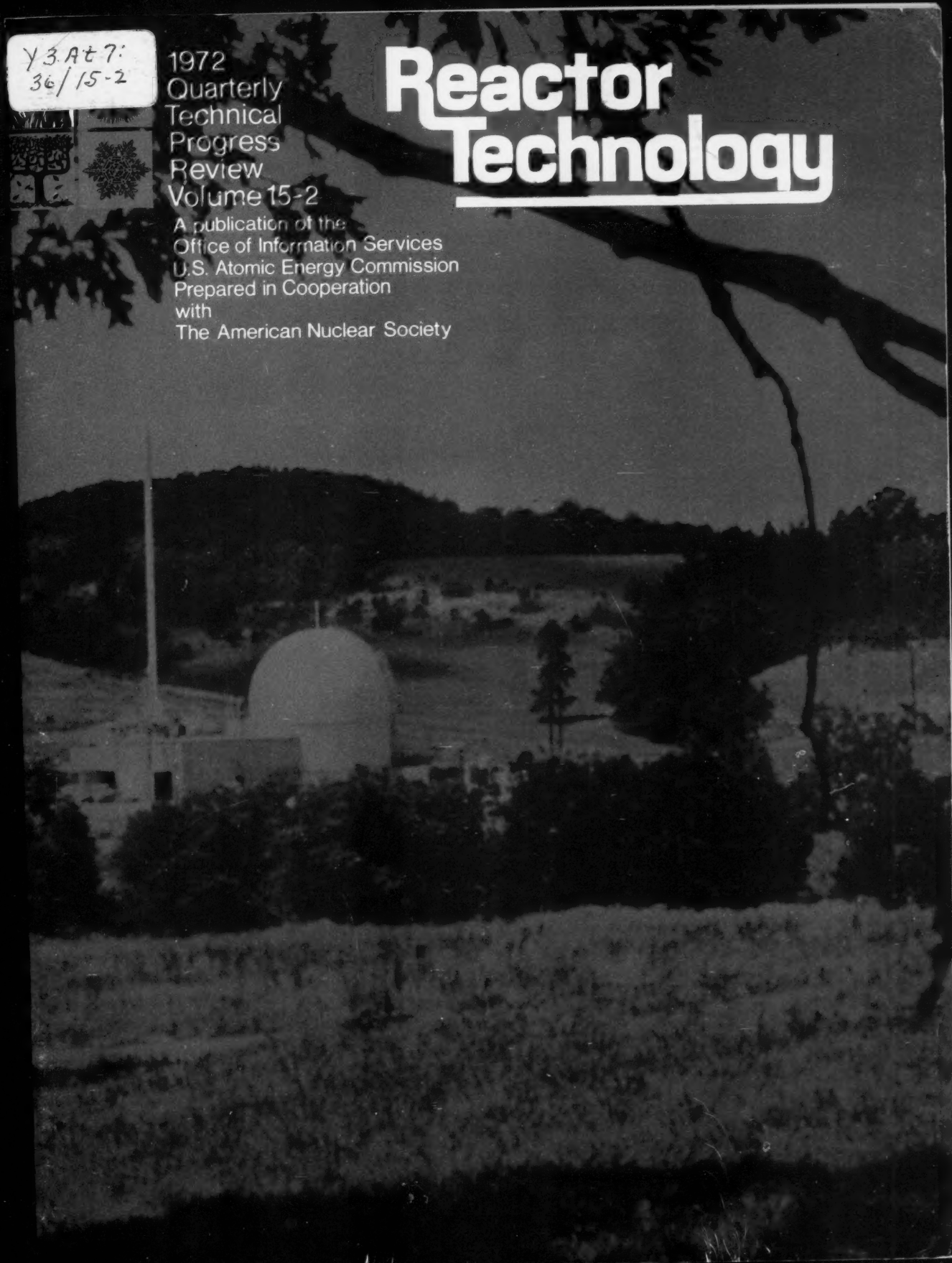

TECHNICAL PROGRESS REVIEWS

The United States Atomic Energy Commission publishes the Technical Progress Reviews to meet the needs of industry and government for concise summaries of current nuclear developments. Each journal digests and evaluates the latest findings in a specific area of nuclear technology and science. *Nuclear Safety* is a bimonthly journal; *Reactor Technology* is a quarterly journal.

Nuclear Safety
Wm. B. Cottrell, W. H. Jordan, J. Paul Blakely, and associates
Nuclear Safety Information Center, Oak Ridge National Laboratory

Reactor Technology
Prepared in cooperation with the American Nuclear Society

Both are available from the U. S. Government Printing Office. See the back cover for ordering instructions.

NOTICE

This journal was prepared under the sponsorship of the United States Atomic Energy Commission. Views expressed in it are not necessarily those of the Commission or its contractors. Neither the United States nor the Commission, nor any of their employees, makes any warranty, express or implied, or assumes any legal liability or responsibility for the accuracy, completeness, or usefulness of any information, apparatus, product, or process disclosed, or represents that its use would not infringe privately owned rights.

Availability of Reports Cited in This Review

United States Atomic Energy Commission (USAEC) reports are available at the libraries listed on the inside front cover of each issue of *Nuclear Science Abstracts*. USAEC reports are also sold by the following governmental and international organizations: (1) National Technical Information Service (NTIS), U. S. Department of Commerce, Springfield, Va. 22151; (2) International Atomic Energy Agency (IAEA), Vienna, Austria; and (3) National Lending Library, Boston Spa, England.

Other U. S. Government agency reports identified in this journal are generally available from NTIS.

Reports from other countries are generally available at the same U. S. libraries as maintain collections of USAEC reports, and from IAEA and the originating country. **United Kingdom Atomic Energy Authority (UKAEA)** reports are sold by Her Majesty's Stationery Office, London. **Atomic Energy of Canada Limited (AECL)** reports are sold by the Scientific Document Distribution Office, Atomic Energy of Canada Limited, Chalk River, Ontario, Canada. UKAEA and AECL reports issued after March 1, 1967, are sold by NTIS to purchasers in the United States and its territories. IAEA publications are sold in the United States by UNIPUB, P. O. Box 433, New York, N. Y. 10016.

Private-organization reports should be requested from the originator.

Y3.AE7
35/15:2

Reactor Technology

Vol. 15, No. 2 Summer 1972

RETNA$_B$ 15(2) 87-184 (1972)

REVIEW ARTICLE

NITRIDE FUELS: PROPERTIES AND POTENTIAL 87
Arthur A. Bauer, Battelle Memorial Institute, Columbus Laboratories

AMERICAN NUCLEAR SOCIETY—CRITICAL REVIEWS

INTRODUCTION 105

INFORMATION FOR AUTHORS 106

DISCRETE-ORDINATES METHODS FOR THE NUMERICAL SOLUTION OF THE TRANSPORT EQUATION 107
K. D. Lathrop, Los Alamos Scientific Laboratory, University of California

DEVELOPMENT OF MATERIALS AND SYSTEMS FOR THE MOLTEN-SALT REACTOR CONCEPT 136
H. G. MacPherson, Department of Nuclear Engineering, University of Tennessee

EFFECTS OF METAL SWELLING AND CREEP ON FAST REACTOR DESIGN AND PERFORMANCE 156
Paul R. Huebotter, Argonne National Laboratory

MISCELLANY

SELECTED RECENT OR RECENTLY RELEASED PUBLICATIONS
Compiled by Reactor Technology Section, AEC Technical Information Center, Oak Ridge, Tenn. 184

IAEA SYMPOSIUM ON NEUTRON MONITORING FOR RADIATION-PROTECTION PURPOSES (ANNOUNCEMENT) 135

IAEA SYMPOSIUM ON NUCLEAR POWER-PLANT CONTROL AND INSTRUMENTATION (ANNOUNCEMENT) 155

COVER: View of Southwest Experimental Fast Oxide Reactor (SEFOR) near Fayetteville, Ark.

ILLINOIS STATE LIBRARY
SEP 20 1972
U. S. Supt. of Documents Deposit

Superintendent of Documents, U. S. Government Printing Office, Washington, D.C. 20402, $3.00 per year.

REACTOR TECHNOLOGY

is a quarterly review of progress and developments in the reactor field including the following subject areas:

Economics	Fuel Cycles
Physics	Fluid and Thermal Technology
Mechanics	Fuel Processing
Construction	Components
Fuel Elements	Operating Performance

Prepared for reactor physicists, reactor operators, designers, fuel-cycle specialists, administrators, and others interested in the field, this journal reviews, summarizes, critically evaluates and interprets the state of the art as reflected in the current literature.

The many reports and publications referenced merit further study, and readers are urged to consult them for additional details.

Qualified authors are invited to contribute review articles for consideration for publication.

U. S. Atomic Energy Commission
Office of Information Services
Washington, D. C. 20545

The General Manager of the U. S. Atomic Energy Commission has determined that the publication of this periodical is necessary in the transaction of the public business required by law of this agency. Use of funds for printing this periodical has been approved by the Director of the Office of Management and Budget through June 30, 1972.

Nitride Fuels: Properties and Potentials

By Arthur A. Bauer*

Abstract: *Interest in nitride fuels centers principally on the use of (U,Pu)N in fast breeder reactors. A review of nitride fuel properties is presented including properties and irradiation behavior of UN, whose major potential application is as a space reactor fuel. Information on UN as presented here serves principally as background to, and to supplement, data on mixed-nitride, (U,Pu)N, fuels.*

Although the mixed nitrides have received less concentrated study, a sufficient technology base appears to exist that will permit an evaluation of mixed nitrides as liquid-metal-cooled fast breeder reactor fuels. The properties of (U,Pu)N related to its irradiation performance, safety characteristics, and fuel-cycle costs are reviewed. Fuel-pin design is discussed, and fuel-performance potential and limitations are outlined. Emphasis is placed on potential advantages resulting from the use of (U,Pu)N to fuel an advanced liquid-metal-cooled fast breeder reactor.

The search for high-performance uranium and plutonium fuels as alternates to the oxides has concentrated on the nitrides and carbides. Oxides, because of their compatibility with the coolant, are uniquely suited for use in water reactors. It is only with other coolants that nitrides and carbides come into serious consideration.

There is a general tendency to refer to nitrides and carbides interchangeably because of their similarities in properties and behavior. However, there are significant differences between the two that eventually will determine which is chosen for exploitation. It is not the intention in this article to compare these fuels, although comparisons at times will be unavoidable, but to review the available data concerning nitride fuels which permit an evaluation of their commercial potential. Since this potential is most evident in a liquid-metal-cooled fast breeder reactor (LMFBR) application, the review will focus on mixed-nitride, (U,Pu)N, fuels. However, interest in uranium mononitride, UN, for high-surface-temperature operation in space power reactors remains active. Consequently UN data also will be reviewed, although principally for the purpose of providing background to the evaluation of the mixed-nitride fuels.

*Battelle Memorial Institute, Columbus Laboratories, 505 King Avenue, Columbus, Ohio 43201.

PHYSICAL PROPERTIES

Constitution and Phase Stability

Compounds associated with UN, U_2N_3, and UN_2 compositions have been identified in the uranium–nitrogen system.[1-3] UN, the most stable and the only one of interest as a fuel material, has a face-centered cubic (fcc) NaCl structure[4-6] and a theoretical density of 14.32 g/cm^3. U_2N_3 has been found to exist in two forms, the body-centered cubic (bcc) alpha and the hexagonal beta structure.[3,7-10] The alpha structure, the lower temperature form, exists at compositions slightly hyperstoichiometric with respect to U_2N_3 and decomposes peritectoidally, with loss of nitrogen, to the beta form, which is slightly deficient in nitrogen with respect to U_2N_3. Under 1 atm nitrogen the alpha-to-beta decomposition on heating occurs at about 1130°C, whereas the beta decomposes to form UN with the evolution of nitrogen at about 1350°C. Alpha U_2N_3 forms a complete series of solid solutions with UN_2, which has an fcc UO_2 fluorite structure; this structure is observed at substoichiometric UN_2 compositions.

The nitrogen decomposition pressure of UN has been studied by a number of investigators with generally good agreement.[2,11,12] These data have been shown[13] to be consistent with a standard heat of formation for UN of −70 kcal/mole, in agreement with calorimetric determinations.[14-16] UN is found to melt

congruently at 2850°C under 2.5 atm nitrogen. At temperatures below this, and down to the melting point of uranium, molten uranium is the equilibrium product of decomposition. Under dynamic conditions, where diffusion of nitrogen in the UN becomes rate controlling, apparent volatilization of UN can occur.[3,17] Two studies of phase stability in the U_2N_3–UN_2 region have been reported.[18,19] Agreement between the studies is generally poor, apparently related to the differences in experimental techniques employed.

The UN phase apparently exists at essentially the stoichiometric composition at room temperature. At temperatures of 1500°C and above, solubility ranges, including N : U ratios, from 0.96 and 0.92 up to 1.04 have been reported.[3,17]

PuN is soluble at all compositions in UN (Ref. 20). The congruent melting point of PuN is estimated[21] as 2830 ± 50°C at a nitrogen pressure of 50 ± 20 atm. Thus, based on an essential ideality of solution between UN and PuN, the congruent melting point of (U,Pu)N alloys is expected to exhibit little variation with U : Pu ratio. The mononitride is the only phase in the plutonium–nitrogen system, and negligible solution of plutonium in U_2N_3 is indicated.[22]

In contrast to UN, (U,Pu)N does not decompose at elevated temperatures, but instead volatilizes such that the metal-to-nitrogen ratio in the solid material remains constant.[23,24] Volatilization is not congruent in a $U_{0.8}Pu_{0.2}N$ alloy, since the plutonium vaporizes at a more rapid rate than the uranium. The result is that, under dynamic conditions, the rate of volatilization is controlled by the diffusion of plutonium in the mixed nitride. The vapor pressures of individual species over UN and $U_{0.8}Pu_{0.2}N$ are summarized in Table 1.

The major contaminants of nitride fuels are oxygen and carbon. UC is completely soluble in UN (Ref. 25) and in PuN (Ref. 26), and the conclusion of complete interchangeability of carbon and nitrogen in the (U,Pu)(C,N) system appears warranted. Oxygen, on the other hand, exhibits only limited solubility in UN (Ref. 27). However, complete solution between UO_2 and UN_2 and of UO_2 with U_2N_3 at temperatures above 1200 to 1300°C is reported.[27-29]

Table 1 Vapor Pressures[24] over UN and $U_{0.8}Pu_{0.2}N$

Temperature, °K	Pressure of indicated species over UN, atm		Pressure of indicated species over $U_{0.8}Pu_{0.2}N$, atm		
	Nitrogen	Uranium	Nitrogen	Plutonium	Uranium
1400	10^{-13}	10^{-13}	3×10^{-11}	2×10^{-10}	10^{-14}
1600	8×10^{-11}	5×10^{-11}	2.5×10^{-9}	1.5×10^{-8}	3×10^{-12}
1800	1.3×10^{-8}	3.0×10^{-9}	8.8×10^{-8}	5.1×10^{-7}	6.3×10^{-10}
2000	6.1×10^{-7}	7.5×10^{-8}	1.1×10^{-6}	6.7×10^{-6}	4.0×10^{-8}
2200	1.3×10^{-5}	1.0×10^{-6}	2.0×10^{-5}	5.8×10^{-5}	7.0×10^{-7}
2400	2.3×10^{-4}	1.1×10^{-5}	5.4×10^{-5}	3.1×10^{-4}	8.1×10^{-6}

Heat Capacity and Thermal Conductivity

Heat-capacity measurements of UN have been made by a number of investigators, and several reviews[13,17,30] of the resulting data have been made. The most recent review[30] provides the data listed in Table 2. Values measured[23] for $U_{0.8}Pu_{0.2}N$ also are given in Table 2.

Thermal-conductivity data for UN have been reviewed,[30,31] with the data given in Table 2 representing preferred values.[30] As a matter of interest, the conductivity of UN is less than that of UC below 1000°K but greater at higher temperatures.[30] Also included are data[23] for $U_{0.8}Pu_{0.2}N$ corrected to theoretical density by the equation[31]

$$\lambda_{T.D.} = \lambda_{meas}\left(\frac{1+\beta P}{1-P}\right)$$

where β is 0.5 and P is the fuel porosity. The conductivity of UN is decreased by the addition of plutonium.

Thermal Expansivity

Linear thermal-expansion coefficients for UN (Ref. 32) and $U_{0.8}Pu_{0.2}N$ (Ref. 22) as a function of temperature are presented in Table 3. Slight increases in expansivity accompany the plutonium addition. The expansivity of nitride fuels is approximately one-half of that of stainless steel, the preferred cladding material for LMFBR application.

Table 2 Heat Capacity and Thermal Conductivity of UN and $U_{0.8}Pu_{0.2}N$

Temperature, °K	UN (Ref. 30)		$U_{0.8}Pu_{0.2}N$ (Ref. 23)	
	C_p, cal/(mole)(°K)	λ, W/(cm)(°K)	C_p, cal/(mole)(°K)	λ, W/(cm)(°K)
10	1.33	0.03		
50	3.76	0.073		
100	6.17	0.095		
200	9.80	0.123		
300	11.4	0.139	11.61	
400	12.3	0.149	11.88	0.135
600	13.1	0.160	12.40	0.149
800	13.7	0.189	12.92	0.163
1000	14.2	0.206	13.44	0.177
1200	14.7	0.226	13.96	0.186
1400	15.2	0.245	14.48	0.195
1600	15.8	0.250	15.00	0.204
1800			15.52	

Diffusivity

The coefficient of self-diffusion for nitrogen in UN (Refs. 33 and 34) as a function of reciprocal temperature is plotted in Fig. 1. The data are presented for a nitrogen pressure of 100 torrs, the diffusivity exhibiting a dependence on nitrogen pressure to the ½ power. The apparent activation energy indicated for constant nitrogen pressure is 62 kcal/mole. Other data have been reported giving diffusion coefficients about an order of magnitude greater[35] than those shown here.

Table 3 Mean Linear Thermal-Expansion Coefficients for UN and $U_{0.8}Pu_{0.2}N$

Temperature range, °C	Thermal expansion, 10^{-6}/°C	
	UN (Ref. 32)	$U_{0.8}Pu_{0.2}N$ (Ref. 23)
20–100	7.4	7.9
20–200	7.6	8.1
20–300	8.0	8.2
20–400	8.2	8.4
20–500	8.4	8.6
20–600	8.6	8.8
20–700	8.8	9.0
20–800	9.0	9.2
20–900	9.2	9.4
20–1000	9.3	9.5
20–1100	9.4	9.7
20–1200	9.5	9.9
20–1300	9.6	10.1
20–1400	9.7	10.2
20–1500	9.8	10.3

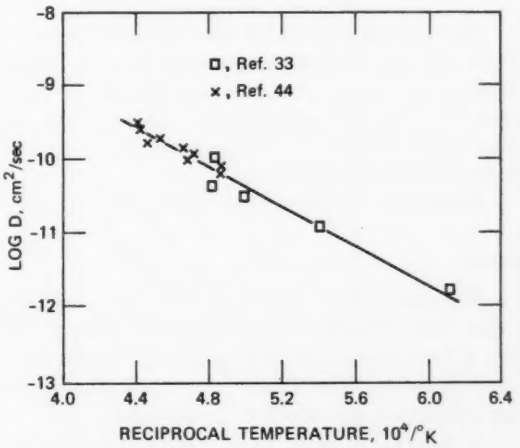

Fig. 1 Self-diffusion of nitrogen in UN (Ref. 33). Data adjusted to a pressure of 100 torrs assuming $D\alpha p^{1/2}$.

The self-diffusivity of nitrogen in $U_{0.8}Pu_{0.2}N$ has been found to be the same as in UN, within the limits of experimental error.[33]

The self-diffusivity of uranium in UN has been determined for low and high nitrogen activities over the temperature ranges 1100 to 1600°C and 1420 to 1830°C, respectively.[36] For low nitrogen activity the diffusivity was described by $D = 3.24 \times 10^{-7}$ exp $(-60{,}000/RT)$, whereas for high nitrogen activity the diffusivity could be expressed as $D = 7.54 \times 10^{-2}$ exp $(-105{,}000/RT)$.

MECHANICAL PROPERTIES

Elastic Properties

The modulus of elasticity for UN has been measured by a number of investigators,[32,37-41] with values ranging from 32×10^6 to 38.4×10^6 psi being determined. The modulus decreases[40,41] essentially linearly with temperature to about 0.9 of its room-temperature value at 1200°C.

Values of Poisson's ratio[37,39,40,42] for UN have been given in the range 0.26 to 0.28. Shear and bulk modulus values ranging from 15.1×10^6 to 16×10^6 psi and from 26.7×10^6 to 29.9×10^6 psi have been reported.[37,39,40]

The elastic modulus for $U_{0.85}Pu_{0.15}N$ has been measured as 29.9×10^6 psi, with Poisson's ratio being 0.275 for the same material.[43]

Hot Hardness

Hot-hardness data for UN are summarized in Fig. 2. Impurities are believed responsible for the higher hardness of some specimens at elevated temperatures.[44] Compared with UC, UN is softer at temperatures below 1000°C but retains hardness to a greater degree at higher temperatures.

No data are available for mixed nitrides.

Creep

Compressive[46,47] and tensile[48] creep measurements have been made with the results shown[49] in Fig. 3. The compressive creep data, in particular, show good agreement when effects of oxygen content and test atmosphere are taken into consideration.

A pronounced dependence of creep resistance on oxygen content of the UN is indicated by the data obtained[47] at about 1100°C under a pressure of 6000 psi. The increase in oxygen content from 400 to 2600 ppM is accompanied by an increase in creep rate of over one order of magnitude.

Comparison of the activation energies for creep obtained from Fig. 3 with those for diffusion in UN suggests that the creep process involves uranium volume diffusion. Creep data obtained in the 1100 to 1350°C range showed activation energies of 62.0 kcal/mole at a stress of 6000 psi and 60.8 kcal/mole at a stress of 8000 psi. These tests were performed in a vacuum of 10^{-6} torr. The higher temperature creep tests, performed under a nitrogen pressure of 200 torrs, provided activation energies averaging 75 ± 10 kcal/mole. The increase in activation energy with nitrogen pressure is consistent with uranium self-diffusion data where an increase from 60 to 105 kcal/mole was determined as the nitrogen pressure increased.

In-pile creep tests have been performed from which the degree of irradiation-induced creep has been calculated.[50] The results are shown in Fig. 4, which includes for comparison similar data obtained for UO_2. It is seen that irradiation-induced creep in UN is an order of magnitude below that in UO_2. The reduced irradiation effect in UN is believed related to the more rapid quenching of thermal spikes or rods in the higher conductivity UN as compared with UO_2.

FUEL FABRICATION

Fuel Synthesis

The most widely used method for laboratory preparation of both UN (Refs. 20, 51, and 52) and (U,Pu)N (Refs. 53 and 54) powders is the hydride–nitride–vacuum degas cycle. The function of the hydride step is to provide a high-surface-area powder product that will react more rapidly with nitrogen than the starting material. The vacuum degas serves to reduce the higher nitride, U_2N_3, formed in the nitride step to the mononitride. The hydriding is accomplished at temperatures in the vicinity of 230 to 250°C, whereas nitriding is performed at temperatures between 400 and 850°C. Reduction to the mononitride is achieved under vacuum at temperatures in excess of 800°C and below 1500°C.

UN powder has also been produced by the direct nitriding of uranium metal followed by reduction to the mononitride.[32,55] The nitriding is apparently best achieved at 850°C, either at reduced pressure or under 1 atm nitrogen. Reduction of the mononitride has been accomplished at 1150 to 1400°C.

Both processes are capable of producing nitride with relatively low levels (200 to 500 ppM) of oxygen contamination. However, depending on the subsequent method of pellet fabrication, high density can be achieved with the relatively coarse, directly nitrided powder only by hot pressing, whereas the finer powder from the hydride–nitride cycle is suitable for the cold pressing and sintering of pellets. Cast alloys of uranium containing 20 wt.% or more of plutonium also are not amenable to the direct nitride cycle but require the intermediate hydride step.

Massive UN forms of the highest purity obtainable, containing less than 100 ppM oxygen, can be routinely fabricated by arc melting.[45,56] The UN can be cast as

either buttons or ingots by tungsten-electrode or consumable-electrode techniques. Producing essentially stoichiometric UN requires a nitrogen overpressure of 20 atm or greater, while melting is performed at a current of 130 to 150 A and an arc potential of 100 V. Attempts to produce mixed nitride by arc melting were discontinued because of the high pressure required and difficulty in producing stoichiometric mononitride.[57]

The process considered to exhibit the greatest commercial potential at the present time is the carbothermic conversion of oxide by reaction with carbon in a flowing nitrogen atmosphere. The reaction is carried out in a fluidized-bed reactor at temperatures of about 1500 to 1700°C. The process has been applied to both UN (Refs. 58 to 60) and (U,Pu)N (Refs. 54 and 61). The relative levels of oxygen and

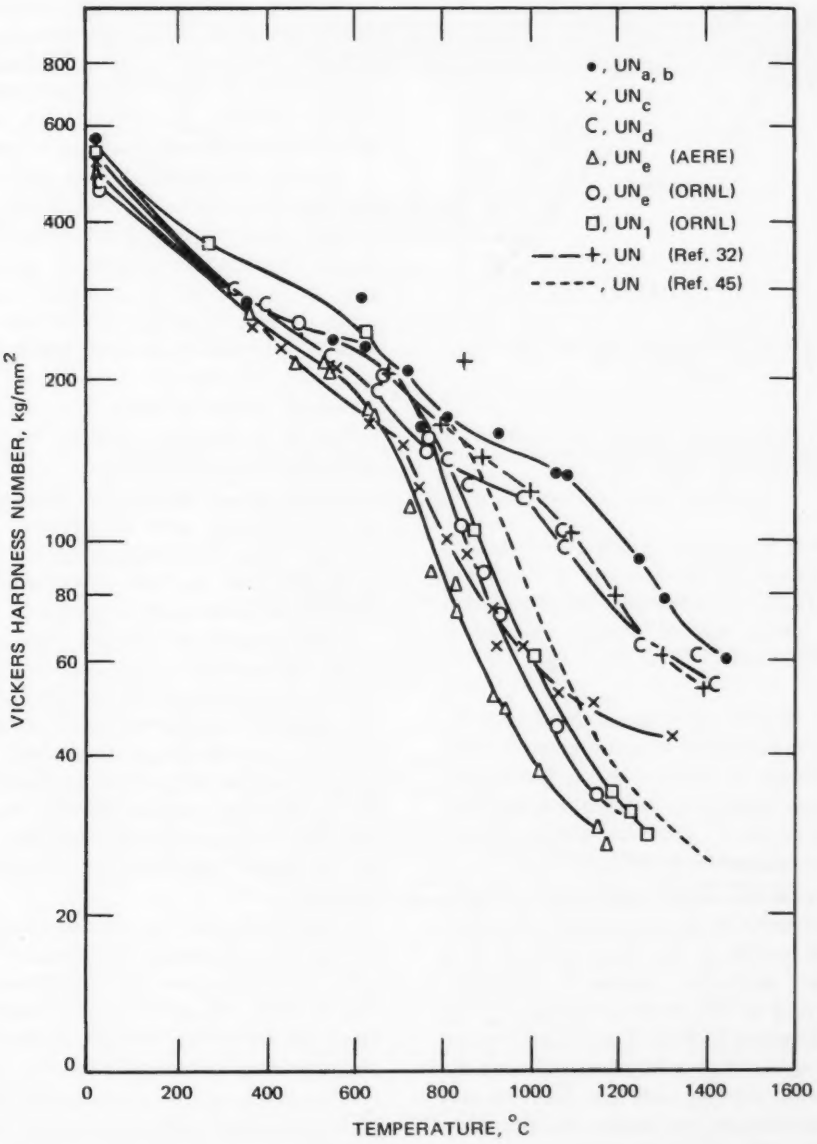

Fig. 2 Hot hardness of various samples of UN corrected to theoretical density.[44]

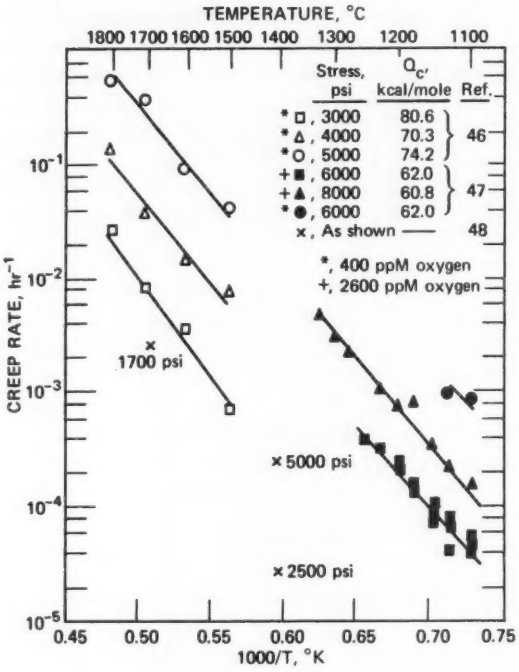

Fig. 3 Steady-state creep rate as a function of temperature for uranium mononitride tested in compression.[49]

carbon retained in the resultant product are functions of the partial pressures of nitrogen and of the carbon monoxide generated in the reaction. It appears that, typically, the lowest residual oxygen and carbon contents achievable are[58,61] in the range 1000 to 2000 ppM.

The use of chemical vapor deposition techniques, as a means of producing UN whereby uranium hexafluoride is reduced by lithium in an atmosphere containing a partial pressure of nitrogen, has also been examined for feasibility.[62] However, work was insufficient to evaluate the potential of this process.

Perhaps one of the more interesting synthesis procedures is applicable to the reprocessing of nuclear fuels and yields nitride as the direct product in a pyrometallurgical separation process.[63] Although applied to date only to UN, the process appears to be applicable also to mixed (U,Pu)N. The process involves the dissolution of the fuel in liquid tin followed by pressurization with nitrogen such that pure UN precipitates from the uranium–tin solution. Because of its higher density, the UN sinks to the bottom where it is subsequently recovered by mechanical separation from the melt. The UN initially produced can be processed through subsequent stages by redissolution in tin under vacuum to decompose the UN followed by reprecipitation to achieve any required decontamination factor. It was estimated that a decontamination factor of 10^6 or higher would be achieved in six stages.

Consolidation

As-synthesized nitride powders are quite resistant to sintering densification and must be comminuted to an average size of $\leqslant 2\,\mu$ to obtain sinter densities of 95% of theoretical. Uniaxial and isostatic hot pressing can be used to obtain similar densities with coarser starting powders. As noted earlier, massive nitride forms can be produced directly by arc melting.

Uniaxial and isostatic hot-pressing techniques have been applied to the fabrication of both UN (Refs. 32, 51, 55, and 64) and (U,Pu)N (Refs. 57 and 65) fuel bodies. Uniaxial hot pressing is accomplished in a graphite die that can be lined with a tantalum foil to act as a barrier to carbon diffusion into the specimen. Uniaxial hot pressing has been performed under both vacuum[64] and nitrogen atmospheres.[55] Degassing of the nitride powder to reduce U_2N_3 before uniaxial hot pressing is not necessary, since the reduction will occur during the hot-pressing cycle.

In the case of isostatic hot pressing,[32] the U_2N_3 must be reduced prior to pressing. The nitride is normally wrapped in tantalum foil and is then inserted in graphite-lined niobium or tantalum cans for the isostatic, hot-gas-pressure compaction.

Cold-pressing and sintering techniques have been studied and applied to the fabrication of UN (Refs. 20, 53, 58, 66, and 67) and (U,Pu)N (Refs. 53, 54, 68, and 69) pellets at a number of sites. The sintering of UN is extremely sensitive to particle size and sintering atmosphere as well as temperature, as illustrated by Figs. 5 and 6. Although vacuum sintering is more effective than either argon or nitrogen sintering, decomposition of UN limits[67] the maximum temperature to below 1600°C.

Attempts to develop sintering aids for nitride fuels have proved unsuccessful.[20,67] Reports concerning the effect of oxygen have been inconsistent,[58,70] and it may be that only when UO_2 is present as a second phase will sinterability increase, whereas small amounts of oxygen decrease sinterability.

Powder prepared from prealloyed uranium–plutonium metal synthesized via the hydride–nitride cycle has proved to be much more amenable to sintering than mechanically mixed powders of UN and

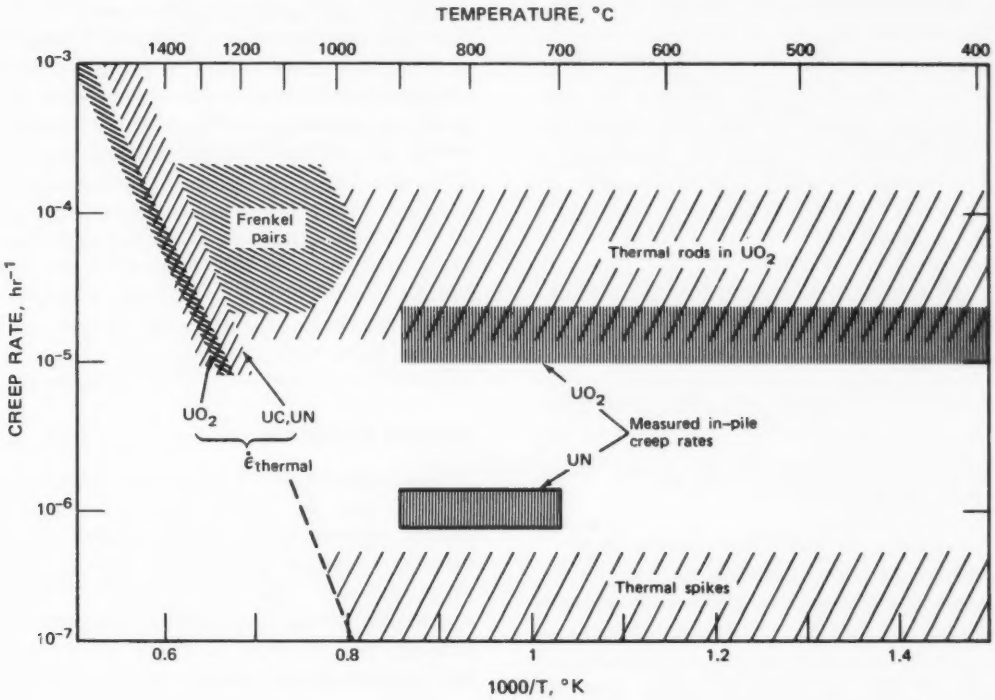

Fig. 4 Ranges of measured in-pile creep rates of UO_2 and UN samples standardized to a fuel density of 96% of theoretical, a fission rate of 2.5×10^{14} fissions/(cm^3)(sec), and a stress of 2 kgf/mm^2. Ranges of estimated rates based on theory are also shown, as are out-of-pile thermal creep rates.[50]

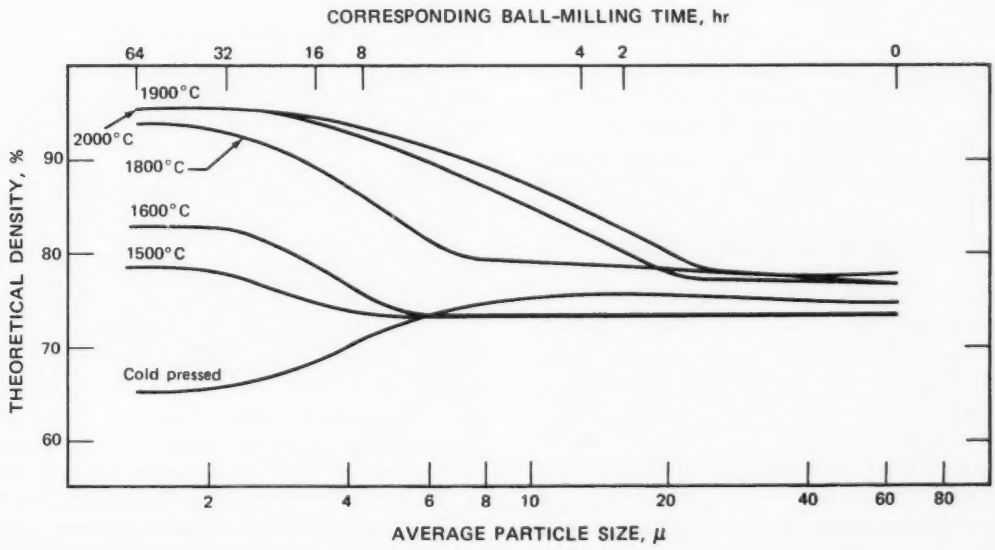

Fig. 5 UN densification as a function of particle size after sintering 3 hr in nitrogen.[67]

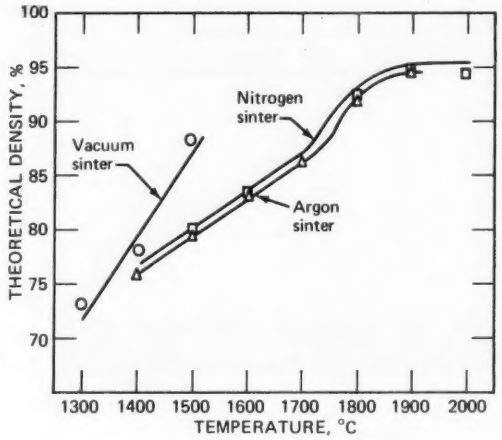

Fig. 6 Effect[67] of atmosphere on the sintering of UN powders ball milled for 32 hr.

PuN (Refs. 53, 54, and 68); in the first case, densities in the range 96 to 97% of theoretical can be obtained by sintering at 1900°C, whereas the density of mechanically mixed powder appears to be limited to a maximum of 90% of theoretical. This limitation appears to result from the Kirkendall effect associated with unequal rates of interdiffusion of the metal atoms in UN and PuN such that voids form at the interface between particles and act as a barrier to further diffusion.[71] Sintering of prealloyed powder is[54] reportedly enhanced by reducing nitrogen pressure at temperatures up to 2150°C.

COMPATIBILITY

Water

The hydrolysis of UN proceeds to completion by the reaction:

$$UN + 2H_2O \rightarrow UO_2 + NH_3 + \tfrac{1}{2}H_2$$

However, this reaction is seldom complete, and U_2N_3 is generally observed along with the oxide.[72] Furthermore, the U_2N_3 forms as an intermediate layer between UO_2 and UN. It has been observed[73] in 300°C water that as U_2N_3 hydrolyzes, the structure changes from the bcc Mn_2O_3-type structure to the fcc UN_2 fluorite structure, although nitrogen is lost in the process so that substitution of oxygen for nitrogen is suggested. This indicates that the hydrolysis proceeds through a continuous series of solid solutions from U_2N_3 to UN_2 to UO_2.

The rate of corrosion of UN has been found to be extremely dependent on stoichiometry,[73] the presence of either free uranium or U_2N_3 being detrimental to corrosion resistance. However, regardless of material quality, corrosion penetration rates exceeding 0.01 mm/hr are reached[74] at temperatures in excess of 250°C. In 100°C water the film that forms on UN affords protection that is lost at higher temperatures as its thickness increases and cracking occurs. The relatively good corrosion resistance of UN as compared with UC is ascribed[72,73] to the coherency of a duplex film of bcc U_2N_3–$U(N,O)_2$ superimposed on UO_2. The fcc array of atoms common to UN, U_2N_3, and UO_2 leads to epitaxial orientation and coherency.

Oxidizing Atmospheres

The oxidation of UN proceeds as in the hydrolysis reaction, with the formation of U_2N_3 as an intermediate product in an adherent, epitaxially related oxidation film. However, unlike the hydrolysis reaction where the final oxidation product is UO_2, U_3O_8 and/or UO_3 (Refs. 73 and 75 to 77) may appear as the final product, although decreasing oxygen pressures favor the formation[73] of UO_2.

The ignition temperature of UN in dry oxygen and air has been found to vary from room temperature for finely divided powders to about 300°C for sintered products and is only slightly sensitive to oxygen pressure.[75]

The oxidation of UN single crystals has been studied in dry oxygen, CO_2, and wet air.[73] The rate of oxidation in wet air was more rapid than in the oxygen, indicating that the rate of reaction in air is controlled by its water content.

Of significance in the storage of these fuels, although UC undergoes severe corrosion due to moisture in air at room temperature, massive UN has shown[73] no significant attack after being exposed to laboratory air for times up to 3 years. Although (U,Pu)N alloys appear less corrosion resistant, the resistance apparently decreasing with plutonium content, sintered specimens of $U_{0.8}Pu_{0.2}N$ have been stored in typical tank-nitrogen glove-box atmospheres for several weeks with only darkening of the specimen surfaces.[78]

Liquid Metals

No indication of reaction between either UN or (U,Pu)N and either NaK or sodium has been evidenced in tests conducted at temperatures ranging from 450 to as high as possibly 1600°C (Refs. 32, 73, and 79 to

81). This is true of observations from irradiation experiments[57,82] as well as from laboratory tests. However, oxide in the sodium, or oxygen in capsule test components which is transported through the sodium, has been observed[79] to react with the fuel to form an oxide phase plus U_2N_3.

Sodium wetting, as indicated by contact-angle measurements in sessile-drop experiments, is found to increase markedly at temperatures above 300°C for UN, $U_{0.8}Pu_{0.2}N$, and 304 stainless steel.[86] The contact angle in all cases approaches 20° or less at a temperature of 550°C, ensuring satisfactory wetting at that temperature or higher in sodium bonds involving these components.

Cladding Materials

Only limited data for nitride fuel–refractory metal systems exist, but these indicate excellent compatibility with UN at and above 1000°C for extended periods of time for all but titanium and zirconium.[84,85] Tungsten exhibits[86] excellent compatibility with UN for times to 1000 hr at 1700°C and for short periods of time to temperatures[87] as high as 2800°C. Molybdenum shows[88,89] no reaction with UN after at least 50 hr at 1200°C, whereas tantalum is used as a diffusion barrier at 1500°C in the hot pressing of UN (Ref. 32) and (U,Pu)N (Ref. 65). Niobium does not react significantly with UN at 1000°C for extended periods of time.[84]

Reaction occurs[84,85] rapidly between UN and nickel at temperatures above 800°C and between UN and aluminum above 500°C. With iron and chromium the only reactions with UN observed at temperatures up to 1000°C have been ascribed to the presence either of U_2N_3 in the fuel or of oxide in the cladding material.[85]

The compatibility of 304 and 316 stainless steels with UN (Refs. 79, 84, 85, and 90) and with (U,Pu)N (Refs. 79, 91, and 92) has been studied extensively, with excellent compatibility indicated for stoichiometric nitride at temperatures up to 1000°C in tests involving both helium- and sodium-bonded fuel. Carbon[84] and oxygen[79] affect this compatibility, as will stoichiometry of the fuel. Free uranium in the fuel undergoes a eutectic melting reaction with the stainless-steel components, whereas chromium nitride appears as a grain-boundary precipitate in stainless steel that is in contact with fuel containing U_2N_3.

The excellent out-of-pile compatibility is confirmed in irradiation tests involving both 304 and 316 stainless steels. Irradiations of UN in 316 stainless-steel[93] cans proceeded to burnups up to 6.3 at.% at cladding temperatures in the range 410 to 760°C with no evidence of reaction, except for several specimens with free uranium in the fuel which reacted with the cladding to form a molten eutectic structure. A series of irradiations involving sodium- and helium-bonded $U_{0.8}Pu_{0.2}N$ clad with 304 stainless steel and proceeding to burnups of 150,000 MWd/metric ton (~18 at.%) at cladding temperatures in the vicinity of 700°C has proceeded with no evidence of reaction between fuel and cladding.[82] The only reaction observed between fuel and cladding occurred when the cladding temperature exceeded 1000°C. These observations are in agreement with results from other irradiation experiments in which cladding temperatures of about 560°C for 316 stainless-steel cladding[94] containing $U_{0.85}Pu_{0.15}N$ fuel and of 1000°C for 304 stainless-steel cladding[91] containing $U_{0.8}Pu_{0.2}N$ were estimated.

The excellent compatibility at high fuel burnups is observed despite predictions, based on thermodynamic considerations, that U_2N_3 will be produced in the fuel as burnup proceeds.[57] As in out-of-pile compatibility tests, evidence of fuel–cladding reaction has been obtained in-pile when $U_{0.8}Pu_{0.2}N$ fuel contained U_2N_3 prior to irradiation.[82] However, no indication of U_2N_3 formation has been obtained in (U,Pu)N fuel at burnups ranging up to 150,000 MWd/metric ton.

IRRADIATION PERFORMANCE

Nuclear Properties

The (n,p) and (n,α) reactions are of significance only with ^{14}N. The thermal-neutron cross section for the (n,p) reaction is about 1.75 barns, and the cross section decreases as $1/v$ with neutron energies up to around 0.1 MeV. Above that energy, resonance effects occur.[57] The (n,α) reaction, on the other hand, is[95] characteristically resonant with a fission-spectrum-averaged cross section of 0.041 barn.

An estimate of the relative amounts of helium and hydrogen production, as compared with the amount of fission gas generated in the core of a mixed-nitride-fueled fast reactor, has been made using group-averaged cross-section data for the (n,p) and (n,α) reactions.[96] A 16% increase in gas generation was calculated, of which about one-third was hydrogen. On the basis of this calculation, a summed nitrogen (n,p) and (n,α) cross section about $^1/_{125}$ of the average plutonium fission cross section can be estimated for a nitride-fueled fast reactor core.

Irradiation Behavior

Relatively large density changes have been observed in low-temperature (i.e., below 250°C) irradiations.[97,98] Quenched-in radiation-induced defects and damage associated with the nitrogen (n,p) reaction are suspected as being responsible for the growth observed.

Irradiations of stainless-steel-clad UN specimens, where fuel centerline temperatures in the range 840 to 1320°C were achieved in conjunction with burnups in the range 16×10^{20} to 22×10^{20} fissions/cm^3, were accompanied by fuel swelling rates that ranged[93] from 0.3 to 0.9% per 10^{20} fissions/cm^3. UN irradiated at linear power ratings near 22 kW/ft operated at centerline temperatures between 840 and 1100°C and exhibited swelling rates of 0.3 to 0.7% per 10^{20} fissions/cm^3. A power rating near 30 kW/ft, where centerline temperatures ranging from 1100 to 1320°C were calculated, was accompanied by swelling rates of 0.7 to 0.9% per 10^{20} fissions/cm^3. Fission-gas bubbles appear to contribute to the swelling at the higher temperatures. Almost total release of hydrogen produced in the nitrogen (n,p) reaction occurred, and fission-gas release rates ranged up to 26%.

Irradiations of UN, clad with either tungsten or W–26 wt.% Re, at linear heat ratings in the range 3 to 10 kW/ft in which cladding temperatures have exceeded 1100°C have shown a strong dependence of swelling and of fission-gas release on temperature.[99–103] At 2100 to 2200°C a gas release from the fuel of 63.5% has been measured,[99] and, at temperatures below 1400°C, releases were below 10%. Single crystals and large-grained cast samples of UN exhibit significantly reduced swelling and fission-gas-bubble coalescence and growth as compared with normal, fine-grained, pressed and sintered UN (Refs. 99 and 101 to 103). It has been observed that fission-gas-induced fuel swelling can be accommodated in the porosity of low-density (76 to 78% of theoretical) fuel.[101,102] The swelling rate of UN, expressed in terms of external dimensional change of the cladding, is shown[103] in Fig. 7. The figure includes swelling rates for UC and UO_2 determined under similar conditions and indicates considerably lower rates for UN as compared with either UO_2 or UC for equivalent surface cladding temperatures. Taking into account differences in thermal conductivity, for equivalent fuel temperatures, UN and UO_2 swelling rates will be essentially the same, whereas the spread between UN and UC remains unchanged from that shown in Fig. 7.

Swelling rates for $U_{0.8}Pu_{0.2}N$ fuel, from a series of irradiations in the Materials Testing Reactor (MTR)

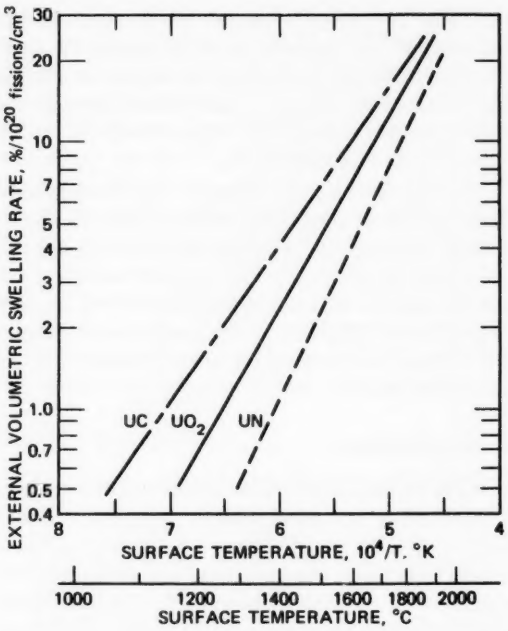

Fig. 7 External swelling rate of UN compared[103] with those for UO_2 and UC. All specimens were clad in W–26 wt.% Re.

and the Engineering Test Reactor (ETR) where the fuel was either helium- or sodium-bonded to 304 stainless-steel cladding, are shown[82] in Fig. 8. Except for two groups of data points, the indicated swelling rate for the mixed-nitride fuel is 0.48% per 10^{20} fissions/cm^3 or less in irradiations performed at linear heat ratings up to 40 kW/ft and to burnups of 150,000 MWd/metric ton. The exceptions occur with fuel that operated with centerline temperatures above 1260°C and with fuel containing U_2N_3 as a second phase in conjunction with relatively high levels of oxygen impurity (3000 to 4000 ppM) as compared with fuels containing only about 500 ppM oxygen.

The effect of fuel centerline temperature on the rate of fuel swelling is illustrated in Fig. 9. At temperatures below about 1300°C, fuel swelling results only from the introduction of individual fission-product atoms into the fuel crystal structure. However, in the range 1300 to 1400°C, fission gases begin to agglomerate, and fuel swelling associated with the growth of fission-gas bubbles is observed. In an analysis performed on a single $U_{0.85}Pu_{0.15}N$ fuel pin irradiated under conditions where a fuel centerline temperature of 1900°C and a fuel burnup of 12,500 MWd/metric ton were achieved, the onset of fission-

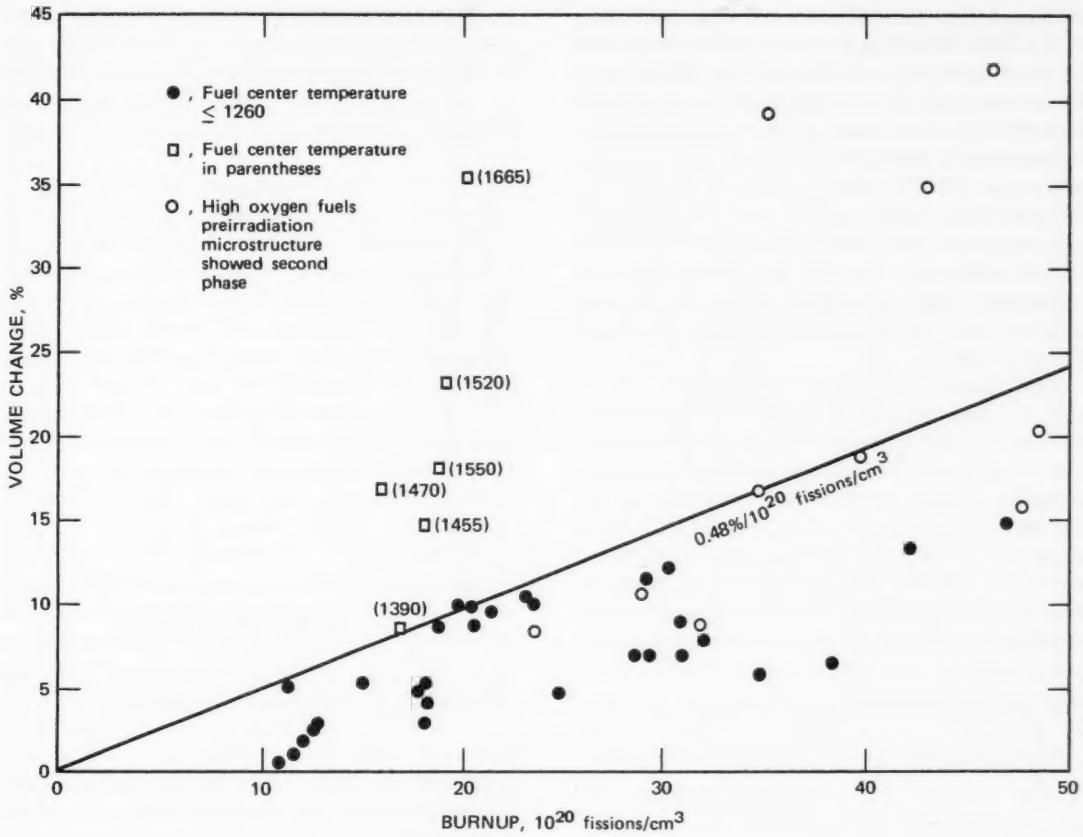

Fig. 8 Volume change of (U,Pu)N vs. burnup.[82]

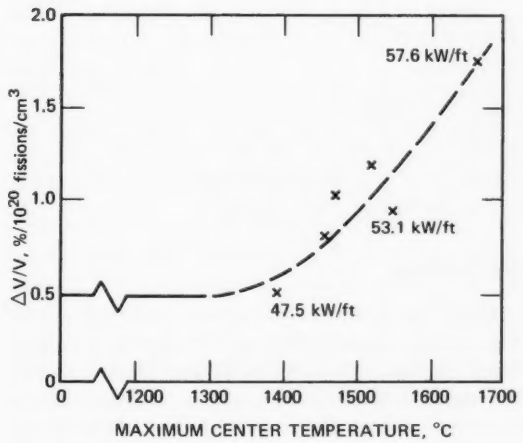

Fig. 9 Temperature dependence of (U,Pu)N swelling.[82]

gas-bubble-induced fuel swelling was estimated[94,104] as beginning at 1260°C.

Fission-gas-release data as a function of density and as a function of burnup for high-density $U_{0.8}Pu_{0.2}N$ fuel are shown[82] in Figs. 10 and 11. Increased rates of gas release are observed at fuel densities below about 85% of theoretical and when fuel burnups exceed 100,000 MWd/metric ton. Increased release at high burnup apparently is associated with microcracking in the high-burnup rim of fuel irradiated in thermal reactors. Increased gas release has also been observed when fuel centerline temperatures exceed 1300 to 1400°C and from fuel containing U_2N_3 stabilized by the presence of high levels of oxygen impurity.

A single fuel pin containing 81.4% dense $U_{0.8}Pu_{0.2}N$ fuel, helium-bonded to 304 stainless-steel cladding, has been irradiated[82] in Experimental Breeder Reactor II (EBR-II) to a burnup of 32,100

MWd/metric ton (3.6 at.%) at a peak linear heat rating of 24.8 kW/ft. The original 4.6-mil radial gap between fuel and cladding was consumed by the swelling fuel, and an additional ½- to 1-mil cladding deformation associated with fuel–cladding mechanical interaction was measured. In view of the initial high fuel centerline temperature (1760°C) estimated before fuel swelling closed the fuel–cladding gap, the pin swelling is judged to be consistent with fuel swelling rates observed in thermal irradiations. Despite the initial high fuel temperatures, fission-gas release in the pin also was consistent with gas-release data obtained in thermal irradiations (see Fig. 10).

Poor capsule performance in irradiation experiments involving UN–20 wt.% PuN fuel clad in 316 stainless steel and irradiated to burnups in the range 2500 to 20,000 MWd/metric ton prevented an accurate assessment of fuel performance.[91] However, it was concluded that thermal decomposition of mixed nitrides was not a problem at fuel centerline temperatures up to 2000°C. This conclusion concerning stability of the mixed nitrides is confirmed by short-term irradiations (~8 hr) of $U_{0.85}Pu_{0.15}N$ at linear heat ratings of 100 kW/ft (3300 W/cm). Maximum fuel centerline temperatures of 2500°C were estimated,[104] but no evidence of fuel decomposition was observed.

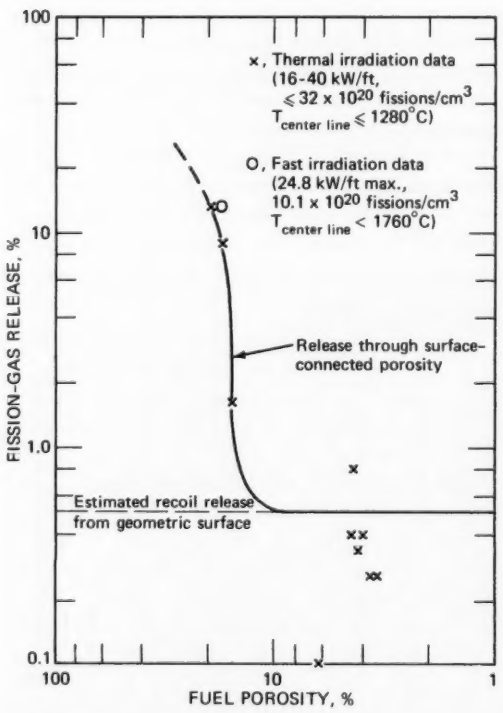

Fig. 10 Fission-gas release dependence on (U,Pu)N pellet porosity.[82]

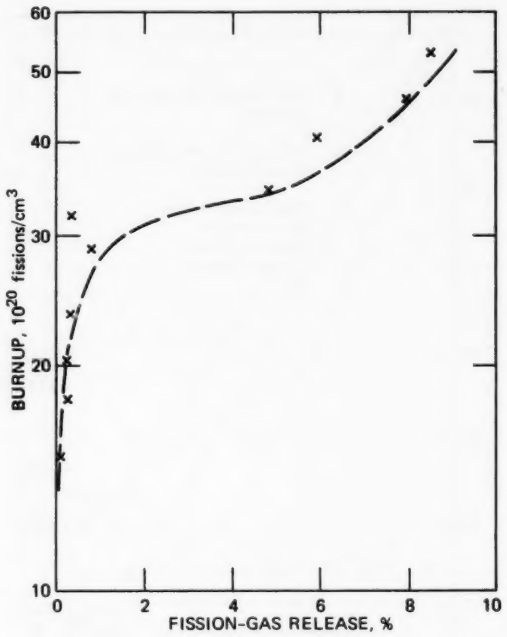

Fig. 11 Fission-gas release as a function of burnup for high-density (>93.8% of theoretical) (U,Pu)N fuel.[82]

DISCUSSION

Interest in UN, as noted at the beginning of this article, is restricted to its possible use at high surface temperatures in space reactor applications. The diametral swelling data presented in Fig. 7 provide excellent support for this interest. Mixed nitrides, on the other hand, are of potential interest as advanced LMFBR fuels. It is this interest which will serve as the focus of discussion in this section.

Fuel-Pin Design

If the high thermal conductivity of nitride fuels is to be used to advantage, two possible approaches exist. In one approach the fuel is helium bonded to the cladding, as with oxide fuel, and its melting point is accepted as the parameter limiting the fuel-pin power rating. In the other approach, sodium bonding is employed between fuel and cladding to reduce the cladding-to-fuel temperature increase, and the tempera-

ture at which swelling rates become excessive, nominally the temperature at which swelling associated with fission-gas-bubble agglomeration occurs, is accepted as limiting pin performance. In either case, significantly higher fuel-pin ratings can be achieved than with oxide fuels.

The first choice has certain inherent limitations. Because of the high fuel temperatures, fuel swelling rates will be high, and, once fuel–cladding contact is established, reliance must be placed on cladding resistance to restrain further swelling. Fission-induced creep, which lowers the fuel creep resistance and permits the cladding to force the fuel to deform into available fuel porosity, is apparently a prime contributor to the successful performance of clad oxide-fuel pins. However, even though fission-induced creep is observed in nitride fuel, the present indication, based on data[50] for UN, is that the creep resistance is an order of magnitude greater than in oxide fuels. Consequently fuel swelling will be more difficult to restrain. Furthermore, relatively low fuel densities may be required if excessive cladding deformation is to be avoided, resulting in a loss in the fuel-loading advantage afforded by high-density nitride fuel.

A sodium bond also results in lower fuel temperatures that minimize the possibility of cladding deformation as a consequence of differences in thermal expansion between fuel and cladding. An increase in average fuel temperature about twice that of the cladding can be tolerated without the occurrence of mechanical interaction. Thus fuel-management concern that power changes accompanying fuel relocation will result in fuel–cladding interaction should be eliminated.

The principal disadvantage associated with the sodium bond arises from the additional cost involved in the loading of a sodium-bonded fuel pin. However, this cost should be more than offset by the potential use of low-cost cladding—possible because the cladding acts only as a container and not as a mechanical structure restraining the swelling fuel. The swelling fuel simply displaces the sodium in the gap as it expands. A 20-mil diametral gap has been estimated[82] as being sufficient with 0.275-in.-diameter fuel pellets to accommodate the fuel swelling associated with a minimum burnup of 150,000 MWd/metric ton. The lack of fuel–cladding interaction also should permit the use of thinner cladding, which will have a beneficial effect on neutron economy.

The use of a sodium gap may introduce an additional problem that has already been encountered with carbide fuels,[105,106] that is, oval cladding deformation produced as the result of fuel-pellet cracking due to thermal stresses. Cracked pellet pieces lodge in the sodium-filled gap and deform the cladding nonuniformly as the fuel grows with increasing burnup. This may not be as serious a problem with nitride fuels, which appear to crack less drastically than carbide fuels. Also, the low swelling rate of nitride fuels permits the use of a relatively small sodium gap, and a smaller gap size has been found to decrease the severity of fuel cracking in nitride fuels.[82] Nevertheless, if fuel cracking does prove to be a problem, a fuel shroud, within the cladding to contain the fuel pieces, can be inserted in the fuel pin.

The performance-boundary limits applicable to mixed-carbide and mixed-nitride fuels are shown[107] in Fig. 12. The limits are based on a minimum pin inside diameter of 0.200 in. (considered the minimum practical pin size fabricable), a minimum specific fuel power of 100 W/g (doubling times become excessive at lower ratings), a maximum heat flux of 2×10^6 Btu/(hr)(ft^2) (limited by cladding thermal stress and sodium heat-removal pumping requirements), and a maximum linear pin power rating of 45 kW/ft. The linear power limit is based on an estimate that excessive fuel swelling can be avoided if fuel centerline temperatures are kept below 1300 to 1400°C. A somewhat more conservative and easily defined limit is the minimum temperature at

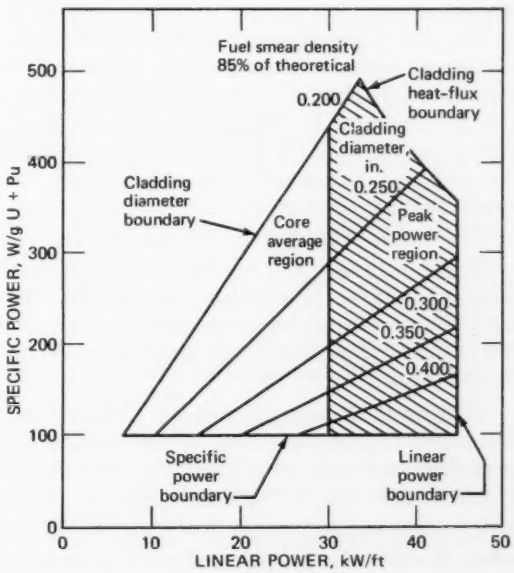

Fig. 12 Performance boundaries of stainless-steel-clad sodium-bonded (U,Pu)C and (U,Pu)N fuel pins in a fast reactor.[107]

which fission-gas-bubble swelling begins; for $U_{0.8}Pu_{0.2}N$, this is[82] about 1350°C, and, for mixed carbide, it appears[105,108] to be below 1300°C. This would tend to decrease the linear power boundary to 40 kW/ft or slightly less, still well above the limit of 19 kW/ft for oxide fuels.

There is a serious need for irradiation data on (U,Pu)N fuel in a fast-flux environment. With the exception of a single helium-bonded pin, all data have been obtained in thermal reactors.[82] However, it should be noted that the performance data reported for the $U_{0.8}Pu_{0.2}N$ fuel are all based on the latter one-half or one-third of the irradiation at which point, because of fuel burnout in the outer region of the fuel, temperature gradients in the fuel have become very similar to those obtained in a fast reactor. Any influence of helium generation in a fast flux is expected to be minor. Also, as long as fuel performance is limited to prohibit fission-gas-bubble swelling in the fuel, and fuel–cladding mechanical interactions are avoided by the use of a sodium bond, it is difficult to see any major effect of differences between thermal- and fast-flux irradiations on the cladding. Thus the thermal irradiations appear a valid means of projecting mixed-nitride fuel behavior.

Safety

A major concern with nitride fuels has been their thermal stability. This concern is based on the behavior of UN, which decomposes in a vacuum with loss of nitrogen at temperatures above about 1600°C. However, as noted earlier, the addition of PuN produces a considerable change in vaporization behavior such that PuN is lost preferentially from (U,Pu)N materials and decomposition is prevented, presumably until such time as all the PuN is vaporized.

The essential stability of the mixed nitrides is confirmed by irradiation experience. Irradiations of $U_{0.8}Pu_{0.2}N$ (Ref. 91) and $U_{0.85}Pu_{0.15}N$ (Ref. 104) have proceeded at fuel centerline temperatures of 2000 and 2500°C, respectively, with no evidence of fuel decomposition.

High-energy neutron capture by ^{14}N has been determined as providing a more negative sodium-void coefficient for a nitride-fueled reactor, compared with a carbide-fueled one.[96] The relative effect in the two fuels is illustrated in Table 4. The importance of this effect is difficult to evaluate, but, if sodium-void characteristics become an important feature in core design, an optimized nitride core could have a beneficial effect on reactor safety and fuel-cycle costs.

Table 4 Sodium-Void Coefficients of Nitride- and Carbide-Fueled Reactors[96]

Sodium loss from	Sodium-void coefficients, % Δk	
	Nitride core	Carbide core
Total reactor	−1.4	−0.8
Core only	+1.0	+1.5

Fuel Synthesis and Fuel-Cycle Costs

There appears little likelihood that the hydride–nitride cycle will provide an economic method for the production of mixed-nitride fuels unless new methods for reduction to metallic uranium and plutonium are developed. Carbothermic reduction coupled with nitridation has received sufficient study to indicate its potential as an economic process, although considerable additional development is required. However, a major question concerning this process is the residual carbon and oxygen impurity levels and their influence on irradiation performance. High levels of oxygen in conjunction with U_2N_3 have been shown to have a detrimental effect on fuel performance that U_2N_3 alone does not have.[82] The effects either of high levels of oxygen alone or of carbon impurity have not been defined.

Other techniques of fuel synthesis certainly deserve examination. Pyrometallurgical reprocessing, permitting direct conversion to nitride, appears extremely promising.[63] One of the attractive features of this process is that it should permit the economic utilization of ^{15}N in mixed-nitride fuel. Such utilization requires ^{15}N recovery and reuse, which are readily accomplished in pyrometallurgical reprocessing.

The interest in ^{15}N stems from the parasitic neutron captures in ^{14}N that have a detrimental effect on breeding characteristics and fuel-cycle costs. Comparative breeding characteristics and fuel-cycle costs for carbide and nitride cores, determined for the same reactor model[96] and assuming equivalent fuel-performance capabilities for both fuels, are shown in Table 5. Fuel-cycle costs for the nitride and carbide cores are essentially equivalent, except for credit for the plutonium produced in the fuel cycle. Slightly increased fuel-inventory requirements are also associated with the nitride core.

These relative differences could be essentially eliminated by the use of ^{15}N. However, costs for its production (90% ^{15}N) are estimated[109] to be about $1.00/g. Although this represents a negligible cost increment to the first core cost, the cost becomes

Table 5 Comparative Breeding Characteristics and Fuel-Cycle Costs for Carbide- and Nitride-Fueled Reactors[96]

	Carbide core	Nitride core
Breeding characteristics		
Core conversion radio	0.81	0.75
Total breeding radio	1.39	1.33
Doubling time, years	8.4	11.7
Fuel-cycle cost, mills/kWh		
Gross cost	1.1242	1.1170
Plutonium credit	0.3743	0.2992
Net cost	0.7499	0.8178

significant relative to the fuel-cycle costs unless the ^{15}N is recycled along with the other fuel components.

CONCLUSIONS

Available fuel-property and -performance data indicate that the nitrides are fuel materials of great potential interest, UN for space reactor and (U,Pu)N for LMFBR applications. The data for (U,Pu)N show that it is thermally stable at least to 2500°C, that swelling rates are extremely low and predictable as long as fuel temperatures that permit the agglomeration of fission gases are avoided, that fission-gas release percentages are low (less than 10% at burnups to 150,000 MWd/metric ton), and that burnups of 150,000 MWd/metric ton can be achieved without degradation in fuel behavior. The data suggest that (U,Pu)N fuels can be best utilized in sodium-bonded fuel pins.

When (U,Pu)N is compared with its principal competitor, (U,Pu)C, as an advanced LMFBR fuel, certain advantages to the use of (U,Pu)N fuel appear to be evident—no evidence of fuel–cladding incompatibility, lower swelling rate, and potentially higher linear power ratings without the initiation of swelling resulting from fission-gas agglomeration. A detrimental effect on breeding characteristics and fuel-cycle costs results from parasitic neutron captures in ^{14}N but may be overcome by the use of ^{15}N.

REFERENCES

1. J. J. Katz and E. Rabinowitch, *The Chemistry of Uranium*, Part I, pp. 232–241, McGraw-Hill Book Company, Inc., New York, 1951.
2. J. Bugl and A. A. Bauer, Phase Relations in the System Uranium–Nitrogen, *J. Amer. Ceram. Soc.*, **47**: 425–429 (1964).
3. R. Benz and M. G. Bowman, Some Phase Equilibria in the Uranium–Nitrogen System, *J. Amer. Chem. Soc.*, **88**: 264–268 (1965).
4. R. E. Rundle, A. S. Baenziger, A. S. Wilson, and R. A. McDonald, The Structures of the Carbides, Nitrides and Oxides of Uranium, *J. Amer. Chem. Soc.*, **70**: 99 (1948).
5. C. P. Kempter, J. C. McGuire, and M. R. Nadler, Uranium Mononitride, *Anal. Chem.*, **31**: 156–157 (1959).
6. M. H. Mueller and H. W. Knott, The Crystal Structure of UN by Neutron Diffraction, *Acta Crystallogr.*, 751–752 (1958).
7. J. Langier and J. M. Martin, Phase Relationships Between the Two Varieties of Uranium Sesquinitride, *J. Nucl. Mater.*, **28**: 215–217 (1968).
8. H. J. Stöcker and A. Naoumidis, Hexagonales Urannitrid, *Ber. Deut. Keram. Ges.*, **43**: 724–728 (1966).
9. S. Yoshihiko and A. Tetsuzo, Nonstoichiometric Hexagonal Close-Packed Uranium Sesquinitride, *J. Amer. Ceram. Soc.*, **53**: 102–105 (1970).
10. R. Benz and W. B. Hutchinson, U + UN_2 Reaction Layer Growths, *J. Nucl. Mater.*, **36**: 135–146 (1970).
11. W. M. Olson and R. N. R. Mulford, The Decomposition and Melting Point of Uranium Mononitride, *J. Phys. Chem.*, **167**: 952–954 (1963).
12. P. A. Vozzella and M. A. DeCrescente, Thermodynamic Properties of Uranium Mononitride, USAEC Report PWAC-479, Pratt and Whitney Aircraft, October 1965.
13. H. Inouye and J. M. Leitnaker, Equilibrium Nitrogen Pressures and Thermodynamic Properties of UN, *J. Amer. Ceram. Soc.*, **51**: 6–9 (1968).
14. B. Neumann, C. Kroger, and H. Haebler, Über die Bildungswärme der Nitride, IV. Uran–Thor–Lanthannitrid, *Z. Anorg. Allg. Chem.*, **207**: 145–149 (1932).
15. P. Gross, C. Hayman, and H. Clayton, Heats of Formation of Uranium Silicides and Nitrides, *Thermodynamics of Nuclear Materials*, Symposium Proceedings, Vienna, 1962, International Atomic Energy Agency, Vienna, pp. 653–659, 1962 (STI/PUB/58).
16. W. N. Hubbard, Thermochemical Studies at Argonne National Laboratory, USAEC Report TID-15554, p. 5, Argonne National Laboratory, February 1962.
17. C. A. Alexander, J. S. Ogden, and W. M. Pardue, Volatilization Characteristics of Uranium Mononitride, *J. Nucl. Mater.*, **31**: 13–24 (1969).
18. J. Bugl and A. A. Bauer, Thermodynamics of the U_2N_3 Phase Region, in International Symposium on Compounds of Interest in Nuclear Reactor Technology, *Nuclear Metallurgy*, Vol. X, pp. 215–224, American Institute of Mining, Metallurgical and Petroleum Engineers, New York, 1964.
19. P. E. Lapat and R. B. Holden, Thermodynamics of the Uranium–Nitrogen System, *ibid.*, pp. 225–236.
20. F. Anselin, Étude des Nitrures d'Uranium, de Plutonium et de Leurs Solutions Solides, *J. Nucl. Mater.*, **10**: 301–320 (1963).
21. K. E. Spear and J. M. Leitnaker, Review and Analysis of Phase Behavior and Thermodynamic Properties of the Plutonium–Nitrogen System, USAEC Report ORNL-TM-2106, Oak Ridge National Laboratory, March 1968.
22. D. L. Keller, Annual Report, Progress on Development of Fuels and Technology for Advanced Reactors During July

1969–June 1970, USAEC Report BMI-1886, pp. A1–A8, July 1970.

23. C. A. Alexander, J. S. Ogden, and W. M. Pardue, Thermophysical Properties of (U,Pu)N, Plutonium 1970 and Other Actinides, in *Nuclear Metallurgy*, Vol. 17, pp. 95–103, American Institute of Mining, Metallurgical and Petroleum Engineers, New York, 1970.
24. D. L. Keller, Annual Report, Progress on Development of Materials and Technology for Advanced Reactors During July 1968–June 1969, USAEC Report BMI-1868, pp. A15–A19, Battelle Memorial Institute, July 1969.
25. J. Williams and R. A. J. Sambell, The Uranium Monocarbide–Uranium Mononitride System, *J. Less-Common Metals*, **1**: 217 (1959).
26. F. Anselin, Preparation and Study of Mixed Carbides–Nitrides of Uranium and Plutonium, French Report CEA-R-2988, June 1966.
27. J. M. Martin, Les Diagrammes de Phases U–UN–UO_2 et UO_2–UN–N_2, *J. Nucl. Mater.*, **34**: 81–85 (1970).
28. R. Benz, UO_2–UN_2–U Phase Equilibria, Report LADC-10417, Los Alamos Scientific Laboratory, 1969.
29. D. L. Keller, USAEC Report BMI-1868, pp. A19–A29, Battelle Memorial Institute.
30. W. Fulkerson, T. G. Kollie, S. C. Weaver, J. P. Moore, and R. K. Williams, Electrical and Thermal Properties of the NaCl Structured Metallic Actinide Compounds, Plutonium 1970 and Other Actinides, *Nuclear Metallurgy*, Vol. 17, pp. 374–385, American Institute of Mining, Metallurgical and Petroleum Engineers, New York, 1970.
31. J. P. Moore, W. Fulkerson, and D. L. McElroy, Thermal Conductivity, Electrical Resistivity, and Seebeck Coefficient of Uranium Mononitride, *J. Amer. Ceram. Soc.*, **53**: 76–82 (1970).
32. E. O. Speidel and D. L. Keller, Fabrication and Properties of Hot-Pressed Uranium Mononitride, USAEC Report BMI-1633(EURAEC-706), Battelle Memorial Institute, May 30, 1963.
33. D. L. Keller, Annual Report, Progress on Development of Fuels and Technology for Advanced Reactors During July 1970–June 1971, USAEC Report BMI-1918, pp. A5–A9, Battelle Memorial Institute, July 1971.
34. J. B. Holt and M. Y. Almassy, Nitrogen Diffusion in Uranium Nitride as Measured by Alpha Particle Activation of ^{15}N, *J. Amer. Ceram. Soc.*, **52**: 631–635 (1969).
35. T. J. Sturiale and M. A. DeCrescente, Self-Diffusion of Nitrogen on Uranium Mononitride, USAEC Report PWAC-477, Pratt and Whitney Aircraft, Sept. 8, 1965.
36. D. K. Reimann and T. S. Lundy, Diffusion of ^{233}U in UN and UO_2 Single Crystals, *J. Metals*, **20**: 54A (August 1968).
37. University of California Lawrence Radiation Laboratory, Advanced Space Nuclear Power Program, Quarterly Report for January–March 1968, USAEC Report UCRL-50004–68–1, p. 17.
38. T. Honda and T. Kikuchi, Porosity Dependence of Elastic Modulus of UN, *J. Nucl. Sci. Technol. (Tokyo)*, **6**: 221–222 (1969).
39. H. L. Whaley, W. Fulkerson, and R. A. Potter, Elastic Moduli and Debye Temperature of Polycrystalline UN by Ultrasonic Velocity Measurements, *J. Nucl. Mater.*, **31**: 345–350 (1969).
40. A. Padel and C. DeNovion, Elastic Constants of the Carbides, Nitrides, and Oxides of Uranium and Plutonium, *J. Nucl. Mater.*, **33**: 40–51 (1969).
41. A. R. Hall, Elastic Moduli and Internal Friction of Some Uranium Ceramics, British Report AERE-R-5650, December 1967.
42. K. M. Taylor and C. H. McMurtry, Synthesis and Fabrication of Refractory Uranium Compounds, Summary Report for May 1959–December 1960, USAEC Report ORO-400, Carborundum Company, February 1961.
43. C. DeNovion, B. Aruce, A. Groff, Y. Guerin, and A. Padel, Mechanical Properties of Uranium- and Plutonium-Based Ceramics, Plutonium 1970 and Other Actinides, *Nuclear Metallurgy*, Vol. 17, pp. 509–517, American Institute of Mining, Metallurgical and Petroleum Engineers, New York, 1970.
44. J. D. L. Harrison and R. P. Pape, Factors Affecting the Hardness of Uranium Mononitride, Plutonium 1970 and Other Actinides, *Nuclear Metallurgy*, Vol. 17, pp. 518–529, American Institute of Mining, Metallurgical and Petroleum Engineers, New York, 1970.
45. R. W. Endebrock, E. L. Foster, and D. L. Keller, Preparation and Properties of Cast UN, USAEC Report BMI-1690, Battelle Memorial Institute, 1964.
46. W. Vandervoort, C. Barmore, and C. F. Cline, Compression Creep of Polycrystalline Uranium Mononitride in Nitrogen, *Met. Trans.*, **242**: 1466–1467 (July 1968).
47. M. F. Fassler, F. J. Huegel, and M. A. DeCrescente, Compressive Creep of UC and UN, USAEC Report PWAC-482(Pt. 1), Pratt and Whitney Aircraft, October 1965.
48. D. L. Keller, USAEC Report BMI-1886, pp. B94–B101, Battelle Memorial Institute.
49. M. S. Seltzer, J. Perrin, A. H. Clauer, and B. A. Wilcox, A Review of Creep Behavior of Ceramic Nuclear Fuels, *Reactor Technol.*, **14**(2): 19 (Summer 1971).
50. D. Brucklacher and W. Dienst, Creep Behavior of Ceramic Nuclear Fuels Under Neutron Irradiation, presented at Basic Science and Nuclear Divisions Joint Fall Meeting, American Ceramic Society, Anaheim, Calif., Nov. 2, 1971.
51. V. J. Tennery, T. G. Godfrey, and R. A. Potter, Synthesis, Characterization, and Fabrication of UN, USAEC Report ORNL-4608(NASA-CR-72764), Oak Ridge National Laboratory, December 1970.
52. A. Nishiyama, T. Kasamatsu, K. Itani, and H. Katsuya, Study of Fabrication of Uranium Nitride Fuel, USAEC Report UCRL-Trans-10074, translated from *Sumitomo Denki*, No. 87, pp. 123–130, 1965.
53. M. U. Goodyear, R. A. Smith, and D. E. Kizer, Sintering Studies on UN and $(U_{0.8}Pu_{0.2})N$, *Trans. Amer. Nucl. Soc.*, **11**: 521 (1968).
54. S. Peterson, Metals and Ceramics Division Annual Progress Report for Period Ending June 30, 1971, USAEC Report ORNL-4770, September 1971.
55. F. Thümmler, G. Ondracek, and K. Dalal, Zur Daretellung und Zum Drucksinter-Verhalten von Uranmononitrid, *Z. Metallk.*, **56**: 535–543 (1965).
56. R. W. Endebrock, E. L. Foster, and D. L. Keller, Characterization and Properties of Arc-Melted Uranium Mononitride, in International Symposium on Compounds

of Interest in Nuclear Reactor Technology, *Nuclear Metallurgy*, Vol. X, pp. 557–563, American Institute of Mining, Metallurgical and Petroleum Engineers, New York, 1964.

57. W. M. Pardue, A. A. Bauer, and D. L. Keller, Potential of Mixed-Nitride (U,Pu)N as a Fast Reactor Fuel, in Proceedings of the International Symposium on Ceramic Nuclear Fuels, pp. 166–178, American Ceramic Society, 1969.
58. J. R. McLaren, R. J. Dicker, J. D. L. Harrison, and L. E. Russell, The Preparation and Sintering Behavior of Uranium Mononitride Made by the Carbothermic Reduction of Uranium Oxides in Nitrogen, in Proceedings of the Second European Symposium on Powder Metallurgy, Stuttgart, May 1968, Paper 8.4.
59. S. Imoto and H. J. Stöcker, Preparation of Uranium Mononitride by the Reaction of Uranium Dioxide with Carbon and Nitrogen, in *Thermodynamics*, Symposium Proceedings, Vienna, 1965, International Atomic Energy Agency, Vienna, 1966 (STI/PUB/109).
60. K. R. Hyde, D. A. Landsman, et al., The Preparation of Uranium Nitride and Carbonitrides from Uranium Oxide in a Fluidized Bed, British Report AERE-R-4650, 1964.
61. W. O. Greenhalgh and E. T. Weber, Carbothermic Synthesis of Mixed Uranium–Plutonium Nitride, USAEC Report BNWL-SA-1866, Battelle–Northwest, August 1968.
62. W. C. Robinson, Jr., and W. R. Martin, A Feasibility Study: Formation of Uranium Nitride Compounds Using Chemical Vapor Deposition Techniques, USAEC Report ORNL-TM-1812, Oak Ridge National Laboratory, May 1967.
63. R. N. Anderson, N. A. D. Parlee, and J. M. Gallagher, Applications of Nitride-Forming Reactions to Reprocessing of Spent Nuclear Fuels, *Nucl. Technol.*, **13**: 29–35 (1972).
64. D. E. Lozier, E. O. Speidel, and D. E. Kizer, Processing of High-Purity Uranium Mononitride by Powder Techniques, Presented at American Ceramic Society Nuclear Division Meeting, Urbana, Ill., 1967.
65. W. M. Pardue, F. A. Rough, and R. A. Smith, Uranium–Plutonium Nitrides: Fabrication and Properties, 1967 AIME Nuclear Metallurgy Symposium on Plutonium Fuels Technology, Phoenix, Ariz., 1967.
66. L. R. McLarken and P. M. W. Atkinson, The Sintering of Uranium Mononitride, *J. Nucl. Mater.*, **17**: 142–148 (1965).
67. M. U. Goodyear, R. A. Smith, W. M. Pardue, and D. E. Kizer, Fabrication of UN–PuN by Sintering Techniques, USAEC Report BMI-1809, Battelle Memorial Institute, 1967.
68. M. U. Goodyear, R. A. Smith, and D. E. Kizer, Development of Sintering Techniques for $U_{0.8}Pu_{0.2}N$ Fabrication, USAEC Report BMI-1826, Battelle Memorial Institute, 1968.
69. E. T. Weber, W. O. Greenhalgh, and R. L. Gibby, Development of Mixed-Nitride Fuel Materials Obtained by Carbothermic Reduction of Oxides, *Trans. Amer. Nucl. Soc.*, **11**: 104 (1968).
70. L. E. Russell, The Sintering of Pyrophoric Powders, *Powder Met.*, **10**: 239 (Autumn 1967).
71. D. L. Keller, USAEC Report BMI-1868, pp. A1–A15, Battelle Memorial Institute.
72. R. M. Dell, V. J. Wheeler, and N. J. Bridger, Hydrolysis of Uranium Mononitride, *Trans. Faraday Soc.*, **63**: 1286–1294 (1967).
73. J. Bugl and A. A. Bauer, Corrosion and Oxidation Characteristics of Uranium Mononitride, Intern. Symp. on Compounds of Interest in Nuclear Reactor Technology, *Nuclear Metallurgy*, Vol. X, pp. 463–476, American Institute of Mining, Metallurgical and Petroleum Engineers, New York, 1964.
74. M. Allbutt and R. M. Dell, Chemical Aspects of Nitride, Phosphide, and Sulphide Fuels, *J. Nucl. Mater.*, **24**: 1–20 (1967).
75. V. J. Wheeler and R. M. Dell, The Oxidation and Ignition Temperature of Uranium Mononitride and Uranium Monocarbide, Part I, British Report AERE-R-4600, 1964.
76. C. Moreau and J. Philippott, Kinetics of the Reaction of Pure Oxygen with Uranium Mononitride, *Compt. Rend.*, **256**: 5366–5369 (1963).
77. E. J. McIver, V. J. Wheeler, R. M. Dell, and E. Watt, The Oxidation and Ignition of Uranium Mononitride and Uranium Monocarbide, Part II, British Report AERE-R-4985, 1965.
78. W. T. Langendorfer, Battelle–Columbus Laboratories, private communication, 1972.
79. J. C. Hebeisen, D. P. Moak, and W. H. Pfeifer, Compatibility of Nitride Reactor Fuels with Austenitic Stainless Steels, USAEC Report BMI-1895, Battelle Memorial Institute, January 1971.
80. D. E. Price and D. P. Moak, in Annual Report, Progress Relating to Civilian Applications During July 1966–June 1967, USAEC Report BMI-1809, pp. A30–A48, Battelle Memorial Institute, July 1, 1967.
81. D. E. Price, F. A. Rough, and D. P. Moak, in Progress Relating to Civilian Applications During March 1966, USAEC Report BMI-1767, pp. C4–C6, Battelle Memorial Institute, April 1967.
82. A. A. Bauer, J. B. Brown, E. O. Fromm, and V. W. Storhok, Mixed-Nitride Fuel Irradiation Performance, in Proceedings of ANS Conference on Fast Reactor Fuel-Element Technology, Materials Science and Technology Division, pp. 785–818, 1971.
83. D. L. Keller, USAEC Report BMI-1868, pp. A56–A66, Battelle Memorial Institute.
84. S. Katz, High Temperature Reactions Between Refractory Uranium Compounds and Metals, *J. Nucl. Mater.*, **6**: 172–181 (1965).
85. D. E. Price, D. P. Moak, W. Chubb, and D. L. Keller, The Compatibility of Uranium Nitride with Potential Cladding Metals, USAEC Report BMI-1760(EURAEC-1591), Battelle Memorial Institute, Feb. 8, 1966.
86. F. E. McGrath, J. A. DeMastry, and M. S. Farkas, Metallography of Ceramic Fuels and Refractory Metal Compatibility Couples, Technical Papers of the 18th Metallographic Group Meeting, USAEC Report NMI-5025, pp. 39–58, Battelle Memorial Institute, 1965.
87. J. Bugl and D. L. Keller, Uranium Mononitride—A New Reactor Fuel, *Nucleonics*, **22**: 66 (1964).
88. S. J. Paprocki, D. L. Keller, G. W. Cunningham, and D. E. Kizer, in Progress Relating to Civilian Applications During September 1960, USAEC Report BMI-1469, p. D-2, Battelle Memorial Institute, Oct. 1, 1960.

89. I. Sheinhartz and Z. L. Zambrow, Dispersion-Type Materials for Fuel Elements, Part I, USAEC Report SCNC-266, Sylvania–Corning Nuclear Corp., June 1958.
90. M. Allbutt and A. R. Junkinson, Some Observations on the Compatibility of Uranium and Plutonium Nitrides with Several Stainless Steel Alloys, British Report AERE-R-5466, 1967.
91. Battelle Memorial Institute, Reactor Fuels and Materials Development Programs, Quarterly Progress Report for October–December 1967, USAEC Report BNWL-668, Battelle Memorial Institute, March 1968.
92. D. L. Keller, USAEC Report BMI-1886, pp. A8–A14, Battelle Memorial Institute.
93. R. L. Martin, W. J. Zielenbach, V. W. Storhok, D. L. Keller, and J. E. Gates, Radiation Stability of Uranium Mononitride, USAEC Report BMI-1731(EURAEC-1431), Battelle Memorial Institute, June 29, 1965.
94. H. Mikailoff, J. P. Mustelier, J. Bloch, J. Leclere, and L. Hayet, Irradiation Behavior of Mixed Uranium–Plutonium Carbides, Nitrides, and Carbonitrides, French Report CEA-R-3223, 1967.
95. H. Alton and C. E. Weber, The Production of Hydrogen and Helium in Metals During Reactor Irradiations, *J. Nucl. Mater.*, **16:** 68–73 (1965).
96. J. F. Fletcher and J. Greenborg, Nitride Fuels for Fast Breeder Reactors: Fuel Cycle Considerations, USAEC Report BNWL-606, Battelle Memorial Institute, February 1968.
97. M. D. Rogers and J. Adam, Radiation Damage and Its Thermal Recovery in Uranium Monocarbide and Uranium Mononitride, British Report AERE-R-4046, June 1962.
98. R. A. Wullaert, J. F. Lagedrost, J. Bugl, and J. E. Gates, Radiation Stability of Uranium Mononitride, USAEC Report BMI-1638(EURAEC-760), Battelle Memorial Institute, June 28, 1963.
99. S. C. Weaver, R. K. Thomas, and V. A. DeCarlo, Irradiation Testing of UN in ORR, *Trans. Amer. Nucl. Soc.*, **12:** 547 (1969).
100. T. N. Washburn, R. K. Thomas, S. C. Weaver, D. R. Cuneo, and E. L. Long, Jr., Examination of UN-Fueled Pins Irradiated at 1400°C Cladding Temperature, *Trans. Amer. Nucl. Soc.*, **13:** 101 (1970).
101. R. F. Hilbert, V. W. Storhok, and W. Chubb, High Temperature Irradiation Behavior of UN, UC, and UO_2 Fuels Compared, *Trans. Amer. Nucl. Soc.*, **13:** 102 (1970).
102. E. D. Albrecht, A. J. Rothman, J. D. Lee, J. M. Johnson, and W. N. Hayes, Jr., A High Temperature Irradiation and Postirradiation Analyses of Uranium Nitride Fuel, USAEC Report UCRL-50727, University of California Lawrence Radiation Laboratory, Aug. 7, 1969.
103. R. F. Hilbert, V. W. Storhok, W. Chubb, and D. L. Keller, Swelling of UC and UN at High Temperatures, Proceedings of ANS Conference on Fast Reactor Fuel-Element Technology, Materials Science and Technology Division, pp. 753–770, 1971.
104. H. Mikailoff, J. Leclere, B. Kryger, J. Bloch, and M. Conte, Irradiation of Mixed Uranium and Plutonium Carbide and Nitride Fuels in the Fast Neutron Loop "MFBS," French Report CEA-N-1186(EURFNR-688), 1969.
105. J. O. Barner, Behavior of Sodium-Bonded (U,Pu)C Fuel Elements After Moderate Burnup, in Proceedings of ANS Conference on Fast Reactor Fuel-Element Technology, Materials Science and Technology Division, pp. 819–847, 1971.
106. B. L. Harbourne, P. J. Levine, T. W. Latimer, and L. A. Numark, The Irradiation Behavior of Sodium-Bonded Mixed-Carbide Fuel Pins, in Proceedings of ANS Conference on Fast Reactor Fuel-Element Technology, Materials Science and Technology Division, pp. 869–894, 1971.
107. T. N. Washburn and J. L. Scott, Performance Capability of Advanced Fuels for Fast Breeder Reactors, in Proceedings of ANS Conference on Fast Reactor Fuel-Element Technology, Materials Science and Technology Division, pp. 741–752, 1971.
108. C. Grando, M. Montgomery, and A. Strasser, Unrestrained Swelling and Fission Gas Release of Fast Reactor Fuels, in Proceedings of ANS Conference on Fast Reactor Fuel-Element Technology, Materials Science and Technology Division, pp. 771–784, 1971.
109. W. C. Corder, Battelle–Columbus Laboratories, private communication, May 1971.

AMERICAN NUCLEAR SOCIETY—CRITICAL REVIEWS

The Atomic Energy Commission has contracted with the American Nuclear Society to prepare for publication on a regular basis detailed Critical Review articles written by experts selected from the ANS membership and reviewed by an advisory committee of top leaders and scientists in the field. In this issue the articles are on pages 107–183.

Members of the Critical Review Advisory Committee are:

Sidney Siegel, *Chairman*	Atomics International
William Chittenden	Sargent & Lundy Engineers
Frank G. Dawson	Battelle—Northwest
Don E. Ferguson	Oak Ridge National Laboratory
F. J. Leitz	WADCO Corporation
Paul Lottes	Argonne National Laboratory
Peter Murray	Westinghouse Electric Corporation
David Okrent	University of Arizona
Herbert Parker	Battelle—Northwest
A. M. Platt	Battelle—Northwest
Joseph Prestele	New York Consolidated Edison
W. C. Redman	Argonne National Laboratory
K. L. Rohde	Idaho Nuclear Corporation
Charles Stevenson	Argonne National Laboratory
Bertram Wolfe	Battelle—Northwest

ANS Critical Review Editor, *Norman H. Jacobson*

ANS Officers:

President, *John W. Landis*

Vice President/President-Elect, *James R. Lilienthal*

Treasurer, *J. Ernest Wilkins, Jr.*

Executive Secretary, *Octave J. Du Temple*

Comments on the articles should be communicated directly to the ANS Critical Review Advisory Committee or Editor, 244 E. Ogden Avenue, Hinsdale, Ill. 60521.

ANS GUIDELINES FOR PREPARING CRITICAL REVIEWS FOR *REACTOR TECHNOLOGY*

One interpretation of the words "Critical Review" emphasizes the word *critical.* That type of article would have as its purpose the discussion of a single subject, which has been uncertain and perhaps controversial, in considerable depth. An example might be a critical review of the values of alpha for plutonium, assessing all the work done and arriving at a best current estimate. This paper is primarily addressed to specialists on the particular subject, and serves as an authoritative source for the information they use.

In the second interpretation of a Critical Review, the emphasis is on the word *review,* in the sense of survey. Such a paper would be broader and probably more descriptive in scope. A paper on "Solubility of Metallic Elements in Liquid Sodium" is an example of this category. Such a paper would be addressed to a much broader group of readers and written in a fashion that would be of interest to the majority of reactor technologists. It would provide enough of an introduction that the specialist from another field could immediately appreciate why the subject is important.

The criteria for these two types of articles may not be very different:

1. The paper should be based on a thorough coverage of relevant work on the subject from many sources. A review based on the work of only one individual or group is better suited for publication in one of the regular society journals. The review should be critically selective, reporting only the most valid results and indicating why some prior results have a questionable status. The review should call attention to significant gaps where more work is required in the subject of the article.

2. The paper should be timely, on a subject of active current interest.

3. The scope of articles acceptable as Critical Reviews includes all the subject areas identified for *Reactor Technology* (Economics, Physics, Mechanics, Construction, Fuel Elements, Fuel Cycles, Fluid and Thermal Technology, Fuel Processing, Components, Operating Performance), as well as Materials (including Source and Special Nuclear), Environmental Effects, and Effluent Management. Not desired are (1) reports of original research proposed for first publication and (2) review articles directed toward the specialist in the field of nuclear safety (which is covered by the AEC's bimonthly review *Nuclear Safety*).

4. The paper should be organized so that it is of immediate practical use to the readers. Such organization requires: attention to consistent use of units, presentation of important data in summary curves or tables, and a fully adequate bibliography to the original literature. Details on size, honorarium, style, etc., can be obtained from ANS.

Discrete-Ordinates Methods for the Numerical Solution of the Transport Equation

By K. D. Lathrop*

Abstract: *The theory, advantages, disadvantages, and capabilities of the discrete-ordinates method for numerical solution of the Boltzmann transport equation are reviewed. To illustrate the simplicity of the method, the author derives the theory directly for the specific case of one-dimensional spherical geometry and thereby provides a clearer picture of the method than is available in more general expositions. On this foundation the essential generalizations of the techniques are made. The major limitations of the method, including orthogonal geometries, negative fluxes, ray effects, convergence requirements, and data storage are discussed in detail, and current work to remedy these limitations is reviewed.*

The capabilities of the discrete-ordinates method are surveyed at length, and numerical programs applying the discrete-ordinates techniques are tabulated and compared. An ancestral chart of current discrete-ordinates programs is provided.

A general guide to the usage of discrete-ordinates programs is given, and the application of the method is illustrated in examples including a shielding bench-mark problem, a reactor core-design problem, a control-rod-worth and radiation heating study, a pulsed-neutron problem, and a shielding parameter survey.

You have a need to know. As a reactor physicist, as a shielding designer, as a weapons physicist, as an astrophysicist, or as a manager in these or related areas, you need to know the number of neutrons or photons within some assembly or in some volume. The form in which you need this information may vary from the power distribution in a reactor to the number of particles emerging from a shield to a stellar albedo, but, to satisfy your need, you must solve the Boltzmann transport equation. Perforce your solution will be numerical. The method of discrete ordinates, often synonymously but incorrectly termed the S_n method, is the most powerful and general tool available for the deterministic solution of the complicated (seven independent variables) and refractory transport equation.

In many situations the diffusion approximation to the transport equation provides adequate solutions; in many others the geometric versatility of Monte Carlo methods provides the only means of solution. But, in a broad class of transport physics calculations, the method of discrete ordinates provides the only feasible means to answer accurately the myriad questions posed in the design of assemblies that produce or contain neutrons or photons. Programs based on the method are available to treat as many as six of the seven independent variables of the transport equation. Programs are available to provide direct or adjoint solutions in each of three common orthogonal geometries in both one and two space dimensions. Both static and time-dependent calculations are possible, and solutions are possible for a variety of isotropic and anisotropic inhomogeneous or scattering sources, a variety of boundary conditions including the specification of incoming particle distributions, and a variety of eigenvalue options.

Although the large number of options available complicates the description of many programs that apply the discrete-ordinates method, the basic method is simple. The method is simple because it is designed to minimize the number of computer arithmetic

*Los Alamos Scientific Laboratory, University of California, Los Alamos, N. Mex. 87544.

operations. Although several expositions of the theory of the method are available, they are written mathematically and technically for the specialist. The basic ideas of the discrete-ordinates method in simple examples, working from the specific to the general, are explained in the next section. A clear understanding of the basic principles of the method will enable the manager or user to see how easily the method can be adapted to his specific problem.

To alert potential users to possible pitfalls and to help them understand and interpret their results, the limitations and defects of the discrete-ordinates method are described in the following section, and in a subsequent section the capabilities of the method as applied in currently available computer programs are reviewed. Both the virtues and defects of these programs are assessed so an intelligent choice of available tools may be made.

A general guide to the usage of discrete-ordinates programs is provided in a later section. Partly philosophy and partly suggestions for reducing cost, this section contains much already known to users and specialists but should be of interest to those newly desiring to use discrete-ordinates programs. Examples of a broad range of applications are also given later, and the review is summarized in the final section.

SIMPLIFIED THEORY OF DISCRETE-ORDINATES METHODS

Presently used discrete-ordinates programs are the evolutionary descendants of S_n programs[1,2] in which the angular variable was represented by n connected straight-line segments, giving rise to the appellation $S(\text{egment})_n$. The label S_n is often used as a synonym for discrete ordinates, although the angular representation is different. In this section the theory of presently used methods is explained without reference to previous expositions.

The analytic transport equation expresses the rate of change of the number of particles in a system as the difference between the production rate and the loss rate for a point in space at a particular velocity. Thus, in addition to time, the equation involves three space variables and three velocity variables. Instead of velocity variables, the energy and two angular variables are frequently used. These three variables plus the three space variables define a six-dimensional phase space in an infinitesimal volume of which, in a nuclear reactor, neutrons may be produced by fission or scattering from other elements of phase space. From the same volume, neutrons may be lost by streaming, absorption, or scattering to other volume elements. For most reactor physics problems, it is sufficient to deal with the linear transport equation, a careful derivation of which is given in Ref. 3, along with an explanation of the assumptions made in the derivation.

The transport equation is complicated, and almost all attempts at its solution begin by simplifying the equation. The greatest simplification is to remove independent variables. The time variable is eliminated by considering steady-state situations when production balances losses. Spatial variables and some angular direction variables are eliminated by considering simple geometries with convenient symmetry properties. The treatment of energy variables is often simplified by making use of the multigroup approximation, in which the transport equation is averaged over energy ranges and the detailed variation of cross sections is replaced by suitable averages. Let us begin our description of discrete-ordinates methods by considering a particularly simple form of the analytic transport equation.

In a sphere in which material properties vary only as a function of distance from the origin, the steady-state transport equation involves only two independent variables: the distance, r, from the origin of the sphere, and the cosine, μ, of the angle between the direction of particle motion and the direction of the vector from the origin to the point r. In this geometry the angular flux $\psi(r,\mu,E)$, that is, the number of particles per unit volume, angle, and energy times the particle speed, is given by the solution to the following equation[4]:

$$\frac{\mu}{r^2}\frac{\partial(r^2\psi)}{\partial r}+\frac{1}{r}\frac{\partial[(1-\mu^2)\psi]}{\partial\mu}+\sigma_t(r)\psi = \frac{\sigma_s(r)}{2}\int_{-1}^{1}\psi(r,\mu')d\mu'+S(r,\mu) \qquad (1)$$

In this equation, σ_t and σ_s represent the macroscopic total and scattering cross sections, respectively. The lower case σ is used by convention to avoid confusion with the capital sigma that occurs repeatedly in sums in numerical work. The scattering is assumed to be isotropic (the probability of a scattering event producing a particle in a direction μ after a collision when traveling in the direction μ' is uniformly $\frac{1}{2}$), but only to simplify the discussion; the source of particles, S, is allowed to be anisotropic, i.e., to depend on μ. The energy variable has been suppressed. All discrete-ordinates programs make use of the multigroup approximation, although a pointwise energy representation is also feasible. In either case, the contribu-

tion of scattering events or other sources that produce particles in the energy range of interest is included in the source, S. This is one of the major simplifications of present discrete-ordinates methods. Each energy range or group can be dealt with separately. In effect, the energy variable is eliminated. Although a solution for each group may be obtained separately, all the fluxes needed for calculating the source to the group are not usually known, and an iterative cycle through the groups is usually performed.

The discrete-ordinates approximation to Eq 1 evaluates the transport equation at a set of discrete directions μ_m, $m = 1, 2, \ldots MM$. The value of the angular flux, or ordinate, in these directions is denoted by $\psi_m(r) = \psi(r,\mu_m)$. Because Eq. 1 contains both an angular derivative and an angular integral, the range of μ is divided into intervals $\Delta\mu_m = \mu_{m+\frac{1}{2}} - \mu_{m-\frac{1}{2}}$, where $-1 = \mu_{\frac{1}{2}} < \mu_{\frac{3}{2}} \ldots < \mu_{MM+\frac{1}{2}} = +1$. This enables representation of the derivative as a difference and representation of the integral as a sum. Thus the discrete-ordinates approximation to Eq. 1 is written

$$\frac{\mu_m}{r^2}\frac{\partial(r^2\psi_m)}{\partial r} + \frac{(1-\mu_{m+\frac{1}{2}}^2)\psi_{m+\frac{1}{2}} - (1-\mu_{m-\frac{1}{2}}^2)\psi_{m-\frac{1}{2}}}{r\Delta\mu_m} + \sigma\psi_{tm} = \frac{\sigma_S}{2}\sum_{\varrho=1}^{MM}\psi_\varrho\,\Delta\mu_\varrho + S_m(r) \qquad (2)$$

This is neither the form of the discrete-ordinates equation as used by Chandrasekhar[5] nor that used in present discrete-ordinates codes; both are more general. For the moment, a description of this generality is postponed.

Equation 2 does preserve one important property of both the currently used methods and the analytic equation. If Eq. 2 is multiplied by $\Delta\mu_m$ and summed over all directions, the term representing the angular derivative vanishes because $\mu_{\frac{1}{2}}^2 = \mu_{MM+\frac{1}{2}}^2 = 1$. The same is true of the μ integral of Eq. 1. The angular derivative accounts for the change of direction of particles as they stream in straight lines between collisions. The net number of particles per unit volume and energy is not affected by this redistribution. If the numerical approximation to Eq. 1 did not preserve this property, local conservation of particles would be lost.

Equation 2 remains a continuous function of r. Let us now discretize this variable and evaluate the equation at the points $r_1, r_2, \ldots r_{IM}$ in the intervals $\Delta r_i = r_{i+\frac{1}{2}} - r_{i-\frac{1}{2}}$ with $0 = r_{\frac{1}{2}} < r_{\frac{3}{2}} < \ldots < r_{IM+\frac{1}{2}}$. The value of the discrete-ordinate angular flux at these points r_i is denoted by ψ_{im}, and Eq. 2 is approximated by

$$\frac{\mu_m}{r_i^2}\frac{(r_{i+\frac{1}{2}}^2\psi_{i+\frac{1}{2},m} - r_{i-\frac{1}{2}}^2\psi_{i-\frac{1}{2},m})}{\Delta r_i} + \frac{(1-\mu_{m+\frac{1}{2}}^2)\psi_{i,m+\frac{1}{2}} - (1-\mu_{m-\frac{1}{2}}^2)\psi_{i,m-\frac{1}{2}}}{r_i\,\Delta\mu_m} + \sigma_{ti}\psi_{im} = \frac{\sigma_{si}}{2}\sum_{\varrho=1}^{MM}\psi_{i\varrho}\,\Delta\mu_\varrho + S_{im} \qquad (3)$$

The domain of the variables μ and r has now been divided into $MM \times IM$ boxes of size $\Delta\mu_m \times \Delta r_i$, and Eq. 3 involves ψ evaluated inside and on the edges of these mesh boxes. Figure 1 shows how these fluxes are oriented for a typical mesh box. The location of r_i within Δr_i and the location of μ_m within $\Delta\mu_m$ does not need to be specified unless the accuracy with which Eq. 3 approximates Eq. 1 is going to be analyzed.

For each box the five angular fluxes shown in Fig. 1 are coupled by Eq. 3. Two of these five fluxes are known, either from boundary conditions or calculations in adjoining boxes. For example, for $\mu_m < 0$ (incoming directions), the commonly used "vacuum" boundary condition means that $\psi_{IM+\frac{1}{2},m} = 0$. Two other equations are required for use with Eq. 3 to allow calculation of the three unknown fluxes. The simple, symmetric, and accurate arithmetic mean relations

$$\psi_{im} = (\psi_{i+\frac{1}{2},m} + \psi_{i-\frac{1}{2},m})/2$$
$$\psi_{im} = (\psi_{i,m+\frac{1}{2}} + \psi_{i,m-\frac{1}{2}})/2 \qquad (4)$$

are frequently used to provide the two extra equations. If it is assumed that $\psi_{i+\frac{1}{2},m}$ and $\psi_{i,m-\frac{1}{2}}$ are known, then the use of Eq. 4 in Eq. 3 permits the center flux to be calculated in terms of these two known fluxes:

$$\psi_{im} = a_{im}\psi_{i+\frac{1}{2},m} + b_{im}\psi_{i,m-\frac{1}{2}} + c_{im}Q_{im} \qquad (5)$$

where the form of a_{im}, b_{im}, and c_{im} is easily determined by performing the substitution and where Q_{im} includes both S_{im} and the scattering source. If $\psi_{i-\frac{1}{2},m}$ is known instead of $\psi_{i+\frac{1}{2},m}$, a similar recursion can be found. For this one-dimensional spherical geometry, it is always possible to proceed from small values of m to large values. For the first value of m, Eq. 5 is used either with values of $\psi_{i,\frac{1}{2}}$ obtained from a special calculation for $\mu = -1$ (see Ref. 6) or with a difference scheme such that $b_{i\varrho} = 0$.

Simple equations like Eq. 5 form the inmost part of almost all numerical programs that solve the discrete-ordinates equations. The complicated partial

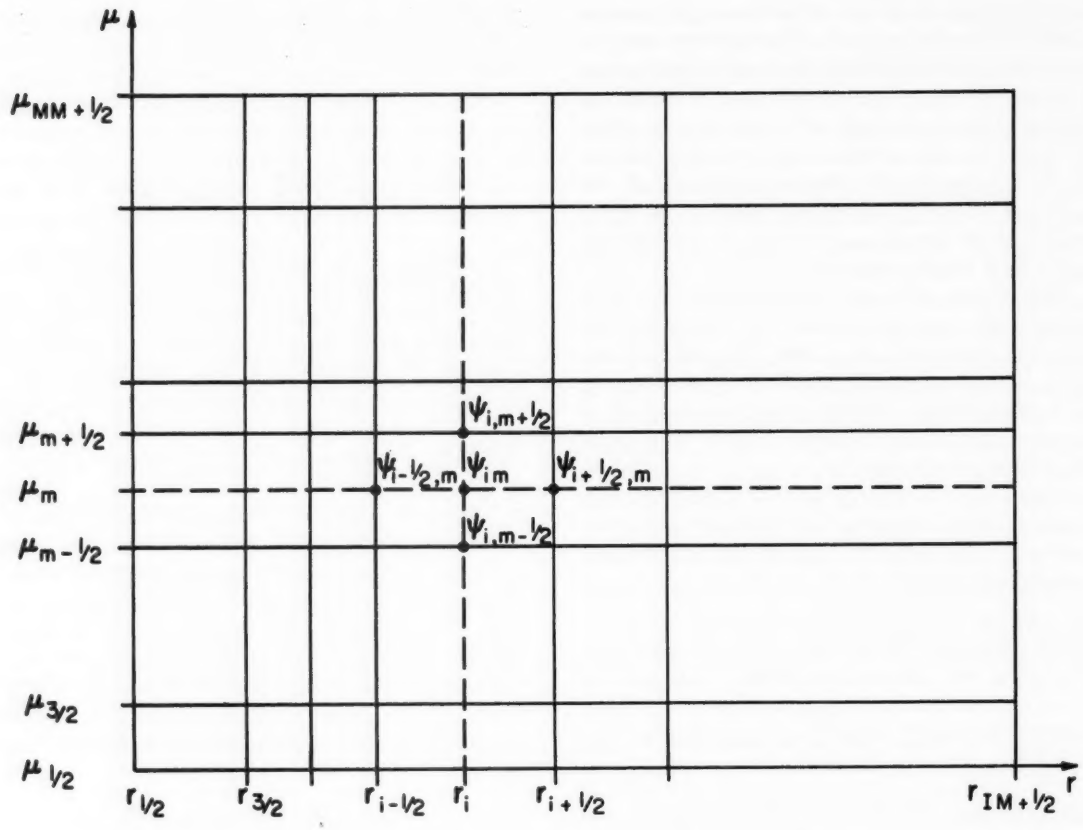

Fig. 1 Typical discrete-ordinates mesh in one-dimensional spherical geometry. Location of cell edge and center fluxes is shown.

differential equation of Eq. 1, or its counterpart in other geometries, is reduced to an algebraic system that can be solved recursively. Every flux on the mesh can be computed by stepping from box to box. Besides being simple, equations like Eq. 5 are very general. The cross sections may be continuously variable from one space interval to the next. Although not indicated in Eq. 3, because most discrete-ordinates codes do not allow it as an option, the cross sections could also depend on angle. A large variety of useful boundary conditions are easily applied. Similar recursions can be developed for the adjoint transport equation so that most discrete-ordinate numerical programs can be used to solve the adjoint transport equation as well. The versatility of such programs will be illustrated later.

Most discrete-ordinates programs for numerical solution of the one-dimensional transport equation use a generalization of Eq. 3, which can be written

$$\frac{\mu_m(A_{i+\frac{1}{2}}\psi_{i+\frac{1}{2},m} - A_{i-\frac{1}{2}}\psi_{i-\frac{1}{2},m})}{V_i} + \frac{(A_{i+\frac{1}{2}} - A_{i-\frac{1}{2}})(\alpha_{m+\frac{1}{2}}\psi_{i,m+\frac{1}{2}} - \alpha_{m-\frac{1}{2}}\psi_{i,m-\frac{1}{2}})}{V_i\Delta\mu_m} + \sigma_{ti}\psi_{im} = \frac{\sigma_{si}}{2}\sum_{\varrho=1}^{MM}\psi_{i\varrho}\,\Delta\mu_\varrho + S_{im} \qquad (6)$$

In this form, $A_{i+\frac{1}{2}}$ is the area of the surface at $r_{i+\frac{1}{2}}$, and V_i is the volume of the cell of width Δr_i in whichever geometry is being considered. For the sphere, $A_{i+\frac{1}{2}} = 4\pi r_{i+\frac{1}{2}}^2$ and $V_i = 4\pi(r_{i+\frac{1}{2}}^3 - r_{i-\frac{1}{2}}^3)$, which leads to a slightly different representation of r_i than that used in Eq. 3. The α coefficients are the analog of $(1 - \mu_{m\pm\frac{1}{2}}^2)$ and are defined so that the two approximate derivatives in Eq. 6 cancel when ψ is a constant, as would the analytic derivatives in Eq. 1. This requires that

$$\alpha_{m+\frac{1}{2}} - \alpha_{m-\frac{1}{2}} = -\mu_m \Delta\mu_m \tag{7}$$

Like $1 - \mu_{\frac{1}{2}}^2$, the first α, $\alpha_{\frac{1}{2}}$ is required to be zero so that Eq. 7 serves as a recursion to determine the rest of the coefficients. With Eq. 7, the use of the arithmetic mean difference relations in Eq. 6 produces a recursion like Eq. 5 which has the same a, b, c coefficients for stepping from left to right or from right to left. This is not true of Eq. 3 unless $\mu_m = (\mu_{m+\frac{1}{2}} + \mu_{m-\frac{1}{2}})/2$, a requirement not satisfied by many useful quadrature sets $(\mu_m, \Delta\mu_m)$.

With equations like Eqs. 4, 6, and 7, one can make a numerical program that treats plane, cylindrical, or spherical geometry simply by using the appropriate definition of A and V, an elegant embedding. Furthermore, when Eq. 6 is multiplied by $\Delta\mu_m V_i$, each term in the equation is identifiable as a number of particles contributing to the gain or loss in the phase space box. For example, the term $\Delta\mu_m \mu_m A_{i+\frac{1}{2}} \psi_{i+\frac{1}{2},m}$ is the number of particles that flow out of the box through the surface at $r_{i+\frac{1}{2}}$, $\Delta\mu_m V_i \sigma_{ti} \psi_{im}$ is the total number removed from the box by collisions, and so on. The approximation to the analytic equation is boxwise conservative, a very useful feature.

The two-dimensional orthogonal geometries (x,y) planar, (ρ,θ) cylindrical planar, and (ρ,z) finite cylindrical can all be treated by using a generalization of Eq. 6:

$$\frac{\mu_m(A_{i+\frac{1}{2},j}\psi_{i+\frac{1}{2},jm} - A_{i-\frac{1}{2},j}\psi_{i-\frac{1}{2},jm})}{V_{ij}} + \frac{(A_{i+\frac{1}{2},j} - A_{i-\frac{1}{2},j})(\alpha_{m+\frac{1}{2}}\psi_{ijm+\frac{1}{2}} - \alpha_{m-\frac{1}{2}}\psi_{ijm-\frac{1}{2}})}{V_{ij} W_m} + \frac{\eta_m B_{ij}(\psi_{i,j+\frac{1}{2},m} - \psi_{i,j-\frac{1}{2},m})}{V_{ij}} + \sigma_{tij}\psi_{ij} = \frac{\sigma_{sij}}{2\pi} \sum_{\ell=1}^{MM} W_\ell \, \psi_{ij\ell} + S_{ijm} \tag{8}$$

Here the subscript j indicates the second spatial direction, with η_m being the cosine of the angle between the direction of particle motion and the direction of the axis along which j distances are measured. In these geometries the angular integral is actually a double integral, but it can be accomplished as a single sum with quadrature weight W. The extra space derivative in Eq. 8 requires the use of another arithmetic mean relation, that is, $2\psi_{ijm} = \psi_{i,j+\frac{1}{2},m} + \psi_{i,j-\frac{1}{2},m}$, but otherwise the solution of Eq. 8 is much like the solution of Eq. 6. In both cases, one starts by assuming that some system exterior-edge values of the flux are known and that the right-hand, or source, sides of the equations are given. Then one uses Eqs. 6 or 8 to calculate the box center flux and equations like Eq. 4 to calculate the other edge fluxes. Having these fluxes, one can move to the next cell to the interior and repeat the process until all fluxes in the system are known. If σ_s is zero, this completes the calculation. If not, the scattering portion of the source is calculated using the latest fluxes. Rather than store the angular flux, one usually accumulates, during the sweep through the mesh, those integrals of the angular flux which are necessary to calculate the scattering source. With the new estimate of the scattering source, the process is iterated. We illustrate this procedure with a very simple, but two-dimensional, example.

For the simple four-space box system shown in Fig. 2, we assume that $\sigma_t = 1$, $\sigma_s = 0$, and that $S = Q$ in

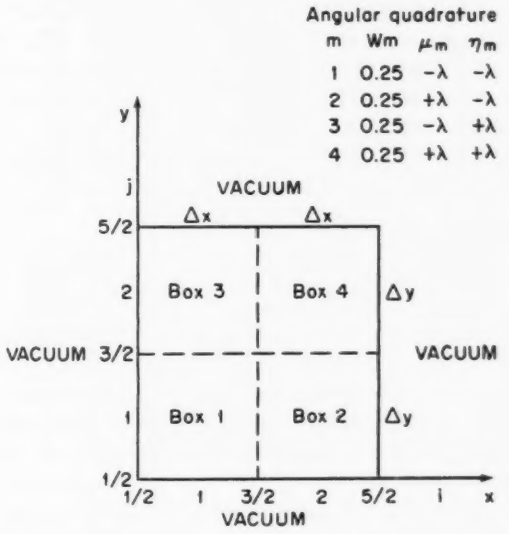

Fig. 2 Geometry for simple two-dimensional test problem.

each box in each direction. That is, the source is constant in space and isotropic in direction. For this geometry, $V_{ij} = \Delta x \Delta y$, $A_{i+\frac{1}{2},j} = \Delta y$, and $B_{ij} = \Delta x$, so that Eq. 8 becomes

$$\frac{\mu_m(\psi_{i+\frac{1}{2},j,m} - \psi_{i-\frac{1}{2},j,m})}{\Delta x} + \frac{\eta_m(\psi_{i,j+\frac{1}{2},m} - \psi_{i,j-\frac{1}{2},m})}{\Delta y} + \psi = Q \tag{9}$$

If the arithmetic mean relations like Eq. 4 are used, Eq. 5 becomes

$$\psi_{ijm} = \frac{2|\mu_m|\Delta y\,\psi_{i+\frac{1}{2},j,m} + 2|\eta_m|\Delta x\,\psi_{i,j+\frac{1}{2},m} + \Delta x\Delta y Q}{2|\mu_m|\Delta y + 2|\eta_m|\Delta x + \Delta x\Delta y}$$

$$= a\psi_{i+\frac{1}{2},j,m} + b\psi_{i,j+\frac{1}{2},m} + cQ \qquad (10)$$

where for the problem at hand, a, b, c are the same for each box for each direction and $a + b + c = 1$. The quadrature uses four symmetrically oriented directions with cosines $\mu = \pm\lambda$ and $\eta = \pm\lambda$. If $\lambda = 1/\sqrt{3}$, the quadrature is the commonly used S_2 set, which has the fewest discrete directions of any S_n quadrature.

To simplify our nomenclature for this problem, we consider only direction 1 and replace the ij subscripts with a box subscript and a letter, using C, L, R, T, and B to denote center, left, right, top, and bottom fluxes in the box. Thus $\psi_{5/2,2,1}$ becomes $\psi_{4,R}$, or the box 4, right-edge flux in direction 1. In box 4, for this direction, $\psi_{4,T}$ and $\psi_{4,R}$ are needed to evaluate Eq. 10 for $\psi_{4,C}$. But, with vacuum boundary conditions, as indicated in Fig. 2, both of these fluxes are zero, and $\psi_{4,C}$ is simply cQ. From Eq. 4, $\psi_{4,L} = 2cQ$ and $\psi_{4,B} = 2cQ$. We can now move to box 3, where the boundary condition implies $\psi_{3,T} = 0$ and where $\psi_{3,R} = \psi_{4,L}$, which was just calculated to be $2cQ$. Thus

$$\psi_{3,C} = a(2cQ) + cQ = (2a + 1)cQ$$

Having this value, we can calculate $\psi_{3,L}$ and $\psi_{3,B}$. At this point, we have generated all the top-row fluxes for direction 1. We now can start direction 2 from box 3, where both boundary fluxes are known, and step to the right. For this simple problem, these fluxes are the same, from left to right, as those we just calculated from right to left. Having traversed from left to right and right to left along the top row of boxes, we have generated all the top-edge fluxes for boxes 1 and 2. These two boxes can then be treated just as if they were at the top of the system, so we can traverse from right to left for direction 1 and from left to right for direction 2 to compute all of these fluxes. We have now reached the bottom of the system, where we can begin solution for the fluxes in directions 3 (right to left traverse) and 4 (left to right traverse). Then we move up to boxes 3 and 4 and complete the calculation. In Fig. 3, we show the magnitudes of all the fluxes for direction 1, in units of cQ. Because of the symmetry of the system, this diagram gives us every angular flux. In fact, the angle-integrated or scalar flux at each cell center is given by

$$\phi_{ij} = \sum_{\ell=1}^{4} W_\ell\,\psi_{ij\ell} = (1 + a + b + a^2 + b^2)cQ$$

It is this flux that would be used to form an isotropic scattering source, if σ_s were not zero. Then the traverse through the mesh would have to be repeated, adding this source to Q. The whole process would have to be iterated until the amplitude of the scattering source converged.

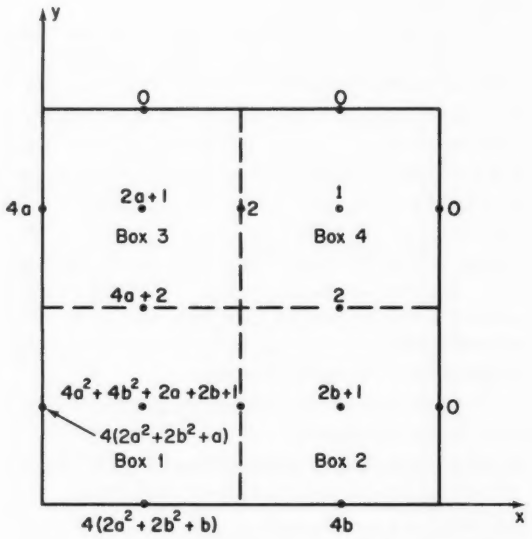

Fig. 3 Angular fluxes for the edges and centers of the in–down direction (units of cQ).

With more directions the traverses are made: (1) inward, beginning at the top-right corner for all in–down directions, and (2) outward, beginning at the top-left corner for all out–down directions. This inward–outward sequence is repeated for each row of the system, beginning at the top and moving to the bottom. Then the inward–outward traverse is begun for all upward directions in the bottom row, and these sequences are repeated a row at a time until the top is reached. This entire cycle comprises one iteration. Anything that reduces the number of iterations or the computational work per iteration shortens the calculation. In the above example, it would have been possible to reduce the number of operations by using the proper boundary condition. For example, if specular reflection had been used as boundary condition for the left and bottom sides of cell 4, only one-fourth as much effort would have been required.

Basically the above procedures for solving the elementary algebraic recursion are very simple and are ideal for implementation on a computer. The programs that implement these procedures are not simple, however, primarily because of the variety of problems each program can handle. We have considered only the portion of the computation known as the inner or within-group iterative cycle. Here we have allowed generality of cross sections, geometry, and boundary conditions. Most discrete-ordinates programs apply algorithms of varying complexity to accelerate the inner iterative process. In two-dimensional geometries, this accelerative algorithm may itself be iterative. Both this process and the inner iterations themselves may form part of an outer iterative cycle. For example, if particles are fed from one group to another by fission or upscattering, then the flux in the group being solved by the inner iteration depends on the flux in groups that have yet to be treated. Another iterative cycle, usually called outer iteration, is required. If the problem is homogeneous, i.e., if it has no sources independent of the flux, an eigenvalue can be determined during the outer iterative process. In neutron problems, k_{eff} is determined during the outer cycle. Most discrete-ordinates programs allow searches for such system parameters as zone thicknesses or material concentrations that guarantee a certain value of k_{eff}. These problems require sequences of outer iterations. A useful example of such a computation is the "time eigenvalue" problem, where the time-dependent flux is assumed to vary as $\exp(\alpha t)$, and a sequence of outer iterations is performed to find that value of α corresponding to a prescribed value of k_{eff}.

Both these parameter iterative sequences and the outer iterative cycle can be accelerated, and many algorithms are used to speed up the computation. In addition to all this machinery, most programs have sophisticated input loading and checking routines, provisions for detailed editing and dumping of computed information, and options for punching, plotting, or passing on information to other programs. The bulk of computation time is spent executing the basic recursion; the bulk of program maintenance time is spent tending the peripheral routines. Options are relatively easy to build into a new program but are much more difficult to thread into existing programs.

The general theory of the methods used in most discrete-ordinates programs is given in Ref. 6; a more detailed exposition of the theory for a specific two-dimensional program is given in Ref. 7 and for a one-dimensional program in Ref. 8. In the next section, defects of these methods are discussed.

LIMITATIONS OF DISCRETE-ORDINATES METHODS

Geometry

The discrete-ordinates method is simple, it is general, and it is most versatile. The method has limitations, however. Foremost of these is its present practical restriction to one- and two-dimensional orthogonal geometries. The reactor shown in Fig. 4 is a

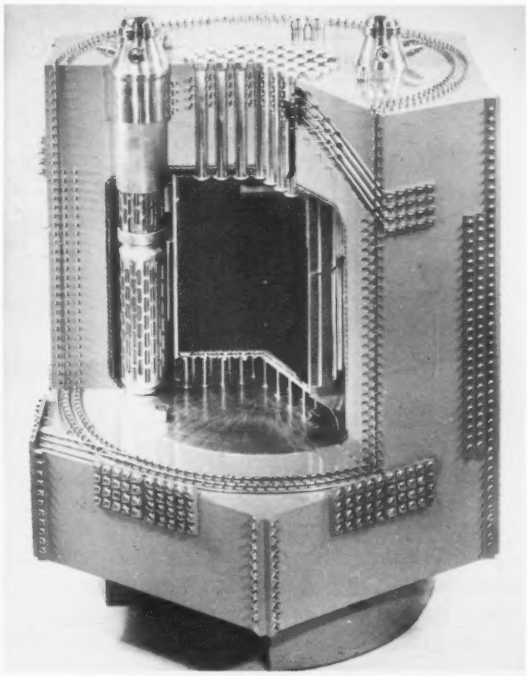

Fig. 4 Real reactor configuration.

piece of precision engineering that was not designed to fit the orthogonal grid of a discrete-ordinates calculation. Figure 5 shows how reality must be forced into artificial boundaries that are the same for each energy. Similarly, Fig. 6 shows a planar cross section of a reactor and Fig. 7 shows the simplified representation when, where possible, advantage is taken of the system symmetry to describe only a fraction of the system. Although Figs. 5 and 6 imply representation of the whole reactor, this is only occasionally possible, and then only with limited description of detail. The number of unknowns, and hence core storage requirements and computational expense, in a discrete-

ordinates calculation is directly proportional to the product of the number of groups, mesh cells, and directions used. In almost any two-dimensional reactor description, the user of a discrete-ordinates program is asked to compromise between accuracy, computational expense, and realistic description of geometry. This need to compromise leads to the popularity of cell calculations in which a representative segment of a reactor core is calculated in great detail to provide

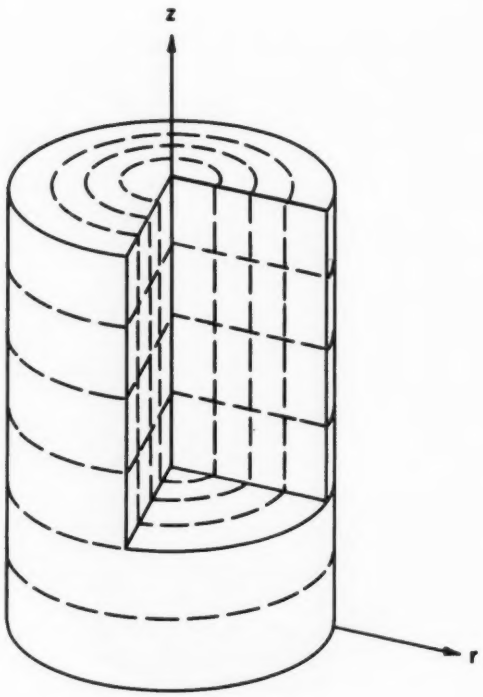

Fig. 5 Orthogonal grid representation of reactor in Fig. 4.

parameters that may be used in cheaper diffusion-theory calculations of the entire system. The need to compromise is also the reason no general three-dimensional discrete-ordinates program has been written. Several existing two-dimensional discrete-ordinates programs perform more arithmetic operations per cell than a three-dimensional (x,y,z) program would require, but the number of mesh cells required for describing real three-dimensional systems is so large that the computational expense would become prohibitive.

Orthogonal grids, then, are inefficient. The coming decade will see the development of discrete-ordinates programs with improved ability to describe geometric detail. Work has already begun[9] on a program to describe planar, regular hexagonal meshes such as that in the real system of Fig. 6. A proposed general triangular mesh for two-dimensional calculations has been described by Reed.[10]

Negative Fluxes

Designers of numerical methods dream of finite-difference schemes that are economically cheap, accurate, and positive. As we have seen, large systems (and large is measured in terms of particle mean free paths over the energy range of interest) strain the capacity of numerical programs with the requirement for large numbers of mesh cells. If the arithmetic mean relations described earlier are used to solve the finite-difference form of the transport equation, large numbers of spatial cells may also be required to ensure that smoothly varying positive fluxes are obtained in situations where the flux should be smoothly varying and positive. These arithmetic mean relations are astonishingly accurate. Not only do errors decrease rapidly as finer mesh intervals are used but also answers obtained with crude meshes are often satisfactory. The relations also lead to cheaply evaluated recursions, as we have seen. They do not guarantee a positive solution, however. By examining the recursion relation in one-dimensional plane geometry, one can easily see that a negative flux could be generated, in the absence of sources, whenever $\sigma_t \Delta x/2\mu_m > 1$, that is, whenever the effective particle path across the cell is large compared to two. Usually, sources are present, or negative fluxes occur only in some directions so that the angle-integrated flux, while being distorted perhaps, does not become negative. Shielding applications, where particles stream through large thicknesses of source-free, absorbing material, are a notable, important exception.

For most practical applications, it is feasible to decrease Δx (or Δr) in one-dimensional calculations until satisfactory fluxes are obtained. This is especially true when corrective recipes are used. In many two-dimensional problems, it is usually not feasible to decrease the size of mesh intervals sufficiently to prevent every negative flux, so considerable effort has gone into developing corrective recipes.[11] All these corrective recipes involve local modification of the arithmetic mean relations but can be divided into two categories: "set-offending-flux-to-zero-and-recompute" algorithms and "switch-to-a-positive-difference-scheme" algorithms. The former is more

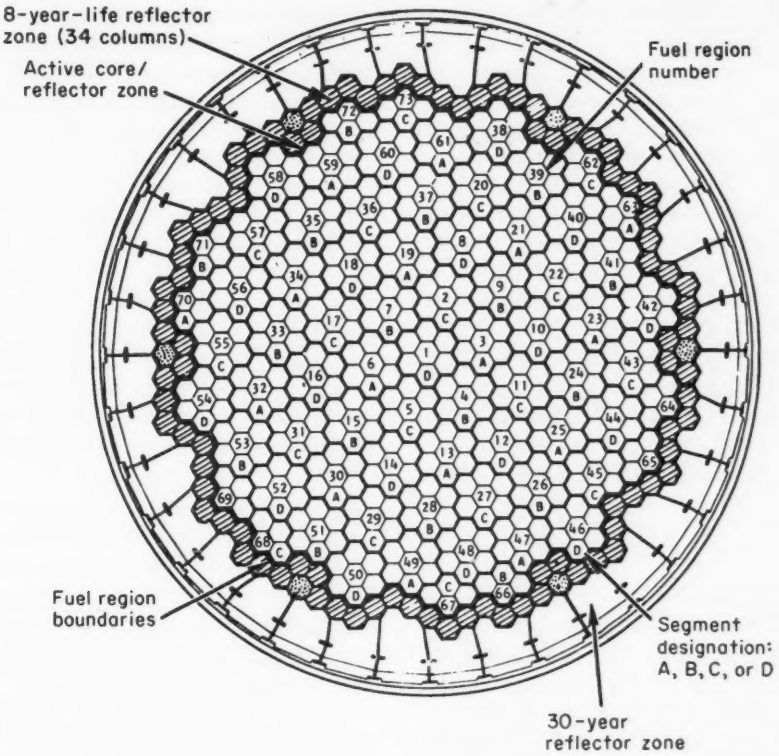
8-year-life reflector zone (34 columns)
Active core/ reflector zone
Fuel region number
Fuel region boundaries
Segment designation: A, B, C, or D
30-year reflector zone

Fig. 6 Actual reactor core configuration.

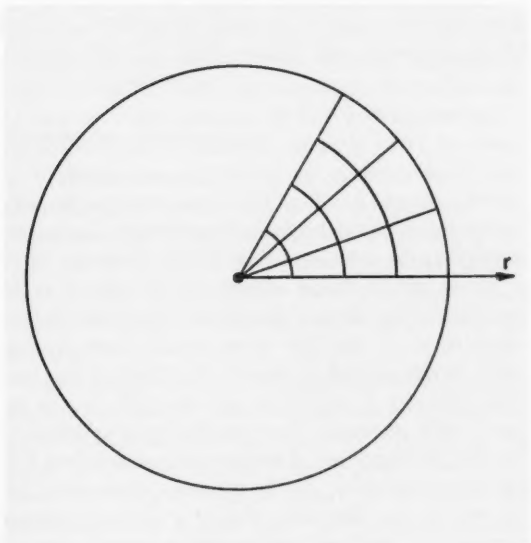

Fig. 7 Orthogonal grid representation of core cross section in Fig. 6.

accurate than the latter, but each requires continuous testing to detect negative fluxes. Thus, in addition to a basic recursion, tests must be made to detect a negative flux, and, if one is detected, extra arithmetic must be performed to calculate a positive flux.

To avoid this proliferation of algorithms and consequent increase of complexity in programs, I have attempted to provide strictly positive difference schemes for the solution of discrete-ordinates equations.[12] Although these schemes have been particularly useful in parameter surveys and although they interact favorably with the iterative process to reduce computational time, their basic inaccuracy is such that one usually returns to the accurate arithmetic mean schemes. In Table 1 the properties of commonly used difference approximations are summarized. The assessment of the properties is based on performance in two-dimensional calculations.

The entries of Table 1 are arranged in order of increasingly positive solution. The more positive the scheme, the better its convergence properties, but the worse its accuracy. This is the kind of tradeoff that

Table 1 Properties of Discrete-Ordinates-Difference Approximations

Scheme	Accuracy	Positivity	Interaction with iterative cycle
Basic arithmetic mean, or diamond scheme[13]	Excellent	No	Fair
Same as above, but with "set-to-zero-and-correct" algorithm included[7,8]	Good to excellent	Yes	Fair to good
Weighted diamond scheme with fixed weights[14]	Good to excellent if weights can be chosen close enough to diamond weights	Yes, provided weights are chosen properly (by trial and error)	Good to excellent
Variable weighted diamond scheme[11]	Fair to good	Yes	Excellent

gives the methods designer nightmares. During the next decade the search for the simple, accurate, positive, and quickly converging scheme will continue. There is some evidence that most of these objectives may be obtained if the explicit nature of the algorithm is sacrificed[15]; i.e., if one is willing to use a relation involving angular fluxes from previous iterations.

Flux Distortions and Ray Effects

In addition to not being positive, the simple, arithmetic mean scheme produces oscillatory distortions of the flux. These can be considered a subcase of the negative-flux syndrome. Note in Fig. 3 that, if a is $<\frac{1}{2}$, the cell-centered flux of box 3 will be less than the right-edge flux for the same cell. Had we used more boxes in the calculation, we could have observed, for $a < \frac{1}{2}$, a spatially damped oscillation of the flux as we progressed inward. Roughly speaking, this oscillation, from cell edge to cell edge, is around the exact solution. Because the cell-centered flux is on a straight line between two edge fluxes, it can be very accurate, and all integral results of discrete-ordinates methods are based on cell-centered fluxes. Occasionally, for instance, when emerging angular fluxes are of interest, these oscillations can become important. They are controlled by the same steps required to make fluxes positive. Normally the oscillations are only an aesthetically annoying price paid for accuracy.

A more serious spatial distortion occurs due to a defect in the discrete-ordinates formulation itself. When we evaluated Eq. 1 at a set of discrete directions to get Eq. 2, we changed the nature of the equation. The analytic transport equation describes the streaming of particles in all directions; the discrete-ordinates equation (even with analytic space derivatives) allows particles to stream only in discrete directions. This is not important in one-dimensional geometries, and the seriousness of the defect was not noticed for many years.

In two-dimensional geometries, for systems including isolated sources in absorbing media, this restricted streaming of particles along discrete directions or rays can lead to serious distortions in the flux. It is not hard to understand why. For the extreme case of an isolated source in a pure absorber, it is easy to find (outside the source) positions in the system not intersected by an allowed straight line from the source. Because the only contribution to the flux at such positions is that due to streaming, the calculated flux is zero. However, such positions can be found adjacent to locations that are intersected by allowed directions. Here the flux is appreciable, so the flux varies rapidly from zero to some significant value. Such a distortion of the true flux behavior is called a ray effect.[16] It can be particularly important if the detailed space variation of the flux is important. Two-dimensional shielding calculations, especially, can be seriously affected by the ray effect. Any time the value of a flux at a point is required and the flux is attenuated by several orders of magnitude in passing from source to detector, the ray effect can cause serious errors.

There are many remedies for the ray effect.[17] Using more directions, or more properly oriented directions,[18] provides more allowed paths from source to detector. Scattering, which provides a local reemission source after a collision, mitigates the effect. It is often possible to calculate, either analytically or very accurately, the flux that has not suffered a collision and use this flux to provide an undistorted source of first collisions to be treated by discrete-ordinates methods.

Perhaps the most powerful remedy for ray effects is the alteration[17] of the equations to make them similar to spherical harmonic equations, which are free from ray effects. The nature of the alteration is the introduction of a special source that emits particles selectively into regions not reached by direct streaming paths.

We show examples of ray effects in the section titled "Applications." One reassuring aspect of calculations performed comparing discrete-ordinates solutions to exact solutions and other solutions free from ray-effect distortions is that solutions that manifest ray effects seem to oscillate about the correct solution. Consequently global quantities can be estimated accurately. For example, the total number of particles emerging from a two-dimensional shield is likely to be accurately predicted, although the precise location of emergence is not.

The next 10 years will see continuing efforts to modify discrete-ordinates equations to eliminate ray effects. The thrust of these efforts will be to make such modifications a minor, easily executed part of the overall calculation.

Convergence Acceleration

The discrete-ordinates method relies heavily on iterative algorithms for solving the transport equation. The size of the $(N \times N)$ matrix involved is simply too large for direct inversion. In two-dimensional calculations, N, the product of the number of space points and the number of directions, can be of the order of a million.

In marked contrast to diffusion-theory methods, the convergence of discrete-ordinates inner iteration algorithms is almost independent of the size of the space mesh or the number of angles used. Nevertheless, there has been a constant effort to accelerate the iterative process. A wide variety of algorithms has been applied. The success of these algorithms has been far from uniform. No straightforward method has been found which works well for all classes of problems.

The most promising of all acceleration procedures are variations of a particle-conserving renormalization suggested by Bell.[2] Now referred to as "coarse-mesh rebalancing," these algorithms determine local factors by which the flux is multiplied to ensure particle conservation. Their theory has been examined by several authors,[19-21] and Reed[22] has recently shown that the method is a nonlinear variant of the synthetic method analyzed by Gelbard and Hageman.[23] By examining the easier to analyze synthetic method, Reed has been able to develop a coarse-mesh rebalancing procedure that works well for even the most difficult of one-dimensional problems. Possibly a version of Reed's technique will also work well in two-dimensional calculations. Present applications of standard coarse-mesh rebalancing techniques have been made to work well in most two-dimensional applications,[7] but only by ad hoc recipes such as periodic application and switching from coarse-mesh to whole-system rebalancing in the event of trouble.

No matter how successful such developments may be, research on accelerative procedures will continue because of the potentially large reward in terms of increased problem-solving capability. A relatively unexplored area of development that seems fruitful is the application of block inversion techniques that rely on the direct inversion of small portions of the equations of the system and the iteration of the coupling between blocks. Such methods have been pioneered in discrete-ordinates computations by Wagner.[24]

Data Storage and Retrieval

One of the big advantages of the discrete-ordinates method, the ability to generate simultaneously the entire space-, energy-, and angle-dependent distribution function, is also a disadvantage of the method because all that data must be handled, stored, and processed.

Most discrete-ordinates programs do not store the angular flux but make an extra iterative cycle to store it if it is needed for output. Moments of the angular flux necessary to generate scattering sources are stored. With increasingly detailed calculations, more and more such moments must be saved. A four-term Legendre scattering expansion requires 10 such moments to be stored in two-dimensional calculations. Each of these moments must be stored for each space mesh for each group.

All the two-dimensional programs now in use solve the transport equation one group at a time. Data required for the calculation of other groups are stored peripherally. More advanced two-dimensional pro-

grams[25] solve the equations one line at a time, as if the equations were one dimensional. Such treatments have been made possible by efficient use of rapid access peripheral storage units. Such developments are indicative of a general trend that will probably continue until the entire angular flux is stored. Moments of the angular flux will then be calculated as needed, rather than stored. With the angular flux available, new difference schemes and new convergence acceleration algorithms are possible.

Part of the data-transfer problem will be alleviated as the ability to transfer data from bulk fast memory to disk or tape units becomes easier, while calculation is in progress. Most discrete-ordinates programs are computation bound. That is, they expend most of their effort in computation rather than in data transfer. Thus it seems feasible that much data transfer could take place without a significant increase in the total computational time. The trend toward increasing spatial and energy resolution in design calculations will speed the development of this capability.

CAPABILITIES OF DISCRETE-ORDINATES METHODS AND PROGRAMS

In previous sections, some capabilities of discrete-ordinates methods were indicated. In this section, all the available capabilities are reviewed, and easily realized additional potentials of the technique are indicated. Not all the capabilities are of immediate interest in any one application, such as reactor-physics design, but most may eventually prove useful. Also reviewed are numerical programs that have been written to apply the method and to evaluate the most generally available modern programs. Programs are categorized in several ways, beginning with their ancestry, and their effectiveness is assessed both in terms of the number of options offered and in terms of the ability to cope with the limitations discussed in the preceding section.

Much fine discrete-ordinates work has been done at the naval reactor laboratories, Bettis and Knolls, and at the weapons laboratories, Livermore and Los Alamos. Some of this effort is undocumented, and some of the resulting numerical programs are not generally available. In this review, no attempt is made to present complete coverage of these programs.

Geometry

Discrete-ordinates programs are available for both time-dependent and static problems in one-dimensional plane, cylindrical, and spherical geometries. Discrete-ordinates programs also can be made to calculate plane-geometry problems in which the angular flux varies as a function of azimuthal angle about the x axis, as well as a function of the cosine of the angle between the particle direction and the x axis.[26] Applications for this capability are most common in astrophysics. In two dimensions, programs exist for solving (x,y) planar, (ρ,θ) planar, (ρ,z) cylindrical, and (r,θ) spherical geometry problems. In this latter geometry, the system is assumed homogeneous in angle of revolution about a pole but can vary as a function of angle from the pole. Developmental work is under way for hexagonal planar geometry[9] and general triangular geometry programs.[10] In the latter work, the triangular grid can be applied to planar or cylindrical geometries. The only time-dependent, two-dimensional geometry program available is for (ρ,z) cylindrical geometry.[27]

Boundary Conditions

Boundary-condition options are quite general. It is possible to specify the angular flux at each boundary point for each incoming direction. Boundary conditions involving the flux being calculated (implicit boundary conditions that may involve iterative solution even in the absence of scattering) are of two types: albedo and periodic. The vacuum boundary condition is a special case of an albedo boundary condition. The most general albedo condition would allow the incoming flux in each direction at each space point for each energy to be an arbitrary linear combination of the outgoing angular fluxes in the same space–energy interval. For the most part, such generality is neither needed nor allowed. The specular reflection (angle of reflection equals angle of incidence) and white (all outgoing particles returned isotropically) boundary conditions are commonly used examples of albedo conditions. Periodic boundary conditions, useful in the representation of periodic lattices in planar geometries or in the representation of periodic variables in cylindrical and spherical geometries, set the incoming angular flux at one boundary equal, angle by angle, to the outgoing angular flux at a periodically located boundary.

Source Options

In addition to being able to specify the incoming angular flux at a boundary, it is also possible to introduce an angularly dependent source at interior surfaces. These are sometimes referred to as "shell" sources. Most discrete-ordinates programs will accept

an isotropic source of particles for every space interval and energy group of the system. Some accept anisotropic distributed sources in terms of the spherical harmonic expansion coefficients of the angular source. In principle, a detailed angular source could be introduced for every space–energy cell.

A source due to first collisions can be entered in most discrete-ordinates programs by using the regular distributed source options, but several programs will automatically calculate such a source and use it for subsequent calculation of the collided flux. At present, the uncollided sources that are calculated are from point, line, or plane sources for which analytic evaluation of the exact flux is simple. Not only do such sources improve accuracy and mitigate ray effects but they also can speed convergence of the interative process. More important, the sources permit the use of lower-order angular resolution for a given accuracy. It is only a matter of time before more general uncollided flux computations are possible.

Angular Quadrature

Much work has been devoted to the development of quadrature sets for discrete-ordinates calculations, that is, to selecting the discrete directions in which the transport equation is evaluated and to selecting the weight associated with each direction.[28–32] Most numerical programs in use accept arbitrary quadrature sets as input, including Gauss Legendre (P_n) and Double P_n for one-dimensional integration, but require that such sets meet certain requirements. Perhaps the most stringent of these is the triangular arrangement of directions on octants of the unit sphere as advocated by Carlson.[28–31] This arrangement is economical of points and permits a two-dimensional angular integral to be executed as a single sum by sweeping over sphere latitudes along which one of the angular variables is constant. The arrangement also satisfies basic symmetry requirements, preventing such unsatisfactory situations as the calculation of two different results for different but equivalent spatial orientations of a system.

Much effort has been devoted to finding an optimum or clearly superior direction set from among the many possibilities within the triangular, symmetry preserving sets. Such a set does not seem to exist. For practical computational purposes, it makes little difference which of the standardly available sets is used, provided the same set is used consistently. In shielding or other applications where the angular flux becomes collimated in streaming, it may be advantageous to use especially tailored quadrature sets. For example, if the emerging angular flux is desired far from a localized source, it is known in advance that most of this flux will be confined to a narrow band of directions. Hence most of the available directions can be clustered in this range. Sometimes special sets can be formed within the framework of standard point arrangements; otherwise minor modifications to programs can be made to permit "asymmetric" quadratures.[33,34] In principle, the discrete-ordinates equations can be solved for any direction sets, but programming treatment of progression through the mesh and setting of boundary conditions may impose limitations.

Convergence and Acceleration Options

With the exception of a direct-inversion program for one-dimensional geometries listed below, all discrete-ordinates programs iterate until input convergence criteria are satisfied. These criteria vary from program to program. In general, the more integral the quantity being monitored, the faster the convergence. For example, k_{eff} converges more rapidly than the fission-energy distribution, which converges more rapidly than the spatial variation of the scalar flux, which converges more rapidly than the pointwise angular flux. Various programs monitor different quantities. Some have options for monitoring pointwise convergence or integral quantities as desired. Others provide for convergence only in spatial zones of interest. A particularly constraining form of convergence criterion insists that coarse-mesh balance be satisfied for the whole system.

For acceleration of convergence, most discrete-ordinates programs apply some form of the particle conservation rebalancing procedure discussed in the preceding section. Most often this rebalance is performed for the whole system in each group to accelerate inner iteration and for the whole system to accelerate upscatter convergence. Other possibilities include coarse-space-mesh rebalance for inner iterations, and coarse-group rebalance for upscatter, fission eigenvalue, or fission plus inhomogeneous source problems.[20,35] Further refinements to pointwise space rebalance[36] and groupwise energy[20,37] rebalance are available.

In addition to rebalancing accelerations, use is also made of Chebyshev acceleration[37,38] and more conventional extrapolation procedures.[37,39] The Chebyshev acceleration works well in one-space dimension but failed catastrophically when applied in one two-dimensional program.[12]

Eigenvalue Options

Because of their common ancestry, most discrete-ordinates programs allow calculation of k_{eff} or system dimension, concentration, or time eigenvalues to achieve desired values of k_{eff}. A "time" or "alpha" eigenvalue is the value of the exponent in an assumed exponential time dependence of the flux. Most programs include provisions for representing leakage in transverse directions by bucklings, and some are capable of searching for values of the buckling required to establish a given k_{eff}.

Special Capabilities

Nonlinear problems can also be treated by discrete-ordinates methods. In photon transport, scattering rates are enhanced by the photon population in the final state. Such effects can be included in the discrete-ordinates equations.[40] Other nonlinearities, such as feedback mechanisms, can also be introduced in the equations. As long as nonlinearities can be treated as sources and calculated iteratively, there seems to be little difficulty in including them.

In time-dependent one-dimensional geometries, it is relatively easy to allow the time variation of the system description, for example, to allow boundaries to move, compositions to change, and so on. Thus discrete-ordinates computations coupled to Lagrangian hydrodynamic calculations are straightforward. In two dimensions, moving boundaries do not usually conform to orthogonal grids, so the situation is more difficult.

In general, most discrete-ordinates programs use the same space and angle mesh for all energies, which is inherently wasteful. It is easily possible to allow the angular resolution to be a function of energy. Most commonly, a switch to diffusion theory is allowed.[41] Similarly it is possible (because the inner iterative cycle is based only on moments of the flux) to gradually increase the number of directions used in inner iteration as the iteration progresses to save effort and possibly accelerate convergence.[42] Also possible, although less simple, is the changing of the space mesh as a function of energy. In the same category is "line deletion" or the use of local grids. At present, a fine space resolution in one region requires mesh lines that run throughout the system, again wasteful. An easily specified, automatic procedure for allowing variable grids would be highly desirable.

Most discrete-ordinates programs require cross sections to be regionwise constant, although a region may be as small as a single mesh box. Many programs allow cross sections to be multiplied by a pointwise function,[7,41] in effect, allowing a continuous density variation of cross sections.

Charged-particle transport[43] or other transport problems with an acceleration term in the transport equation can be treated with discrete-ordinates programs. For example, it is relatively easy to introduce a speed derivative into the finite-difference algorithm.

Specific Programs

Many different numerical programs with approximately the same capabilities have been written to solve the discrete-ordinates equations. To differentiate between programs, one will find it helpful to understand their genesis. Figure 8 shows the genealogy of the codes developed since the method originated at Los Alamos. Some of the early programs were written in very efficient but special machine languages, such as FLOCO.[44] These languages hid the inner workings of the program and kept those who understood the physics of particle transport separate from those who understood the numerical solution techniques. With the gradual emergence of FORTRAN as a common language, this barrier disappeared, leading not only to the proliferation of new programs but also to the local modification of programs for special applications. The programs DTF-IV[7] and ANISN,[41] which have been used at installations around the world, exist in different versions at each installation. In one dimension, an up-to-date version of either of these programs should satisfy most needs. ANISN was developed in an IBM computing-system environment, and DTF-IV evolution began on IBM machines, switched to the UNIVAC-1108, and continued on CDC-6600/7600 computers. ANISN offers certain options (e.g., shell sources and group selection of diffusion theory) not available in DTF-IV and in certain guises provides more sophisticated input and output options. DTF-IV has perhaps been seasoned longer in a wider variety of applications but, except for more sophisticated versions like 1DFX,[37] is probably somewhat less economical to use than ANISN. A selection between the two might well hinge on how easy the initial acquisition would be.

In Table 2 most of the "last-generation" one-dimensional programs of Fig. 8 are categorized in terms of options. The programs XSDRN[45] (ANISN) and GTF[46] (DTF-IV) are programs for calculating space-dependent spectra for use in forming multigroup cross sections. The speed of one-dimensional calculations has progressed to the point that few hundred-group calculations, even in the thermal range, are feasible.

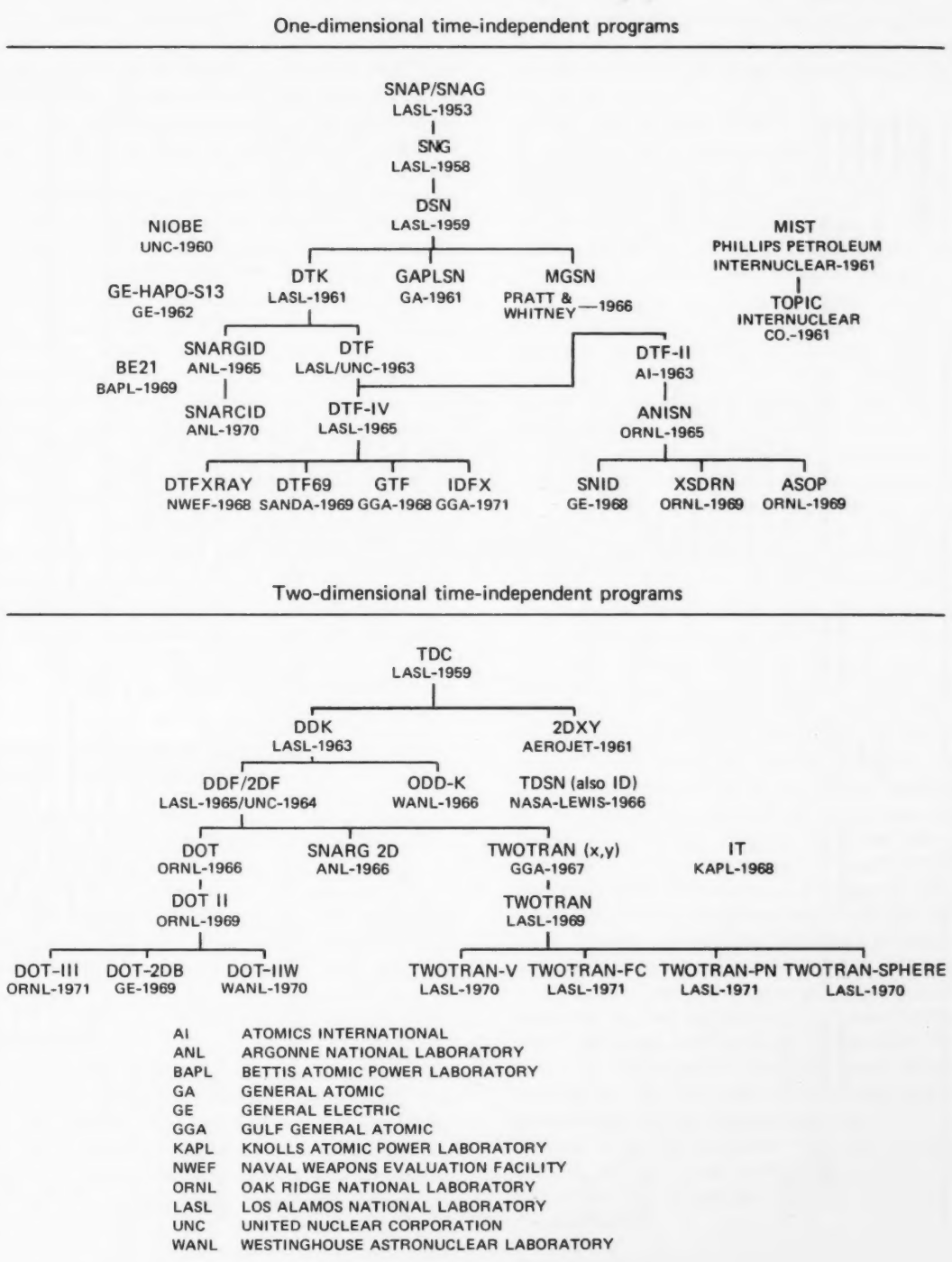

Fig. 8 Ancestry of one- and two-dimensional discrete-ordinates transport programs. Chart is reasonably complete but not exhaustive. Year of development is approximate.

Table 2 Properties of One-Dimensional Discrete-Ordinates Transport Codes*

Name	Boundary conditions†	Source options‡	Acceleration options§	Negative-flux correction Algorithm¶	Eigenvalue options**	Special features or comments	Ref.	Abstract available: Argonne code center number	Abstract available: Radiation shielding information center number
ANISN	0,1,2,3,4,5	0,3	1,3,4	2	0,1,2,3,4,5,6	Pointwise density option, option to allow out-of-core storage of enough data to permit problem execution, diffusion-theory solution optional by group; anisotropic scatter order variable by zone	41	151	82
DTF-IV	0,1,2,3	0	1,4	1	0,1,2,3,4,5	A more advanced version of this program is available from the author	8	209	42
SN1D	0,1,2,3,4,5	0,3	1,3,4,6	2	0,1,2,3,4,5,6	Same as ANISN plus free format input, group and zone bucklings options, void streaming corrections, temperature correction of thermal cross sections	48		
1DFX	0,1,2,3,5	0,1	1,2,5,6,7,8	1	0,1,2,3,4,5	Automatic use of fluxes from one problem in subsequent problems in same run; restart and output dumps	37		
DTF-69	0,1,2,3,5	0	1,4,8	1	0	Uncollided-flux calculation for plane parallel and point source, automatic minimization of cross-section storage, special features for photon transport	49		130
ASOP	See ANISN for properties		1,3,4	See ANISN for properties		Performs shield optimization by solving sequences of transport calculations and dose-constraint equations	50		126
SNARC1D (SNARG1D)	0,1,2,3	0,2	1	1	0,1,2,3,4,5	Pointwise density option, group diffusion option, fission matrix option; limited to P_1 scattering; built-in S_n constants option	51	288	

*All codes treat plane, cylinder, or sphere geometries and perform direct or adjoint calculations and, except for SNARC1D, allow general-order anisotropic scattering.

†0, vacuum; 1, reflecting; 2, periodic; 3, white; 4, albedo; and 5, input flux.

‡0, isotropic distributed; 1, anisotropic distributed; 2, linear shell source; and 3, angular shell source.

§0, none; 1, whole-system rebalance; 2, coarse-mesh rebalance; 3, pointwise rebalance; 4, one-factor upscatter rebalance; 5, multigroup-upscatter rebalance; 6, fission-source extrapolation; 7, flux extrapolation; and 8, Chebyshev acceleration.

¶0, none; 1, set-to-zero; and 2, switch to positive scheme.

**0, inhomogeneous source; 1, k_{eff}; 2, time eigenvalue; 3, radius; 4, zone thickness; 5, concentration; and 6, buckling.

A similar categorization is given for two-dimensional programs in Table 3. The choice of most versatile programs is between a version of DOT[4,7] or TWOTRAN,[7] and again depends to some extent on the ease with which the program can be acquired. Both are large programs making extensive use of peripheral storage, overlays, etc., so that local computer-system configurations are much more important than for the one-dimensional program. DOT was developed for and has been used extensively in shielding applications. By contrast, TWOTRAN originated in a thermal reactor environment and includes many convergence acceleration features. The SNARG2D program is greatly limited in capability. Its limitations illustrate the developmental trend toward general anisotropic scattering, sophisticated convergence acceleration algorithms, negative-flux corrections, and generalized source options.

Finally, in Table 4 we tabulate information for time-dependent discrete-ordinates programs.

All the programs noted in Tables 2 to 4 compactly and automatically store data for each problem to minimize fast-memory usage. This feature permits problems with any combination of input parameters to be executed, provided total storage does not exceed fast memory. As noted in the tables, others do even better, automatically utilizing peripheral storage.

USAGE GUIDE FOR DISCRETE-ORDINATES PROGRAMS

Suppose you have obtained a discrete-ordinates program from one of the code centers or direct from the author. You have made the changes necessary to implement the program on your computer and successfully executed the test problems that accompanied the program. What next? A discussion of this question and advice about the general usage of such programs follow.

Expectations

One of the first things to do is to calibrate the program in terms of cost, reliability, and accuracy. You probably already know how well your other programs do; running several problems with your discrete-ordinates program will give you a feel for relative running time. Because of the convergence insensitivity of discrete-ordinates methods to number of space intervals or number of directions, it is easy to estimate the cost of subsequent computer runs once a problem of the applicable type has been run. Execution times are almost directly proportional to the total number of space intervals or directions. Provided the addition of groups does not alter the upscattering or fission coupling, execution time is proportional to the number of groups.

Checking accuracy usually requires that the number of both intervals and directions be increased. If the arithmetic mean relations are used, doubling the number of either should reduce the error by a factor of 4. It is also possible to estimate absolute errors in this fashion. It is also necessary to check convergence precisions to see how much solutions change. A too tight convergence wastes much machine time. Once acceptable accuracy has been established, it should be maintained for all problems of a parameter survey. For example, if fuel zone widths are being varied, the same relative number of space intervals per zone should be maintained.

While becoming familiar with a discrete-ordinates program, get to know the physics of particle transport as well. The unaccelerated inner iterative process consists in accumulating the solution by adding together the flux due to no collisions, one collision, two collisions, etc. The use of any negative-flux correction recipe forces more particles from the affected cell. Such forcing may be acceptable when shielding situations are considered because it can lead to an overestimate of the escape probability, but may not be so satisfactory for predicting breeding ratios. Learn the idiosyncrasies of flux streaming in voids in curved systems which can either enhance or deplete a void central flux, depending on the flux angular distribution at the edge of the void. Learn to use the correct boundary conditions. Programs are dumb and will accept specular reflection as an outer boundary condition in cylinders or spheres. The programs will also return a solution with infinite gradient in such conditions, although a zero gradient solution is probably the one you seek. (This pathology leads to the development of the "white" or isotropic return boundary condition for cell calculations.[60]) Learn to choose angular direction sets pertinent to a problem. Some sets in (x,y) geometry have too many directions pointing in the transverse (z) direction and will underestimate leakage from such systems.

Once a general familiarity with the program is acquired, most problems can be run acceptably. There will always be exceptions. Common problems are discussed below.

Convergence

The more absorbing and leaky a group, the faster it will converge by the ratio of sources proportional to

Table 3 Properties of Two-Dimensional Discrete-Ordinates Transport Codes*

Name	Geometries†	Boundary conditions‡	Acceleration options§	Negative-flux correction¶	Source options**	Restrictions	Special features and comments	Ref.	Abstract availability: Argonne code center number	Abstract availability: Radiation shielding information center number
DOT	1,2,3	0,1,2,3,4,5	1,3,4	2,3	0,2,3		Can store angular flux	47		89
DOT-IIW	1,2,3	0,1,2,3,4, 5,7	1,3,8,9	2,3	0,2,3	Chebyshev acceleration not reliable	Can store angular flux; allows asymmetric quadrature; has zone of interest convergence option	52		
DOT-2DB	1,2,3,and 5 for diffusion theory	Same as DOT	1,7,8	2,3	0,2,3		Allows diffusion theory by groups; diffusion solution can be used as guess for transport calculation	53	459	151
TWOTRAN (x,y)††	1	0,1,4,5	1,2,5,6,9	0 or 3	0,1,2,3	Chebyshev acceleration not reliable	Because it is specialized, it is faster than TWOTRAN	54	358	129
TWOTRAN	1,2,3	0,1,2,3,4, 5,6	1,2,5,6	1	0,1,2,3,4,8		Built in S_n constants; point wise density variation; available in variable weight or first collision source or spherical harmonic versions	7	358	129
TWOTRAN sphere	4	0,1,2,3,4	1,2,5,6	2	0,1,2	Uses much fast memory	Special separable quadrature required to treat two angular derivatives	55		
SNARG2D	1,2	0,1,2,3	1,4,10	0	0	P_1 scatter only	Built in S_n constants option	56		
IT	1,2,6	0,1,2	Synthetic method	Not applicable	0	Isotropic scatter only source and k_{eff} options only	Synthetic iteration of integral equation offering groupwise diffusion-theory or simplified P_n solution; only discrete-ordinates option is in evaluation of integrals which is done stochastically to avoid ray effects	57		
DOT-III	1,2,3	0,1,2,3,4, 5,6,7,8	1,3,8,9	0,2,3	0,2,3,4,5, 6,7,8		Can store angular fluxes externally or store fluxes and moments in or out of core; allows anisotropic scatter by group and zone; allows asymmetric quadrature; outer iterations on	47		

					neutron groups only of coupled neutron-gamma problem; will store externally angular fluxes at specified radial and/or axial interior boundary; allows diffusion-theory solution by group and is flexibly dimensioned with free-form input for IBM/360	

*All codes treat direct or adjoint problems, allow eigenvalue options 1 to 5 of Table 2, and permit general-order anisotropic scattering as noted.

†1, (x,y); 2, (ρ,z) cylinder; 3, (ρ,θ) cylinder; 4, (r,θ) sphere; 5, triangular; and 6, hexagonal.

‡0, vacuum; 1, reflection; 2, periodic; 3, white; 4, input right; 5, input top; 6, input bottom; 7, albedo, and 8, input left.

§0, none; 1, whole-system rebalance; 2, coarse-mesh rebalance; 3, pointwise rebalance; 4, one factor upscatter rebalance; 5, coarse-mesh upscatter, 6; coarse-mesh eigenvalue; 7, fission-source extrapolation; 8, flux extrapolation; 9, Chebyshev; and 10, two-pass scaling for implicit boundary conditions.

¶0, none; 1, set-to-zero; 2, switch to positive scheme; and 3, use positive scheme exclusively.

**0, isotropic distributed; 1, anisotropic distributed; 2, right boundary; 3 top boundary; 4, bottom boundary; 5, left boundary; 6, interior radial boundary; 7, interior axial boundary; and 8, first collision source.

††The (x,y) program of greatest capability is that of Bettis Atomic Power Laboratory.[25]

Table 4 Time-Dependent Discrete-Ordinates Transport Programs*

Name	Geometries	Acceleration options	Type of first collision source	Initial conditions	Special features or comments	Ref.
TDA†	1D slab, cylinder and sphere	Pointwise rebalance for inner iteration, exponential predictor	Normally incident on slab face, line, or point source	Zero or complete angular flux	Implicit weighted diamond difference equations,[11] with switch to exponential difference scheme allowed; variable time step allowed, moving boundaries under development	58
TIMEX	1D slab, cylinder and sphere	Pointwise rebalance and exponential predictor–corrector	Same as above	Zero, isotropic, or complete angular flux	Explicit (noniterative) time-difference scheme, moving boundaries, time-dependent material, zone, source, fission spectrum, and pointwise density variations allowed; time-step size variable by group	59
TRANZIT	2D cylinder (ρ,z)	Coarse-mesh rebalance for inner iterations and for upscatter interations	Point on axis of cylinder	Zero	Pointwise z variation of density allowed; implicit, generalized weighted diamond scheme[11]; variable time-step size allowed	27

*All programs allow the same type of boundary conditions as their static counterparts.

†*T*ime *D*ependent *A*nisn.

the flux divided by losses proportional to the flux. In thick homogeneous zones, this ratio approaches the within-group scatter cross section divided by the total cross section. The closer the ratio to unity, the more difficult a group is to converge. In fact, in "alpha" eigenvalue searches [$\exp(\alpha t)$ time dependence], this ratio can exceed unity when α is negative and no convergence is possible.

The more local the convergence criterion, the more slowly convergence will be obtained. We have earlier noted the oscillations due to the arithmetic mean difference equations. Either these alone or in conjunction with negative-flux fixups can produce slowly damped oscillations as a function of the iterative cycle. Hence a pointwise convergence criterion may converge slowly, whereas an integral criterion may converge rapidly.

Certain acceleration algorithms can delay or prevent convergence. Simple overrelaxation can fail catastrophically if the relaxation factor is not kept within bounds. The pointwise rebalancing algorithm such as used in ANISN[36] can fail if not modified as indicated by Reed.[22] For this reason the algorithm is applied only every third iteration in ANISN. The Chebyshev acceleration in the earlier TWOTRAN (x,y) program[54] can prevent convergence.

Convergence may be prevented by a too-tight criteria. On a UNIVAC-1108, a criteria of 10^{-8} convergence will fail because the result of subtracting two nearly equal numbers may differ by this much. An outer iterative precision should be larger than an inner precision because the error in the outer cycle can be the cumulative error of all the inner cycles.

For the above reasons, most discrete-ordinates programs have provisions to limit the number of inner iterative cycles. Such provisions not only prevent endless iterations but they can also be used to save computation time. In any problem expected to run through several outer cycles, no more than 10 inner cycles should be allowed per group. As the outer cycle progresses, convergence of the inner cycles is also obtained without undue iteration in early outer cycles. When convergence is limited, most programs monitor the ultimate residual error, allowing a user to decide whether more iteration is necessary or not.

When one shifts to one program from another, it is important that he be familiar with the effectiveness of the different criteria. TWOTRAN[7] criteria are often two orders or more of magnitude more effective than those of DDF.[61] The DOT program has very useful "zone-of-interest" criteria[34] allowing selective convergence. All programs have a hierarchy of convergence precisions, and, if the user has the option, he should decrease the required precision in the general order of local to global. For instance, inner cycles should be converged most tightly, then upscatter or rebalance error for the whole system, and then eigenvalue errors.

Negative Fluxes

If the program has a fixup or uses a positive difference scheme, the only legitimate source of a negative flux is the existence of a negative source. Negative sources can arise due to the use of a truncated spherical harmonic scattering expansion. When this expansion is evaluated at the discrete directions of the problem at hand, it may be negative. Such expansion occurs frequently in first-collision source problems in which the uncollided flux is often completely collimated. Consequently its spherical harmonic moments do not decrease, and the scattering expansion for the collided flux is likely to be negative. Normally only angular fluxes are negative in such situations, and the angle-integrated flux remains positive, especially the total of collided and uncollided fluxes. Usually negative fluxes from such causes can be tolerated.

Another reason for negative fluxes is an error in input cross sections. A mispunched exponent in a scattering transfer matrix can wreak havoc with the size of a scattering source. This leads us to the most frequent source of unsatisfactory problem runs.

Input Errors

Although most discrete-ordinates programs use sophisticated loading routines to count, check, and print input data and although most programs check the input to guarantee that nonphysical or nonsensical options are not specified, input errors remain the largest cause of problem failure. Not every type of error is anticipated by the checking routines. For example, it is assumed, not always correctly, that users specify positive convergence precisions.

Certain classes of input errors can be determined from the printed output of the calculation. Advisory messages are printed by checking routines whenever cross-section sets are inconsistent in the sense that the absorption implied by the input total cross section and scattering matrix does not correspond to the independently entered absorption cross section. Balance tables are prepared during the course of the calculation and are a sensitive measure of cross-section inconsistencies. If the group sum of the outscattering rate does not equal the group sum of the inscattering rate, while at the same time group neutron balance is not in error,

then some cross section is incorrect (or there is code error). The neutron-balance monitor also provides clues. It is a global measure of the equality between losses and sources. Balance suffers when a group or groups are not converged or when, for example, a high-order anisotropic scattering source is used with a low-order discrete quadrature, which will not correctly integrate the spherical harmonic coefficients of the scattering source and will thus cause an erroneous addition to the balance equation.

Balance tables and summaries are excellent means of monitoring changes to discrete-ordinates programs. Neutron or particle balance is extremely sensitive to any error in formulation; consequently the balance tables provide excellent diagnostic aid in debugging.

APPLICATIONS

In this section several examples of the application of discrete-ordinates methods are discussed. These have been selected from problems that show a variety of different, but typical, uses of the method. Because the examples are ones with which the author has been associated, the programs used are those available to him.

Calibration of the Method: A Shielding Bench-Mark Problem

In addition to executing test problems and comparing results with those from similar programs, it is extremely useful to measure the performance of the method in real problems where exact solutions are known. Naturally it is very difficult to pose realistic problems for which exact or very accurate solutions are available. The Mathematics and Computations Division of the American Nuclear Society has compiled a book of such bench-mark solutions[62] of which the problem below not only models a realistic shielding situation but also provides a means for assessing the severity of the ray effect. The problem is a two-group (x,y) geometry model of a central source emitting in a highly absorbing medium. The geometry for the problem is shown in Fig. 9, and the two-group material cross sections including linearly anisotropic scattering are given in Table 5. The portion of the system shown is approximately 13 by 14 mean free paths in extent, and the secondaries ratio, σ_s/σ_t, is a highly absorbing 0.16 in the first group. A P_{19} evaluation of the exact-kernel solution for the infinite medium model of this problem is available for comparing solutions. This solution is applicable everywhere except near the right boundary,

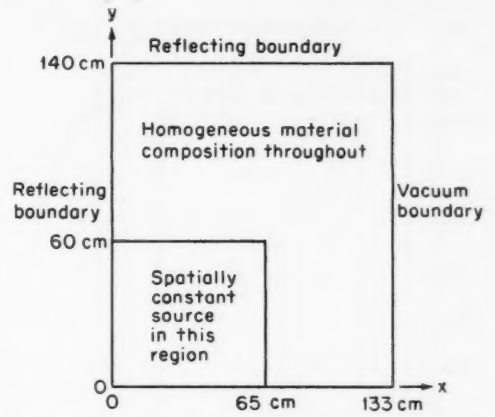

Fig. 9 Geometry and boundary conditions for bench-mark problem. Solutions are compared along the lines $y = 80$ and $y = 140$.

Table 5 Cross Sections and Sources

	Group 1	Group 2
	Isotropic, cm^{-1}	
Σ_a	0.061723	0.096027
$\nu\Sigma_f$	0.0	0.0
Σ_t	0.10108	0.108529
$\Sigma_{s0g\to g}$	0.015923	0.012502
$\Sigma_{s0g-1\to g}$	0.0	0.023434
	Linear Anisotropic, cm^{-1}	
$\Sigma_{s1g\to g}$	0.008976	0.003914
$\Sigma_{s1g-1\to g}$		0.009016
	Source Density, neutrons/cm^3	
	0.0065460	0.017701

where a vacuum boundary condition is specified. This enables the effect of the boundary to be assessed.

In Fig. 10 we compare the x variation of an S_{12} discrete-ordinates solution to this bench-mark problem to the x variation of the kernel solution along the line $y = 80$. The approximate solution is naturally lower than the infinite medium solution near the right boundary; otherwise it is close to the kernel solution but oscillates about it. These oscillations are due to the ray effect. The further from the source, the larger the distortion, as evidenced in Fig. 11, where the approximate solution is compared to the exact solution near $y = 140$ or the top edge of the system. Also shown in

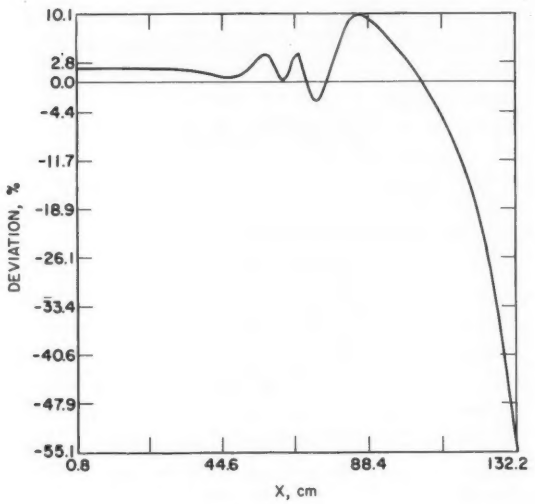

Fig. 10 Percent deviation of S_{12} solution from "exact" solution at $y = 80$ cm. Exact solution is for infinite medium so that S_{12} solution, which was computed with a vacuum right-boundary condition, is correctly smaller. Oscillations are ray effects.

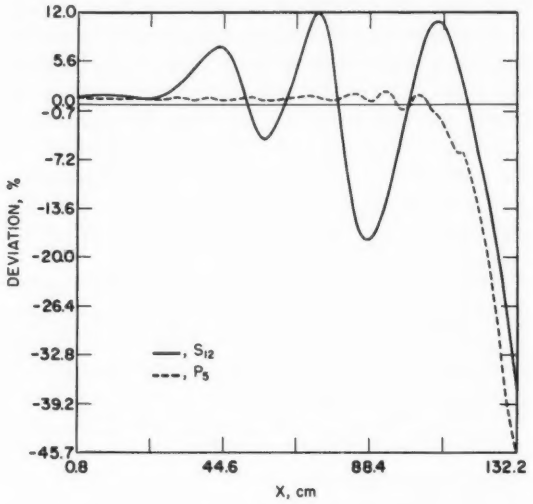

Fig. 11 Percent deviation of S_{12} and P_5 solution from "exact" solution at $y = 140$ cm. S_{12} solution shows increased ray effect, whereas P_5 solution eliminates the effect. (Oscillations in the P_5 solution are due to space differencing.)

Fig. 11 is a spherical harmonic-like solution of order P_5 obtained from a modification of the discrete-ordinates method.[11] Figure 12 shows the same two solutions compared to the kernel solution, except that a reflecting boundary condition was used with the P_5 solution. In this case the P_5 solution deviates less than 3% from the kernel solution.*

In assessing these results, one should note that the flux in group one falls by more than four orders of magnitude as a function of y from the bottom of the system to the top near $x = 0$. The flux at the top further decreases by more than a factor of 30 as a function of increasing x from $x = 0$ to the right boundary. Consequently the problem is a severe test of discrete-ordinates methods in a shielding-type situation. Except, of course, near the right boundary, the S_{12} flux solution is nowhere more than 18% in relative error, which is remarkably good agreement. Similar results were obtained for the second group.

The problem as a whole provides an excellent check-out of a multigroup, two-dimensional, anisotropic-scattering transport program.

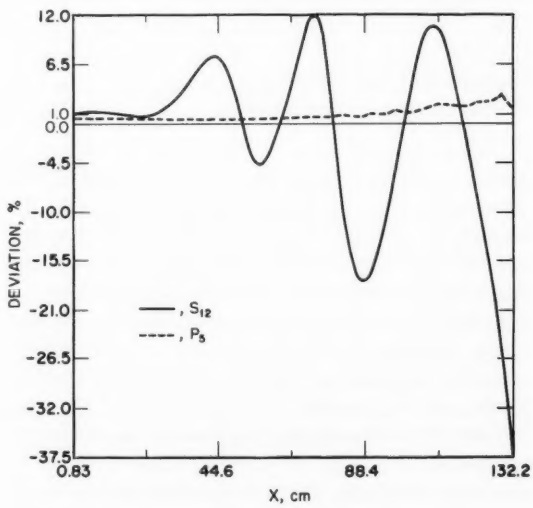

Fig. 12 Same comparison as Fig. 11 except P_5 solution was calculated with a reflecting boundary to provide a direct comparison with "exact" solution.

Reactor Core-Design Optimization

In the preliminary design of a reactor core, many parameters are at the core physicist's disposal. To optimize performance, he is likely to perform a series

*The P_5 solution was obtained from a modified version of TWOTRAN[7] using a discrete-ordinates approach.[17] Much more arithmetic and iterative effort is required for the P_5 solution.

of cheap, one-dimensional transport calculations. Typical of such a design effort are the calculations performed and described by Adler[63] for the Kinetic Intense Neutron Generator (KING) reactor.[64] In this reactor type the aqueous fuel solution is cooled after passing through the active core. For a beryllium-reflected, light-water-moderated version of this system,[64] Adler varied the fuel concentration and central-flux-trap radius in a series of one-dimensional, cylindrical geometry, 16-group k_{eff} critical zone thickness and concentration search problems. The results from these problems permitted the determination of the optimum value of the Feinberg[65] performance index, as illustrated in Fig. 13. The most complex of these calculations required no more than a few minutes computation (CDC-6600). With the advent of the CDC-7600, such parameter surveys are becoming feasible for two-dimensional calculations.

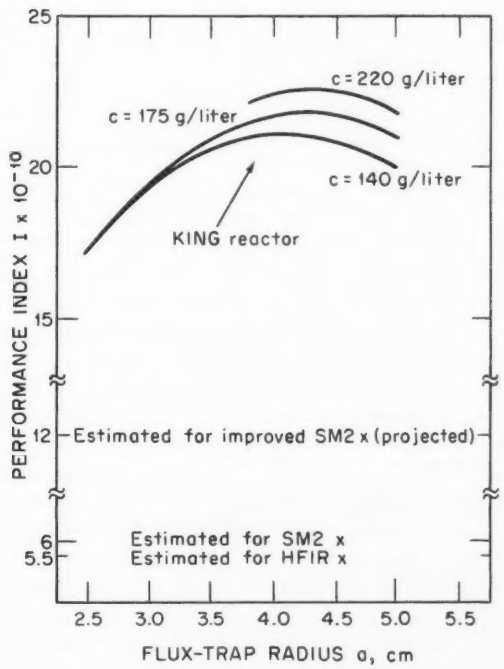
c = 220 g/liter
c = 175 g/liter
c = 140 g/liter
KING reactor
Estimated for improved SM2 x (projected)
Estimated for SM2 x
Estimated for HFIR x
PERFORMANCE INDEX I x 10⁻¹⁰
FLUX-TRAP RADIUS a, cm

Fig. 13 Variation of performance index with flux-trap radius and fuel-solution concentration.

Reactor Control-Rod Worth and Radiation Heating Calculations

For the Kinglet reactor configuration shown in Fig. 14, Malenfant[66] has recently reported results of

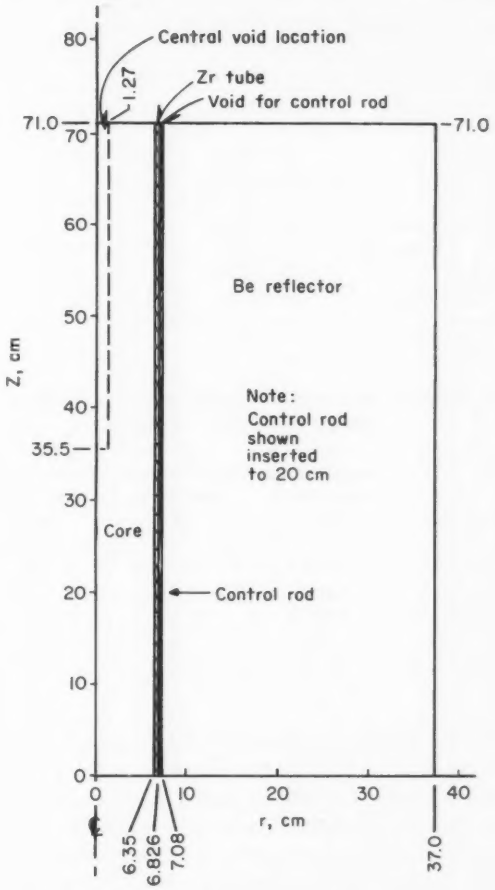

Fig. 14 Kinglet reactor calculation configuration.

one-dimensional neutronic and gamma-ray heating calculations and of two-dimensional control-rod worths. The composition of the system is shown in Table 6. The comparatively routine heating calculations produced axial average neutron and gamma heating rates for each material for 36 radial intervals. These results are summarized by zones in Table 7.

The more unusual control-rod-worth and central-void-worth calculations were performed by Malenfant using the TWOTRAN[7] program and were compared with experimental results obtained by Wimett.[66] In the experiment the control-rod worth for a 0- to 8-in. rod insertion was determined by integrating differential worths. During the experiment the system was kept near critical by varying the depth of a 1-in.-diameter central void. The calculations indicate that the cumulative measured rod worth for the full 8-in. insertion would

Table 6 Kinglet Material Description

Region	Composition atom/barn-cm	Composition g/cm³
Core	H, 0.0648	H, 0.10845
	O, 0.0351	O, 0.93239
	U, 0.000216	U, 0.084349
Zr tube	Zr, 0.0429	Zr, 6.497
Control rod	Cd, 0.0162	Cd, 3.02
	Fe, 0.0345	Fe, 3.20
Reflector	Be, 0.122	Be, 1.825

Table 7 Summary of Kinglet Radiation Heating Normalized to 10^{18} Fissions

Region	Gamma-energy deposition, MJ	Neutron-energy deposition, MJ	Total energy deposition, MJ
Core	0.494	0.421	0.915
Zr tube	0.261		0.261
Be reflector	0.825	0.250	1.075
Total	1.580	0.671	2.251

be a function of void position, due to a displacement of the flux peak from the midplane as the rod was inserted. The experimental results were not corrected for this effect. Both calculational and experimental results are summarized in Table 8. The worth of the fully inserted rod was calculated with no void and with the full void. These two results should bracket measured rod worth. Similarly the calculated worth of the 35.5-cm, 1-in.-diameter central void in the presence and absence of the control rod should bracket the experimentally measured void worth. The agreement between calculation and experiment is excellent.

In Fig. 15 the axial shift of the power density due to control-rod insertion is shown. Figure 16 shows a contour plot of the two-dimensional flux in the thermal group. Note the severe perturbation caused by the control rod and the interesting profile of the reflector flux peak. Contour plots and projective plots of fluxes are a standard option of TWOTRAN.

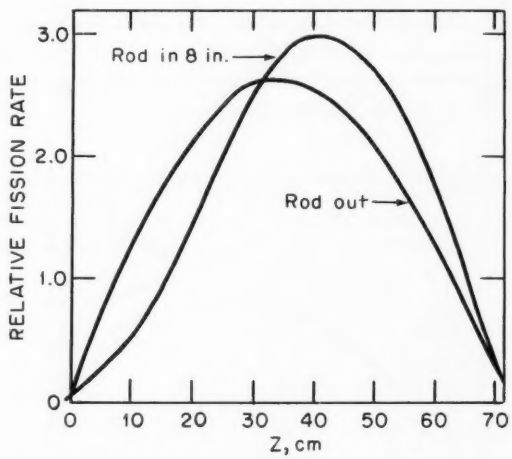

Fig. 15 Kinglet axial power-density distributions for control rod fully inserted and completely out.

Table 8 Kinglet Calculational and Experimental Results

Configuration*	Calculated k_{eff}	Calculated worth, dollars	Experimental worth, dollars
Rod out, no void	1.05397		
Rod in, 1-in.-diameter void	1.04249		
Rod in, no void	1.01866		
Rod in, full 1-in.-diameter void	1.00271		
Rod out, 1-in.-diameter void		1.44	
1-in.-diameter void with no correction for void–rod interaction			1.75
Rod in, 1-in.-diameter void		1.99	
8-in. rod insertion, no void		4.41	
8-in. rod worth with no correction for void–rod interaction			5.00
8-in. rod insertion, 1-in.-diameter void		4.97	

*1-in.-diameter void is understood to extend from top of core to z = 35.5 cm.

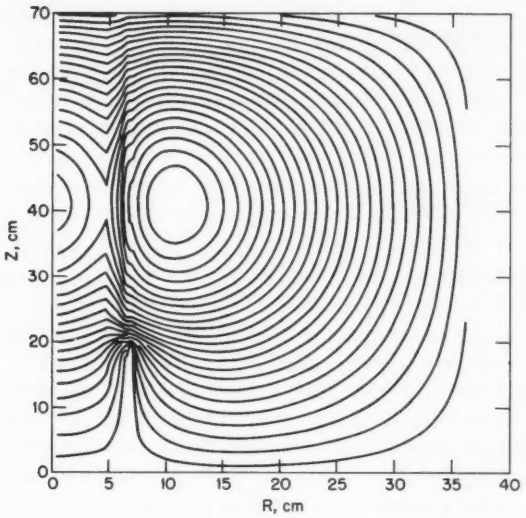

Fig. 16 Kinglet thermal-group-flux contour plot showing effect of control rod and location of reflector-flux peak. Not all contours are drawn in the vicinity of the control rod.

Pulsed-Neutron Calculations

Suppose a point burst of neutrons is produced on the axis of a finite cylinder. What is the space–time evolution of the flux? Such questions are answered by time-dependent discrete-ordinates calculations, an example of which is shown in Fig. 17. Here the time dependence of the leakage and absorption rates from a discrete-ordinates calculation is compared with Monte Carlo results. In this problem a point-burst source was located at $\rho = 0$, $z = 1.9$ inside a cylinder of 1-cm radius and 2-cm height in a medium with $\sigma_s/\sigma_t = 0.2$. Inflections in the curves of the figure are visible at times associated with the uncollided wave front reaching the bottom surface, reaching the right surface, and leaving the system. A more complete description of this calculation is given in the manual describing the TRANZIT program[27] used to perform the discrete-ordinates calculation. A similar calculational result obtained with this program is shown in Fig. 18, where contours of energy deposition in an exponential atmosphere are plotted for the time 1 to 2 sec after a point burst of neutrons at a height of 26 km at $t = 0$.

Shielding Survey Calculations

As part of a design effort, it was desired to calculate the flux of photons from a ^{60}Co source and other gamma sources located at one end of a cylindri-

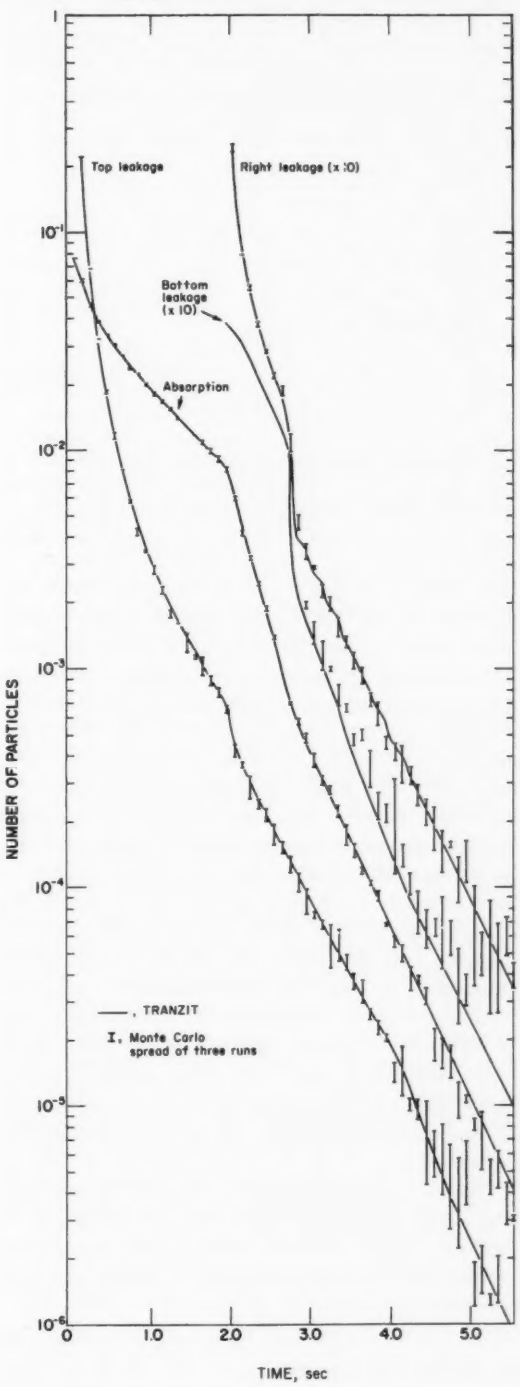

Fig. 17 Time variation of leakage and absorption rates after point burst of particles on cylinder axis.

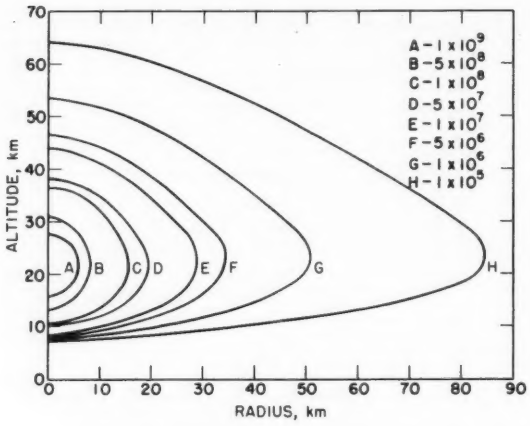

Fig. 18 Energy-deposition contours for time interval 1 to 2 sec after point air burst of particles. Shape of contours reflects the effects of varying air density.

cal container immersed in water. In particular, the objective of the calculations was to shield a small region inside the cylinder (housing electronic gear) subject to strict weight and size limitations. Figure 19 shows a picture of one such problem in the sequence as it is drawn by the computer output of the TWOTRAN program.[7] The location of the source and detector regions has been added to the figure. An iron barrier is interposed between the source and detector, and a uranium can surrounds the detector. Water surrounds the whole assembly, and a white boundary condition is used to ensure an overestimate of the reflected flux from the water. This problem was run with 28 radial intervals and 88 axial intervals in a three-group representation. An S_8 quadrature was used. This particular problem required about 2 min (CDC-7600) of computer time. Although this is very cheap, many such calculations were run since various barriers, encapsulating configurations, and source spectra were tried. To save calculational effort, the following steps were taken:

1. Only one calculation in a particular sequence was computed using anisotropic scattering. As it happened in this problem, isotropic scattering gave an overestimate (because of reflection from the water) of the detector flux.

2. The water end caps were included in only one problem in each sequence.

3. The positive difference scheme version of TWOTRAN was used to ensure smooth solutions and rapid convergence. As noted previously, this scheme tends to overestimate the flux reaching the detector, which is a safe error.

4. Space meshes and group structures were kept crude but consistent. Thus relative comparisons could be made without having to obtain absolute accuracy.

SUMMARY

The review has covered the theory, capabilities, limitations, and applications of discrete-ordinates methods and programs for the solution of the transport equation. In general terms, the method is more expensive but is a more accurate approximation than diffusion theory. The method is less geometrically versatile than Monte Carlo techniques but is usually more economical. For two- or three-dimensional geometries, and especially for time-dependent situations, a Monte Carlo estimate of localized or integral

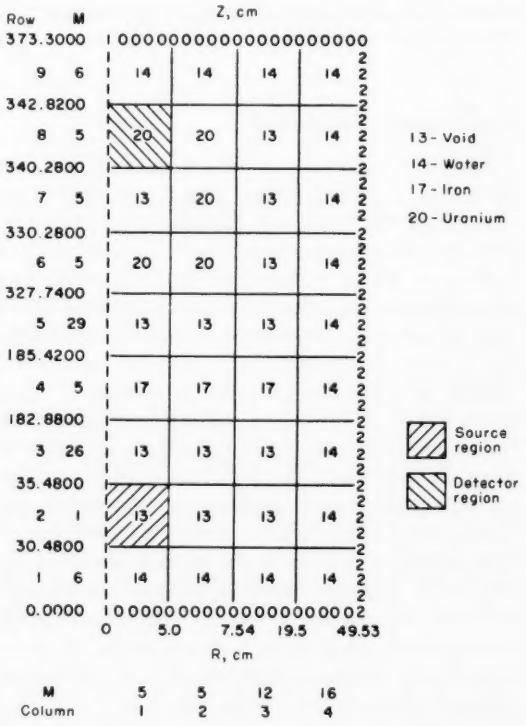

Fig. 19 Geometry for shielding survey calculations. Picture is a redrawn copy of computer output from TWOTRAN with the border of the figure indicating boundary conditions: 0, vacuum; 1, reflective; and 2, white. The number of uniform fine-mesh intervals per coarse-mesh interval is shown in the left column and bottom row.

quantities may be less expensive than a discrete-ordinates calculation, but, whenever the detailed solution is required in every volume element of the system (e.g., power distribution, gamma heating rate, neutron-energy deposition, and angular flux), the discrete-ordinates method is cheaper. It is also easier to perform parameter surveys with discrete-ordinates methods than with Monte Carlo programs. The ease with which both direct and adjoint solutions are obtained has led to the development of many programs to perform perturbation calculations with the output of discrete-ordinates programs.

In discussing limitations and usage of discrete-ordinates methods, our intention has been to create awareness of the pitfalls rather than to inspire mistrust. Used with care and intelligence, the method has been, and will continue to be, an extremely useful tool.

REFERENCES

1. B. G. Carlson, Solution of the Transport Equation by S_n Approximations, USAEC Report LA-1599, Los Alamos Scientific Laboratory, 1953.
2. B. G. Carlson and G. I. Bell, Solution of the Transport Equation by the S_n Method, in *Proceedings of the Second United Nations International Conference on the Peaceful Uses of Atomic Energy, Geneva, 1958,* Vol. 16, p. 535, United Nations, New York, 1958.
3. G. I. Bell and S. Glasstone, *Nuclear Reactor Theory*, p. 11, Van Nostrand Reinhold Company, New York, 1970.
4. G. I. Bell and S. Glasstone, *Nuclear Reactor Theory*, p. 31, Van Nostrand Reinhold Company, New York, 1970.
5. S. Chandrasekhar, *Radiative Transfer*, Oxford University Press, Inc., Fair Lawn, N. J., 1950.
6. B. G. Carlson and K. D. Lathrop, in *Computing Methods in Reactor Physics*, H. Greenspan, C. N. Kelber, and D. Okrent (Eds.), Gordon and Breach, Science Publishers, Inc., New York, 1968.
7. K. D. Lathrop and F. W. Brinkley, Theory and Use of the General-Geometry TWOTRAN Program, USAEC Report LA-4432, Los Alamos Scientific Laboratory, 1970.
8. K. D. Lathrop, DTF-IV, a FORTRAN-IV Program for Solving the Multigroup Transport Equation with Anisotropic Scattering, USAEC Report LA-3373, Los Alamos Scientific Laboratory, 1965.
9. R. Protsik, Users Manual for SN2D, A Two-Dimensional Multigroup Discrete Ordinates Transport/Diffusion Code with Anisotropic Scattering, Report NEDE-13747, General Electric Company, 1971.
10. W. H. Reed, Triangular Mesh Difference Schemes for the Transport Equation, USAEC Report LA-4769, Los Alamos Scientific Laboratory, 1971.
11. K. D. Lathrop, *J. Comput. Phys.*, **4**: 475 (1969).
12. K. D. Lathrop, TWOTRAN, A FORTRAN Program for Two Dimensional Transport, USAEC Report GA-8747 Gulf General Atomic, 1968.
13. B. G. Carlson and K. D. Lathrop, TWOTRAN, A FORTRAN Program for Two Dimensional Transport, USAEC Report GA-8747, Gulf General Atomic, 1968.
14. N. K. Madsen, Convergence of the Weighted Diamond Difference Approximations to the Discrete Ordinates Equations, in Proceedings of a Conference on New Developments in Reactor Mathematics and Applications, USAEC Report CONF-710302(Vol. 2), pp. 565–576, 1971.
15. William H. Reed, New Difference Schemes for the Neutron Transport Equation, *Nucl. Sci. Eng.*, **46**(2): 309 (1971).
16. K. D. Lathrop and N. S. Demuth, Biorthogonal Angular Polynomial Expansion of the Two-Dimensional Transport Equation, *Nucl. Sci. Eng.*, **32**(1): 120 (1968).
17. K. D. Lathrop, Remedies for Ray Effects, *Nucl. Sci. Eng.*, **45**(3): 255 (1971).
18. E. M. Gelbard, Recent Research, a talk given at the Los Alamos Transport Conference, January 1971; also, Arrangement of Ordinates in Deep-Penetration Cylindrical and X-Y S_n Calculations, in Conference on New Developments in Reactor Mathematics and Applications, USAEC Report CONF-710302, p. 617, 1971.
19. R. Froehlich, A Theoretical Foundation for Coarse Mesh Variational Techniques, USAEC Report GA-7870, Gulf General Atomic, 1967.
20. B. E. Clancy and I. J. Donnelly, Outer Iteration Scaling in Neutron Transport Codes, *Nucl. Sci. Eng.*, **39**(3): 398 (1970).
21. S. Nakamura, A Variational Rebalancing Method for Linear Iterative Convergence Schemes of Neutron Diffusion and Transport Equations, *Nucl. Sci. Eng.*, **39**(2): 278 (1970).
22. W. H. Reed, The Effectiveness of Acceleration Techniques for Iterative Methods in Transport Theory, *Nucl. Sci. Eng.*, **45**(3): 245 (1971).
23. E. M. Gelbard and L. A. Hageman, The Synthetic Method as Applied to the S_n Equations, *Nucl. Sci. Eng.*, **37**(2): 288 (1969).
24. M. R. Wagner, Application of the Block Inversion Technique to Multidimensional Reactor Calculations, in Conference on The Effective Use of Computers in the Nuclear Industry, USAEC Report CONF-690401, pp. 211–233, 1969.
25. C. J. Pfeifer, S_n Programming Techniques, in Conference on New Developments in Reactor Mathematics and Applications, USAEC Report CONF-710302, p. 557, 1971.
26. R. J. Rodgers and F. R. Mynatt, Differential Neutron and Gamma Current Albedos for Concrete, in Neutron Physics Division Annual Report, USAEC Report ORNL-4280, p. 93, October 1968. The applicable equation is given on p. 316 of *Linear Transport Theory* by K. M. Case and P. F. Zweifel, Addison-Wesley Publishing Company, Inc., Reading, Mass., 1967.
27. K. D. Lathrop, R. E. Anderson, and F. W. Brinkley, TRANZIT: A Program for Multigroup Time-Dependent Transport in (ρ,z) Cylindrical Geometry, USAEC Report LA-4575, Los Alamos Scientific Laboratory, 1965.
28. B. G. Carlson and C. E. Lee, Mechanical Quadrature and the Transport Equation, USAEC Report LAMS-2573, Los Alamos Scientific Laboratory, 1961.
29. K. D. Lathrop and B. G. Carlson, Discrete Ordinates Angular Quadrature of the Neutron Transport Equation,

USAEC Report LA-3186, Los Alamos Scientific Laboratory, 1965.

30. B. G. Carlson, Transport Theory: Discrete Ordinates Quadrature over the Unit Sphere, USAEC Report LA-4554. Los Alamos Scientific Laboratory, 1970.
31. B. G. Carlson, Tables of Equal Weight Quadrature EQ_n over the Unit Sphere, USAEC Report LA-4734, Los Alamos Scientific Laboratory, 1971.
32. R. K. Disney, J. Jedruch, R. G. Soltesz, R. S. Kaiser, and S. K. Zeigler, Report WANL-TME-3704, Westinghouse Electric Corp., Astronuclear Laboratory, 1971.
33. R. J. Cerbone and K. D. Lathrop, S_n Calculation of Highly Forward Peaked Neutron Angular Fluxes Using Asymmetrical Quadrature Sets, *Nucl. Sci. Eng.*, **35**(1): 139 (1969).
34. F. R. Mynatt, F. J. Muckenthaler, and P. N. Stevens, Development of Two-Dimensional Discrete Ordinates Transport Theory for Radiation Shielding, USAEC Report CTC-INF-952, Union Carbide Corporation, Computing Technology Center, 1969.
35. K. D. Lathrop and F. W. Brinkley, Theory and Use of the General-Geometry TWOTRAN Program, USAEC Report LA-4432, Los Alamos Scientific Laboratory, p. 10, 1970.
36. W. W. Engle, Jr., and F. R. Mynatt, A Comparison of Two Methods of Inner Iteration Convergence Acceleration in Discrete Ordinates Codes, *Trans. Amer. Nucl. Soc.*, **11**(1): 193 (1968).
37. R. Archibald, K. D. Lathrop, and D. Mathews, 1DFX: A Revised Version of the 1DF (DTF-IV) S_n Transport Theory Code, Report Gulf GA-B-10820, Gulf General Atomic, 1971.
38. L. A. Hageman, The Chebyshev Polynomial Method of Iteration, USAEC Report WAPD-TM-537, Bettis Atomic Power Laboratory, 1967.
39. C. E. Barber. A FORTRAN-IV Two-Dimensional Discrete Angular Segmentation Transport Program, Report NASA-TN-D-3573, National Aeronautics and Space Administration, 1966.
40. K. D. Lathrop, Discrete Ordinates Treatment of Induced Scattering, USAEC Report LA-4646-MS, Los Alamos Scientific Laboratory, 1971.
41. W. W. Engle, Jr., A Users Manual for ANISN, A One Dimensional Discrete Ordinates Transport Code with Anisotropic Scattering, USAEC Report K-1693, Union Carbide Corporation, 1967.
42. R. E. Sullivan, L. K. Albers, and D. Yu, Reduction of Machine Time in Discrete Ordinates Calculations, in Conference on The Effective Use of Computers in the Nuclear Industry, USAEC Report CONF-690401, p. 234. 1969.
43. D. R. Bartine, R. G. Alsmiller, Jr., F. R. Mynatt, W. W. Engle, Jr., and J. Barish, Low-Energy Electron Transport with the Method of Discrete Ordinates, USAEC Reports ORNL-TM-3318 and ORNL-TM-3438, Oak Ridge National Laboratory, 1971.
44. B. G. Carlson, C. S. Kazek, Jr., and C. E. Lee, FLOCO Manual, USAEC Report LAMS-2339, Los Alamos Scientific Laboratory, 1959.
45. N. M. Green and C. W. Craven, Jr., XSDRN: A Discrete Ordinates Spectral Averaging Code, USAEC Report ORNL-TM-2500, Oak Ridge National Laboratory, 1969.
46. R. J. Archibald and K. D. Lathrop, GTF: A Space Dependent Thermal Spectrum Code, USAEC Report GA-8775, Gulf General Atomic, 1968.
47. F. R. Mynatt, A User's Manual for DOT, Report K-1694, Union Carbide Corporation, 1967.
48. R. Protsik, S. C. Crick, and J. M. Kelley, SN1D: A One-Dimensional Discrete Ordinates Transport Code with General Anisotropic Scattering, Report GEAO-0064(Rev. 1), General Electric Company, 1970.
49. J. H. Renken and K. G. Adams, An Improved Capability for Solution of Photon Transport Problems by the Method of Discrete Ordinates, USAEC Report SC-RR-69-739, Sandia Laboratories, 1969.
50. W. W. Engle, Jr., A Users Manual for ASOP, ANISN Shield Optimization Program, USAEC Report CTC-INF-941, Union Carbide Corporation, Computing Technology Center, 1969.
51. G. J. Duffy, H. Greenspan, S. D. Sparck, J. V. Zapatka, and M. K. Butler, SNARG-1D, A One-Dimensional Discrete-Ordinate, Transport-Theory Program for the DCD-3600, USAEC Report ANL-7221, Argonne National Laboratory, 1969. See also USAEC Report ANL-7717, 1971.
52. R. G. Soltesz and R. K. Disney, User's Manual for the DOT-11W Discrete Ordinates Transport Computer Code, USAEC Report WANL-TME-1982, Westinghouse Electric Corp., Astronuclear Laboratory, 1969.
53. R. Protsik and E. G. Leff, Users Manual for DOT2DB: A Two-Dimensional Multigroup Discrete Ordinates Transport/Diffusion Code with Anisotropic Scattering, USAEC Report GEAP-13537, General Electric Company, 1969.
54. K. D. Lathrop, User's Guide for the TWOTRAN (x,y) Program, USAEC Report LA-4058, Los Alamos Scientific Laboratory, 1969.
55. K. D. Lathrop and F. W. Brinkley, TWOTRAN SPHERE: A FORTRAN Program to Solve the Multigroup Transport Equation in Two-Dimensional Spherical Geometry, USAEC Report LA-4567, Los Alamos Scientific Laboratory, 1970.
56. G. J. Duffy, H. Greenspan, S. D. Sparck, J. V. Zapatka, and M. K. Butler, SNARG-2D: A Two-Dimensional Discrete Ordinates Transport Theory Program for the CDC-3600, USAEC Report ANL-7426, Argonne National Laboratory, 1968.
57. J. P. Friedman and B. W. Crawford, A Two-Dimensional Transport Theory Program in a Modular System Environment, in Conference on the Effective Use of Computers in the Nuclear Industry, USAEC Report CONF-690401, p. 248, 1969.
58. S. A. Dupree, H. A. Sandmeier, G. E. Hansen, W. W. Engle, Jr., and F. R. Mynatt, Time-Dependent Neutron and Photon Transport Calculations Using the Method of Discrete Ordinates, USAEC Report LA-4557, Los Alamos Scientific Laboratory, 1971.
59. W. H. Reed, TIMEX: A Time Dependent Explicit Discrete Ordinates Program for Solution of the Multigroup Transport Equation, Report LA-4800, Los Alamos Scientific Laboratory, to be published.
60. H. C. Honeck, The Calculation of the Thermal Utilization and Disadvantage Factor in Uranium/Water Lattices, *Nucl. Sci. Eng.*, **18**(1): 49 (1964).

61. M. Shapiro, 2DF, Abstract No. 173 in Argonne Code Center Compilation of Program Abstracts, USAEC Report ANL-7411, Argonne National Laboratory, 1971.
62. Argonne Code Center: Benchmark Problem Book, USAEC Report ANL-7416, Argonne National Laboratory, 1968.
63. F. T. Adler and K. D. Lathrop, Flux Optimization for a KING Reactor, *Trans. Amer. Nucl. Soc.*, **14**(2): 717 (1971).
64. L. D. P. King and T. F. Wimett, The KING Reactor Concept: Its Dynamic Test and Safety Evaluation, *Trans. Amer. Nucl. Soc.*, **14**(2): 716 (1971).
65. S. M. Feinberg, High-Flux Stationary Research Reactors and Their Outlook, I. V. Kurchatov Institute of Atomic Energy, Moscow, 1968, USAEC Report LA-4399-TR, translated by Helen J. Dahlby from Report IAE-1693.
66. R. E. Malenfant, Neutronic and Radiation Heating Calculations for Kinglet, Memorandum N-2-8473, Los Alamos Scientific Laboratory, 1971.

IAEA SYMPOSIUM ON NEUTRON MONITORING FOR RADIATION-PROTECTION PURPOSES

Vienna, Austria, Dec. 11–15, 1972

This symposium will be held to facilitate discussions on current problems among radiation-protection specialists with particular emphasis on detectors, instruments, and techniques for neutron monitoring and accuracy in dose estimating. Major topics to be covered are:

- General considerations
- Instruments and techniques
- Interpretation of measurements
- Standardization and calibration

Nominations for participation will be accepted only if presented by the government of a Member State of the International Atomic Energy Agency or by an international organization invited to participate.

For complete information about participation, submission of papers, etc., persons in the United States should write

Mr. John H. Kane
Office of Information Services
U. S. Atomic Energy Commission
Washington, D. C. 20545

and persons outside the United States should write

Miss C. H. de Mol van Otterloo
Administrative Secretary
Division of External Relations
International Atomic Energy Agency
Kärntner Ring 11
P. O. Box 590, A-1011
Vienna, Austria

Development of Materials and Systems for the Molten-Salt Reactor Concept

By H. G. MacPherson*

Abstract: *Interest in molten-salt-fueled reactors stems largely from the ease and relatively low cost of purifying and reconstituting the fuel. Molten-salt thermal breeder reactors—graphite moderated and with salt constituents that absorb few neutrons—will have low enough inventories and doubling times to greatly ease the future requirements for uranium mining and for enrichment facilities.*

Among the reactor designs that have been studied, the favorite is a single-fluid breeder fueled with a mixture of ^{7}LiF, BeF_2, ThF_4, and $^{233}UF_4$. The chemical characteristics of such salts and the behavior of fission products in them are quite well understood from many years of research and from the operation of the Molten Salt Reactor Experiment (MSRE). A number of processes for removing the soluble fission products (and protactinium) from the salt have been explored in recent years. Of these, reductive extraction into bismuth is being developed most vigorously. A bubble generator and centrifugal gas stripper are being developed to ensure the speedy removal of the noble-gas fission products, which are only sparingly soluble.

Unresolved problems receiving current attention include the control of tritium arising from neutron reactions with lithium, surface fissures in Hastelloy N probably arising from fission-product attack, the retention of the radiation resistance of Hastelloy N to high temperatures, and the development of a steam generator.

The use of a molten salt as the fuel material has been proposed for many different reactor types, much as UO_2 is used as the fuel for a variety of different reactors. Conceptual designs have been prepared for ship and aircraft propulsion systems as well as for fast breeders and thermal reactors for central-station power generation. Nearly all of the recent development work has been directed toward a graphite-moderated thermal breeder.

*Department of Nuclear Engineering, University of Tennessee, Knoxville, Tenn. 37916.

The principal attraction of a molten-salt fuel is the ease of fuel preparation and reprocessing. This ease leads with certainty toward a low fuel-cycle cost. Furthermore, the possibility of rapid processing, including the rapid removal of ^{135}Xe, makes the molten-salt system the only one in which breeding with a reasonably short doubling time appears to be economically possible in a thermal reactor.

The fuel salt for these thermal reactors is a mixture of ^{7}LiF and BeF_2 in a mole ratio somewhat greater than 2:1, with the addition of as much UF_4, PuF_3, or ThF_4 as is required to make the reactor critical or to provide the desired amount of fertile material. For example, the composition of the salt used in the most recent conceptual design is ^{7}LiF–BeF_2–ThF_4–UF_4 in the mole ratio 71.7:16:12:0.3. It has a melting point of about 500°C (930°F) and a vapor pressure of less than 0.1 mm Hg at a mean operating temperature of 620°C (1150°F). This salt has about 3.3 times the density of water, about 10 times the viscosity of water (11 cP at 620°C), and a thermal conductivity and heat capacity per unit volume comparable to water. These properties are favorable for heat transport; particularly important in this respect is the high heat capacity per unit volume which allows large amounts of heat to be transported with moderate salt flow rates.

The high melting temperature is an obvious limitation, requiring careful design to keep the system hot. Concern is also frequently expressed about corrosion of the system, containment of the radioactive liquids and gases, reliability of the equipment, and maintenance of the highly radioactive system. Operation of the 7.5-MW Molten Salt Reactor Experiment (MSRE) from early 1965 to December 1969 provided favorable first-order answers to these questions. MSRE operation

also called attention to two new problems. One problem is the necessity for controlling the tritium that is produced in large amounts from the lithium in the fuel. The other problem is a moderate grain-boundary attack on the nickel-based container alloy that appears to be associated with the presence of some fission product, probably tellurium.

The present development work is directed toward providing the additional technology required for building the much larger and longer lasting reactors needed for power production. In addition to the tritium and grain-boundary problems, particular current attention is being devoted to the development of chemical processing methods, improvement of the radiation resistance of the nickel-based alloy, and the gaining of confidence in the handling of the sodium fluoroborate salt that has been proposed for use as the intermediate coolant to transfer heat from the fuel salt to the steam generator.

An extensive review of molten-salt reactor technology at Oak Ridge National Laboratory (ORNL) through mid-1969 is given in a series of articles in the February 1970 issue of *Nuclear Applications and Technology*.[1-8] Included in this series is a discussion of the rationale for the development of molten-salt reactors, showing that they, like the Liquid-Metal-Cooled Fast Breeder Reactor (LMFBR), have the capability of solving our long-range energy supply problem.[1] Further progress in ORNL's development program and the current reference design of a molten-salt breeder are described in Ref. 9. Other relatively recent articles giving a broad view of molten-salt reactors and citing their virtues are those listed in Refs. 10 to 14.

The sections that follow give a somewhat historical account of the major reactor configurations and design concepts that have been proposed using molten-salt fuels, followed by descriptions of the recent progress and the current status of important areas of molten-salt reactor technology.

REACTOR CONFIGURATIONS AND CONCEPTS

Since the start of the Molten Salt Reactor Program, conceptual designs, revised frequently, have guided the development program. The first designs were for aircraft propulsion, taking advantage of the high-temperature possibilities.[15] At the start of the civilian power program, homogeneous reactors were considered, the only moderation being that provided by the fluorine and beryllium in the salt.[16] With such reactors, breeding was not quite possible, and only converter reactors were considered. By late 1958 enough experimental information about graphite in contact with fluoride fuel salt in a radiation environment was available to shift the design effort to graphite moderation. It was quickly found that the optimum performance usually occurred with 10 to 20% of the core volume occupied by molten-salt fuel and the remainder by graphite. At that time the most feasible reactor still seemed to be a converter, partly because complete chemical processing procedures were unknown but also because it was not easy to find plausible designs for two-region reactors.

For breeding, the two-region reactor seemed necessary to prevent leakage from consuming too many neutrons. It was realized, though, that, if the reactor were made big enough, say a 20-ft-diameter right cylinder, the leakage could be kept to about 0.05 neutron per neutron absorbed in fissile atoms, a value low enough to allow breeding if rapid processing schemes could be developed.[17] Such a large reactor seemed impractical because, with its large inventory, it would be suitable only for power levels of 1000 MW or greater, a size unheard of at that time. There was a tendency to discount the value of reflector regions because they would have to be cooled with fuel salt and would generate some power and some neutrons. In later years all these prejudices were overcome.

In the early 1960s the major conceptual design effort shifted to two-region two-fluid breeder reactors, with the ^{233}U fuel in one fluid and the fertile thorium in the other fluid. Reasonable designs were generated in which the fuel flowed through the core in graphite pipes and the fertile salt not only surrounded the core as a blanket but also permeated the core, bathing the outside of the fuel tubes and flowing through channels in the graphite moderator.[18] With uranium and thorium in separate salt streams, the processing steps could be greatly simplified. A useful breeder could be designed using only the fluoride-volatility process, or that plus vacuum distillation to recover the carrier salt from the rare-earth fission products. An improvement on the performance of this two-fluid reactor was indicated when it was discovered that protactinium could be selectively removed from the blanket salt by reductive extraction into a bismuth carrier.

A continuing concern with the reliability of the graphite plumbing in the two-fluid core led to more refined calculations of the possibilities of a single-fluid breeder. These calculations have evolved into the presently favored three-region single-fluid breeder.[19] The salt that serves as the single fluid contains both

thorium and enriched uranium, in a ratio of about 50:1. A central core zone containing about 13 vol.% salt is surrounded by a "blanket" region with 37 vol.% salt. With less graphite, the blanket region is undermoderated, enhancing the resonance absorptions in thorium relative to the fission absorptions in uranium. This reduces the leakage, and a 2-in.-thick salt annulus at the outside edge of the blanket aids in this function. The third region is a graphite reflector about 75 cm thick which is cooled with the minimum amount of salt, about 1 vol.%. The reflector not only saves neutrons but it also reduces the fast flux at the reactor vessel. Concurrent improvements in chemical processing, described in a later section, made the breeding performance of this single-fluid system attractive.

Capital-cost estimates for molten-salt reactors have been made a number of times, and they usually fall within the range of such costs for light-water reactors. The significance of the exact number is usually clouded by the inclusion of a rather large contingency, the magnitude of which depends on the confidence of the estimator. The capital cost estimated for a 1000-MW(e) three-region single-fluid breeder of the type described above was $203 million, based on January 1970 construction costs. The number for a light-water reactor, on the same basis, was estimated at $201 million. The direct cost of the molten-salt system is about $12,000,000 lower for the turbine plant equipment because of the higher temperature steam, but this advantage is used up in such items as an auxiliary boiler ($3,000,000), maintenance equipment ($4,500,000), and extra allowance for contingencies ($6,000,000). The power production cost was estimated at about 5.5 mills/kWh.

Along the way to this latest design, a number of interesting modifications have been suggested. A simple one that is surely worthy of future experimentation is a two-fluid two-region reactor with the regions separated by a metal membrane.[20] In this case the core salt would contain both uranium and thorium to allow some breeding in the core, but leakage from the core would be usefully absorbed in the blanket salt, which would contain thorium but no uranium. Such a reactor could have less leakage and a lower inventory than the single-fluid reactor, provided the metal membrane can be made sufficiently thin.

A much more inventive modification involving lead cooling was suggested by Bettis.[21] In this reactor the fuel salt is cooled by direct contact with a falling shower of lead droplets, and their momentum transfer is used to provide circulation of the fuel, thereby replacing the fuel pumps. A big advantage would be the reduced inventory of fuel achieved by the elimination of the external heat-exchanger circuits. This would be particularly advantageous for a fast molten-salt reactor, which would use a chloride salt for the single fuel and fertile stream. Only a small amount of development work has been done on lead-cooled systems, but such a system is being considered seriously in the United Kingdom for fast reactor use.[22]

Taube,[23] first in Poland and now in Switzerland, has proposed fast molten-salt reactors using either aluminum chloride or mercury as a boiling coolant, in direct contact with the fuel. He has outlined the long list of development problems that must be solved to make such a system practical but sees great advantages in the compactness of the reactor and in its large negative temperature coefficient of reactivity. Another variant of the family of molten-salt reactors, the epithermal MOSEL concept, has been studied at Jülich.[24] In connection with this reactor, the pros and cons of internal vs. external cooling are discussed by Gat.[25]

The next reactor proposed for construction by ORNL is a breeder experiment, the Molten Salt Breeder Experiment (MSBE).[26] The purpose of the MSBE would be to serve as a true pilot plant for a large breeder reactor. It must be capable of operation at power densities and fast-neutron fluxes at least as high as would be encountered in a power breeder and would incorporate facilities of continuous chemical processing. The components should be of such a size that only modest scaling-up would be required for the power breeder. For economy, the size should be as small as possible and still meet these requirements. This minimum size is determined primarily by the requirement for high power density and the desire to keep the neutron-energy spectrum and fuel concentrations reasonably close to those for the power breeder. A reactor of about 150 MW(t) is planned.

Although it was desired that the MSBE have a breeding ratio approaching 1.00, the actual demonstration of breeding does not seem as important as high power density from a technical point of view. The problem of achieving a breeding ratio above 1.00, still maintaining the neutron spectrum soft enough to be representative of the ultimate breeder, is that it would require a rather large low-leakage core. With the high-power-density criterion, this would mean a reactor of perhaps 250 MW(t) and extra cost. It should be possible to obtain an accurate check on the ultimate breeding performance of a large reactor by comparison of the calculated and actual performance of a MSBE whose conversion ratio is in the range 0.9 to 1.0. So far

the reactor-physics calculations seem to be in very good shape, as judged in part by the accuracy with which the critical concentrations of fuel were calculated for the two loadings of the MSRE. The greatest uncertainty in the calculation of breeding is in the value of eta for ^{233}U; and the value used has been validated by measurements of alpha for ^{233}U in the MSRE.[27]

Recently ORNL has carried out a design study of a 300-MW(e) "prototype" reactor.[28] The principal criterion for this reactor was that it should require as little development effort as possible and still be economically attractive as far as running costs are concerned. The purpose of the reactor would be to demonstrate the feasibility and delineate the problems of construction of a large molten-salt-reactor power station. The minimum development requirement led to the decision that it be a converter, without sophisticated chemical processing, rather than a breeder. Also, the core size was made large, about 6.4 m in diameter, with a correspondingly low power density, so that the graphite could be expected to last for the lifetime of the reactor. No attempt would be made to seal the graphite pores to keep out xenon, and the tritium problem would be handled by using a nitrite–nitrate salt in a third loop between the primary-coolant salt and the steam system.

Recent reactor-physics and fuel-cycle studies have examined the effects of increasing the core size for larger reactors to reduce the graphite replacement problem.[29] For a 1000-MW(e) breeder, the principal effect of increasing the core diameter to 8.7 m (providing a 30-year graphite life) was to increase the fissile inventory by 50%, and the fuel-cycle cost by 0.2 mill/kWh. Other such studies have examined the use of plutonium as the startup fuel for a breeder and as makeup fuel for a converter. A tentative conclusion is that the use of plutonium rather than ^{235}U gives a comparable fuel-cycle cost.[30] The use of plutonium in molten-salt reactors is of special interest to the Indian Atomic Energy Commission, and they have started some work on the chemistry of PuF_3 in molten fluoride salts.

The success of the MSRE gave rise to an increase in industrial interest in molten-salt reactors. An industrial study group headed by Black and Veatch[31] reported favorably on the promise of the system and proposed the construction of a prototype reactor that could be completed in 1976. A group headed by Ebasco Services, Inc., has made a similar study, and they have now been given the role of undertaking the major design effort in the United States, under contract to ORNL. They have compiled a rather complete summary and evaluation of molten-salt technology[32] and have concluded that the existing technology is sufficient to justify the construction of a demonstration plant which could be made to work and from which a great deal would be learned about the cost of construction and operation.

THE FUEL SALT

Previous reviews[3,33,34] have described how the presently favored molten-salt constituents and proportions were chosen. The mixture of ^{7}LiF and BeF_2 as the major brew to which the fissile and fertile species are added is probably unique in its combination of properties of low neutron cross section, stability against radiation damage and thermal decomposition, low vapor pressure, and tolerable melting point. Since the fuel is the heart of the reactor, the importance of understanding its basic properties and reactions cannot be overstressed.

There are several ways of broadly characterizing the chemical state of a fused fluoride-salt mixture. The different ways are not completely independent, but each emphasizes or correlates certain aspects of the chemical behavior and physical properties. One of these ways for characterization arises from the relative proportions of the major constituents and is related to their tendencies to form complex ions. BeF_2 added to LiF tends to form the ion BeF_4^{2-}, and ThF_4 tends to form the ion ThF_7^{3-}. In each case the complex ions tie up or immobilize fluoride ions coming from LiF. By analogy with the silicate system, the BeF_4^{2-} and the ThF_7^{3-} ions can be thought of as "basic," and any remaining unassociated (or free) F^- ions can be regarded as "acidic."[35]

The excess or deficit in the free fluoride-ion content can be placed on a rough scale,[36] as follows:

$$\text{Excess free fluoride} = \text{mole \% LiF} - 2(\text{mole \% } BeF_2) - 3(\text{mole \% } ThF_4)$$

This excess (or deficit) influences many of the properties of the salt. For example, it has been shown to have a strong influence on the activity coefficients of various metallic-ion species dissolved in the salt mixtures. This is particularly apparent in measurements of the ease with which bismuth containing lithium can reduce and extract rare earths from the fuel salt.[37] Also, for example, it affects the solubility of BF_3 in the fuel since BF_3 tends to form the BF_4^- ion, which it can do most readily in a salt with free fluoride ions.[38]

A polymer model developed by Baes[39] is related in concept. Starting with the observation that solid BeF_2 consists of the tetrahedral ions BeF_4^{2-} arranged in a three-dimensional network, he studied the polymeric character of $LiF–BeF_2$ melts using activities derived from electromotive-force (emf) measurements and from liquidus data. In the concentration range of BeF_2 of interest for reactors, the model gave best fit to experimental data with most of the beryllium in the BeF_4^{2-} ion, and with only small amounts of $Be_2F_7^{3-}$ ion.

With respect to physical properties, salts with a high percentage of BeF_2 are undesirable because their polymeric structure results in a very high viscosity. For a recent summary of the physical properties of a variety of salt compositions, reference should be made to a report edited by Cantor.[40]

A second and perhaps more important way of characterizing the chemical state of a fuel-salt mixture is its effective potential for oxidation or reduction. This redox potential is directly related to the valence states that are assumed by those metal ions in the salt mixture that are capable of existing in different valence states. The greatest importance of the redox potential is that, to a large extent, it controls the corrosive tendency of the fuel mixture toward the Hastelloy N container alloy. The major constituents of this alloy are nickel, molybdenum, chromium, and iron; of these, chromium, constituting about 7% of the alloy, is by far the most easily oxidized. Accordingly, any corrosive tendency of the fuel salt acts selectively on the chromium of the alloy.

Lithium, beryllium, and thorium in their fluorides LiF, BeF_2, and ThF_4 have neither higher nor lower valence states. They cannot be oxidized and can be reduced only to the metals, and then only by reducing agents very much stronger than the constituents of Hastelloy N. Mixtures of these materials would not be expected to be corrosive, and this was confirmed by the almost immeasurably small corrosion of Hastelloy N by the $LiF–BeF_2$ coolant salt in the MSRE.[41] Uranium, on the other hand, has several stable valences; its known fluorides include UF_3, UF_4, UF_5, and UF_6. Salts containing UF_5 and UF_6 have redox potentials so high as to be very corrosive and will be excluded from the circulating fuel system. In the absence of extraneous strong oxidants, such as HF, FeF_2, and NiF_2, the redox potential is determined by the relative concentrations of UF_4 and UF_3.

In this situation the corrosion occurs through the reaction

$$Cr + 2UF_4 \rightleftharpoons 2UF_3 + CrF_2$$

with all fluorides remaining as solutes in the salt. Equilibrium is reached with quite small concentrations of UF_3 and CrF_2, and the UF_3/UF_4 ratio of an isothermal system can be adjusted so that the extent of reaction is negligible. However, the reaction is temperature dependent, and there are small changes in the equilibrium concentrations as the temperature changes. In the reactor, therefore, there will be some surface depletion of chromium in the hot zones and formation of a surface layer rich in chromium in the cold zone. A satisfactory equilibrium is established[3] if the U^{3+}/U^{4+} ratio is above 0.005. In the MSRE, this condition was usually maintained (although not always), and the corrosion rate was about 0.1 mil/year, with some indication that much of this was associated with the admission of air during shutdown periods.[42]

The direct relation of the U^{3+}/U^{4+} ratio to the corrosion reaction suggests that it would be the ideal measure of the redox potential of the salt. As far as corrosion is concerned, the higher this ratio, the less corrosive the salt will be, but an upper limit, beyond which one should not go, is set by the disproportionation reaction by which UF_3 is converted to UF_4 and uranium metal. This limit is rather high, corresponding to 20% or more of the uranium occurring[3] as UF_3. In the presence of graphite, disproportionation can produce uranium carbide instead of uranium metal, and recent experiments[43] suggest that this reaction goes more readily, placing an upper limit of about 0.06 for the UF_3/UF_4 ratio to prevent formation of uranium carbide. There seems to be adequate leeway to maintain the small ratio needed to keep corrosion low.

In the MSRE, the U^{3+}/U^{4+} ratio was determined by the occasional analysis of a sample of fuel salt withdrawn from the reactor. The analytical method involved sparging the sample with hydrogen and measuring the amount of HF evolved as the various species were reduced.[44] Although the results obtained were useful, the method had many difficulties.[45] Since then a relatively simple voltammetric method has been developed that seems suitable for automated in-line analysis.[46] The method involves measuring the difference between the equilibrium potential of the melt, as indicated by an inert platinum electrode, and the voltammetric equivalent of the standard potential of the U^{4+}/U^{3+} couple. The measurement has been automated and is now undergoing test in a molten-salt thermal-convection loop.[47] It gives promise of being applicable to an operating reactor.

The fission process tends to increase the oxidation potential of the salt[3] since the active metal fission products are not produced in sufficient quantity to

match up with all the fluorides liberated by the destruction of UF_4. Therefore it is necessary to adjust the redox potential to keep it within the desired range. In the MSRE, the redox potential was adjusted by the occasional addition of some reducing metal (beryllium), suspending it in a basket in the pump bowl until it dissolved.[2] Presumably the potential could also have been adjusted by introducing hydrogen into the gas-stripping system; indeed, this is the method of regulating the redox potential of the salt as it is prepared for use. The designs for breeder reactors include the continuous processing of a side stream of fuel so that, for these reactors, hydrogen treatment will probably be the normal method of adjustment.

Long and Blankenship[48] have carried out measurements of the concentration ratio of UF_3/UF_4 that is in equilibrium with various mixtures of hydrogen and HF. From these data an equivalence of HF concentration in hydrogen to the U^{3+}/U^{4+} ratio can be obtained as a function of temperature. For example, at 600°C a U^{3+}/U^{4+} ratio of 0.01 in the molten salt is in equilibrium with hydrogen at 1 atm pressure containing about 20 ppM HF.

Baes[49] has published a very useful summary of the thermodynamic information available in 1969 pertaining to reactions in molten fluoride salts. He gives equilibrium constants as a function of temperature for many heterogeneous reactions and indicates how they can be applied to the control of impurities in molten-salt reactors. Of particular interest to this discussion are his curves of the concentration of various corrosion and fission products to be expected as a function of the redox potential expressed as the UF_4/UF_3 ratio.

The redox potential also determines the balance between different valences of other metals. For example, if protactinium is in the salt, it can exist in either the 4+ or 5+ valence state. At the redox potential regarded as optimum for the reactor, protactinium exists as Pa^{4+}, but, by sparging the salt with HF, it can be oxidized[50] to Pa^{5+}. This oxidation reaction is favored by increasing the temperature.

During MSRE operation, there were short periods when the fuel was quite oxidizing, with the calculated U^{3+}/U^{4+} ratio falling below 0.004. During these periods the fission-product niobium appeared in solution in the fuel salt,[51] indicating the oxidation of niobium from Nb^0 to Nb^{3+} or Nb^{4+}. On one occasion the fuel was apparently sufficiently oxidizing for Fe^{2+} to appear in solution. The presence of niobium in solution in the fuel could perhaps be used as an indicator of an excessively high oxidation potential, one at which corrosion could become a problem.

The stability of niobium fluorides in molten salts is being investigated by Weaver and Gill.[52] They find that NbF_4 is remarkably stable in the mixture $2LiF–BeF_2$, much more so than as a solid. The niobium gradually disappears from solution at 700°C, presumably by disproportionation, producing NbF_5 gas. They conclude that niobium is slightly more noble than chromium and considerably more reactive than iron.

The fuel salt has a limited tolerance for oxide ion, depending on the proportions of the major constituents. If the solubility for oxide ion is exceeded, metals will precipitate as oxides in a definite sequence. If protactinium is oxidized to the 5+ valence, it is the first to precipitate.[53,54] This unique position is being investigated as a possible processing step for separating the protactinium from the fuel.[55] The tetravalent oxides are the next to precipitate; if there is a preponderance of ZrF_4 over UF_4, it will precipitate separately, before uranium or thorium. Advantage was taken of this fact in the MSRE, adding ZrF_4 to protect against the possible precipitation of UO_2. If the oxide content is further increased, the uranium and thorium come down together as a mixed oxide, which is high in UO_2 until the uranium is depleted.[56] Finally, if enough oxide is present, BeO is precipitated. Pu^{3+} does not precipitate as oxide from fuel salt even in the presence[57] of excess BeO or ThO_2.

The trifluoride species, PuF_3, UF_3, and the rare earths, have a limited solubility in fluoride-salt mixtures and tend to coprecipitate when their solubility is exceeded. This naturally caused some concern over the use of plutonium as a fuel, so a number of measurements were carried out. Barton et al.[58] measured the solubility of CeF_3 in a large variety of molten-fluoride compositions between 550 and 800°C. In mixtures of the two constituents, LiF and BeF_2, they found a minimum solubility for the composition with about 37 mole % BeF_2. The solubility was greatly enhanced by replacing BeF_2 with ThF_4, presumably because the Ce^{3+} ion, with a charge-to-size ratio z/r of about 3, can compete for F^- ions better with Th^{4+} ions ($z/r = 4$) than with Be^{2+} ions ($z/r = 6$). The solubility also increased sharply in compositions with a very high value of the free fluoride-ion content.

Measurements at ORNL[59] and at the Bhabha Atomic Research Center in India[60] have shown the solubility of PuF_3 in the single-fluid breeder salt (72 mole % LiF, 16 mole % BeF_2, and 12 mole % ThF_4) to be nearly identical to the solubility of CeF_3 measured by Barton. The solubility is about 0.8 mole % at the liquidus temperature of about 500°C and increases to

about 5.5 mole % at 800°C. These values are adequate for the use of plutonium as a fuel and would allow the accumulation of rare-earth fission products for as long as 10 years without processing if this were thought desirable. The measurements of PuF_3 solubility are being extended to other compositions by the Bhabha Atomic Research Center.

BEHAVIOR OF FISSION PRODUCTS

In an ordinary reactor, most of the fission products will remain within the fuel can, but the mobility that is inherent in a fluid-fuel reactor makes it necessary to trace the paths that the individual fission products take. For a molten-salt fuel, there are three broad classes of fission products: those whose fluorides are stable in the salt at its redox potential (the soluble fission products), the noble gases, and the noble metals. A great deal of practical information on the disposition of these different fission-product groups was provided by operation of the MSRE.

The major soluble fission products are the rare earths (including yttrium), zirconium, barium and strontium, rubidium and cesium, and iodine and bromine. Metal coupons exposed in the MSRE core showed only very small deposits of these soluble fission products, generally corresponding to the amounts that might be expected from fission-product recoil or as a residue from deposited precursors.[61] Slightly more was found on the graphite, presumably reaching there via motion of aerosols into the graphite pores. Similarly, very small amounts of these soluble fission products were found in the off-gas system, presumably carried there by an aerosol mist and by gaseous precursors.

Xenon and krypton gases constitute about 27% of the stable fission products, but other stable or long-lived fission products spend a transient period as noble gases. The noble gases are very sparingly soluble in molten salt and take the first opportunity to migrate to any gas phase in contact with the fuel. The competitive sinks for noble gases are the pore spaces in the moderator graphite and the circulating bubbles of the cover gas. The reactor designer tries to encourage migration to the gas bubbles so that the xenon can be stripped from the salt to reduce the ^{135}Xe neutron poison. The assumption has generally been made that it will be possible, by sealing the pores of the graphite and by efficient gas stripping, to keep the loss of neutrons to ^{135}Xe at about one-tenth of the value for a solid-fuel reactor.

In the MSRE the graphite surface was not sealed, and only 4% of the fuel flow was sent through a degassing spray ring in the pump bowl. The volume fraction of bubbles in the circulating salt varied from less than 0.05 to about 0.7%. The poison fraction for ^{135}Xe varied from 0.001 to 0.009, depending on the bubble fraction and on whether helium or argon was used as the stripping gas. For most of the MSRE operation (using helium), the ^{135}Xe poison fraction was about 0.003, as compared to an expected value of 0.015 had there been no xenon stripping. The variations in xenon poison fraction with volume fraction of the circulating cover gas and with the nature of the gas have been explained adequately by a model developed by Engel[62] that takes into account the solubility of the cover gas as a function of temperature.

Fission products that spend seconds to hours as noble gases and then decay to other elements can migrate into the graphite pores as a gas and deposit there as a solid. Concentration profiles as a function of depth below the graphite surface for such fission products are consistent with what would be expected from gaseous diffusion during their half-life as a gas.[61] In similar manner, some of these solid fission products were found in the off-gas system after their transitory existence as noble gases.

Another major group of fission products, consisting largely of Nb, Mo, Tc, Ru, Rh, and Te, does not form fluorides that are stable at the redox potential of the fuel salt and is therefore called "noble." Because they are born within the salt, these elements must act somewhat like the noble gases since they are not appreciably soluble, are not wet by the salt, and tend to migrate to the salt surfaces. The deposits of these noble metals on metal and graphite coupons exposed in the core of the MSRE were, with the exception of niobium, which forms a stable carbide at reactor temperatures, heavier on the metal surfaces than on graphite surfaces.[63] By a postmortem gamma scan of the heat exchanger, Houtzeel, Blumberg, and Dyer[9,64] found a heavier deposit of noble metals than would have been expected from the samples exposed in the reactor core. The deposits were further enhanced by as much as a factor of 3 in the regions of high turbulence caused by the heat-exchanger baffles.

Noble metals were also found in the pump bowl of the MSRE, both as a film on the surface of the salt and in the gas space. Evidence for the surface film was provided by the fact that sampling capsules always emerged from the salt with a deposit of noble metals on the outside surface. The gas samples that were collected from the space above the liquid level also showed the presence of noble metals. Blankenship has proposed that the ejection of noble-metal atoms from

the surface of the molten salt should be expected as a result of the conversion of the surface energy of a nonwetting species to kinetic energy.[65]

By observing the relative concentrations of an isotope pair ($^{103}Ru/^{106}Ru$) having different half-lives, Bohlman and Compere[63] were able to measure the age of the noble-metal fission-product deposits. Their results are consistent with a model that involves a "storage pool" from which the noble metals are redistributed after a time. The metals leave the salt soon after their birth; some are deposited immediately on metal and graphite surfaces, but some are delivered to the storage pool, presumably in the pump bowl, where they are held up for periods of from 45 to 90 days. After this period, some of the metals from the pool are distributed to the graphite and metal surfaces, and some go into the off-gas system.

In a power reactor, it is important to know the distribution of these noble-metal fission products so that the afterheat generation in various reactor components can be calculated. Briggs[66] has estimated this distribution using a model based on mass-transfer theory. The distribution between the surfaces of graphite, metal, and bubbles is then taken as proportional to the products of the mass-transfer coefficients and the surface areas. In this way, it was estimated that, in a power reactor, 10% would deposit on the graphite, 40% on the metal surfaces, and 50% would go into the off-gas system with the bubbles. The model gives results reasonably consistent with the data obtained from the MSRE.

COOLANT SALTS AND TRITIUM CONTROL

In all serious studies of molten-salt reactors, an intermediate coolant has been proposed to carry heat from the fuel salt to the steam generators. A steam leak directly into the fuel salt would cause rapid precipitation of oxides, including UO_2, and make the fuel salt corrosive by the formation of HF. Since such a leak is a likely event and the consequences are serious, a protective intermediate coolant loop seems necessary. Many coolants have been repeatedly considered for this role, but only lead and various salt compositions have received sustained attention.

The MSRE used a salt with a molar composition of 66% ^7LiF–34% BeF_2 as the coolant, a choice made for maximum safety. With such a salt, leakage into the fuel salt would be completely harmless and, except for a potential health hazard, leakage into the radiator air would be uneventful. For power reactors, its disadvantages of high cost and relatively high melting point (455°C, 850°F) seem to outweigh its advantages. Although other salts are occasionally considered, the current choice is a eutectic mixture of sodium fluoride and sodium fluoroborate with a molar composition of 8% NaF–92% $NaBF_4$. It is inexpensive, has reasonable heat-transport properties, and has a liquidus temperature of 725°F. Its vapor pressure is relatively high,[67] with about $\frac{1}{3}$ atm pressure of BF_3 gas at the expected maximum operating temperature. As a result, the cover gas must contain an equilibrium partial pressure of BF_3 to avoid a gradual change in composition in the direction of NaF. After some slight initial difficulty, this has been accomplished on a routine basis in circulating loops.[68]

The sodium fluoroborate salt is considerably more corrosive than the fuel salt. Corrosion losses are quite sensitive to impurities, particularly water vapor, and corrosion rates of several mils/year have been observed for short times. With reasonable impurity levels, an average corrosion rate of 0.7 mil/year has been measured. One loop,[69] operated with high-purity salt and at rather extreme temperatures (hot leg 687°C and cold leg 438°C), has given the best performance with a corrosion rate of 0.2 mil/year. During periods of high corrosion, caused by high impurity levels, there has been a tendency for deposits, which seem to consist largely of Na_3CrF_6, to occur in the cold leg, leading to the possibility of plugging. It may be necessary to use cold traps to alleviate this situation. Evidently much more good experience is needed in the operation of loops in which adequate purity of the salt is maintained before one can be assured of obtaining a satisfactory life for heat exchangers and steam generators.

When the sodium fluoroborate salt is mixed with the fuel salt, it reacts to produce two immiscible liquids accompanied by an increase in BF_3 pressure.[70] For a small heat-exchanger leak, the excess pressure could be handled without difficulty by the fuel off-gas system, but larger leaks can cause sudden generation of large quantities of gas, increasing the pressure by an order of magnitude. A more thorough investigation of the mixing kinetics is in order. In similar vein, the planned experiments related to steam leaks into the coolant salt would seem quite important.

When public attention began to be focused on the environmental effects of the radioactive effluents from power reactors, serious calculations of the disposition of tritium from molten-salt reactors were begun. A 1000-MW(e) molten-salt reactor will produce tritium at a rate of about 2420 Ci/day, with more than 98%

coming from (n,α) reactions with lithium isotopes. At the temperature of operation of a molten-salt reactor, iron- and nickel-based alloys are nearly transparent to hydrogen, and it was feared that the tritium would flow through the coolant salt to the steam in the steam generators.

Briggs[71] has studied the problem extensively and devised a model to describe the transport of tritium. He assumed that tritium would appear in the fuel salt either in molecular hydrogen form (T_2, HT) or as tritium fluoride, with the relative proportions determined by the redox potential of the salt. These gases would migrate to surfaces: graphite, metal, or gas. At the metal surfaces, some of the molecular tritium would dissociate into atoms, dissolve in the metal, and diffuse to the outer surface. Tritium fluoride would release some tritium atoms by reaction with the metal, but this is thought to be a comparatively slow reaction. The T_2, TH, or TF that did not diffuse through the walls or absorb on the graphite would find its way into the fuel off-gas system.

With a reasonable choice of parameters, the model gave a good fit to the observed distribution of tritium in the MSRE. The measurements of the tritium distribution in the MSRE were somewhat erratic, but between 46 and 56% was found in the fuel off-gas system, 15% on the graphite, between 5 and 9% in the reactor cell, and a similar amount in the cooling air coming from the radiator heat dump. As much as 20% of the calculated production is unaccounted for, but there is good reason to believe that most of this was retained in a hydrocarbon residue in the pump bowl or off-gas system. (The hydrocarbons came from a small oil leak into the fuel pump.)

Applied to a large power reactor, this model indicated that as much as 60% or 1500 Ci/day could end up in the steam system of the turbogenerator plant. Handling this amount of tritium in the steam system would be awkward, although not impossible if one were allowed to approach the stated maximum permissible concentration (MPC) values. This does not seem desirable, however, and so a tentative goal of the development program is to reduce the plant effluent to the level proposed as a design objective for light-water reactor plants, about 10 Ci/day. A number of possible approaches are under investigation, but only two, both involving trapping tritium in a coolant salt, will be mentioned here.

In relatively pure fluoroborate salt, OH ions are not stable; when small amounts of NaOH or $NaBF_3OH$ are added, the OH ions disappear by thermal decomposition or by hydrogen-producing reactions with the Hastelloy N container.[72] However, there is evidence that in the presence of higher concentrations of oxide and Cr^{3+} ions, steady-state concentrations of hydrogen as high as 30 ppM can be maintained as hydroxyl in fluoroborate test loops. Exchange of hydrogen isotopes in such hydroxylated fluoroborate melts has been observed, although the rates of exchange have not been measured. It seems likely that tritium entering the coolant salt will exchange with the hydrogen already there and thereby be retarded from passage into the steam system. Such a holdup mechanism combined with a side-stream processing scheme which removed the hydroxyl ion would permit the safe storage of the tritium. The tritium so obtained would be diluted with hydrogen, but, if such dilution were less than a factor of 10^4, the volume could be handled readily.

The other method of preventing the tritium from getting into the steam system which has received considerable attention is the use of a secondary coolant salt, a mixture of $NaNO_3$, $NaNO_2$, and KNO_3 known as HTS or Hitec, to isolate the steam generator from the primary-coolant salt. If the tritium were oxidized to water, the Hitec would effectively trap tritium, but its use has the obvious disadvantage of adding a third loop and increasing the capital cost.

The Hitec salt as a replacement for the primary-coolant salt has not been given serious consideration for several reasons. The mixture may not be sufficiently stable at the higher temperatures it would experience in the primary heat exchanger, and extensive testing would be necessary to ensure its stability to the radiation field in the heat exchanger. A leak of Hitec into the fuel would cause precipitation of UO_2, and a large leak would probably result in rapid reaction with the moderator graphite.

Current development work relating to the tritium problem includes measurement of the solubilities and diffusion constants needed in the model describing tritium behavior. The hydrogen content of the sodium fluoroborate salt is still under investigation, as is the means for recovery of the hydrogen and tritium from it. The high-temperature stability of the Hitec salt is also under investigation, should there be a necessity for using it.

RADIATION BEHAVIOR OF HASTELLOY N AND GRAPHITE

Hastelloy N was developed specifically as the container material for use with molten fluorides. It was tailored to have good high-temperature strength, good air-oxidation resistance, good fabrication properties,

and to be resistant to corrosion by the fuel salt. However, Hastelloy N has been found to suffer from the high-temperature radiation embrittlement common to most iron- and nickel-based alloys. This embrittlement results from internal generation of helium either by thermal-neutron absorption in boron impurities or by fast-neutron reactions with nickel. At high temperatures the helium gathers at the grain boundaries and greatly reduces the tolerance for strain before fracture. Under some conditions the strain before rupture is less than 0.5%.

A development effort to improve the high-temperature radiation performance of the alloy has been under way for some years.[9] The general approach has been to produce a fine carbide precipitate within the grains and at grain boundaries. By this means the helium is inhibited from migrating to the grain boundaries, and the grain boundaries are strengthened. The first modification consisted in reducing the molybdenum from 16 to 12%, reducing the silicon from 0.5 to 0.1%, and adding 0.5% titanium. This alloy was satisfactory at temperatures up to 650°C, but its properties deteriorated above that temperature. The cause of the deterioration was shown to be the conversion of the finely dispersed MC-type carbide to a much coarser carbide of the type MC_2. (The metal "M" in these carbides is a mixture, high in molybdenum.) Recent development work has shown that improved ductility and strength at higher temperatures can be obtained by somewhat larger additions of various metals, such as Ti, Nb, Zr, and Hf. The niobium seems to provide improvement only in combination with the others, and zirconium makes the alloy difficult to weld satisfactorily. In laboratory-prepared samples, the hafnium greatly improved the ductility, but later commercially produced heats did not perform so well. At present the best solution seems to be an alloy containing about 1.5 to 2.0% titanium, which gives promise of having a ductility of 4% or more when irradiated at temperatures up to 760°C and of having other properties that are satisfactory. There is some concern that the phenomenon of conversion of MC-type carbides to MC_2-type carbides provides a new upper limit to the temperature excursions allowable in a molten-salt reactor. It seems probable that short-time overheating beyond the temperature for which the alloy is tailored will allow the formation of coarse carbide precipitates, thus rendering the irradiated alloy brittle and endangering future reactor operation. If this proves true, it will provide an additional engineering constraint in design, but one that can probably be met without too much difficulty.

The appearance of fissures between the surface grains was a new problem encountered with the Hastelloy N alloy during the operation of the MSRE.[73] Fissures were first observed in core surveillance specimens on which tensile tests were run. Although no decrease in tensile strength was observed, photomicrographic examination of the specimens after being elongated by the test revealed fissures to a depth of about 5 mils, the thickness of the surface grains. Extensive examination of many specimens after the MSRE was shut down showed that these cracks occurred wherever the alloy was exposed to fuel salt, but almost never anywhere else. For example, the surface of the heat-exchanger tubes exposed to the fuel salt showed fissures, but the opposite side of the tubes, exposed to the coolant salt, showed no attack. Similarly the surface of the control-rod thimbles exposed to fuel salt was attacked, but not the other side which saw a gaseous atmosphere.

Two possible explanations are being explored. One is that the fuel was quite oxidizing during part of the MSRE operation, and there might have been excessive grain-boundary removal of chromium during this period. The other explanation, which now appears more likely, is that some fission product, probably tellurium, is responsible, probably by forming an intermetallic compound. This subject is under intensive investigation at present. Surface grain-boundary defects have been produced artificially, both by exposure to a highly oxidizing salt and by heat treating with tellurium introduced as a surface impurity. The effects with tellurium seem to resemble those seen in the reactor, leading to the belief that tellurium is the primary responsible agent. Until further information on the rate and extent of the attack and its mechanism is known, it is difficult to assess whether the matter is serious or not.

In a power reactor the displacement damage to graphite produced by fast neutrons will create some problems. At the high temperature of the molten-salt reactor, the principal harmful effect will be the gross dimensional changes. The usual graphites at first shrink as a result of a contraction of the hexagonal graphite crystals in their "a" direction. After receiving a fluence of about 2×10^{22} neutrons/cm^2 with energy greater than 50 kV, the graphites begin to expand, reaching their original dimensions at about 3×10^{22} neutrons/cm^2. After this, they expand at an ever-increasing rate, presumably to destruction.

Most graphites are highly anisotropic, and thus the dimensional changes are quite different along different axes, but this effect can be kept small by choice of raw

materials, primarily by the use of rounded particles instead of needle-shaped ones. With this "isotropic" graphite,[74] the linear shrinkage before the expansion starts may be as much as 2.5%. As the temperature of irradiation increases, the maximum shrinkage decreases, but the rapid expansion phase occurs at a lower fluence.

The graphite in a reactor will see a nonuniform fluence at nonuniform temperatures, so that a careful stress analysis is required.[6] Fortunately the graphite also undergoes radiation creep, and this helps to keep the stress problem from being serious. Similarly the changes in reactor physics resulting from dimensional changes have been investigated and found to be acceptable.

How long the graphite moderator can remain in the reactor core before it is replaced is a matter of judgment. As the expansion from radiation damage progresses, the graphite will become more porous, and the breeding performance will gradually show a slight deterioration due to the absorption of fission products and to the displacement of some fuel from the reactor core. At some point the expansion could cause binding and possible breakage of the graphite. For practical purposes, it has been assumed that the graphite life in the reactor will be determined by the time it takes for the graphite to return to its original volume after the shrinkage phase has been completed. With this restriction the graphite life is about 4 years if the maximum power density in the reactor core is 70 kW/liter. The replacement of the graphite core every 4 years is expected to cost[19] about 0.2 mill/kWh.

Graphites that do not follow the above-described pattern of shrinkage and expansion under radiation have been made. This gives hope that some improvement in graphite longevity can be obtained. Development work is currently directed at understanding the deviations that have been observed in radiation behavior, of course, with the hope that some improvement can be made.

FUEL PROCESSING

A number of studies have been made of the dependence of breeding performance and fuel-cycle costs on the cycle times for removing fission products from the fuel of a molten-salt reactor.[8,75-77] The breeding performance, of course, improves with rapid fuel processing, but the net fuel-cycle cost shows remarkably little variation between the extremes of virtually no processing and the rather sophisticated processing required to get the optimum breeding characteristics. With little processing the reactor has a conversion ratio between 0.8 and 0.95, and, when operated as a breeder, the breeding ratio is about 1.07. With a specific power of about 1.5 MW(t)/kg, the breeder has a fissile production credit of about 0.1 mill/kWh. As far as fuel-cycle cost is concerned, what the converter loses in fuel production credit and fuel purchase cost, it makes up for in decreased cost of the processing plant and its operation. In both cases the fuel-cycle cost has been calculated to lie between 0.6 and 0.8 mill/kWh, although recent capital-cost estimates of the processing plant[78] will lead to higher values. With the wide range of processing speeds economically interesting, a number of different combinations of individual processing steps have been explored.

All of the reactor performance calculations assume that ^{135}Xe is removed on rapid enough cycle to keep the xenon poisoning to 0.005 neutron per neutron absorbed in fissile atoms. The problem here is to prevent the xenon from entering the porous graphite moderator. In the past it has been assumed that this could be accomplished by a rapid purge of the fuel with helium or other gas, combined with some method of sealing the surface pores of the graphite. A remarkably good method of sealing the graphite pores was developed,[4] involving heating the graphite to about 900°C and alternating between evacuation and admission of a hydrocarbon gas such as butadiene. Unfortunately the low permeability was not retained after irradiation to a fast-neutron fluence of about 10^{22} neutrons/cm^2. Development of sealing techniques is continuing, both with the "pulse-impregnation" technique described above and with isotropic pyrolitic coatings put on at a somewhat higher temperature. Occasional samples have retained their low permeability to fluences of over 10^{22} neutrons/cm^2, but it is by no means certain that large-scale success will be achieved.

Additional attention is being given to the possibility of removing part of the iodine precursor of xenon by giving a mild HF treatment to the side stream of fuel going to the off-gas system.[79] If this proves practical, the xenon poisoning can be kept within the specified 0.005 limit without any special sealing of the graphite pores. If neither pore sealing nor iodine removal becomes practical, the xenon poisoning can be kept to between 0.01 and 0.02 by the planned gas-purging system, and the loss from design performance will be about 0.01 in breeding or conversion ratio and less than 0.02 mill/kWh in fuel-cycle cost.

Protactinium is a fairly serious neutron poison for the breeder since, for each neutron absorbed, a potential ^{233}U atom is also destroyed. At a specific power of 1.5 kW(t)/g, the present reference-design reactor would have a breeding-ratio loss of about 0.05 if the protactinium were allowed to decay in the reactor fuel. It is therefore desirable to remove the protactinium from the fuel soon after it is formed and to store it somewhere outside the reactor until it decays to ^{233}U. Removing the protactinium on a 10-day cycle[8] reduces the breeding-ratio loss to about 0.01.

It would be most desirable to remove the protactinium without also having to remove the uranium, and this may be possible through an oxidation process. Early work[80] showed that the addition of excess amounts of BeO, CaO, or ThO_2 would precipitate protactinium from fluoride melts and that the protactinium could be brought back into solution by HF treatment. More recently, it has been shown[53,54] that, if protactinium is first oxidized to the 5+ valence, it can be precipitated as Pa_2O_5 with a clean separation from uranium. Bell and McNeese[55] have described a possible flow sheet for a processing plant using this process.

Another way to remove the protactinium, currently the favorite, is by reductive extraction from the fuel salt into bismuth in a multistage countercurrent extraction column. The reductant is lithium dissolved in the bismuth, in such amount that the thorium it extracts will not exceed the thorium solubility in bismuth. Many experiments have shown that the distribution coefficients for uranium, protactinium, and thorium are widely different, allowing for clean separations. Since uranium is preferentially extracted, it must be removed from the salt first, either by prior reductive extraction or by fluorination.

Once the protactinium is extracted into the bismuth, it is converted back into a fluoride by treatment with HF, and the protactinium fluoride is transferred into a separate recirculating salt stream. This salt stream is then fluorinated to separate and recover the ^{233}U as it is produced from the protactinium. The reductive extraction process has now been demonstrated successfully in a flowing system, transferring uranium from salt to bismuth in a packed column.[81,82]

The reductive extraction process requires a construction material that is compatible both with fluoride salt and with bismuth containing dissolved lithium. Corrosion tests have shown that molybdenum and graphite should be suitable from this point of view,[9] but both materials are brittle and present problems in fabrication. A considerable development effort has been expended on the forming and joining of molybdenum. It has been found that short sections of pipe up to 12 cm in diameter can be made by back extrusion, as can suitable end caps with the desired protuberances. A series of Fe–Mo–C brazing alloys for joining molybdenum has been developed which may be usable with bismuth, but their suitability for long-term use has not yet been demonstrated. Since welds in molybdenum are brittle at room temperature, all welded joints will be either back brazed or strengthened by brazed-on sleeves. Tight joints have been made both with a gasketed mechanical coupling that can be disassembled and by roll bonding.[83] The progress that has been made in the technology of fabricating equipment from molybdenum is impressive. Plans are also under way to make increasing use of graphite, especially for such equipment as mixer–settler tanks that can be fabricated by simple machining operations.

As noted above, the reductive extraction method for isolating the protactinium requires the prior removal of uranium. The complete removal of the uranium from the fuel salt on as short a cycle as 10 days is an ambitious undertaking, requiring a method that offers little chance for loss of uranium before it is reconstituted in the fuel. Several methods that appear to meet this requirement are available. One is reductive extraction into bismuth, and this method was considered along with an electrolytic method of putting the uranium back into the fuel salt after the protactinium had been removed.[84] A number of factors, including the amount of reductant required and the difficulty of developing a continuous electrolytic process, caused this method to be abandoned in favor of fluoride volatility.

Fluoride volatility is a proven method for the recovery of uranium from molten fluoride salts. This process involves sparging the molten salt with a mixture of fluorine and helium, converting the UF_4 to gaseous UF_6. As a batch process, this method was used to recover the ^{235}U from the first charge of fuel salt that was used in the MSRE. With some modifications the equipment used for the MSRE could be used for the infrequent processing of a converter reactor. For the larger-scale uranium removal needed by the breeder reactor, a continuous fluorinator is considered to be necessary.

The most troublesome point of such a device is corrosion at the liquid–gas interface. Where the metal surface is exposed only to gas, a protective fluoride film is formed, but this film is dissolved whenever it is

contacted by the molten salt. To overcome this problem, we plan to operate the fluorinator with a layer of frozen salt lining the vessel walls. This requires the combination of an internal heat source to keep the salt molten and external cooling to provide the frozen layer on the walls. When the reactor is operating with irradiated fuel, the radioactivity will provide the internal heat, but, in the development of the equipment, we plan to use induction or resistance heating of the salt. The first such experiment with molten salts should be under way soon.[85]

After the xenon poisoning has been limited to a low value, more than 85% of the neutron losses to the remaining fission products are due to the rare earths. If the rare earths are removed continuously from a small stream of fuel with equivalent cycle times of 20 to 50 days, the total fission-product poisoning can be kept to less than 0.02 neutron per neutron absorbed in fissile atoms, a very satisfactory level for a breeder reactor. The preferred method for removal of the rare earths is the so-called "metal-transfer process."[86] In this process the rare earths are first extracted from a fuel-salt stream into lithiated bismuth in the same manner as the protactinium, after all the uranium and protactinium have been previously removed. An additional step is necessary because it is difficult to separate the rare earths from the thorium cleanly by this first extraction. The second extraction step is from the bismuth to a stream of LiCl, which discriminates strongly against thorium. The concentration of rare earths in the LiCl is kept low by a further extraction into a very strongly reducing stream of molten Li–Bi alloy. An extra bonus of the metal-transfer process is that barium and strontium are also separated.

The process has been demonstrated in a small engineering experiment[87] in which lanthanum and neodymium were transferred from a fuel salt to the final Li–Bi alloy and concentrated relative to thorium by a factor of 10^5.

If the oxidation process has been used to remove the protactinium, it will then be necessary to remove uranium as an extra step prior to the metal-transfer process. This can be a smaller operation than the uranium removal prior to the protactinium extraction because the cycle time is likely to be more nearly 50 days than 10 days. The fluoride-volatility process is still a valid way to do this, but there is also the possibility of removing the uranium by precipitating it as the oxide.

Taking advantage of oxide-equilibria studies by Bamberger and Baes,[56] which showed that uranium might be precipitated somewhat preferentially in the presence of thorium, Bell and McNeese[82] have proposed a process flow sheet. Experimentation is currently being carried out with encouraging results. A salt containing both uranium and thorium is being treated with water vapor as an oxidant. Early results indicate that the initial precipitate, high in UO_2, does not equilibrate with the lower concentration of uranium remaining in the solution. Taking advantage of this fact should make possible the precipitation of most of the uranium in a single stage without removing much thorium. The principle of uranium oxide precipitation seems to be well established, and, although its embodiment into an engineering process is in its infancy, rapid progress is expected.

Although the metal-transfer process appears to give the best fuel-salt purification for a high-performance breeder, there are other possibilities for rare-earth removal that are perhaps worth keeping in mind. If the bismuth-contacting systems prove expensive or if unseen difficulties develop, the other methods may be applicable, especially at some sacrifice in breeding performance.

When two fluid breeders with separate salt streams for fuel and fertile materials were in vogue, distillation was the reference method for freeing the fuel salt of rare-earth fission products. Many experiments[88] on the relative volatility of the different constituents indicated that, by continuous operation of a still at 1000°C, it would be possible to recover the carrier salt as a distillate with its composition 66 mole % LiF and 34 mole % BeF_2. For this composition of distillate to appear, the composition of the liquid in the still would be about 88 mole % LiF and 12 mole % BeF_2 at the start of distillation, although the concentration of rare earths would gradually build up during the course of the distillation. If the still bottoms were recycled through a 400-ft^3 holdup tank, it was estimated that their disposal could be deferred for the life of a 1000-MW plant.[89]

Batchwise distillation was carried out on an engineering scale, both with nonradioactive salt and with a portion of the fuel salt of the MSRE. The results were in accord with expectations, except that there may have been some carry-over of nonvolatile species by mist in the runs on the MSRE fuel.[90] In the nonradioactive tests the separation factor for rare earths from LiF was in excess of 1000, but with the MSRE fuel the indicated separation factor became as low as 100 (for cerium).

With the shift of attention to the one-fluid breeder, in which the ThF_4 and UF_4 are in the same salt, interest in distillation diminished because the 1000°C

distillation would not recover the thorium, and, for a breeder to be effective in conserving fuel, the thorium must be recycled. Smith, Ferris, and Thompson[91] indicate that distillation at 1200°C might make the recovery of thorium possible, but the problem of construction materials for this higher temperature discouraged further consideration at the time. The possible construction materials for the 1200°C still are molybdenum and graphite; since these are also the materials that must be used for the now-popular reductive extraction process, and the problems of constructing equipment from them are being faced anyway, it may be worth considering distillation again.

In some recent experiments an attempt was made to precipitate plutonium from a molten-salt solution by oxidation, and it was found to be very stable. There was no loss of plutonium from solution[57] even in the presence of ThO_2 and BeO. From the similarity of plutonium chemistry to that of the rare earths, it is probable that they also are difficult to precipitate as oxides. This suggests that, after the protactinium and uranium have been precipitated as oxides, the thorium may also be separated out in this way, leaving the carrier salt containing the rare earths ready for distillation. There are obvious difficulties with this suggestion, but it is made to indicate that there may be other future possibilities for processing.

Similarly Grimes[3] has repeatedly suggested that the precipitation of mixed trifluorides, perhaps using natural CeF_3 as the saturating fluoride, could be used to remove the rare earths. Perry[92] estimated that the use of this method for a relatively high-performance breeder would require about 35 tons of cerium per year for a 1000-MW reactor. With these and other possibilities for chemical processing relatively unexplored, there seems to be much room left for interesting investigation.

DESIGN AND DEVELOPMENT OF ENGINEERING COMPONENTS

Most of the recent design and development work on components has been directed to items that need to be changed significantly from those used on the MSRE. A prime example is the off-gas system proposed for a power reactor. The MSRE used a simple spray ring in the pump bowl to establish contact between the fuel salt and the purge gas, which was introduced primarily down the annulus around the pump shaft. The plan for a power reactor is to have specially designed gas-bubble injectors and centrifugal gas separators in a side stream of fuel salt. Extensive experiments have been carried out with such devices, using water and water–glycerine mixtures. Several different bubble generators have been tested and appear workable, and good efficiency has been obtained with a gas separator.[93] Tests with a closed aqueous loop are in progress, and a molten-salt test loop is under construction.[94]

The MSRE had no steam generator, so that work in this area is new. The preference at ORNL is for a supercritical steam generator, primarily because it is expected to lead to fewer difficulties in adapting it to the high melting point of the fused-salt intermediate coolant but also because of its high thermal efficiency. The design studies that have been made are based on modifications of the TVA Bull Run supercritical power station.[95] The Foster Wheeler Company, under contract to ORNL and the AEC, has started a design study leading to a development program. In the meantime the compatibility of the Hastelloy N alloy with high-temperature steam is being tested in a cooperative program[9] between ORNL and the TVA. These corrosion tests have shown a metal removal rate of less than 0.00063 cm/year at 538°C (1000°F). Tube burst tests to determine if there is a stress effect on the corrosion are under way.

The sodium fluoroborate intermediate coolant salt has been circulated for 11,500 hr at 750 gal/min in an Inconel loop without excessive corrosion or visible attack on the pump impeller.[96] The biggest difficulty was the nearly complete plugging of the bubbler tube used to indicate the liquid level in the pump bowl. A new engineering-scale pumped loop of similar size is being constructed out of Hastelloy N piping taken from the coolant loop of the MSRE. It will have several side streams that can be used for a variety of purposes,[97] but the principal function will be to serve as a vehicle for testing the control of the chemistry of the coolant salt. High on the priority list will be trial of schemes for the control of tritium in the coolant salt.

In the engineering design of molten-salt power plants, a great deal of attention has been given to safety and maintainability. The experience in maintaining the MSRE has been drawn upon generously. The philosophy of maintenance is "remove, replace, and repair or discard."[98] To remove and replace requires that all service lines be accessible for disconnection and connection by long-handled tools. The major equipment items must be laid out so that they are visible from the maintenance area, and their positions must be accurately fixed so that replacement equipment will fit in place. Flanges were used to connect the major pieces of equipment in the MSRE, but the larger-sized piping for the power reactors will

require welding in preference to flanges. A program to develop a machine for remotely cutting, facing, positioning, and welding pipe has been under way for some time, and the machine appears quite promising for molten-salt reactor use.[99]

Although there is optimism about maintenance based on the experience with small pieces of equipment in the MSRE, it must be recognized that replacement of major reactor cell equipment will be very difficult and probably time consuming, at least until some experience is gained. Consequently even greater than usual emphasis must be placed on reliability of equipment.

Another problem that has received some attention is that of replacing the graphite core when its life has ended. One plan is to lift the whole core out as a unit in a cage,[19] along with the roof of the reactor vessel. The steps by which this might be done have been worked out and appear to be feasible. The magnitude of the task is comparable to the proposal in the "hot-cell" maintenance concept of the LMFBR to lift the reactor head with its shielding as a unit. Other designers may prefer to group the graphite sticks in bundles and remove the bundles one at a time.

Particular attention has been given to the design of the drain tank and its method of cooling.[19] The great desire is to provide a safe "walk-away" situation in case of a severe accident, with the fuel automatically drained into a tank that is always cooled by natural convection and requires no engineered safeguards. Several plausible methods have been proposed.

The safety engineering has naturally been concerned with accident situations, mostly those in which circulation of the fuel salt or the coolant salt has been lost. In such cases the afterheat produced by deposited noble-metal fission products must be taken into account. For example, studies have been made of the peak temperature that would be reached by the intermediate heat exchanger if it were drained of both fuel and coolant salts. Here it would be desired to use a tube bundle enclosed in an inner shell so that it could be replaced as a unit, but the extra heat-transfer barrier presented by the inner shell makes its use problematical.[100]

Some of the problems of safety of a molten-salt reactor will be different from those of other reactors. No accidents comparable in chain of events to the loss-of-coolant accident in light-water reactors or the pump-coastdown-without-scram accident in LMFBRs have yet been postulated for molten-salt reactors, so that there is reason for somewhat less concern with big accidents. On the other hand, a large MSBR plant will have its radioactivity normally spread over a larger area and in more pieces of equipment, and great care must be taken to avoid containment leaks. This problem can be faced squarely only when a serious design is undertaken for a reactor that will be constructed.

SUMMARY

Any appraisal of the current status of molten-salt reactor development or any proposal as to what should be done next must be a personal one reflecting the experience and interests of the writer. However, three separate groups of engineers who have studied the molten-salt system agree that the present technology is adequate to justify starting the design and construction of either a power-producing prototype or a reactor experiment of significant size and performance, such as the proposed MSBE, or both. For the smooth progression to a molten-salt reactor power-producing industry, these are the most urgently needed steps, for they will lead to the development of full-size equipment, to the realistic facing of difficult design decisions, and to the all-important operating experience.

That there is adequate information for a decision to proceed with plant design and construction projects does not mean that the development is completed; all such proposals allow a long time, such as 7 or 8 years, for the expected completion of such a plant. During that time the larger pieces of equipment would be designed and tested, and a number of opportunities for altering the details of design would be available. New knowledge from a concurrent research and development program could be utilized.

I will try to summarize the status of the development program in the approximate order of the preceding technical sections.

The understanding of the basic chemistry of the fuel salt seems to be adequate at present for any normal, and for some abnormal, operating conditions of a reactor. Further work on the effects of an increased oxidation potential (to very low ratios of UF_3/UF_4) on the compatibility limits of the fuel should be valuable since some of the fuel-processing steps may leave the fuel salt quite oxidizing. The compatibility with both Hastelloy N and graphite should be explored under these oxidizing conditions, at both normal and high temperatures.

The voltammetric method of measuring the redox potential of the fuel is a very important development. Some of the chemistry research should be devoted toward improved or alternate methods of determining the chemical condition of a fuel salt under the highly

radioactive conditions that exist in a reactor plant. Along the same line, more work seems to be justified on methods for adjusting the redox potential of a reactor, including the kinetics of the reactions.

The behavior of the gaseous and the soluble fission products seems to be well enough understood. For the noble metals the situation is not as good, and much more experimentation is required. Such experimentation is difficult because it is not easy to simulate the physical situation that a newborn fission-product atom sees. Subjects needing attention are agglomeration, adhesion to surfaces, transport in purge gas—in fact, any knowledge that bears on the mode of transport and the place and permanence of deposition. Also, the evidence in the MSRE of different conditions of surface tension of the fuel salt, which may have been associated with fission products, needs attention. Reactions of the various fission products with the graphite should be studied to learn the conditions of temperature and redox potential that will cause carbides to be formed.

Although sodium fluoroborate will probably turn out to be satisfactory as the coolant salt, much more needs to be learned about it before one can predict a 30-year life for the heat exchanger or the steam generator. Basic chemistry studies related to its corrosive tendencies are needed, leading to knowledge of purity requirements and methods of control. The events that occur when it is mixed with fuel salt also need further elucidation. The sodium fluoroborate salt was chosen because of its low cost, low melting point, and because one could recover readily from some contamination of the fuel salt. Recently the fact that its small hydrogen content may provide a means for control of tritium has counted in its favor. Other salts have been proposed, and I believe it is worthwhile to keep up some activity exploring the other possibilities. It may be possible to find a different set of compromises that are as acceptable as those associated with the sodium fluoroborate salt.

Research on the habits and control of tritium is already intense and should be continued until its behavior is understood and a method of control is assured. Experience with the MSRE left some questions about absorption of tritium in graphite and about a reaction of tritium with hydrocarbons that should be explored. In my opinion the tritium can be controlled satisfactorily; the question is just how and at what cost.

Improvement in the resistance of Hastelloy N to helium embrittlement is well along, and this work should be completed without too much difficulty. More needs to be learned about the effects of inadvertent overheating of irradiated Hastelloy N. The investigation of its suitability for steam-generator use needs to be continued, and, if it should turn out not to be suitable, some modification or substitute must be found.

The investigation of the surface fissuring of Hastelloy N in the MSRE fuel salt is in too early a stage to estimate the outcome. It is encouraging that out-of-pile experimentation methods are showing the effect, so that much more can be learned quickly about the reactions involved, their dependence on fission-product concentration, their kinetics, and the ultimate extent of the attack. Some consideration had already been given to using a cladding metal for the primary system, and work along this line should probably be encouraged as a possible way to cope with the surface fissuring.

Graphites suitable for molten-salt reactors can be manufactured with present technology, but their limited life in the fast-neutron environment adds inconvenience and cost. The fact that different graphites show different radiation behavior provides hope that some improvement in radiation resistance can be achieved. The subject should be explored until the causes of the observed differences are better understood because the subject is of long-term importance. However, one should not expect more than modest improvements over the performance of presently known types of graphite.

It has not been many years since the time when molten-salt reactor engineers could only *hope* that suitable chemical processing methods would be developed, basing that hope on the expectation that the liquid state of the fuel would make chemical processing easier and on faith in the ingenuity of the chemists. Now there seems to be a relative abundance of possible methods, at least two for each needed step. At present, all that can be advised sensibly is to continue the development of the reductive extraction and the oxidation methods for removal of protactinium, the metal-transfer process for the periodic removal of rare earths, and the oxidation and fluoride-volatility methods for extraction of uranium. Other processes, such as distillation, should not be completely forgotten. It is important to keep several options open because the relative cost of the different chemical processing steps will increase in importance as commercial reactor operation nears.

The responsibility for keeping a low xenon level in the reactor lies with the engineers, and current experi-

ments on the introduction and stripping of bubbles should do the major job. The work on sealing the graphite pores should not be abandoned until the utility of depositing thinner layers of pyrolysis products is fully explored. Lighter deposits may retain their integrity under radiation better. In this connection it should be remembered that the gaseous permeability measurement used as a measure of the degree of surface sealing may yield a pessimistic estimate of the effect of the salt–graphite interface in the prevention of xenon entry into the graphite.

A great deal more experience is needed in the handling of the coolant salt, including control of its chemistry during operation. Any corrosion products must be kept from plugging small passages. One of the experiments with the coolant salt should involve a small steam generator so that any compatibility problems will be encountered early. The full development of a steam generator is of great importance; experience in this area is perhaps the most glaring omission to date.

The MSRE operated well and provided much useful information on the reliability of its equipment. Its size was small, for its main purpose was to demonstrate that a molten-salt reactor could be run successfully. It accomplished its purpose admirably, and, in the normal course of events, the next step would be to proceed to the construction of a larger reactor that could serve as the proving ground for larger and higher power-density equipment. The construction of a larger reactor costs much more money and raises the question, "Is it worth it?"

As far as can be determined, without constructing and operating a power reactor, the answer is "Yes, if it is worth developing an alternate to the LMFBR." Some possible reasons for wanting an alternate breeder reactor are: (1) The molten-salt system is devoted to the use of the thorium reserves and may be better for this purpose than the fast reactor; (2) although the LMFBR will surely be a technical success, with all the resources being devoted to it throughout the world, there may still be some reservations about its universal use, such as siting restrictions, cost of power, or just plain prejudice, and all of these are in evidence to some extent; (3) with its complete on-site operation of the fuel cycle, practical even for a single unit, the molten-salt reactor offers a different mode of industry operation, avoiding the necessity for fuel-element fabrication and keeping complete control of the fuel cycle in the hands of the operator; (4) competition between reactor suppliers would have a stronger basis if the products they sold were significantly different.

There has been gradually increasing industrial interest in the United States and Europe[101] and increased interest by the Indian government. Although the exact mechanism is not apparent to me, this interest could, and I believe should, be focused on a reactor construction project, either an MSBE or a prototype power reactor.

REFERENCES

1. M. W. Rosenthal, P. R. Kasten, and R. B. Briggs, Molten-Salt Reactors: History, Status, and Potential, *Nucl. Appl. Technol.*, 8: 107 (1970).
2. P. N. Haubenreich and J. R. Engel, Experience with the Molten-Salt Reactor Experiment, *Nucl. Appl. Technol.*, 8: 118 (1970).
3. W. R. Grimes, Molten-Salt Reactor Chemistry, *Nucl. Appl. Technol.*, 8: 137 (1970).
4. H. E. McCoy, R. L. Beatty, W. H. Cook, R. E. Gehlbach, C. R. Kennedy, H. W. Koger, A. P. Litman, C. E. Sessions, and J. R. Weir, New Developments in Materials for Molten-Salt Reactors, *Nucl. Appl. Technol.*, 8: 156 (1970).
5. M. E. Whatley, L. E. McNeese, W. L. Carter, L. M. Ferris, and E. L. Nicholson, Engineering Development of the MSBR Fuel Recycle, *Nucl. Appl. Technol.*, 8: 170 (1970).
6. Dunlap Scott and W. P. Eatherly, Graphite and Xenon Behavior and Their Influence on Molten-Salt Reactor Design, *Nucl. Appl. Technol.*, 8: 179 (1970).
7. E. S. Bettis and R. C. Robertson, The Design and Performance Features of a Single-Fluid Molten-Salt Reactor, *Nucl. Appl. Technol.*, 8: 190 (1970).
8. A. M. Perry and H. F. Bauman, Reactor Physics and Fuel-Cycle Analyses, *Nucl. Appl. Technol.*, 8: 208 (1970).
9. M. W. Rosenthal, P. N. Haubenreich, H. E. McCoy, and L. E. McNeese, Recent Progress in Molten Salt Development, *At. Energy Rev.*, 9(3): 605 (1971).
10. M. W. Rosenthal, E. S. Bettis, R. B. Briggs, W. R. Grimes, P. N. Haubenreich, H. E. McCoy, and L. E. McNeese, Advances in the Development of Molten-Salt Breeder Reactors, in *Proceedings of the Fourth International Conference on the Peaceful Uses of Atomic Energy, Geneva, 1971*, A/CONF.49/P-048, United Nations, New York (in press).
11. M. Grenon and J. J. Geist, Les Reacteurs a Sels Fondus, *Energ. Nucl. (Paris)*, 13(2): 86 (1971).
12. M. W. Rosenthal, R. C. Robertson, and E. S. Bettis, Molten Salt Breeder Reactors, *Nucl. Eng. Int.*, 14: 420 (1969).
13. P. N. Haubenreich and M. W. Rosenthal, Molten Salt Reactors, *Sci. J.*, 5(6): (June 1969).
14. H. G. MacPherson, Molten Salt Reactors, in *Proceedings of the International Conference on Constructive Uses of Energy*, Washington, D. C., November 1968, American Nuclear Society, March 1969.
15. E. S. Bettis, R. W. Schroeder, G. A. Cristy, H. W. Savage, R. G. Afbel, and L. F. Hemphill, The Aircraft Reactor

Experiment: Design and Construction, *Nucl. Sci. Eng.*, **2**: 804 (1957).
16. J. A. Lane, H. G. MacPherson, and F. Maslan, *Fluid Fuel Reactors*, Addison-Wesley Publishing Company, Inc., Reading, Mass., 1958.
17. Report of the Fluid Fuel Reactors Task Force, USAEC Report TID-8507, February 1959.
18. R. C. Robertson, R. B. Briggs, O. L. Smith, and E. S. Bettis, Two-Fluid Molten-Salt Breeder Reactor Design Study (Status as of Jan. 1, 1968), USAEC Report ORNL-4528, Oak Ridge National Laboratory, 1970.
19. R. C. Robertson (Ed.), Conceptual Design Study of a Single-Fluid Molten-Salt Breeder Reactor, USAEC Report ORNL-4541, Oak Ridge National Laboratory, 1971.
20. P. R. Kasten, E. S. Bettis, and R. C. Robertson, Design Studies of 1000-MW(e) Molten-Salt Breeder Reactors, USAEC Report ORNL-3996, p. 140, Oak Ridge National Laboratory, 1966.
21. E. S. Bettis, Molten-Salt Reactor Program Semiannual Progress Report,* USAEC Report ORNL-4037, p. 223, Oak Ridge National Laboratory, 1966.
22. R. V. Moore and S. Fawcett, Present and Future Types of Fast Breeder Reactors, in *Fast Breeder Reactors*, pp. 99-113, Pergamon Press, London, 1967.
23. M. Taube, M. Mielcarski, S. Poturog-Gutniak, and A. Kowalew, New Boiling Salt Breeder Reactor Concepts, *Nucl. Eng. Design*, **5**: 109 (1967).
24. P. R. Kasten, The MOSEL Reactor Concept, in *Proceedings of the Third International Conference on the Peaceful Uses of Atomic Energy, Geneva, 1964*, Vol. 6, p. 363, United Nations, New York, 1965.
25. Uri Gat, Cooling Concepts for a Compact MOSEL (Molten Salt) Reactor, *Nucl. Eng. Design*, **5**: 113 (1967).
26. R. B. Briggs, Summary of the Objectives, the Design, and a Program of Development of Molten-Salt Breeder Reactors, USAEC Report ORNL-TM-1851, Oak Ridge National Laboratory, 1967.
27. G. L. Ragan, MSPR, USAEC Report ORNL-4622, p. 31, Oak Ridge National Laboratory, 1970.
28. E. S. Bettis, C. E. Bettis, C. W. Collins, W. K. Furlong, H. A. McLain, J. R. McWherter, and H. L. Watts, MSPR, USAEC Report ORNL-4676, p. 22, Oak Ridge National Laboratory, 1971.
29. H. F. Bauman, MSPR, USAEC Report ORNL-4676, p. 43, Oak Ridge National Laboratory, 1971.
30. A. M. Perry and H. F. Bauman, MSPR, USAEC Report ORNL-4622, p. 26, Oak Ridge National Laboratory, 1970.
31. R. J. Jenson and E. Swanson, Utility Application of Molten Salt Breeder Reactor, *Proc. Amer. Power Conf.*, **31**: 222 (1969).
32. D. R. deBoisblanc and J. R. Trinko, Molten Salt Reactor Technology, Ebasco Services, Inc., New York, 1971.
33. W. R. Grimes, Chemical Research and Development for Molten-Salt Breeder Reactors, USAEC Report ORNL-TM-1853, Oak Ridge National Laboratory, 1967.
34. W. R. Grimes, MSPR, USAEC Report ORNL-3708, p. 214, Oak Ridge National Laboratory, 1964.
35. F. F. Blankenship to W. R. Grimes, personal communication, 1958.
36. M. A. Bredig to W. R. Grimes, personal communication 1968.
37. J. H. Shaffer, D. M. Moulton, and W. R. Grimes, MSPR, USAEC Report ORNL-4344, p. 176, Oak Ridge National Laboratory, 1969.
38. S. Cantor and W. T. Ward, MSPR, USAEC Report ORNL-4676, p. 98, Oak Ridge National Laboratory, 1971.
39. C. F. Baes, Jr., *J. Solid State Chem.*, **1**: 159 (1970).
40. S. Cantor, Physical Properties of Molten Salt Reactor Fuel, Coolant, and Flush Salts, USAEC Report ORNL-TM-2316, Oak Ridge National Laboratory, 1968.
41. H. E. McCoy, MSPR, USAEC Report ORNL-4622, p. 119, Oak Ridge National Laboratory, 1970.
42. R. E. Thoma, MSPR, USAEC Report ORNL-4548, p. 93, Oak Ridge National Laboratory, 1970.
43. L. M. Toth, MSPR, USAEC Report ORNL-4676, p. 118, Oak Ridge National Laboratory, 1971.
44. J. M. Dale, R. F. Apple, and A. S. Meyer, MSPR, USAEC Report ORNL-4119, p. 158, Oak Ridge National Laboratory, 1967.
45. J. M. Dale, A. S. Meyer, R. F. Apple, J. E. Caton, and C. M. Boyd, MSPR, USAEC Report ORNL-4344, p. 188, Oak Ridge National Laboratory, 1968.
46. H. W. Jenkins, D. L. Manning, Gleb Mamantov, and J. P. Young, MSPR, USAEC Report ORNL-4396, p. 201, Oak Ridge National Laboratory, 1969.
47. J. M. Dale and T. R. Mueller, MSPR, USAEC Report ORNL-4676, p. 138, Oak Ridge National Laboratory, 1971.
48. G. Long and F. F. Blankenship, The Stability of Uranium Trifluoride, Part II. Stability in Molten Fluoride Solution, USAEC Report ORNL-TM-2065(Pt. 2), Oak Ridge National Laboratory, 1969.
49. C. F. Baes, Jr., Symposium on Reprocessing of Nuclear Fuels, *Nucl. Met., Met. Soc. AIME*, **15**: 617 (1969); also, USAEC Report CONF-690801, 1969.
50. R. G. Ross, C. E. Bamberger, and C. F. Baes, Jr., MSPR, USAEC Report ORNL-4676, Oak Ridge National Laboratory, 1971.
51. R. E. Thoma, MSPR, USAEC Report ORNL-4548, p. 96, 1970.
52. C. F. Weaver and J. S. Gill, MSPR, USAEC Report ORNL-4676, p. 85, Oak Ridge National Laboratory, 1971.
53. R. G. Ross, C. E. Bamberger, and C. F. Baes, Jr., MSPR, USAEC Report ORNL-4622, p. 92, Oak Ridge National Laboratory, 1970.
54. J. C. Mailen, MSPR, USAEC Report ORNL-4676, p. 245, Oak Ridge National Laboratory, 1971.
55. M. J. Bell and L. E. McNeese, MSPR, USAEC Report ORNL-4676, p. 237, Oak Ridge National Laboratory, 1971.
56. C. E. Bamberger and C. F. Baes, Jr., *J. Nucl. Mater.*, **35**: 177 (1970).
57. C. E. Bamberger, R. G. Ross, and C. F. Baes, Jr., MSPR, USAEC Report ORNL-4548, p. 142, Oak Ridge National Laboratory, 1970.
58. C. J. Barton et al., *Inorg. Chem.*, **9**: 307 (1970).
59. C. E. Bamberger, R. G. Ross, and C. F. Baes, Jr., MSPR, USAEC Report ORNL-4622, p. 91, Oak Ridge National Laboratory, 1970.

*Hereafter abbreviated MSPR.

60. Molten Salt Breeder Reactor Concept, Quarterly Report for Period Ending April 30, 1971, USAEC file No. 18955, Bhabha Atomic Research Center, 1971.
61. F. F. Blankenship, E. L. Compere, and S. S. Kirslis, MSPR, USAEC Report ORNL-4548, p. 104, Oak Ridge National Laboratory, 1970.
62. J. R. Engel and R. C. Steffy, Xenon Behavior in the Molten Salt Reactor Experiment, USAEC Report ORNL-TM-3464, Oak Ridge National Laboratory, 1971.
63. E. L. Compere and E. G. Bohlmann, MSPR, USAEC Report ORNL-4622, p. 60, Oak Ridge National Laboratory, 1970.
64. A. Houtzeel, R. Blumberg, and F. F. Dyer, MSPR, USAEC Report ORNL-4548, p. 11, Oak Ridge National Laboratory, 1970.
65. F. F. Blankenship, MSPR, USAEC Report ORNL-4622, p. 70, Oak Ridge National Laboratory, 1970.
66. R. B. Briggs, MSPR, USAEC Report ORNL-4396, p. 62, Oak Ridge National Laboratory, 1969.
67. S. Cantor, MSPR, USAEC Report ORNL-4254, Oak Ridge National Laboratory, 1968.
68. R. B. Gallaher and A. N. Smith, MSPR, USAEC Report ORNL-4449, p. 74, Oak Ridge National Laboratory, 1969.
69. J. W. Koger, MSPR, USAEC Report ORNL-4676, p. 197, Oak Ridge National Laboratory, 1971.
70. D. M. Richardson and J. H. Shaffer, MSPR, USAEC Report ORNL-4548, p. 136, Oak Ridge National Laboratory, 1970.
71. R. B. Briggs, Tritium in Molten-Salt Reactors, *Reactor Technol.*, **14**(4): 335 (Winter 1971–1972).
72. S. Cantor and R. M. Waller, MSPR, USAEC Report ORNL-4676, p. 88, Oak Ridge National Laboratory, 1971; J. B. Bates, H. W. Kohn, J. P. Young, M. M. Murray, and G. E. Boyd, MSPR, USAEC Report ORNL-4676, p. 94, Oak Ridge National Laboratory, 1971.
73. B. McNabb and H. E. McCoy, MSPR, USAEC Report ORNL-4676, p. 147, Oak Ridge National Laboratory, 1971.
74. P. R. Kasten, E. S. Bettis, W. H. Cook, W. P. Eatherly, D. K. Holmes, R. J. Kedl, C. R. Kennedy, S. S. Kirslis, H. E. McCoy, A. M. Perry, R. C. Robertson, D. Scott, and R. A. Strehlow, Graphite Behavior and Its Effects on MSBR Performance, USAEC Report ORNL-TM-2136, Oak Ridge National Laboratory, 1969.
75. L. E. McNeese, Engineering Development Studies for Molten-Salt Breeder Reactor Processing No. 2, USAEC Report ORNL-TM-3137, pp. 5-21, Oak Ridge National Laboratory, 1971.
76. L. E. McNeese, Engineering Development Studies for Molten-Salt Breeder Reactor Processing No. 3, USAEC Report ORNL-TM-3138, pp. 14-30, Oak Ridge National Laboratory, 1971.
77. L. E. McNeese, Engineering Development Studies for Molten-Salt Breeder Reactor Processing No. 5, USAEC Report ORNL-TM-3140, pp. 12-13, Oak Ridge National Laboratory, 1971.
78. L. G. Carter and E. L. Nicholson, USAEC Report ORNL-TM-3579, Oak Ridge National Laboratory, (in press).
79. F. F. Blankenship, Chemical Separations in Molten Fluorides, in *Thorium Fuel Cycle*, Gatlinburg, Tenn., May 3–6, 1966, R. G. Wymer (Coordinator), AEC Symposium Series, No. 12 (CONF-660524), p. 647, 1968.
80. J. H. Shaffer, W. R. Grimes, G. M. Watson, D. R. Cuneo, J. E. Strain, and M. J. Kelly, The Recovery of Protactinium and Uranium from Molten Fluoride Systems by Precipitation as Oxides, *Nucl. Sci. Eng.*, **18**: 177 (1964).
81. L. E. McNeese, Engineering Development Studies for Molten Salt Breeder Reactor Processing No. 7, USAEC Report ORNL-TM-3257, pp. 52-58, Oak Ridge National Laboratory, 1971.
82. L. E. McNeese, Engineering Development Studies for Molten-Salt Breeder Reactor Processing No. 8, Report ORNL-TM-3258, Oak Ridge National Laboratory, (in press).
83. J. R. DiStefano, MSPR, USAEC Report ORNL-4676, p. 218, Oak Ridge National Laboratory, 1971.
84. L. E. McNeese, Engineering Development Studies for Molten Salt Breeder Reactor Processing No. 3, USAEC Report ORNL-TM-3138, pp. 6-14, Oak Ridge National Laboratory, 1971.
85. L. E. McNeese, personal communication, January 1972.
86. L. E. McNeese, Engineering Development Studies for Molten-Salt Breeder Reactor Processing No. 5, USAEC Report ORNL-TM-3140, pp. 2-15, Oak Ridge National Laboratory, 1971.
87. L. E. McNeese, Engineering Development Studies for Molten-Salt Breeder Reactor Processing No. 9, Oak Ridge National Laboratory (in press).
88. J. R. Hightower, Jr., and L. E. McNeese, Measurement of Relative Volatilities of Fluorides of Ce, La, Pr, Nd, Sm, Eu, Ba, Sr, Y, and Zr in Mixtures of LiF and BeF_2, USAEC Report ORNL-TM-2058, Oak Ridge National Laboratory, 1968.
89. W. L. Carter and M. E. Whatley, Fuel and Blanket Processing Development for Molten Salt Breeder Reactors, USAEC Report ORNL-TM-1852, Oak Ridge National Laboratory, 1967.
90. J. R. Hightower, Jr., L. E. McNeese, B. A. Hannaford, and H. D. Cochran, Jr., Low-Pressure Distillation of a Portion of the Fuel Carrier Salt from the MSRE, USAEC Report ORNL-4577, Oak Ridge National Laboratory, 1971.
91. F. J. Smith, L. M. Ferris, and C. T. Thompson, Liquid-Vapor Equilibria in Lithium Fluoride–Beryllium Fluoride and Lithium Fluoride–Beryllium Fluoride–Thorium Fluoride Systems, USAEC Report ORNL-4415, Oak Ridge National Laboratory, 1969.
92. A. M. Perry, personal communication, Jan. 17, 1969.
93. D. Scott and C. H. Gobbard, MSPR, USAEC Report ORNL-4622, p. 35, Oak Ridge National Laboratory, 1970.
94. D. Scott and W. K. Furlong, MSPR, USAEC Report ORNL-4676, p. 51, Oak Ridge National Laboratory, 1971.
95. E. S. Bettis and R. C. Robertson, The Design and Performance Features of a Single-Fluid Molten-Salt Reactor, *Nucl. Appl. Technol.*, **8**: 204 (1970).
96. A. N. Smith, MSPR, USAEC Report ORNL-4676, p. 52, Oak Ridge National Laboratory, 1971.
97. A. I. Krakoviak, MSPR, USAEC Report ORNL-4676, p. 57, Oak Ridge National Laboratory, 1971.
98. R. Blumberg, Maintenance Development for Molten-Salt

Breeder Reactors, USAEC Report ORNL-TM-1859, Oak Ridge National Laboratory, 1967.
99. P. P. Holz, Feasibility Study of Remote Cutting and Welding for Nuclear Plant Maintenance, USAEC Report ORNL-TM-2712, Oak Ridge National Laboratory, 1969.
100. J. R. Tallackson, MSPR, USAEC Report ORNL-4676, p. 32, Oak Ridge National Laboratory, 1971.
101. M. Grenon and J. J. Geist, Nuclear Breeding, An Argument for Alternative Concepts, *Power Eng.*, p. 42, (December 1971).

IAEA SYMPOSIUM ON NUCLEAR POWER-PLANT CONTROL AND INSTRUMENTATION

Prague, Czechoslovak Socialist Republic, Jan. 22–26, 1973

This symposium is designed to provide specialists from Member States an opportunity for a comprehensive exchange of information on the current international status of the field. It will emphasize problem areas and recent experience in the design, operation, and maintenance of control and instrumentation systems, including relevant aspects of safety and economy.

Topics to be included are:

- Nuclear and process instrumentation: design, reliability, and economic considerations
- Application of experience gained from operating nuclear power plants
- On-line computer applications and related operational, reliability, and safety considerations
- Engineering standards for control and safety systems: considerations of quality control
- Installation testing and in-service inspections
- Potential failure detection: measurement techniques, signal analysis and interpretation, and equipment design

The nomination of a participant will be accepted only if it is presented by the government of a Member State of IAEA or an international organization invited to participate.

For details, persons in the United States should write

Mr. John H. Kane
Office of Information Services
U. S. Atomic Energy Commission
Washington, D. C. 20545

and persons outside the United States should write

Miss C. H. de Mol van Otterloo
Administrative Secretary
Division of External Relations
International Atomic Energy Agency
Kärntner Ring 11
P. O. Box 590
A-1011 Vienna, Austria

CORRECTION

Wayne K. Lehto, one of the authors of the article on pages 345-353 of Vol. 14, No. 4, of this journal, has submitted a correction for the last sentence of the first paragraph in the right-hand column on page 345. That sentence says ". . . this technique . . . has not as yet been applied to thermal reactors at power . . . ." Lehto has learned that such a reactivity-measurement technique was in fact used at Peach Bottom, operating at 25 MW(t). The reference for this added information is: H. Long, R. Schlicht, K. Van Howe, and A. Weiman, Use of On-Line Reactivity Computer To Calibrate Control Rods at Power, USAEC Report GA-8104, Gulf General Atomic, July 12, 1967.

Effects of Metal Swelling and Creep on Fast Reactor Design and Performance

By Paul R. Huebotter*

Abstract: *Dimensional instability of stainless steel, due to radiation-induced swelling and radiation-enhanced creep, profoundly affects the design and performance of fast reactors. This article reviews the design literature in an attempt to clarify the impact of swelling and creep and to scope the options available for accommodating these recently discovered fast-neutron irradiation effects. In this critical review the problems of swelling and creep are stated for selected reactor components, and contemporary-design thinking on each component is presented. The subject is then discussed on a reactor-by-reactor basis with either a summary description of the design strategy to accommodate swelling and creep or, in the case of reactors designed prior to discovery of these phenomena, the impact of swelling and creep that has been experienced or is foreseen. Finally the probable effect of swelling and creep on fast reactor economics is conjectured. This effect is translated into an incentive for research and development focused toward a metallurgical solution to the problem.*

Austenitic (AISI 300 series) stainless steels have long enjoyed favored status as structural materials in the high-flux high-temperature regions of fast reactor power plants or test facilities.[1] Many fast reactors (including Experimental Breeder Reactors I and II, Enrico Fermi 1, Dounreay Fast Reactor, Rapsodie, and BR-5) were designed before irradiation effects on stainless steel had been experienced to even 1% of the fast-neutron fluence now thought to represent the threshold of potentially economic fuel-cycle costs. In the liquid-metal-cooled fast breeder reactor (LMFBR), this commercial threshold is generally regarded as $\sim 2 \times 10^{23}$ neutrons/cm^2 ($E > 0.1$ MeV), although twice that value is desired for target plants in the $\geq$1000-MW(e) size range. The early reactors, of course, were built as irradiation test facilities and/or to demonstrate breeding, operability of sodium systems, technical feasibility of certain fuel-cycle concepts, etc. In the design of these early fast reactors, stainless steel was assumed to be dimensionally stable other than from thermal expansion. The reduction in ductility due to irradiation was acknowledged; however, this ductility loss was generally recognized by designers to be partially compensated by strength enhancement (in solution-treated material) from neutron bombardment. The major objectives in the strategy of core structural design were: (1) to maintain stresses sufficiently low to not challenge the uncertain limits of ductility and (2) to maintain a spatial fuel configuration that is constant or changes predictably and safely during operating transients.

The first of the early reactors to pass the fluence milestone of 5×10^{22} neutrons/cm^2 was the Dounreay Fast Reactor (DFR), and, as it did so, a new and unexpected irradiation effect became apparent in the stainless-steel cladding on experimental mixed-oxide fuel elements. Diametral increases that greatly exceeded the presumed ductility limit were seen. On detailed examination, including immersion-density measurements and transmission electron microscopy (TEM), swelling of 7% $\Delta V/V$ at 7.8×10^{22} neutrons/cm^2 (all energies) and 500°C was revealed and reported.[2] Within months the phenomenon was confirmed in stainless steel irradiated in Experimental Breeder Reactor II (EBR-II).[3,4]

Since these early papers, additional in-reactor data, metallurgical theories, extrapolations, and out-of-reactor simulation in ion-bombardment facilities have become abundant. These activities, and the trend of progress toward a metallurgical solution to the swelling

*Materials Science Division, Argonne National Laboratory, Argonne, Ill. 60439.

problem, were recently reviewed by Kangilaski.[5] Although today's designer has a more complete understanding of fast-neutron irradiation effects than that enjoyed by his predecessors, considerable extrapolation of existing data is required to predict swelling in future reactors. Illustrating this point, Fig. 1 shows[6] the status of swelling data vs. the objectives of the U. S. LMFBR program (in terms of fast fluence) and the EBR-II operating time needed to acquire fluence. Actually the required extrapolations are greater than suggested in Fig. 1 because all of the high-fluence data from EBR-II safety- and control-rod thimbles apply to solution-treated 304 stainless steel at temperatures below 850°F. Fast Flux Test Facility (FFTF) and demonstration plant designers require data on 316 and other stainless steels, annealed as well as cold worked, to temperatures around 1400°F to cover cladding hot-spot conditions with uncertainty factors.

Thus, since swelling was discovered in 1967, the major challenge in the field of fast reactor core design has been to predict the nature of dimensional changes in reactor components and to accommodate these changes by design provisions compatible with the other properties of reactor materials, the general characteristics of fast reactors (including neutronic sensitivity to fuel movement), and the objectives and constraints of specific reactors. The literature on design implications of, and design solutions to, the swelling phenomenon was sparse during the first 2 years. This silence was due in part to the traumatic and unsettling effect of this discovery on "preswelling" approaches to core design, including the approaches revealed in the two rounds of AEC-sponsored 1000-MW(e) LMFBR design studies.[7-16] Another reason for the dearth of literature in the 1968–1969 era was the tendency for design judgments to be withheld as having proprietary value, in contrast with metallurgical data, theories, and extrapolations which largely flowed from government-sponsored base-technology programs. In any case, the past 2 years have produced a more open disclosure of the position of core designers on the swelling issue.

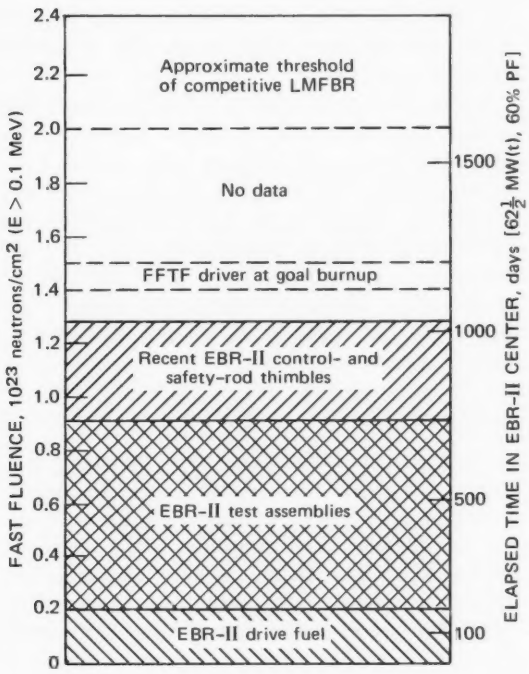

Fig. 1 Status of swelling data and required test time vs. program objectives.

The phenomenon of radiation-enhanced creep, poorly characterized and generally ignored by designers before the discovery of swelling, has emerged as a very important property in certain strategies of designing for swelling. It is now the usual practice of core designers to discuss both subjects together, as will be done in this article. The metallurgical literature on radiation-enhanced creep has been recently reviewed by Gilbert.[17] Core designers of the FFTF have mostly used a creep equation furnished by Gilbert and Blackburn.[18] As in the case of swelling, considerable extrapolation of existing data (at least a factor of 10) was required to produce a design equation for target-fluence conditions in the FFTF and the U. S. demonstration plants. Unfortunately the models for this extrapolation are not completely resolved, a fact that results in wide differences in high-fluence creep estimates among researchers in this field. This point is illustrated by Fig. 2, which shows the 1970 FFTF creep expression in terms of creep rate as a function of temperature for a single value of stress and two values of fluence. The fluence dependence arises from a transient term in the design equation which saturates at relatively low fluence and contributes little to the total creep strain at high fluence and hence nothing to the creep rate at that time. Figure 2 also shows some Argonne National Laboratory (ANL) estimates of radiation-enhanced creep rate under equivalent conditions.* These estimates, based on a "climb-

*The comparison is made at an arbitrary stress of 30 ksi. At 10 ksi the ANL creep rate would be reduced by a factor of 9 and the FFTF estimates by a factor of 3. At high temperatures (>900°F), this brings the two models into closer agreement, but, in the important 600 to 900°F temperature range, the models are even more divergent at low stress.

controlled" model of radiation-enhanced creep proposed by Harkness, Tesk, and Li,[19] have changed in minor detail as a result of recent work, but the comparison illustrates the present dilemma of the designer with respect to this important property.

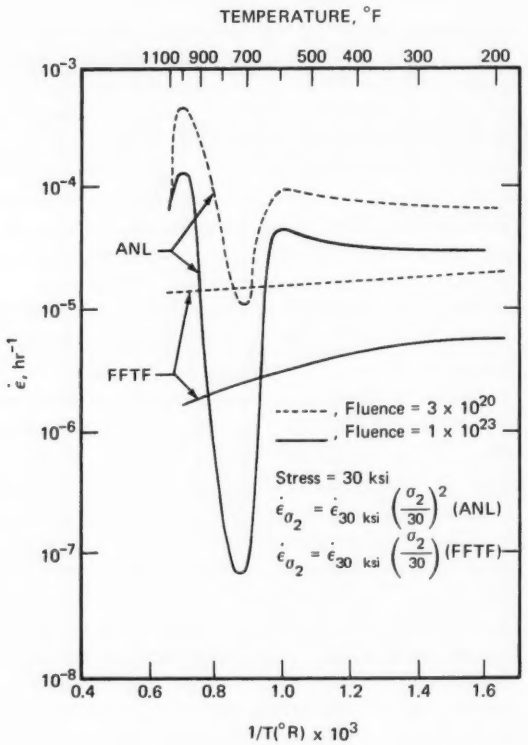

Fig. 2 Estimated radiation-enhanced creep rates from two different models.

The present design climate, therefore, is characterized by uncertainty in the amount of swelling and creep that will occur in the next generation of fast reactors. Designers with a tendency to use design equations literally are reminded by Häfele et al.[20] that "the existence of a mathematical expression should . . . mislead nobody about the large errors and uncertainties involved." Most core designers, including those attached to the FFTF project, employ upper and lower confidence limits on the swelling and creep design equations. Ideally, although this climate of uncertainty persists, key reactor components should be designed for flexibility to operate satisfactorily over a wide range of combined swelling–creep behavior.

EFFECTS ON KEY REACTOR COMPONENTS

Although swelling and creep of core structural material can affect the design strategy of the entire plant, it is convenient to analyze separately the effects of these phenomena on individual reactor components. In doing this analysis, it is helpful to divide the reactor components into two categories as follows: (1) items whose service lives are short compared to that of the plant, so that they are packaged for routine replacement by the fuel-handling machine; and (2) items not easily changed during the life of a particular plant, so that they are designed for 20 to 40 years of service.

Generally items in the first category have no inherent design permanence, and inadequate provisions for swelling and creep can be rectified at a cost of a few years' operation with somewhat reduced service from these expendable units. Although this cost is not trivial, it is considerably less than that of foreshortened plant lifetime; thus, where uncertainties in materials properties exist, the designer can employ a "bootstrapping" strategy rather than one of ultraconservative design. Components in this category include: fuel, blanket, and control elements; fuel, blanket, and control assembly internals; and ducts,* although somewhat less flexibility may exist here since duct design is closely tied to core-restraint design, thus implicating hardware in category 2.

Components in the second category require special caution and conservatism in design because, if the effects of swelling and creep are badly estimated, the operation of the reactor may be interrupted for a long maintenance outage or be aborted completely. The core-restraint system, load-support structure, and instrument tree are examples of components in this category. The effects of swelling and creep on the design and performance of selected reactor components are reviewed below.

Fuel Elements

Prior to the swelling discovery, American fuel-element designers were divided in their relative preference for strength or ductility in the inevitable trade-off between these properties when selecting a cladding alloy. The British, on the other hand, have always preferred strength, which accounts for the appearance of cold-worked stainless steel in the devel-

*Also known as wrapper tubes, channels, housings, shrouds, hex cans, and boxes. Throughout this article, the nomenclature used in the FFTF project has been adopted.

opment program of the U. K. Atomic Energy Authority (UKAEA) prior to the discovery of swelling. Now, Bishop generalizes that "cladding of low strength and greatest ductility appears to show greatest swelling, and vice versa,"[21] and so the UK designers' preference for strength is even greater. Alloys FV 548, a stabilized stainless steel of composition similar to AISI 318, and Nimonic PE16, a high-nickel precipitation-type alloy, are being developed as future cladding materials. The low-swelling tendencies of the latter, if ion-bombardment results are confirmed by high-fluence neutron irradiation, could make it especially valuable as a future duct material.

The empirically established swelling resistance of cold-worked 316 stainless steel has produced a general consensus favoring its use for fuel-element cladding in near-term facilities in the United States, although other stainless steels, especially carbon-stabilized ones, are being evaluated.[22]

The Edison Electric Institute (EEI), speaking for potential U. S. customers for fast reactor power plants, sounded an early alarm about the implications of the swelling discovery.[23] The EEI panel focused their concern on the issue of fuel-element lifetime, suggesting the need to discount successful irradiations of mixed-oxide fuel elements in EBR-II and DFR by a factor of 3 to 4 in burnup, equivalent to the neutron-flux differential between these small test reactors and the target commercial plants. Figure 3 illustrates this point showing swelling-induced cladding dilation as a function of burnup for a typical mixed-oxide fuel element in the EBR-II, the FFTF, and a commercial LMFBR. The estimates of both absolute and relative swelling depend on the swelling correlation in use,* but clearly more cladding swelling per unit burnup is to be expected in reactors with greater high-energy flux.

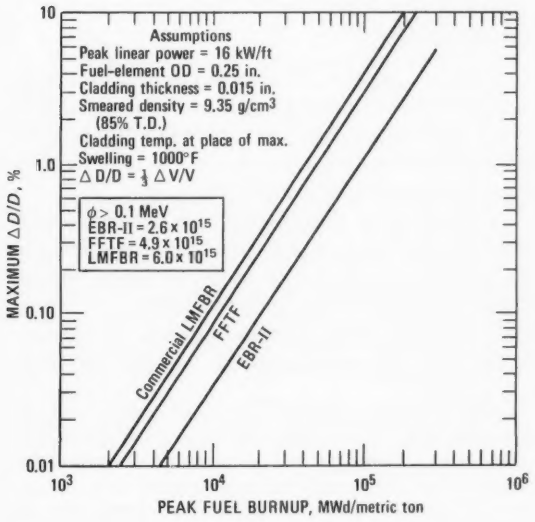

Fig. 3 Cladding dilation from radiation-induced swelling in three fast reactors.

For the past 3 years, two important issues relevant to the EEI concern have been debated. These are:

1. Is the additional cladding dilation good or bad in terms of fuel-element lifetime?
2. How much of the diametral increase measured in test elements is due to swelling and radiation-enhanced creep (thought by many to be innocuous), and how much is due to fuel–cladding mechanical interaction and thermal creep from gas pressure (the accepted failure causes)?

Selected excerpts from that debate are given below:

Bump[24]: "One consequence of cladding swelling is the provision of more room for gas in the fuel, thus lowering the pressure of that gas and, in turn, the pressure exerted on the cladding by fuel swelling."

Boltax et al.[25]: "Figure 4*a* shows the [cladding] stress accumulation when stainless-steel swelling is comparatively small . . . e.g., in EBR-II and DFR . . . . Figure 4*b* shows the behavior of the hoop stress when stainless-steel swelling is large, as in the case of high fluence/burnup pins [in a commercial LMFBR]."

Bagley et al.[26]: "It has been found . . . that pin strain normally correlates well with clad swelling so that void-development tendencies may validly be inferred from fuel pin [diametral increase]."

Jackson et al.[27] The measured diameter increase of these two fuel pins [PNL 2-3 and 2-6] is almost entirely a result of cladding swelling, and the small difference between measured and predicted diameter is error."

Neimark et al.[28]: "Mechanisms other than cladding swelling alone are contributing to the diametral increases [of NUMEC Group C elements with burnup of ~10%]."

Craig et al.[29]: "Smeared fuel density *appears* to have a major effect on the diametral increases of these [NUMEC D-5 and General Electric F2 series with burnups up to ~12%] fuel pins."

*The estimates in Fig. 3 conservatively assume a fluence exponent of 1.5 and no saturation of swelling beyond the range of current experience.

Boltax et al.[30]: "The results [of computer studies] reveal the major effect of fuel pellet density on total plastic strain of the cladding. The benefits obtained from lowering the fuel pellet density are reduced significantly at cladding temperatures where thermal creep becomes important ($T > 550°C$)."

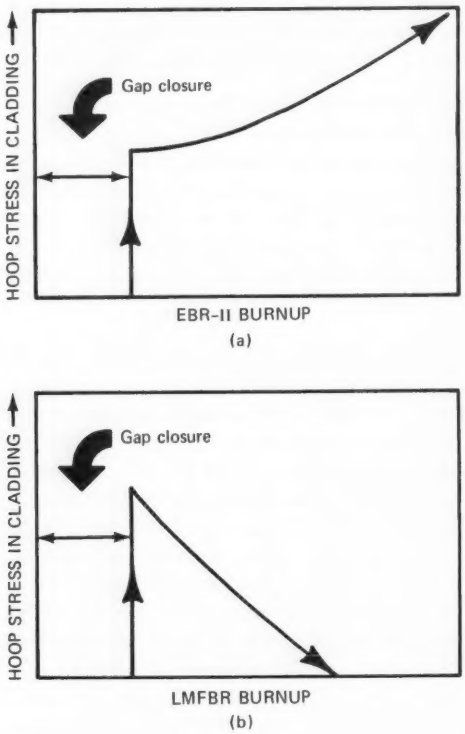

Fig. 4 Postulated cladding-stress history in EBR-II and a commercial LMFBR.

In a recent review paper on mixed-oxide fuel technology for the LMFBR, Leggett[31] concludes that: "Cladding swelling presents few significant problems to *fuel pin performance* [emphasis in original] but must be completely defined for assembly design and compatibility with the rest of the core components." In another recent assessment of the critical factors in mixed-oxide fuel-element design, Roake[32] observes that: "We have come full circle since 1966; i.e., pin design life was governed (in chronological sequence) by (1) fission gas pressure and fuel swelling, (2) stainless-steel swelling, (3) radiation-enhanced creep and swelling gradients, and now, but at a higher burnup, (4) fuel swelling."

It is interesting that, other than the recognized need to consider swelling resistance as a major criterion for cladding selection, the debate over the effects of swelling on fuel-element performance has produced negligible fuel-element design changes. Table 1 gives some of the principal design parameters for fuel elements in oxide-fueled sodium-cooled fast reactors of comparable size. Note that there is no obvious pattern of design difference between fuel elements designed before the swelling–creep problem came to light (BN-350, PFR, and Phenix) and those designed after the problem was recognized (SNR, FFTF, and the U. S. demonstration plants designed by Atomics International, General Electric, and Westinghouse).*

The current consensus of both development and design people is that swelling should not be regarded primarily as a "cladding problem" or a "fuel-element problem." It is also recognized, however, that a burnup limit on fuel elements could result if designers do not properly cope with swelling in the design of other core components. Fuel-element designers now work on the optimistic assumption that core-swelling effects will not limit fuel burnup, and fuel elements are designed as the components pivotal to core lifetime; hence, essentially the same as before swelling was discovered. If this assumption proves wrong, and allowable fuel burnup is dictated by core-swelling effects, the economic loss can be partially recouped through the use of higher smeared density and the relaxation of fabrication specifications that purchase burnup capability beyond the usable range.[6]

Fuel Assemblies

Table 2 presents selected fuel-assembly design parameters for the same group of oxide-fueled sodium-cooled fast reactors. As in the case of fuel elements, no revolution in design practice appears to have resulted from the discoveries of swelling and creep.

The wire-wrap spacer system has been chosen in both the preswelling and postswelling design eras, as has the principal alternative—compliant grids. Neither is free of problems arising from swelling and creep. Both systems must be carefully designed for accommodation of differential swelling between the fuel-

*One of the few apparent correlations in Table 1 is that most reactors in the first group have bottom-end gas plenums and most in the second group have top-end plenums. Since the bowing of fuel assemblies is exaggerated by top-end plenums, this difference is clearly not a conscious reaction to the swelling problem. Instead, it appears to be a U. S. vs. European difference of opinion on the safety implications of gas stored upstream from the core.

Table 1 Fuel-Element Design Parameters in Oxide-Fueled LMFBRs Under Design and Construction*

Parameter	Reactors designed before swelling was discovered			Reactors designed after swelling was discovered				
	BN-350	PFR	Phenix	SNR	FFTF	AI demonstration	GE demonstration	Westinghouse demonstration
Fuel form	Annealed pellets	Annealed pellets	Solid pellets	Solid pellets	Solid pellets	Solid pellets		
Smeared density, %	73	80	78	80	85.5	80		
Target burnup (av.), MWd/kg				55	45	75	40†/84‡	75
Target burnup (peak), MWd/kg	46	69	50†/100‡	80	80	110	124‡	103
Linear power (peak), kW/ft	13.4	15.1	14.1	13.8	13	14.5	11.7†/14.5‡	13.8
Location of fission-gas plenum	Top	Bottom	Bottom	Bottom	Top	Top	Top†/vent at top‡	
Fission-gas plenum length, in.	<3	28 (red. diameter)	16.5	25.6	42	26	30	
Fuel length, in.	41.8	36	33.5	37.4	36	44	30	35
Cladding material	"Russian 316"	316 S.S., 20% C.W.	316 S.S.	Open	316 S.S., 20% C.W.	316 S.S., C.W.	321 S.S.	316 S.S., 20% C.W.
Fuel-element diameter, in.	0.240	0.23	0.260	0.236	0.23	0.27	0.25	0.25
Cladding thickness, in.	0.014	0.015	0.018	0.015	0.015	0.016	0.015	0.016

*Missing values are not available in the open literature. †First core. ‡Target core.

Table 2 Fuel-Assembly Design Parameters in Oxide-Fueled LMFBRs Under Design and Construction*

Parameter	Reactors designed before swelling was discovered			Reactors designed after swelling was discovered				
	BN-350	PFR	Phenix	SNR	FFTF	AI demonstration	GE demonstration	Westinghouse demonstration
Type of hold-down	Hydraulic	Hydraulic	Hydraulic	Hydraulic	Hydraulic	Hydraulic	Hydraulic	Mechanical
Sodium velocity (max.), ft/sec	26	20 (free stream)	24	20 (free stream)	25	31.2		20.6 (free stream)
Type of duct material	"Russian 316"	S.S., C.W.	316 S.S.	Open	316 S.S., 20% C.W.	316 S.S., C.W.	321 S.S.	316 S.S., 20% C.W.
Fuel-element pitch/diameter (dimensionless)	1.15	1.26	1.16	1.29	1.24	1.17	1.28	1.24
Type of fuel-element support	Wire wrap (alt. pins)	Honeycomb grid	Wire wrap	Grid	Wire wrap	Wire wrap	Wire wrap (ref.)	Honeycomb grid
No. of fuel elements/assembly	169	325	217	169	217	271	127	217
Fuel-assembly width, A/F, in.	3.780	5.54	4.87	4.34	4.575	5.570	3.849	
Fuel-assembly in-core pitch, in.	3.859	5.7	5.01		4.715	5.887	4.009	5.122
Duct thickness, in.	0.079	0.115 (min.)	0.138	0.110	0.120	0.125	0.086	

*Missing values are not available in the open literature.

element bundle and the duct, and the wire-wrap system must also accommodate some differential swelling between the wire and cladding. Greater swelling of the cladding than an initially taut wire has produced pronounced helical distortion of high-burnup fuel elements[28] but no known failures in the U. S. fuel-development program. These swelling differentials can arise from temperature differentials (typical values are shown in Fig. 5, taken from Ref. 33) or from differences in composition or temper possibly so subtle as to be presently unrecognized as significant variables in swelling behavior. A problem in grid design is how to attach it to the duct. Creep will tend to round the ducts by as much as 0.070 in. per flat, based on contemporary creep estimates* and fuel-assembly design parameters, and this rounding could distort a grid attached directly to the duct. Hanger straps and other concepts that permit duct–grid differential deflection are under development to solve this recently recognized problem. In Core A of Enrico Fermi 1, grids are fixed to vertical tie rods, thus creating a "birdcage" structure which slips into the duct and is anchored to it at the lower end.[35] This avoids the problem of direct attachment to the duct but tends to promote more peripheral flow than is desired. Grids were chosen for Fermi 1 because of the use of a square pitch in which the wire wrap is unstable. The EBR-II, designed in the same era, uses wire wraps and a triangular pitch.[36]

Speaking for the British designers, whose Prototype Fast Reactor (PFR) uses grids attached to the duct for fuel-element support, Bishop[21] offers the opinion that it is less difficult to avoid the undesirable extremes of mechanical interference and vibration in the gridded concept than in the concepts that employ non-compliant fins or wires on the cladding. Westinghouse, with considerable experience with gridded spacer systems in pressurized-water reactors and in the U–10 wt.% Mo core of Enrico Fermi 1, shares the British preference for grids in LMFBRs. They contend that, if the duct, cladding, and wire should follow swelling laws that differ from one another in the adverse direction, metal swelling could impose a burnup limit on the wire-wrap concept as low as 30,000 MWd/metric ton in a high-flux LMFBR.†[37] Wire-wrap

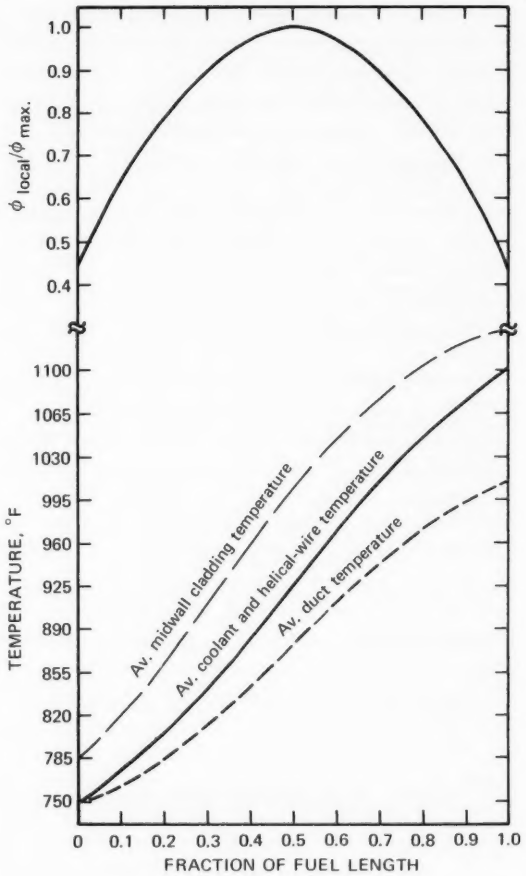

Fig. 5 Typical axial profile of average metal temperatures in an LMFBR fuel assembly.

proponents contend that this conclusion is valid only if the wire-wrap design is unnecessarily handicapped by little or no internal clearance at beginning of life. General Electric (GE) core designers have selected the wire wrap as their reference demonstration-plant fuel-element support concept, although a grid spacer concept which is "potentially more attractive than the wire wrap with respect to differential swelling, fuel performance and thermal hydraulics" is under development.[38] The reference GE wire-wrap system provides radial compliance to accommodate differential swelling by: (1) initial clearances built into the assembly, (2) staggered-start wires, and (3) omitted wires on selected elements. Atomics International (AI) has unequivocally chosen the wire-wrap system as a result of their fabrication and test program, which satisfied

*The EBR-II driver-fuel duct rounding has been observed at a total fluence of only 1.9×10^{22} neutrons/cm^2, and it agrees with calculated rounding within the range and accuracy of measured values.[34]

†This analysis did not include the effects of radiation-enhanced creep which tend to mitigate the consequences of adverse differential swelling.

them that the small-amplitude bowing of the multiplicity of fuel elements within the duct will exert sufficient mechanical interaction to avoid vibration, fretting, and wear even when the planar clearance is enough to absorb differential swelling.[39] Atomics International prefers the wire wrap because of lower cost, twice the interchannel mixing, and only two-thirds as much pressure drop compared with gridded designs.[40]

As part of a general assessment of the design, research, and development implications of metal swelling in fast reactors, Huebotter et al.[6] concluded that: (1) sufficient design accommodation could safely be made for the differential axial and radial swelling likely to occur in wire-wrap support systems in near-term LMFBRs; (2) the fuel-element support system is unlikely to emerge as the burnup-limiting component of near-term cores; (3) the choice of a fuel-element support system is not an irrevocable 30-year decision but is one that can be reconsidered for follow-on cores when metal swelling and other pertinent behaviorisms are better characterized; and (4) since the adequacy of the wire-wrap system at fluence targets for commercial fast reactors is still a matter of industrial disagreement, opportunities should be sought to test representative grid designs. On the basis of such reasoning, the FFTF project has chosen the wire-wrap concept for initial use, but the U. S. LMFBR program is supporting grid-development projects at GE and Westinghouse, which will both include testing in EBR-II as adjuncts to fuel-element irradiation programs.

In principle, differential dilation between the duct and the contained fuel elements can produce cladding overheating by restriction of coolant passages. In practice, however, this effect is of minor concern. It has been estimated, for example, that the hot-spot temperature of the PFR cladding is increased only 11°F due to a uniform 1% increase in fuel-element diameter over the entire 36-in. core length with no compensating duct dilation.[21] In actual reactor operation the effect would be even less for either whole-core or partial-core refueling strategies. With whole-core refueling the differential dilation develops in all assemblies at approximately the same rate. Therefore a general increase in hydraulic resistance would be compensated by increased pump speed to maintain constant core flow and mixed-mean outlet temperature. With partial-core refueling, increased hydraulic resistance in the older fuel assemblies would tend to be offset by their decline in heat generation due to fissile-atom burnup. Leduc et al.[41] point out that bowing of the duct relative to the fuel elements increases the overall hot-channel factor for the cladding by changing random (statistical) geometric aberrations into systematic (multiplicative) ones. Other than in fuel-element bundles with a very low pitch/diameter ratio, however, swelling is not regarded as a significant factor in normal heat removal from the LMFBR core.

A design-sensitivity study by Burchill and Menzel[42] has shown that, if the successful accommodation of swelling and creep requires some form of positive core restraint (see below), fuel-assembly dimensions might well be influenced. Hoop stresses, for example, vary as the duct diameter cubed and inversely as the pad thickness squared. In large assemblies, duct stresses can be the limiting factor in design.

Core Restraint

Observers on both sides of the Atlantic[21,43] regard the core-restraint system as presenting the greatest design challenge with respect to successful accommodation of swelling and creep in core stainless steel. In fact, the term "core restraint" has found common usage only since the discovery of the swelling phenomenon, implying the recognition of new problems and a higher degree of design emphasis. Unlike fuel elements and fuel assemblies, the core-restraint system implicates reactor internals not easily changed during the life of the plant. Therefore the strategy of periodic upgrading of design as more and better materials data are acquired does not pertain to the core-restraint system as it does to expendable core components.

The functional requirements of the core-restraint system can be summarized as follows:

1. *Reactivity Control.* Produce a safe, calculable, and reproducible structural response of the core to steady-state and transient operation.

2. *Alignment.* Maintain desired juxtaposition between the in-core and above-core components of the nuclear control system and between reactor-assembly effluent streams and downstream instrument sensors.

3. *Refueling.* Provide adequate clearance and achieve adequate duct straightness for reactor assemblies to be inserted and removed within an acceptable range of vertical forces.

Fast reactor core-restraint systems, including those designed before swelling and radiation-enhanced creep were discovered, fall into three categories. For each of these categories, the essential design features and general response to swelling and creep are discussed below.

Positive Restraint. Designs in this category employ external mechanisms, such as the hold-down assembly in Enrico Fermi 1 or the peripheral clamps in the FFTF, to gather at least the high-worth reactor assemblies into a tight array before criticality is approached. With this tight cold array, in which the centerline location of each assembly is known at specific elevations, one of which is in or near the core, structural reactivity effects are calculable with an accuracy limited only by uncertainties in spatial temperature distribution. Alignments are assured, usually by making the downstream end of the assembly one of the elevations of fixed radial position, and refueling clearances are produced by release or withdrawal of the restraint mechanism.

In positive-restraint systems the characteristic interaction between thermal expansion effects, swelling, and creep is shown[44] in Fig. 6. When only thermal strains are considered, the bowing profile of all assemblies except that at the core center line is qualitatively represented by Fig. 6(*a*). Differential swelling alone would produce such shapes as that shown in Fig. 6(*b*), and the additive effect of thermal and swelling strains is represented by Fig. 6(*c*). In suppressing free bowing in the direction that would be produced by differential thermal elongation and differential swelling elongation, the core-restraint system imposes high bending stresses. The relaxation of these stresses, by radiation-enhanced creep, alters the bowing profile markedly [Fig. 6(*d*)]. The shapes qualitatively depicted in Fig. 6 are a function of time, location in the reactor, and the design equations for swelling and creep.

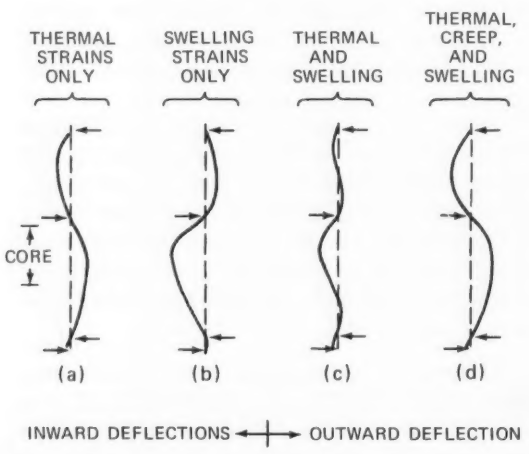

Fig. 6 Assembly-deflection patterns characteristic of positive core restraint.

When the core is released for fuel handling, the assemblies assume shapes of a basically different character, as shown[44] in Fig. 7. Again, it is convenient to analyze separately the three factors responsible for distortion. With the reactor at zero power, the thermal strains are removed, and the assemblies would be

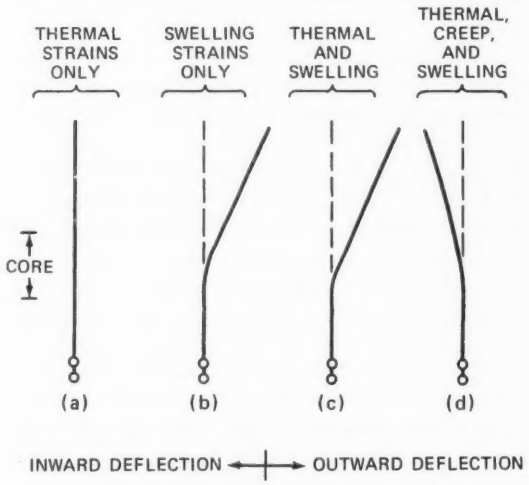

Fig. 7 Typical assembly-deflection patterns after removal of positive core restraint.

straight [Fig. 7(*a*)] if no other distortion mechanisms were operative. Differential swelling is not reversible, however, and so the upper ends would tend to splay outward [Figs. 7(*b*) and 7(*c*)] when freed of restraint. With sufficient stress relaxation at power, however, the profile at zero power can actually be reversed [Fig. 7(*d*)]. The position of the top end of each reactor assembly, which must be known within fairly close limits for blind fuel handling,* is a strong function of swelling and radiation-enhanced creep.

Passive Restraint. Designs in this category, which include EBR-II, Rapsodie, and Phenix, have the following generic features:

1. Core assemblies are cantilevered from their inlet nozzles and are vertically aligned by two-point support thereon.

2. The top ends of core assemblies are radially unrestrained other than by mechanical interference

*In existing fast reactors the allowable uncertainty in handling-head position in the r,θ plane is 0.25 to 0.5 in. Improved fuel-handling designs are being developed to increase the allowable uncertainty to 1 in. or more.

with, and the longitudinal stiffness of, outboard rows of blanket and/or reflector assemblies. Forces tightening the core at a spacer-pad plane are generated when "free-flowering" edge-core assemblies are opposed at the top ends by these straight outboard rows.

3. Refueling clearance is provided exclusively by the cold clearances between spacer pads, which are typically at one elevation in or near the core.

Mechanical interactions are produced between assemblies in the passive-restraint concept, and these are capable of inducing sufficient stress to affect the final shape of assemblies through radiation-enhanced creep. Figure 8 illustrates[45] the calculated time-dependent mechanical interactions affecting a high-fluence test assembly in EBR-II. Compared to the positive-restraint designs, however, one is less likely to encounter reactor assemblies with creep-dominated residual shapes because the thermal bowing is unrestrained over at least part of the power range. An ideal design strategy has been suggested[46] to be one in which all or most of the thermal bowing is allowed to occur without restraint while resisting the additional bowing caused by differential swelling. This permits creep to mitigate the permanent bowing of core assemblies without risking the concave (relative to the core center line) bowing produced by relaxation of stresses incurred in suppressing thermal bowing. These concave curvatures can produce an undesirably loose core at low power.

No Restraint. In designs of this category, assemblies are cantilevered from their nozzles* or from a support point between the nozzles and the core† and are unrestrained at the top end over the entire power range. The structural reactivity effect is dependably

*An example is the Gulf General Atomic gas-cooled fast reactor demonstration plant.[47]

†An example is the British Prototype Fast Reactor.[48]

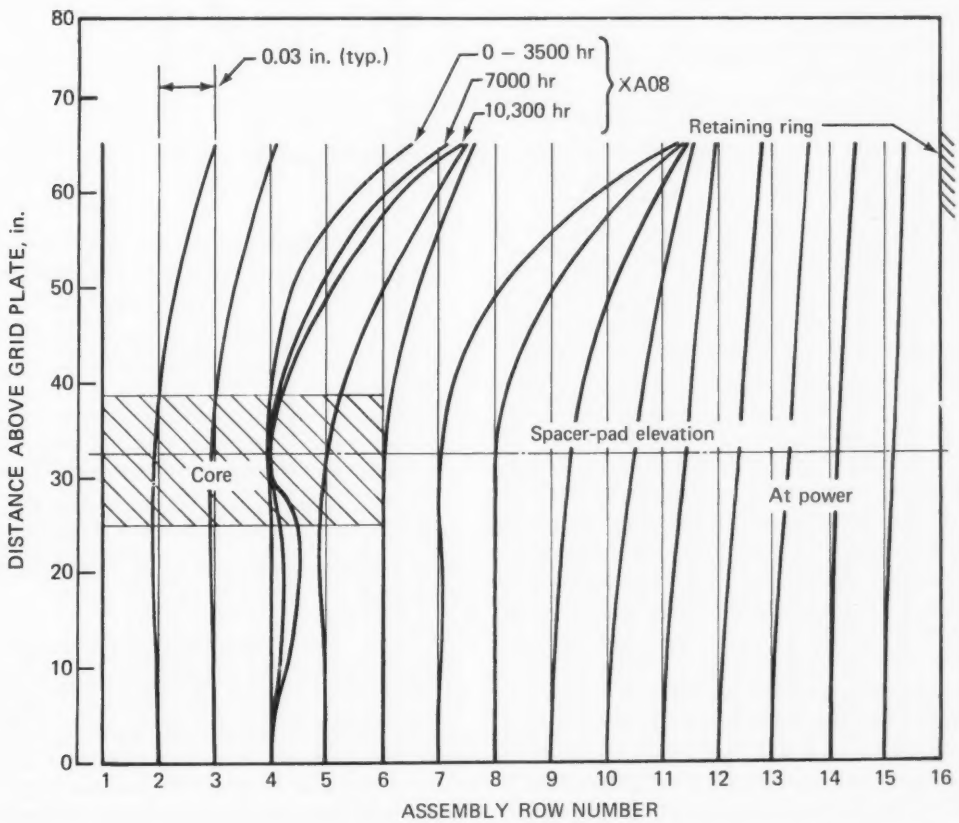

Fig. 8 Time-dependent mechanical interactions between assemblies in EBR-II.

negative since thermal bowing moves fuel away from the core center line.

In this approach, creep is not a design factor because bending stresses are not produced. Thus the assemblies assume the residual swelling-dominated curvatures [Fig. 7(*c*)] resulting from flux and temperature gradients. Periodic rotation is generally envisaged as the operational strategy to preclude an unacceptable degree of bow from the standpoint of alignment and fuel handling. Whether periodic rotation will be an acceptable operational practice in commercial fast reactors will depend on the frequency with which it must be done.

Both thermal bowing and bowing from differential swelling are a strong function of duct length downstream from the core. Figure 9 shows[6] the typical contribution to overall bowing from the portions of the duct containing the fuel, the upper axial blanket, and a downstream gas plenum. For minimization of bowing, particularly important in this category of core-restraint design concepts, the upstream gas plenum is advantageous.

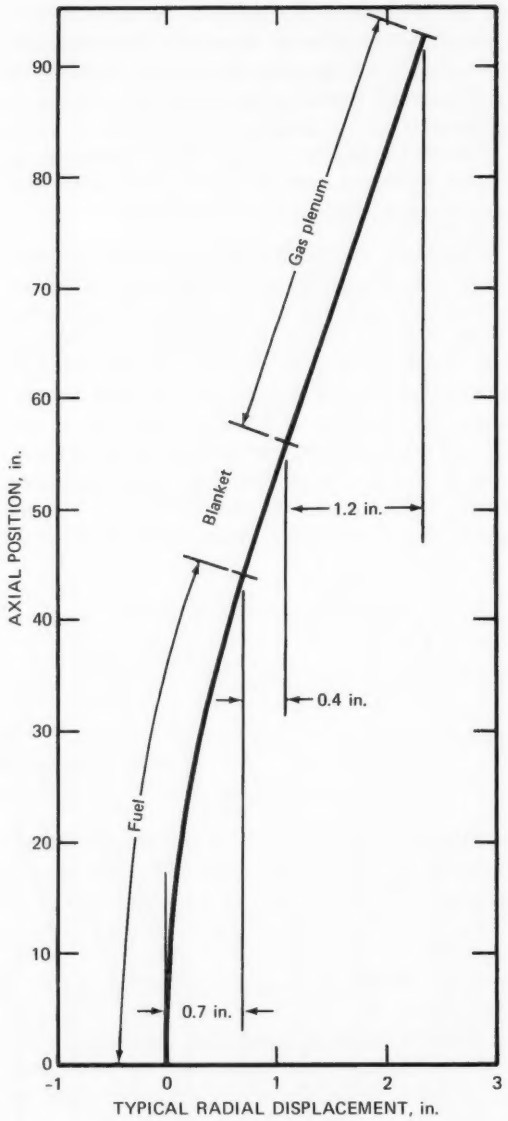

Fig. 9 Typical contributions of fuel and above-fuel length to free bowing.

Other Reactor Components

The extent to which other reactor components are implicated in the general problem of radiation-induced swelling and radiation-enhanced creep of stainless steel is difficult to assess in general terms because of wide variations in the design of reactor internals other than those discussed above. Some specific observations, such as those given below, can be made, however.

1. Elongation of assemblies, and differences in elongation, will complicate the design of fuel-handling equipment somewhat. Figure 10 shows[6] end-of-life elongations of reactor assemblies in the AI 1000-MW(e) design[12] based on the 1969 FFTF swelling predictions for 20% cold-worked 316 stainless steel.[25] More flexibility in the fuel-handling equipment is needed than when the assembly lengths are constant and uniform. With only a 14-in.-long core, EBR-II duct elongations have been limited to $\frac{3}{8} \pm \frac{1}{16}$ in., but these have caused handling difficulties because they were unanticipated in the design.[49]

2. Some reactors employ a sweep arm or similar device to assure that assemblies are properly seated on the grid plate. Length increases will tend to mask the evidence of improper seating, particularly in a core containing both old (long) and new (short) assemblies.

3. Aside from its incompatibility with significant length increases, the EBR-II fuel-handling system has been given much of the credit for successful operation despite unanticipated swelling effects.[50] The key feature is the hold-down mechanism that spreads the six assemblies adjacent to the one being inserted or withdrawn, thus creating the necessary local clearance.

4. Swelling of the grid plate, instrument plate, and other core-proximity "permanent" hardware will probably be avoided by the fluence limits imposed to retain the desired ductility (generally $< 10^{22}$ neutrons/

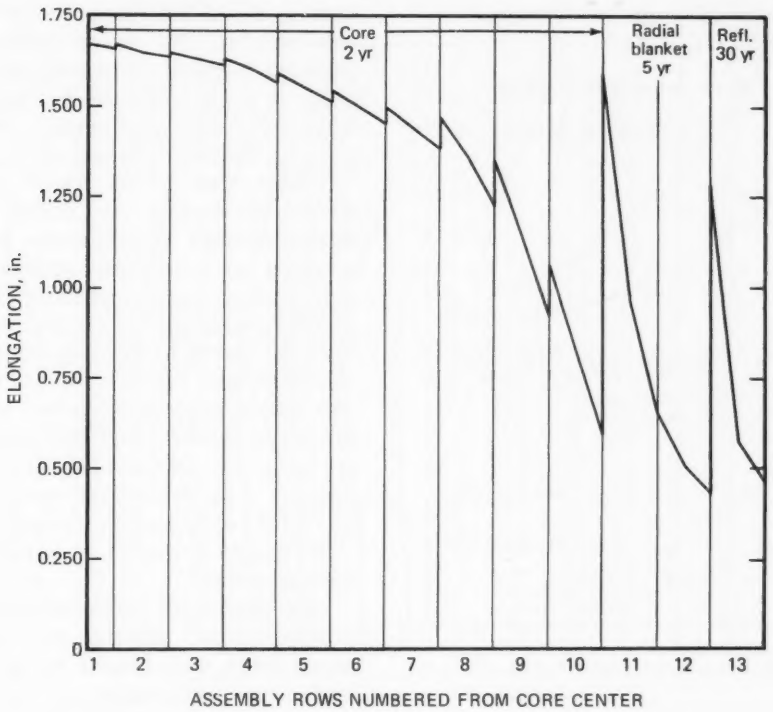

Fig. 10 Component elongations due to swelling in a 1000-MW(e) LMFBR.

cm^2). Extra shielding of components beyond the ends of the assemblies is conveniently purchased with small increases in axial blanket lengths. Figure 11 shows[6] the effect of blanket length on grid-plate and instrument-plate flux in the AI 1000-MW(e) design.[12] Grid plates, whose designs are generally governed by deflection criteria rather than stress criteria, cannot be permitted to undergo significant differential swelling. Fortunately theoreticians[51] believe that low flux will produce less swelling than high flux to the same fluence. This works to the advantage of the core-proximity hardware of long life expectancy.

EFFECTS ON SOME PRESENT AND FUTURE FAST REACTORS

The effects of swelling and creep have been felt in operating fast reactors, which in no case were designed to accommodate these effects but can still yield valuable engineering insight into how to design future reactors. This group is represented by EBR-II and Enrico Fermi 1.

In the next grouping are the Russian BN-350, the British PFR, and the French Phenix, all scheduled for criticality between late 1971 and early 1973. These facilities were in an advanced stage of design when the swelling–creep properties gained recognition. In general, these phenomena were not permitted to perturb the designs significantly.

Finally, indications of how fast reactor designers have responded to the problems of swelling and creep in an overall sense are available in the literature describing reactors still in design or in the early stages of construction. This group of reactors includes the German-Benelux SNR, the FFTF, and the U. S. demonstration plants being designed by Atomics International, Combustion Engineering, General Electric, Gulf General Atomic, and Westinghouse.

As we have already seen, major differences in design philosophy are not found in the design of fuel elements and assemblies. Therefore this reactor-by-reactor assessment of the impact of swelling and creep on design and performance will concentrate on the core-restraint system and the other reactor internals sensitive to the swelling–creep phenomena.

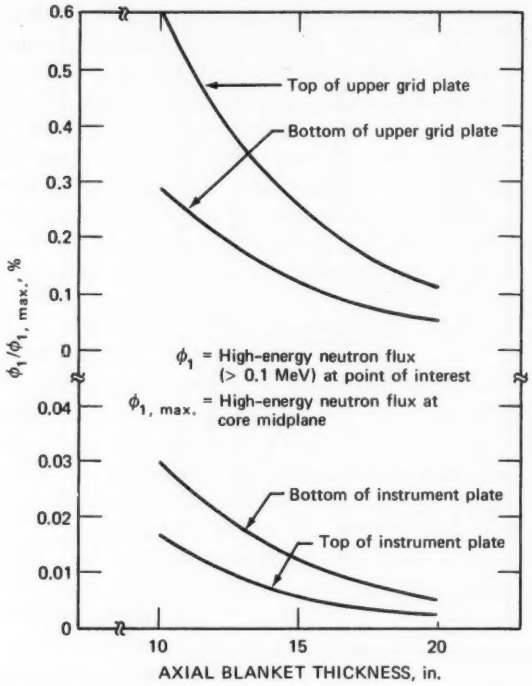

Fig. 11 Effect of axial blanket thickness on flux at above- and below-core components.

EBR-II (Refs. 36, 50)

The EBR-II core plan employs hexagonal ducts of 2.290 in. across outside flats, with a nominal cold clearance between assemblies of 0.030 in. One $\frac{3}{8}$-in.-diameter spacer pad (produced by indenting the inside surface of the duct) is provided at the center of each flat about 1 in. above the core midplane. The nominal height of each pad is 0.014 in., and so the nominal gap between pads is 0.002 in. cold and zero at operating temperature.

The lower adapter (nozzle) of each assembly fits into locating holes in two horizontal support (grid) plates. The upper plate supports the weight of the assembly and provides a pivot point by means of a spherical seat. The amount of free pivoting is limited mainly by the 0.004-in. radial clearance in the lower grid-plate hole. Core radial restraint of the passive type is provided by the eight to nine rows of radial reflector and/or blanket assemblies similarly cantilevered from their respective inlet nozzles and also equipped with spacer pads. A retaining ring 0.030 in. beyond the final row, near the top of the assemblies, is also present. This ring was installed as an aid to peripheral-row fuel handling and is believed to play no essential role in core restraint. The use of hydraulic hold-down, pioneered in EBR-II, circumvents the need for top-end fixity, so the assemblies are free to deflect under the influences of differential swelling, creep, and thermal gradients. The latter (the only effect recognized during the design phase of the EBR-II project) produces top-end interferences just beyond the core edge, creating inwardly directed forces at the pad plane according to calculations employing the BOW-V code.[52] These forces maintain a tight core during operation and also produce a small positive structural-reactivity coefficient owing to the compressibility of mid-flat pads on the relatively thin (0.040-in.) ducts. This positive component is greatly overridden by fuel and sodium expansion and other negative components of the power coefficient.[53] Most of the above-described design features and operating characteristics of EBR-II are illustrated[6] schematically in Fig. 12, a preswelling-era conception of EBR-II core-component bowing behavior.[54]

The reactor has performed well in the face of radiation-induced swelling and radiation-enhanced creep, neither phenomenon having been recognized until 10 years after design, and the plant factor has increased steadily during 7 years of operation. Core components not limited by fuel-burnup restrictions, i.e., control- and safety-rod "thimbles" (guide tubes), have functioned to world-record exposures up to 1.7×10^{23} neutrons/cm^2 (all energies) before swelling effects forced their removal. Although the thimbles operate at relatively low temperature (700 to 850°F), this solution-treated* 304 stainless steel has exhibited[55] up to 11.7% $\Delta V/V$, believed to be the highest yet seen from neutron exposure.

Curiously, elongation and dilation, rather than bowing, eventually forced the removal of these high-fluence components. Elongations of $\frac{3}{8} \pm \frac{1}{16}$ in. were experienced,[49] well beyond anything anticipated in the design of the fuel-handling equipment. Dilation up to 0.090 in. has been seen,[49] more than enough to fill the nominal 0.030-in. gaps separating thimbles from neighboring assemblies which, for the most part, contain low-burnup driver fuel and therefore experience little duct dilation to further aggravate the local congestion.

Examination of high-fluence ducts and thimbles from EBR-II has produced two "surprises," both

*These hexagonal thimbles, like the ducts on driver and fuel-test assemblies, contain some cold work at corners and spacer pads but are essentially in an annealed condition.

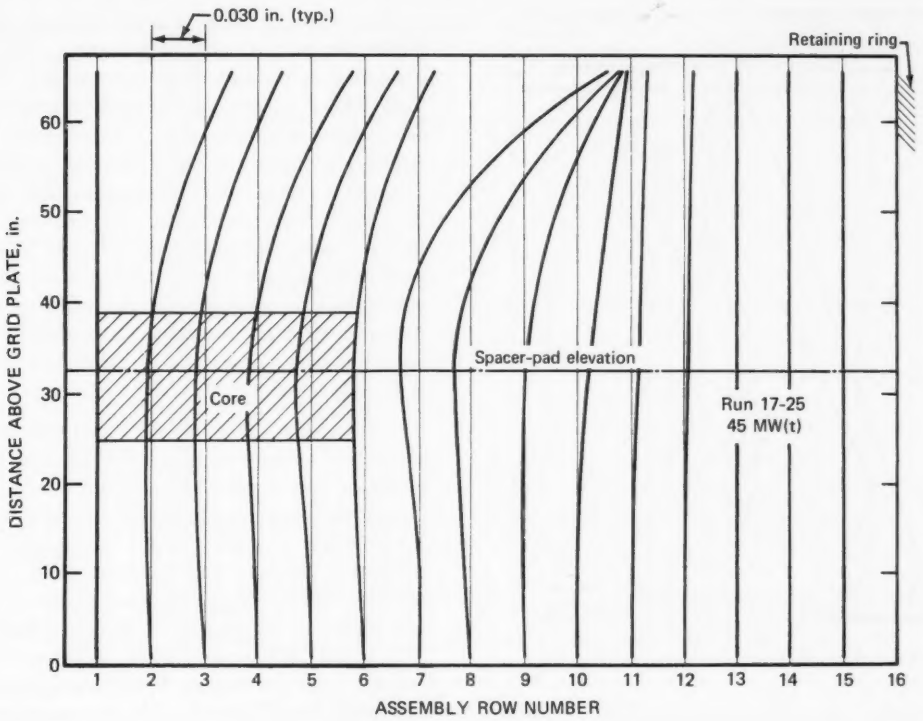

Fig. 12 Thermal deflections of EBR-II assemblies.

relevant to the search for a simple and reliable core-restraint design to accommodate the calculated effects of swelling. These are (1) the amazing degree of longitudinal straightness of these components and (2) the near constancy of duct diameter measured across spacer pads (although these pads are located on the highest swelling portion of the duct) while considerable duct dilation is found ½ in. away.

The first phenomenon is illustrated[56] by Fig. 13. In the three high-fluence thimbles removed from the reactor in July 1970, note that measured bowing was less than predicted bowing by factors of 6 to 12, depending on the swelling expression used for the predictions. Thimbles discharged more recently show the same tendency of straightness beyond any reasonable expectation. On the basis of the only thimble completely characterized by destructive measurements of density as of this writing (5A3), radiation-enhanced creep is not responsible for this straightness, although the straightening effects of creep have been calculated on a high-fluence fuel-test assembly.[45] The second surprise, that associated with spacer-pad behavior, is illustrated[46] in Fig. 14. This is being evaluated as a creep phenomenon, and one that gives rise to hope that reactors with in-core spacer pads are not doomed to low-burnup capability.

Both of the above-described phenomena in EBR-II, as well as fuel-element longitudinal bow and duct rounding, are being studied at ANL to test the reliability of contemporary swelling and creep expressions, albeit on solution-treated 304 stainless steel.[34,45,56-63] Also, of course, the surprising capability of the passive EBR-II core-restraint system to maintain straight components with absolute swelling up to 11.7% by volume must be understood before it can be reliably extrapolated to the next generation of fast reactors, as some experimenters have suggested doing.[6,46,64]

Enrico Fermi 1 (Refs. 35, 65)

Enrico Fermi 1, designed in the same era as EBR-II, has a more positive means of producing core radial restraint, not unlike the clamped-core concepts that have emerged since the discovery of swelling, except that radial restraint is produced by fixing the top ends of core assemblies rather than by direct side loading.

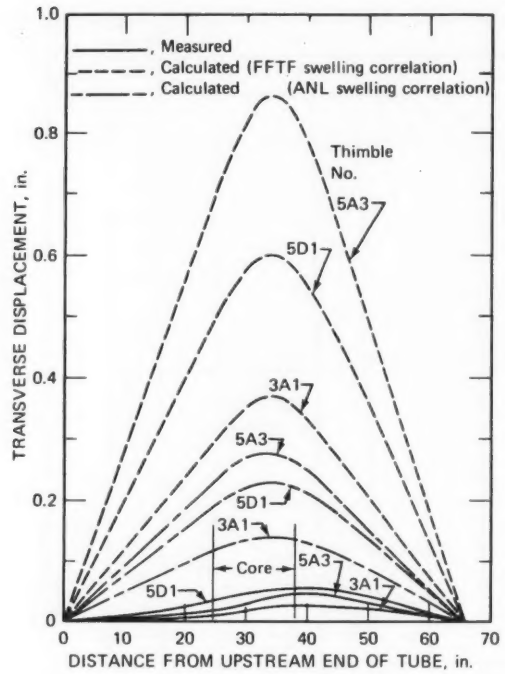

Fig. 13 Measured and calculated bowing of EBR-II safety and control thimbles.

In this reactor the square cold-worked 347 stainless-steel ducts of 2.646-in. width and 0.096-in. thickness are vertically oriented in a double support plate that receives tubular nozzles in close-fitting holes. A plane of spacer pads exists 4.5 in. above the midplane of the 30.5-in.-long core. These pads, made of Colmonoy, are welded to the corners of the ducts and machined to close tolerances to produce the 2.693-in. square pitch of core assemblies.

The handling head of each core and inner radial blanket assembly is captured by a stiff hold-down finger projecting downward from a horizontal hold-down plate. This finger prevents lifting from hydraulic forces and also precludes radial displacement of the assembly's upper end from thermal bowing or differential swelling. The center-to-center spacing of hold-down fingers is slightly less than the center-to-center spacing of support-plate holes. Accordingly, when the hold-down plate is lowered (as it always is before reactor startup) and the handling heads are captured by their respective hold-down fingers, an inward gathering of assemblies occurs, and all clearance at the spacer-pad plane is eliminated.

This design, known as the "tight-core concept" is illustrated[66] schematically in Fig. 15. The design has produced very dependable reactivity effects, including a negative structural component of the power coefficient, which was the primary design objective. Unfortunately the operating experience of this reactor has been limited to low fluence, and so the capability of this design to accommodate swelling effects has not been tested. The most pertinent analogous experience resulted from the October 1966 fuel-melting incident, during which brief period a few core assemblies became badly distorted as a result of high thermal gradients.[66]

The potential of this reactor to accommodate swelling and creep effects has been estimated.[6] No significant swelling would be expected during the remainder of the reactor operations with low-burnup metallic Core A fuel, although creep effects may be seen, probably as residual longitudinal bowing concave with respect to the reactor center line. When the proposed UO_2 core is installed and operated at its intended 400-MW(t) power level, the peak total flux (6.5×10^{15} neutrons/cm^2) will be such as to produce

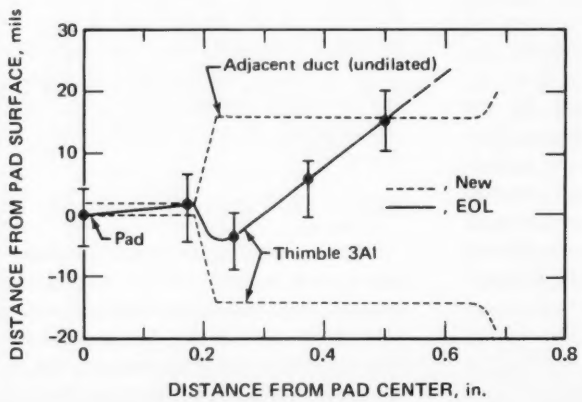

Fig. 14 Measured dilation in spacer-pad region of EBR-II thimble 3A1.

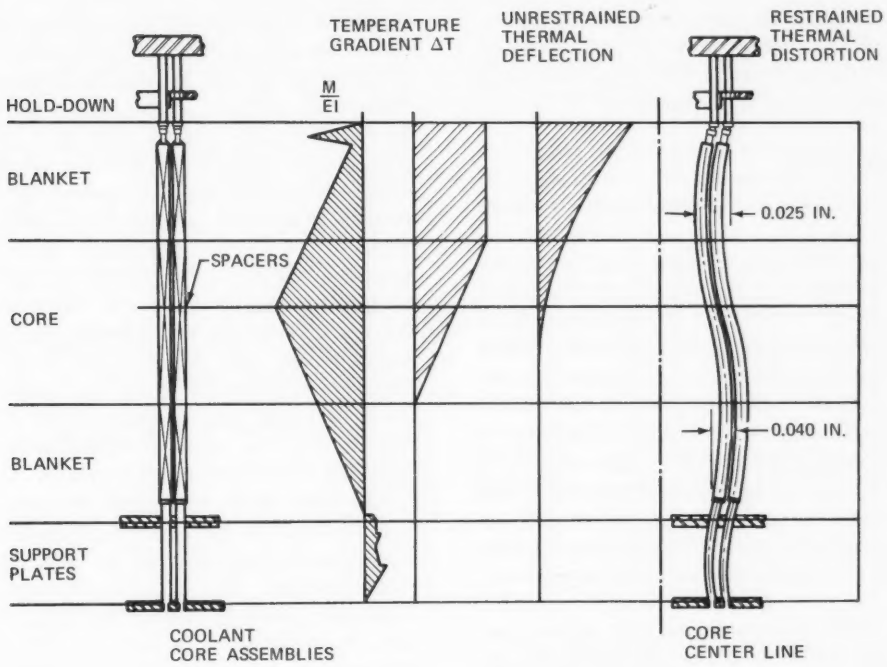

Fig. 15 Core-restraint design in Enrico Fermi 1.

a burnup/fluence ratio similar to that of future LMFBRs, and swelling could become a major factor.

Duct elongation due to swelling can be accommodated by compression of the nozzle spring, a feature originally intended to provide for differential thermal expansion. Clearance for dilation accommodation, assuming the use of the full 0.047-in. interassembly gap, is slightly greater than EBR-II.* Because of the in-core spacer pads, however, the usefulness of the full interassembly gap is not assured. Substantial creep distortion around the pads is required. Although this phenomenon is not understood sufficiently to assure that dilation accommodation will not be restricted by in-core pads, the indications are favorable. The stress required for the creep rate to match the swelling rate in Fermi[1] has been estimated[6] to be less than that required in EBR-II.† At this time it appears that the limiting factor in the ability of the Fermi design to accommodate swelling and creep is the necessity of the handling heads to mate with the hold-down fingers when the hold-down plate is lowered following refueling and prior to startup. This operational requirement constrains the allowable bowing due to swelling and creep. The nominal allowable mismatch is ¼ in. An inspection facility has been built, which, among other things, can provide direct measurements of assembly straightness. The facility is a portable, heated, shielded hot cell that can be stationed at the mouth of the reactor exit port to receive assemblies one at a time. Originally designed and built for the requalification of irradiated fuel assemblies[6,7] suspected of having sustained minor damage in the October 1966 fuel-melting incident, this facility can be used to monitor the effects of swelling and creep, although a more efficient procedure has been developed to monitor bowing alone. This procedure involves the use of an under-sodium periscope built into a diving-bell structure that is lowered down the exit port onto the handling head of an assembly that has been placed in a special gauging pot in the transfer rotor. Bowing is measured optically, i.e., by photoanalysis, to a quoted[6,8] precision of ±0.015 in. in magnitude and ±5°

*The interassembly gaps in Fermi 1 and EBR-II represent linear clearances of 1.77 and 1.31%, respectively.

†This result is highly dependent on the creep and swelling expressions used. The calculations referred to were based on expressions that yield lower swelling and higher creep estimates for the cold-worked Fermi ducts relative to the solution-treated EBR-II ducts under the same conditions.

in angular direction. This procedure, already used to measure bowing in a complete core loading, offers the capability for further study of integral swelling–creep effects as reactor operation proceeds.

BN-350 (Refs. 69, 70)

The BN-350, being built at the Caspian Sea in the USSR, is designed to produce 150 MW(e) and an equivalent 200 MW(e) for seawater desalination. The plant was scheduled for criticality[71] at the end of 1971 and should be the first of the generation of high-flux intermediate-size [250 to 500 MW(e)] reactors to operate at power.

The core design of BN-350 (like that of the test reactor BOR-60) was frozen without allowance for stainless-steel swelling, although the design schedule for BN-600 (the next in the Russian series of LMFBR power plants) allows ample time for such provisions to be made within the constraints imposed by a fixed-size vessel.[70] BN-350 uses the passive type of core restraint provided by the annulus of radial blanket and shield assemblies cantilevered from long inlet nozzles supported at two points in a conventional double grid plate offering hydraulic hold-down. Spacer pads, which occupy 0.059 in. of the nominal 0.079-in. interassembly gap, are apparently located on the fueled length of the duct. These similarities with EBR-II might be expected to promote similar response to swelling and creep, except that the dissimilarities in spacer-pad design, shown[70] in Fig. 16, could produce two important differences.[6]

First, the 0.020-in. clearances in the spacer-pad plane (vs. 0.002 in. in EBR-II) could produce a

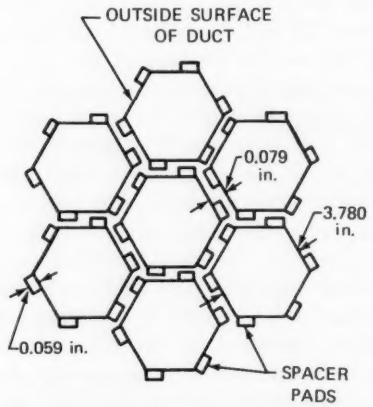

Fig. 16 BN-350 core-assembly pattern.

significant positive structural-reactivity coefficient over part of the power range during early core lifetime. This results from thermal bowing and bowing due to differential swelling, producing top-end contact between adjacent rows of assemblies, hence inward deflection of the fueled span of the assemblies to the extent allowed by pad-plane clearances. After metal swelling absorbs this clearance (at a peak burnup of ~30,000 MWd/metric ton based on U. S. swelling estimates[6]), the positive feedback potential is exchanged for another threat, this one to fuel-handling feasibility. Note that in this design, which uses "one-sided" spacer pads (see Fig. 16), duct dilation of ⩾0.020 in. below the spacer-pad plane will trap assemblies in the core and prevent their removal other than by forceful extrusion or sequential unloading, beginning with the outermost assemblies.

An upper limit on burnup capability, based on U. S. swelling estimates,[6] is ~70,000 MWd/metric ton. This assumes utilization of the full 0.079-in. gap accommodating the dilation produced by ~6% volumetric swelling. Burnup capability of the early cores is calculated to be only ~46,000 MWd/metric ton, owing to fission-gas pressure.[70] (Note, in Table 1, that the BN-350 fuel element has a negligible fission-gas plenum.) Assuming that swelling limitations permit, later cores may be extended to higher burnup with the BN-600 fuel-element design featuring integral axial blankets and a long fission-gas plenum below the core.

Prototype Fast Reactor[48,72,73]

In the patented[74] PFR core-restraint concept, each fuel assembly, in groups of six, leans on a central structural member externally similar to the fuel-assembly duct. In most cases the "leaning posts" also serve as guide tubes for control or safety rods. This design approach, therefore, produces a characteristic rosette pattern of fuel and absorber assemblies, as shown[72] in Fig. 17.

Contact between the assembly and its assigned leaning post is brought about by an out-of-plumb alignment of two nozzle-support points. A bending bar, concentrically located in the fuel-assembly nozzle ("spike" in PFR nomenclature), deflects elastically under the force needed to insert the nozzle into its receiving socket,* producing a contact force of at least 50 lb between duct and leaning-post spacer pads located well below the core. Among the relatively few

*It is intended that this force be no more than the assembly's deadweight.[74]

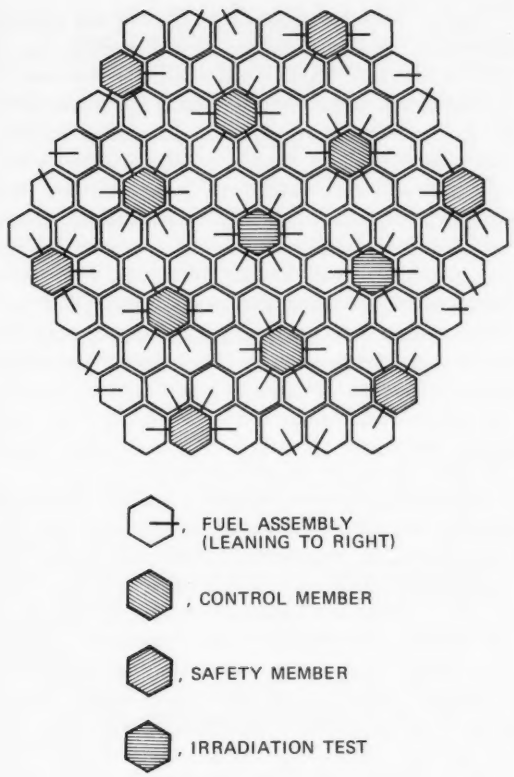

Fig. 17 Core plan of the PFR.

PFR design alterations resulting from the discovery of swelling, the spacer-pad location was chosen as a compromise between minimizing swelling at the pads (by keeping them well below the core) and minimizing flow-induced vibration (by keeping the support points as high as possible). To allow this location to be changed in the future, possibly as a result of better swelling data, the designers have made the leaning posts more readily removable. The finite life of the leaning post itself, due to swelling effects, also prompted this design alteration.[75]

Swelling-induced elongation of fuel assemblies is apparently not restricted, and dilation accommodation is relatively generous* for a reactor designed before swelling was recognized. Swelling-induced bowing of core assemblies is the greatest threat to the success of this design concept as a viable engineering solution to the swelling problem. Without restraining stresses, radiation-enhanced creep cannot play a correcting role to the effects of swelling. Periodic rotation of fuel assemblies, and possibly of leaning posts as well, is the operational "fall-back" position if bowing becomes excessive. The required frequency and operational practicality of duct rotation can be meaningfully assessed only through reactor operation, which is scheduled to begin (initial criticality)[71] at the end of 1972.

The PFR design strategy places a high premium on the development of a duct material with low-swelling tendencies. The current British favorite is Nimonic PE16 (Ref. 21). If a low-swelling duct material is found, the absence of restraint (eliminating radiation-enhanced creep as an important determinant of core mechanical behavior) would be a design asset to go with the many other attributes of this approach.[6]

Phenix[76-79]

This French LMFBR prototype uses the pot-type layout (like the PFR), is rated at 250 MW(e), and is scheduled for criticality in early 1973 (Ref. 71). The core design is an extrapolation of Rapsodie, the highly successful mixed-oxide-fueled test reactor operated at 20 and 24 MW(t) from 1967 to 1970 and more recently at 40 MW(t) with the replacement "Fortissimo" core.

With respect to core restraint, Rapsodie and Phenix are similar to EBR-II. That is:

1. Reactor assemblies are cantilevered from a two-point nozzle support employing a double grid plate with hydraulic hold-down.
2. Unrestrained top ends of reactor assemblies "flower outward," in response to thermal gradients produced by the characteristic radial flux profile, until top-end interference is met.
3. Lateral support is provided by the longitudinal stiffness of many rows of "straight" assemblies radially beyond the core.

The Phenix core consists of 103 hexagonal fuel assemblies 4.87 in. across flats and six control assemblies in guide tubes of the same dimensions. The high-pressure (110-psi) plenum also serves 90 radial blanket assemblies, 216 steel-reflector assemblies, and 41 storage positions. Radially beyond the cylindrical grid box, comprising the high-pressure plenum, the core load support, and the two-point lateral nozzle support, is a "false grid." This false grid provides vertical orientation, although no forced convection, to

*The 0.16-in. gap in the 5.7-in. lattice spacing allows nominal dilation accommodation for a peak swelling of 8.7% $\Delta V/V$, sufficient for the estimated swelling of 5% in PFR.[21]

937 lateral shield assemblies, which theoretically are also part of the lateral restraint system. These contain graphite, boron graphite, or steel rods and have a circular cross section either 4.88 or 6.22 in. in diameter.

The interassembly gap is 0.218 in., offering a 2.63% linear dilation accommodation, equivalent to a maximum of 7.9% volumetric swelling. The spacer pads, as in EBR-II and Rapsodie, are on the mid-flats and formed out of the 316 stainless-steel duct. Originally, the pads were to be placed at or near the core midplane. One of the few concessions to the swelling phenomenon* has been to relocate these pads,[41] probably to above the core where they will result in a small positive bowing coefficient well overridden by the Doppler coefficient.

The Phenix fuel elements are designed for a peak burnup of 100,000 MWd/metric ton; the minimum expectation is half of that.[77] Irrespective of fuel performance, the operation of Phenix will provide the earliest indication of whether the EBR-II-type core-restraint approach, so successful in EBR-II and Rapsodie, is practical for commercial LMFBR power plants.

SNR[80,81]

This 300-MW(e) LMFBR station is being designed by an industrial consortium that includes firms in West Germany, Belgium, and the Netherlands. Construction of this loop-type prototype is scheduled to begin in 1972 on its site in West Germany. In contrast with the other European prototypes, the timing of this project has permitted deliberate design steps to offset the effects of swelling and creep. At this writing, however, those steps have not been publicly revealed in detail.

The 150 hexagonal fuel assemblies are relatively small (~4.3 in. across flats) and contain 169 elements supported by a system of intermittent grids. The assemblies are freestanding and cantilevered from a double grid plate incorporating hydraulic hold-down. An overhead instrument plate, hung from the top shield, provides an emergency stop against lifting of assemblies but does not interfere with swelling-induced elongation. Dilation is accommodated by interassembly gaps. A value of 8% has been mentioned[20,82] as the maximum expected volumetric swelling of core stainless steel.

Spacer pads are attached to all core and blanket assemblies, apparently outside the high-swelling region. Outside the radial blanket, which averages five rows in thickness, and at elevations matching the spacer pads, are ferritic steel rings that provide core radial restraint. Owing to differential thermal expansion between ferritic and austenitic steel, this passive system will produce fuel-handling clearances under isothermal reactor conditions and peripheral restraint against thermal and swelling-induced bowing at operating temperatures. As in the other European designs (PFR and Phenix), fuel-assembly bowing is reduced through the use of upstream plenums for fission-gas storage within the fuel elements.

FFTF

Most of the open literature on the effects of swelling and creep on reactor components, and the possibilities for mitigation of these effects through core-restraint design, has been produced by the FFTF project. Initially a literature review on the subject of fast reactor core restraint was conducted.[83] When early swelling correlations predicted that irreversible differential elongation of edge-core assemblies would produce several inches of free top-end deflection at the burnup and temperature targets of the Fast Test Reactor (FTR),[84] previous core-restraint design effort was seen as having limited relevance. A peripherally clamped core was chosen as the reference-design solution, and an extensive engineering-mechanics effort was inaugurated.

At first, only the effects of swelling were analyzed.[85,86] Dilation and bowing of core assemblies, as free bodies and in an idealized *r,z* plane of the core, were computed based on a procession of swelling predictions. These predictions have trended downward from 1969 to the present, at least for 20% cold-worked 316 stainless steel, which had been chosen for cladding and ducts.

The recognition that radiation-enhanced creep would be an important determinant of FTR mechanical behavior stimulated the development of analytical tools not formerly required for fast reactor design. Responding to this need, Sutherland et al. produced the finite-element codes CRASIB[87] and AXICRP.[88] CRASIB is specifically oriented to statically indeterminate beams of arbitrary cross section. The code calculates time-dependent loads, stresses, and shapes of ducts using any functional representation for swelling and creep, although interassembly mechanical interactions of the type evaluated by the BOW-V code[52]

*Other important modifications have been made to the fuel-handling system to tolerate distorted (bowed) assemblies and to facilitate periodic rotation if this should prove necessary.[41,78]

cannot be simultaneously solved. AXICRP is more general than CRASIB in that it can evaluate creep effects in plane-strain, plane-stress, and axisymmetric-bodies-of-revolution problems. Of the open-literature codes, cross-sectional distortion of hexagonal ducts can best be analyzed with AXICRP. In addition to these, several private and proprietary finite-element codes are known to exist in the United States and Europe for estimating the time-dependent effects of swelling and creep on core components.

Thus evolved the capability to analyze the complex interacting effects of differential thermal expansion, differential swelling, and radiation-enhanced creep in a reactor with positive core restraint. During this evolution the FTR fuel-assembly design had become relatively firm. Figure 18 shows the main features of core-assembly ducts. Not shown is the interassembly gap of 0.140 in., allowing a 3% linear dilation of adjacent ducts before contact is made other than at the two above-core planes of load pads. Analyses of the response of these ducts to swelling, creep, and thermal gradients have been published[44] and are still in progress.

Perhaps because of the many contributions of the FFTF project toward a coordinated engineering attack on the problems of dimensional instabilities of stainless steel in fast reactor cores, the peripherally actuated core clamp approach is currently the favored design strategy in the United States (see below). Concerned with the reliability of these complex active clamps, however, the AEC has sponsored a study to evaluate the feasibility of a simpler passive restraint system patterned as much as possible after the unexpectedly successful EBR-II design approach.

U. S. Demonstration Plant Designs

Most of the design descriptions and analyses pertaining to U. S. demonstration plant designs have not yet been widely distributed, and the designs are evolving rapidly as of this writing. There is, however, sufficient open literature on each plant to provide a general understanding of how swelling and creep have been factored into the respective designs. The following synopses are gleaned from the open literature available as of December 1971.

Atomics International.[40,89,90] At 500 MW(e) the AI plant is the largest of the "first-generation" LMFBR demonstration plants being designed under the current U. S. breeder program. The AI plant also has the tallest core (44 in.) and the largest duct (5.57 in. across flats), which are important variables in the design of the active-clamp system of core radial restraint, which is the focal point of the design strategy to combat the effects of dimensional instability of stainless steel. Use of the active clamp with above-core and top-end load pads makes this design resemble the FTR to a greater extent than the others in this group. The active clamp was selected to achieve the dual benefits of: (1) large clearances to facilitate fuel handling and (2) operational tightness at the load-pad planes to minimize reactivity anomalies, ensure a negative power coefficient, and allow reproducible core performance.

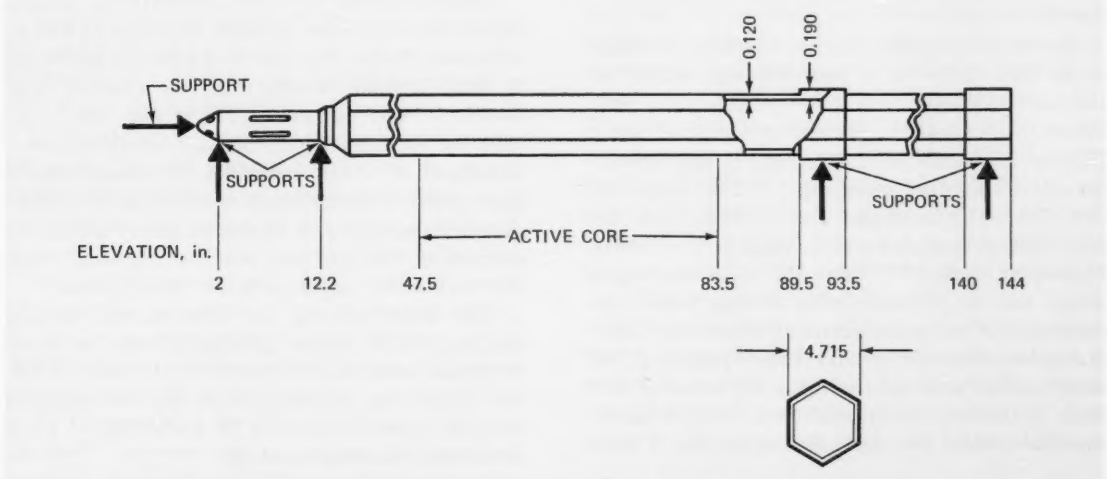

Fig. 18 Driver-fuel-assembly duct in the FTR.

The 0.3-in. interassembly gap was sized to preclude assembly-to-assembly contact (other than at the pad planes) by dilation and bowing. With AI's current swelling and creep estimates (nominals), this gap is sufficient to prevent duct–duct mechanical interaction for the entire 2-year (four-cycle) residence time, during which the peak total fluence will reach 4×10^{23} neutrons/cm^2. Nominal swelling under these conditions is 4.2% $\Delta V/V$. At the 3σ upper limit of swelling (6.6% $\Delta V/V$), in conjunction with nominal to minimum creep, assembly rotation is required to avoid contact of ducts near the core periphery, where bowing tendencies are greatest. The maximum swelling-accommodation potential of the design is given as 15% $\Delta V/V$, based on the dilation allowance for the peak-fluence (central) assembly.

A half-scale full-core mockup including the six clamping segments has been built and operated in room-temperature air to study the mechanical response of the core to peripheral clamping forces with straight assemblies and simulated bowed assemblies. On the basis of calculation, the required clamping force is 33,000 lb per segment, considerably higher than the FFTF, due primarily to the increased duct diameter. The clamp is actuated by a system of hydraulic cylinders using sodium as the working fluid.

Combustion Engineering.[91,92] The only current U. S. LMFBR design advertised as a "second-generation demonstration plant," this 500-MW(e) design uses high-performance mixed-carbide fuel that, with a peak linear power of 32 kW/ft (19 kW/ft av.), permits a more compact core than the AI design with the same electrical rating.*

For design purposes, peak metal swelling was taken to be 10% $\Delta V/V$ at a peak discharge burnup of 100,000 MWd/metric ton, corresponding to a peak fluence of 2.3×10^{23} neutrons/cm^2 ($E > 0.1$ MeV). Dilation is accommodated by a ~0.3-in. gap between hexagonal assemblies measuring 5.932 in. across outside flats. This contrasts with 0.050-in. gaps for fuel-handling allowance used in previous Combustion Engineering designs.[9,14] For the more challenging design task of accommodating bowing within the constraints of acceptable reactivity effects, four alternatives were evaluated, that is (1) active peripheral core clamps and an articulated assembly, (2) decreased duct width to eliminate the articulation, (3) "unrestrained" core that permits free mechanical interaction of ducts and some lateral movement, and (4) development of a suitable low-swelling duct material.

Design options were affected by the following ground rules: (1) the bowing coefficient must be negative, (2) no duct–duct mechanical interaction except at load pads, (3) no load pads in regions of significant swelling, and (4) assemblies must be restrained at a minimum of one level above the grid plate. Under the constraints of these requirements and certain economic criteria, the first alternative was chosen as the basic concept for swelling–creep accommodation.

The six mechanically actuated compliant peripheral clamps apply a constant force on load pads located on the ducts at elevations 6 and 48 in. above the top of the core. Bottom support of assemblies uses a conventional double grid plate and hydraulic hold-down. Because of the large duct diameter and the resultant high stresses that the core-restraint system would impose on a conventional duct, it was deemed necessary to articulate the fuel assemblies with a double joint between the upper grid plate and the bottom of the fuel elements. The articulation is essentially a hollow open-ended dumbbell supported in two sockets. Radial blanket assemblies do not have the articulation joints, but instead have a floating-collar type of upper load pad to maintain stresses at allowable values by permitting 0.25 in. of unrestrained top-end radial movement. This type of load pad was avoided in the core because it tends to produce a positive bowing coefficient which the lower-end articulation scheme does not.

General Electric.[38,93] The 350-MW(e) GE demonstration plant has the smallest duct size (3.849 in. across hex flats) of any plant in the present generation of U. S. LMFBR designs. With the resulting large number of fuel assemblies (276 in two enrichment zones in the target core), the unit worth is low—prototypic of larger assemblies in proportionately larger plants. Although safety is the prime motivation, clamping loads and duct stresses are greatly reduced by selection of this duct size, other factors being equal. The interassembly gap in the GE design is 0.160 in.

The design strategy for core restraint involves clamping, but it differs significantly from the active peripheral clamps used in the FFTF, AI, and Combustion Engineering reactor concepts and the peripheral clamping system designed by GE for SEFOR.[94] Three interacting systems are involved:

1. Banding ring segments positioned to form a hard outer boundary.

*Height, 36 vs. 44 in.; diameter, 74 vs. 76 in.

2. Spring clamps within this outer boundary and surrounding the radial blanket.

3. Internal core clamps that are expanded to take up the duct-spacing clearance.

The distinguishing feature is the third system. The internal clamps are distributed in a uniform pattern with each clamp surrounded by six fuel assemblies. In the core the clamp mechanisms are mounted in absorber-assembly guide tubes, thus distributing the absorber positions in a symmetry resembling that of the PFR.

The reference core-restraint design has, as one of its aims, increased flexibility for accommodating the wide range of possible materials behavior. With compliance to absorb swelling, thermal expansion, and dimensional tolerance provided at the blanket periphery, the mechanical response of the core to temperature increase, for example, should be as a single structure with calculable and reproducible neutronic effects. The actual clamping forces, however, are generated locally and need not be transmitted across many rows of assemblies to achieve the intended planes of tightness at the load-pad elevations. The design should, therefore, be tolerant of higher friction coefficients at the load pads.

Like SEFOR, the GE demonstration plant uses the open-reactor, hot-cell refueling approach. Among other reasons for selecting this concept, the feasibility of remapping fuel-assembly handling heads, should they become misplaced due to swelling and creep effects, has been mentioned.[38]

Gulf General Atomic.[47,95] The only gas-cooled fast reactor (GCFR) concept to be reviewed here, the 300-MW(e) GGA (Gulf General Atomic) demonstration plant is also the smallest in the current generation of U. S. breeder reactor designs. Owing in part to the differences between sodium and helium as reactor coolants, this design shows some major differences in core support and hence in the gross strategy of accommodating swelling and creep. Along with these differences, there are many similarities with respect to core materials, temperatures, and fuel-element designs. The similarities are often deliberate to capitalize on the LMFBR research and development program in areas of fuels and materials development and reactor physics. An FFTF correlation for 20% cold-worked 316 stainless steel[25] has been used to estimate the amount of swelling in the GGA plant. The maximum swelling, at GCFR demonstration plant conditions, is estimated at 10% $\Delta V/V$ for a fluence of 1.8×10^{23} neutrons/cm^2 ($E > 0.1$ MeV), corresponding to a maximum fuel burnup of 100,000 MWd/metric ton.

The reactor loading contains 118 fuel and 93 radial blanket assemblies featuring very large (6.5 in. across flats) hexagonal ducts. They are supported from, and rigidly attached to, a top-mounted single grid plate. The assemblies project downward from this grid plate, and fuel handling is performed from beneath the core (control rods are driven from above). In this "free-hanging" array of core assemblies, as in the freestanding array in the PFR, duct bowing due to differential thermal expansion and differential swelling is unsuppressed. Therefore radiation-enhanced creep does not have the importance it has in restrained-core concepts. Instead, duct dilation and bowing are accommodated by a 0.25-in. interassembly gap that extends along the entire 10-ft length of duct, and swelling-induced bowing will be held to acceptable values by periodic rotation of assemblies. It is anticipated that annual rotation, at times coinciding with partial-core refueling, will reduce duct–duct interferences to an acceptably small degree. Both 180 and 120° rotation increments have been evaluated, with no significant difference in the calculated degree of interference.

Westinghouse.[96-98] This 330-MW(e) (gross) plant was designed to accommodate 20% maximum stainless-steel swelling (by volume). All structural material in the core, including cladding, spacer grids, and ducts, is 20% cold-worked 316 stainless steel; and the maximum burnup, based on a 6-month refueling cycle, is 103,000 MWd/metric ton.

The reference core-support and core-restraint concepts were chosen after a trade-off study that evaluated various methods of accommodating swelling and creep phenomena. Both hydraulic and mechanical hold-down designs were studied. Mechanical over-the-core hold-down was chosen, a selection that runs counter to the present trend of U. S. and European LMFBR design practice. Simplicity and improved predictability are cited as the reasons for this choice. With the top ends of assemblies securely fixed in a massive hold-down structure, and the lower nozzles captured in receptacles that offer two-point positioning, radial restraint can be somewhat less elaborate than designs utilizing active clamps. In the Westinghouse concept, radial restraint is assisted by a single row (72) of longitudinally flexing "restraint-spring" assemblies surrounding the core system of 367 hexagonal assemblies.* Beyond that, a

*The design consists of 153 fuel, 16 control (based on a 6-month refueling cycle), 132 radial blanket, and 66 radial reflector assemblies.

nonyielding "former plate" provides a fixed outer diameter and limits total radial free space. The radial restraint strategy also requires rotation of some core and blanket assemblies every 12 months, based on existing data.

As in Fermi 1, axial thermal expansion and swelling-induced elongation of assemblies are accommodated by a nozzle spring, in this case made of Inconel X-750. Dilation is absorbed by an interassembly gap that is unobstructed over the length of duct that will experience significant swelling. There are two levels of load pads above the core and one below. Pads are located at the same elevation on all assemblies from core center to the peripheral restraint system. The protrusion of the pads beyond the duct varies with the type of assembly and the axial elevation, but dimensions across pads are always slightly less than the cold pitch established by the spacing of holes in the support plate and hold-down plate. If this embodiment produces any positive bowing effects, they are overshadowed by negative constituents of the power coefficient. The overall power coefficient is monotonically negative over the whole power range, having an average value of −0.29 cent/MW(t) and a value of −0.13 cent/MW(t) at full power.

Although the reference design requires semiannual refueling, with about 30 fuel and 13 radial blanket assemblies replaced each time, the ultimate objective is annual refueling, although this will require more favorable materials irradiation data than are now in hand, or mechanical releases in the passive restraint assemblies. Uneven swelling of core components is said to be the greatest mechanical disadvantage of long refueling intervals.

EFFECTS ON FAST REACTOR ECONOMICS

The general view of fast reactor designers is that the need to accommodate swelling and creep will increase the cost of energy production, but not by so much as to undermine the role of the breeder reactor as a major future energy source for the world.

Capital costs are subject to increase from (1) larger reactor size resulting from space needed to accommodate swelling in the core and (2) complex reactor internals not heretofore utilized, e.g., core clamps.

The only component of the energy-cost increase calculable on first principles is the cost of the enlarged interassembly gap reflected through decreased breeding ratio and specific power. This cost has been calculated as ~0.08 mill/kWh for 15% swelling accommodation[6,99] and proportionately less for lesser amounts of swelling. The upper boundary on fuel-cycle cost increase has been suggested as 0.35 mill/kWh, based on the worst-case assumption that fuel burnup would need to be reduced by half.[6]

Several design approaches have been suggested that represent more radical departures from preswelling LMFBR design practice. All involve penalties in fuel-cycle costs which generally fall between the limits given above.[6] Some of these concepts, and the nature of the economic penalty, are given below.

1. *"Cold-Wrapper Tube".*[6,100] The duct is maintained in a temperature range below the swelling threshold, a task requiring a reactor-inlet sodium temperature of only ~600°F. The penalty arises from the less-than-optimum core-outlet temperature of probably ~950°F.

2. *Refractory-Metal Core Structure.*[6,101-104] Refractory metals, such as niobium or molybdenum, which apparently resist swelling at temperatures in the range of interest for fast reactors,[105] are substituted completely or strategically for stainless steel in the core. Penalties arise through adverse neutronic properties of these materials and higher fabrication costs.

3. *Periodic Annealing.*[6,106] Analogous to the method of coping with graphite swelling in some gas-cooled reactors, swollen core components are periodically shrunk to original size by a brief annealing treatment at ≥1400°F, which is effective in eliminating voids.[107] The penalty arises through reactor unavailability and/or increased on-site fuel inventory.

4. *Periodic Rotation.*[6,108] This concept is a currently favored strategem to limit the extent of swelling-induced bowing. Loss-of-plant availability is translatable to an energy-cost penalty.

5. *^{233}U–Th Cycle.*[6,109,110] Higher fission cross sections and the feasibility of breeding at intermediate neutron energies ($E < 0.1$ MeV) greatly reduce the swelling/burnup ratio in the ^{233}U–Th cycle relative to the ^{239}Pu–U cycle. The penalties are a substantial loss of breeding ratio and a heavy sacrifice of existing technology on which to design commercial breeders for the 1980s.

Returning to the $(U,Pu)O_2$-fueled LMFBR with a stainless-steel core structure, it appears that the swelling phenomenon has thwarted the development of core features that could have produced a step increase in core-fuel fraction, with resultant increases in breeding ratio and specific power. Figure 19 shows[6] the effect of breeding ratio and specific power on fuel-cycle cost (other parameters constant) and a thumb-shaped zone

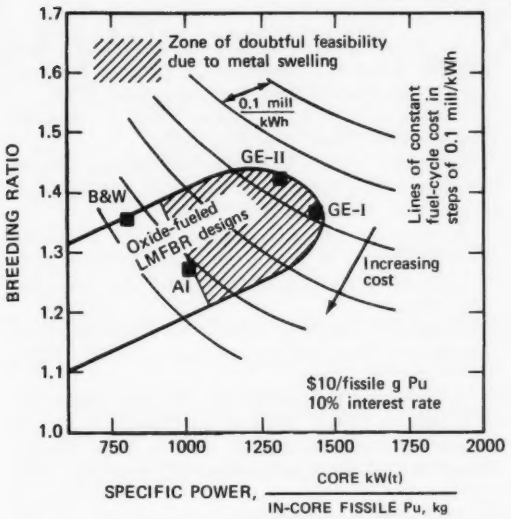

Fig. 19 Effects of specific power and breeding ratio on fuel-cycle costs and potential impact of swelling.

defining these values in all LMFBR studies reported to date. Notice that the leading edge of the thumb, representing most favorable economics, is defined by two GE designs[111] that featured nonfreestanding ducts and essentially no interassembly sodium gaps, and hence the highest possible fuel fraction. Since these features now seem impractical in view of the need to accommodate swelling, the portion of the thumb whose leading edge is defined by the AI[12] and Babcock & Wilcox (B&W)[13] 1000-MW(e) concepts now seems to be a more practical design regime. The B&W design had considerable subsequent study related to the impact of swelling and the evaluation of various modifications.[112]

Taking the "physics" value of increased interassembly sodium gaps as the minimum cost of accommodating swelling and a 50% burnup reduction as the maximum cost, a cost–benefit analysis for development of low-swelling alloys has been made.[6] The analysis indicated that the cost savings of having to accommodate only 5% $\Delta V/V$ in U. S. breeder reactors to be built over the period 1970–2020 (Ref. 113), rather than 15% $\Delta V/V$, have a 1970 present worth of from $860,000,000 to $5,600,000,000.

CONCLUSIONS

Fast reactor designers have now had 4 years in which to evolve design strategies to cope with the various problems posed by radiation-induced swelling and radiation-enhanced creep in core stainless steel. At this time, no worldwide consensus can be presented, since (1) the open literature on design strategies is almost entirely American and (2) no reactor specifically designed for swelling and creep effects is even close to operation, and only one (the FFTF) is under construction. Certain trends are apparent in the open design literature, however. Those which seem noteworthy to this reviewer are:

1. Despite the sophistication with which swelling and creep effects are analyzed and predicted in fuel elements, these phenomena have affected fuel-element designs very little. There is no clear trend to higher smeared densities, as might be justified by enhanced cladding dilation; nor have fuel-element designs become noticeably less conservative, as might result from a general resignation that swelling and creep effects, rather than intrinsic burnup capability of high-quality fuel elements, would limit core lifetime.

2. Internal design features of fuel assemblies have also been relatively unaffected. The helical wire wrap still dominates the field of candidates for fuel-element support, but more built-in clearances or other schemes to produce radial compliance are used than in the "preswelling era."

3. Fuel-assembly dilation is accommodated by increased gaps between assemblies, with the gaps continuous over the duct length where significant swelling is expected. Designers have abandoned the in-core pads featured for safety reasons in earlier and smaller fast reactors.*

4. Swelling-induced elongation of core components is considered a minor problem, especially in the majority of designs where the use of hydraulic hold-down leaves the top ends of reactor assemblies free to grow.

5. Restraint of swelling-induced bowing of reactor assemblies is favored over no restraint. Active peripheral clamps, which generate comfortable refueling clearance, are the most popular current concept for providing this radial restraint. Reliable mechanisms and reproducible complete or near-complete compaction are system requirements under development.

*A redeeming characteristic of large fast reactors, offsetting their higher swelling/burnup ratio (Fig. 3), is their decreased neutronic sensitivity to radial movement of fuel. This neutronic sensitivity, expressed as $\delta k/k$ per mil change in core radius, is inversely proportional to the core radius as a first approximation.[114]

6. In the restrained-core concepts, uncertainties in swelling and creep combine in equal measure, according to the principles of superposition, to uncertainties in duct deformation during service.

7. Although a metallurgical solution to the problems of swelling and creep is widely desired by reactor designers, it is generally hoped and expected that this solution will be found within the Fe–Cr–Ni family of alloys, rather than in the refractory metals.

8. Temperature and burnup goals for commercial LMFBRs have not been lowered due to swelling and creep phenomena, and the economic impact of these properties is considered tolerable even without a metallurgical breakthrough.

As for the nearly completed high-flux reactors designed with little or no deliberate provision for swelling, Häfele appears to represent European opinion in saying that "6–8% $\Delta V/V$ can be lived with."[82] This is a plausible prediction in view of the successful operation of EBR-II with over 11% swelling of certain "permanent" core internals, although the reasons for this unexpected success are not well understood and could be unique to EBR-II. Prevailing metallurgical opinion is that cold-worked and/or stabilized stainless steels will not reach 6 to 8% $\Delta V/V$ until somewhat beyond 10^{23} neutrons/cm^2, an adequate achievement for the European demonstration plants.

For the future, optimism or pessimism on the swelling–creep issue seems to pivot around materials data rather than design solutions. Some investigators are more optimistic about cold-worked stainless steel than given above, predicting as little as 5% $\Delta V/V$ for burnups of the order of 100,000 MWd/metric ton (Ref. 71), which is far below the estimates promulgated 2 to 3 years ago. Significantly, this "interim metallurgical solution" has been found within the family of preferred commercial alloys for fast reactor construction. As a systematic search for improved alloys is conducted, assisted by larger and more prototypic irradiation facilities and an expanded theoretical base, it appears probable that fast reactors designed near the turn of the century will be little affected by swelling.

To put the swelling problem in perspective, Bishop[21] observes that stainless steel heated from room temperature to ~1000°F undergoes a 3% volumetric expansion. Therefore, if this recent optimism proves accurate, the swelling problem has been reduced to magnitudes of dimensional change with which designers of complex equipment are familiar.

REFERENCES

1. J. G. Yevick (Ed.), *Fast Reactor Technology: Plant Design,* Chap. 11, Description of Fast Reactors, pp. 677-746, The MIT Press, Cambridge, Mass., 1966.
2. C. Cawthorne and E. J. Fulton, Voids in Irradiated Stainless Steel, *Nature,* **216:** 575 (1967).
3. J. J. Holmes and H. R. Brager, Fast Reactor Induced Swelling by Void Formation in Type 304L Stainless Steel, *Trans. Amer. Nucl. Soc.,* **11:** 479 (1968).
4. T. Lauritzen, G. Ferguson, L. Seacrist, and F. Comprelli, Density Changes in Several Austenitic Stainless Steels After Irradiation in EBR-II, *Trans. Amer. Nucl. Soc.,* **11:** 479 (1968).
5. M. Kangilaski, Minimizing Swelling and Embrittlement of Fast-Reactor Fuel Claddings, *Reactor Technol.,* **14**(3): 213 (Fall 1971).
6. P. R. Huebotter, T. R. Bump, W. T. Sha, D. T. Eggen, and P. J. Fulford, Design, Research, and Development Implications of Metal Swelling in Fast Reactors, USAEC Report ANL-7786, Argonne National Laboratory, April 1971.
7. C. Klotz et al., Large Fast Reactor Design Study, USAEC Report ACNP-64503, Allis-Chalmers Mfg. Co., Atomic Power Development Associates, Inc., and Babcock & Wilcox Co., 1964.
8. D. T. Eggen et al., Feasibility Study of a 1000-MW(e) Sodium-Cooled Fast Reactor, USAEC Report NAA-SR-11378, Atomics International, 1966.
9. S. Visner et al., Liquid Metal Fast Breeder Reactor Design Study, USAEC Report CEND-200, Combustion Engineering, Inc., 1964.
10. M. J. McNelly, Liquid Metal Fast Breeder Design Study, USAEC Report GEAP-4418, General Electric Company, 1964.
11. F. M. Heck et al., Liquid Metal Fast Breeder Reactor Design Study, USAEC Report WCAP-3251, Westinghouse Electric Corp., 1964.
12. Atomics International, 1000 MW(e) LMFBR Follow-On Study, Conceptual System Design Descriptions, USAEC Report AI-AEC-12791.
13. Babcock & Wilcox Co., 1000 MW(e) LMFBR Follow-On Study, Task II and III Report, Conceptual System Design Descriptions, USAEC Report BAW-1328(Vols. 1 and 2), February–March 1969.
14. Combustion Engineering, Inc., 1000 MW(e) LMFBR Follow-On Study, Task II and III Report—A Reference Conceptual Design of a 1000 MW(e) LMFBR, USAEC Report CEND-337, Vol. 1, 1968.
15. General Electric Company, 1000 MW(e) LMFBR Follow-On Study, Task II Report, Conceptual Plant Design, System Descriptions, and Costs for a 1000 MW(e) Sodium-Cooled Fast Reactor, USAEC Report GEAP-5678, December 1968.
16. Westinghouse Electric Corp., 1000 MW(e) LMFBR Follow-On Study, Task II and III Report, Conceptual Design, USAEC Report WARD-2000-97, 1969.
17. E. R. Gilbert, In-Reactor Creep of Reactor Materials, *Reactor Technol.,* **14**(3): 258 (Fall 1971).
18. E. R. Gilbert and L. D. Blackburn, Irradiation-Induced Creep in Austenitic Stainless Steel, USAEC Report WHAN-FR-30, WADCO Corporation, October 1970.

19. S. D. Harkness, J. A. Tesk, and C-Y. Li, An Analysis of Fast Neutron Effects on Void Formation and Creep in Metals, *Nucl. Appl. Technol.*, **9**: 24 (1970).
20. W. Häfele et al., Fast Breeder Reactors, *Ann. Rev. Nucl. Sci.*, **20**: 393 (1970).
21. J. F. W. Bishop, The Significance of Fast-Neutron-Induced Voids in the Design and Performance of Fast Reactors, in *Voids Formed by Irradiation of Reactor Materials*, Conference Proceedings, Reading, England, March 24–25, 1971, pp. 301-318, British Nuclear Energy Society.
22. C. N. Spalaris and E. L. Zebroski, Consideration of Stabilized Stainless-Steel Alloys for LMFBR Fuel Cladding, *Trans. Amer. Nucl. Soc.*, **14**(Suppl. 1): 3 (1971).
23. Edison Electric Institute, Fast Breeder Reactor Report, April 1968.
24. T. R. Bump, Mechanical and Thermal Analysis of Cylindrical Fuel Elements During Off-Normal Conditions After Extended Burnup, *Nucl. Appl. Technol.*, **9**: 301 (1970).
25. A. Boltax, P. Murray, and A. Biancheria, Fast Reactor Fuel Performance Model Development, *Nucl. Appl. Technol.*, **9**: 326 (1970).
26. K. Q. Bagley, J. I. Bramman, and C. Cawthorne, Fast Neutron Induced Voidage in Non-Fissile Metals and Alloys, in *Voids Formed by Irradiation of Reactor Materials*, Conference Proceedings, Reading, England, March 24–25, 1971, pp. 1-26, British Nuclear Energy Society.
27. R. J. Jackson, R. D. Leggett, J. W. Weber, and L. A. Pember, Comparison of Measured and Predicted Diameter Increase of Two Stainless-Steel-Clad Mixed-Oxide Fuel Pins in a Fast Reactor, *Trans. Amer. Nucl. Soc.*, **14**(Suppl. 1): 10(1971).
28. L. A. Neimark et al., Performance of Mixed-Oxide Fuel Elements: ANL Experience, *Trans. Amer. Nucl. Soc.*, **14**(Suppl. 1): 22 (1971).
29. C. N. Craig et al., Steady-State Irradiation Performance of UO_2–PuO_2 Fast Reactor Fuels, *Trans. Amer. Nucl. Soc.*, **14**(Suppl. 1): 23 (1971).
30. A. Boltax, T. P. Soffa, and A. Biancheria, Sensitivity of Fuel Pin Behavior to Void Swelling and Irradiation Creep of Stainless Steel, *Trans. Amer. Nucl. Soc.*, **14**: 631 (1971).
31. R. D. Leggett, Plutonium Fuels for LMFBR—An Extrapolation, presented at the Fourth International Conference on Plutonium and Other Actinides, Santa Fe, N. Mex., October 5–9, 1970, USAEC Report WHAN-SA-51, WADCO Corporation.
32. W. E. Roake, FTR Driver Fuel Development Program Status, *Trans. Amer. Nucl. Soc.*, **14**(Suppl. 1): 22 (1971).
33. P. R. Huebotter and T. R. Bump, Implications of Metal Swelling in Fast Reactor Design, in *Radiation-Induced Voids in Metals*, Albany, N. Y., June 9–11, 1971, James W. Corbett and Louis C. Ianniello (Eds.), AEC Symposium Series No. 26 (CONF-710601), pp. 84-124, 1972.
34. T. R. Bump, in ANL Reactor Development Program Progress Report for November 1971.
35. Power Reactor Development Company, Technical Information and Hazards Summary Report on the Enrico Fermi Atomic Power Plant, September 1962.
36. L. J. Koch et al., Hazard Summary Report: Experimental Breeder Reactor II (EBR-II), USAEC Report ANL-5719, Argonne National Laboratory, May 1957.
37. Westinghouse Electric Corp., FFTF Fuel Pin Spacer Mechanical Performance Study, Report WARD-BDR-362-15, October 1969.
38. L. F. Fidrych, Description of 350 MW(e) LMFBR Demonstration Plant, presented at the American Power Conference, Chicago, Ill., April 1971.
39. R. Balent and W. H. Hirst, Design and Development of Fast Reactor Fuel Assemblies, *Trans. Amer. Nucl. Soc.*, **13**(Suppl.): 42 (1970).
40. R. Balent and D. J. Stoker, Design of the Atomics International Fast Breeder Demonstration Plant, presented at the ASME Nuclear Engineering Division Conference on Fast Reactors, Palo Alto, Calif., March 1971.
41. J. Leduc et al., Developpement en France de la Technologie du Coeur de Reacteurs Rapides Refroides au Sodium, et Perspectives D'Avenir, in *Monaco Symposium on Sodium-Cooled Fast Reactor Engineering*, March 1970, International Atomic Energy Agency, IAEA-SM-130/29.
42. W. E. Burchill and G. Menzel, Sensitivity Analysis of Subassembly Shroud Mechanical Performance, *Trans. Amer. Nucl. Soc.*, **14**(Suppl. 1): 3 (1971).
43. D. R. Riley, The Status of LMFBR Core Design, *Trans. Amer. Nucl. Soc.*, **14**: 300 (1971).
44. R. J. Jackson, W. H. Sutherland, and I. L. Metcalf, Metal Swelling and Irradiation Creep Effects upon the Fast Test Reactor Core Component Performance, USAEC Report BNWL-1430, Battelle–Northwest, 1970.
45. T. R. Bump, in ANL Reactor Development Program Progress Report, USAEC Report ANL-7872, pp. 5.25-5.27, Argonne National Laboratory, October 1971.
46. P. R. Huebotter, T. R. Bump, P. J. Fulford, L. J. Koch, and J. T. Madell, A Backup Concept for Core Restraint in the Fast Test Reactor, to be published.
47. W. N. Thomas and R. H. Simon, The 300 MW(e) Gas-Cooled Fast Breeder Reactor Demonstration Plant, presented at the American Power Conference, Chicago, Ill., April 1971.
48. G. O. Jackson, C. Betts, and F. Buckley, PFR Core Support, in *Monaco Symposium on Sodium-Cooled Fast Reactor Engineering*, March 1970, International Atomic Energy Agency, IAEA-SM-130/16.
49. R. D. Phipps, Nondestructive Examination of High-Fluence EBR-II Thimbles, *Trans. Amer. Nucl. Soc.*, **14**: 601 (1971).
50. L. J. Koch, EBR-II: An Experimental LMFBR Power Plant, *Reactor Technol.*, **14**(3): 286 (Fall 1971).
51. S. D. Harkness and C-Y. Li, A Study of Void Formation in Fast Neutron Irradiated Metals, *Met. Trans.*, **2**: 1457 (1971).
52. D. A. Kucera and D. Mohr, BOW-V: A CDC-3600 Program to Calculate the Equilibrium Configurations of a Thermally Bowed Reactor Core, USAEC Report ANL/EBR-014, Argonne National Laboratory, January 1970.
53. D. Mohr and A. Gopalakrishnan, Prediction and Measurement of Reactivity Effects Due to Thermal Bowing of EBR-II Subassemblies, *Trans. Amer. Nucl. Soc.*, **14**: 2 (1971).

54. T. R. Bump, Effect of Reactor Temperatures on Bowing of EBR-II Subassemblies, *Trans. Amer. Nucl. Soc.*, **10:** 661 (1967).
55. P. R. Okamoto et al., in ANL Reactor Development Program Progress Report, USAEC Report ANL-7854, pp. 5.1-5.2, Argonne National Laboratory, August 1971.
56. T. R. Bump, in ANL Reactor Development Program Progress Report, USAEC Report ANL-7825, pp. 5.38-5.41, Argonne National Laboratory, April–May 1971.
57. T. R. Bump, in ANL Reactor Development Program Progress Report, USAEC Report ANL-7783, pp. 62-64, Argonne National Laboratory, February 1971.
58. T. R. Bump, in ANL Reactor Development Program Progress Report, USAEC Report ANL-7798, pp. 75-77, Argonne National Laboratory, March 1971.
59. T. R. Bump, in ANL Reactor Development Program Progress Report, USAEC Report ANL-7833, pp. 5.20-5.21, Argonne National Laboratory, June 1971.
60. T. R. Bump, in ANL Reactor Development Program Progress Report, USAEC Report ANL-7854, pp. 5.22-5.23, Argonne National Laboratory, August 1971.
61. T. R. Bump, in ANL Reactor Development Program Progress Report, USAEC Report ANL-7861, pp. 5.34-5.35, Argonne National Laboratory, September 1971.
62. T. R. Bump and P. R. Huebotter, Analysis of EBR-II Core-Component Deformations, *Trans. Amer. Nucl. Soc.*, **14:** 157 (1971).
63. T. R. Bump, F. D. McGinnis, R. D. Phipps, and R. V. Strain, Analyses of EBR-II Core-Component Deformations, *Trans. Amer. Nucl. Soc.*, **14:** 601 (1971).
64. L. J. Koch, Mechanical Requirements of the LMFBR, *Nucl. News*, **13:** 11, 61 (1970).
65. Atomic Power Development Associates, Inc., Enrico Fermi Atomic Power Plant, Report APDA-124, January 1959.
66. W. H. Jens and H. R. Michael, Behavior of Fermi Fuel Assemblies in High Thermal Gradients, *Trans. Amer. Nucl. Soc.*, **13:** 115 (1970).
67. J. Matte III, Requalification Examination of Irradiated Fermi Subassemblies, *Trans. Amer. Nucl. Soc.*, **14:** 884 (1971).
68. J. Matte III, oral remarks following prepared paper, Ref. 67.
69. A. I. Leipunski et al., Nuclear Power Plant BN-350, presented at ANS National Topical Meeting on Fast Reactor Technology, Detroit, Mich., April 1965, USAEC Report ANS-100(Suppl.), pp. 15-26, American Nuclear Society.
70. Soviet Power Reactors—1970, Report of the USA Nuclear Power Reactor Delegation Visit to the USSR, June 15–July 1, 1970, USAEC Report WASH-1175, August 1970.
71. G. Vendryes, G. Denielou, and L. Vautrey, Developments in Breeder Reactors, *Nucl. News*, **14:** 59 (October 1971).
72. A. G. Frame et al., Design of the Prototype Fast Reactor, in *Fast Breeder Reactors*, Conference Proceedings, London, May 1966, P. V. Evans (Ed.), pp. 291-315, Pergamon Press, Oxford, 1967.
73. R. H. Campbell, Progress on the Prototype Fast Reactor, in *Monaco Symposium on Sodium-Cooled Fast Reactor Engineering*, March 1970, International Atomic Energy Agency, IAEA-SM-130/12.
74. Nuclear Reactor Core Support Structure, U. S. Patent No. 3,383,287, May 14, 1968.
75. R. H. Campbell, Current Status of the British Fast Reactor Construction Programme, presented at the ASME Nuclear Engineering Division Conference on Fast Reactors, Palo Alto, Calif., March 8–10, 1971.
76. R. Carle et al., The Phenix Reactor, in Proceedings of the ANS National Topical Meeting on Fast Reactors, USAEC Report ANS-101, pp. 3-39–3-59, American Nuclear Society, April 1967.
77. R. Carle et al., Phenix: Status of the Design Before Construction, USAEC Report ANL-7520(Pt. 2), pp. 243-253, Argonne National Laboratory, November 1968.
78. Y. G. Adda et al., Phenix Design and Preliminary Studies on 1000 MW(e) Fast Reactors, presented at the ASME Nuclear Engineering Division Conference on Fast Reactors, Palo Alto, Calif., March 8–10, 1971.
79. Phenix Prototypes Fast-Neutron Nuclear Power Station, USAEC Report AEC-tr-7130, translated from Bulletin D'Informations Scientifiques et Techniques, No. 138, June 1969.
80. M. Köhler and H. Rothfuss, Design of the Reactor Vessel for the SNR Prototype, in *Monaco Symposium on Sodium-Cooled Fast Reactor Engineering*, March 1970, International Atomic Energy Agency, IAEA-SM-130/50.
81. R. Harde, Design Considerations and Experimental Program for the Common Development of a 300 MW(e) Sodium-Cooled Fast Breeder Prototype SNR by a Belgium–Dutch–German Consortium, USAEC Report ANL-7520(Pt. 2), pp. 130-146, Argonne National Laboratory, November 1968.
82. W. Häfele, Basic Problems of the Development of Fast Breeder Reactors, in International Conference on the Safety of Fast Reactors, Aix-en-Provence, France, September 19–22, 1967.
83. M. T. Jakub and W. H. Sutherland, Core Radial Constraint Theory and Applications to the FTR, USAEC Report BNWL-1170, Battelle–Northwest, November 1969.
84. L. M. Finch and R. E. Peterson, Impact of Stainless Steel Swelling on Fast Reactor Core Design, *Trans. Amer. Nucl. Soc.*, **12:** 316 (1969).
85. G. R. Waymire and C. L. Mohr, Core Clamping System Design for Fast Reactors, *Trans. Amer. Nucl. Soc.*, **12:** 797 (1969).
86. R. J. Jackson, C. L. Wheeler, G. R. Waymire, and W. W. Little, Metal Swelling Effects on FTR Core Components, USAEC Report BNWL-1286, Battelle–Northwest, March 1970.
87. W. H. Sutherland and V. B. Watwood, Jr., Creep Analysis of Statically Indeterminate Beams, USAEC Report BNWL-1362, Battelle–Northwest, 1970.
88. W. H. Sutherland, A Finite Element Computer Code (AXICRP) for Creep Analysis, USAEC Report BNWL-1142, Battelle–Northwest, October 1969.
89. E. B. Baumeister, AI LMFBR Core Design Methods, *Trans. Amer. Nucl. Soc.*, **14:** 300 (1971).
90. R. J. Beeley and E. B. Ash, Atomics International

LMFBR Demonstration Plant, presented at the American Power Conference, Chicago, Ill., April 1971.
91. G. Menzel, S. A. Caspersson, and R. C. Noyes, Core Design of CE LMFBR Demonstration Plant, *Trans. Amer. Nucl. Soc.*, **14:** 714 (1971).
92. W. E. Burchill et al., An LMFBR Core Design for Swelling Accommodation, *Trans. Amer. Nucl. Soc.*, **14:** 714 (1971).
93. P. Greebler and P. R. Pluta, Project Definition Phase Core Design of the General Electric 350 MW(e) LMFBR Demonstration Plant, *Trans. Amer. Nucl. Soc.*, **14:** 301 (1971).
94. N. P. Hansen, SEFOR Core Clamping System, *Trans. Amer. Nucl. Soc.*, **12:** 321 (1969).
95. H. Hopkins, D. Buttemer, and J. Dee, Accommodation of Radiation Swelling in the GCFR, *Trans. Amer. Nucl. Soc.*, **13:** 776 (1970).
96. W. M. Jacobi, Westinghouse LMFBR Demonstration Plant Design, presented at the American Power Conference, Chicago, Ill., April 1971.
97. C. A. Anderson, Jr., Westinghouse LMFBR Demonstration Plant Core Design, *Trans. Amer. Nucl. Soc.*, **14:** 302 (1971).
98. M. W. Dyos, The Nuclear Design of the Westinghouse 300 MW(e) LMFBR Demonstration Plant, *Trans. Amer. Nucl. Soc.*, **14:** 715 (1971).
99. J. T. Madell, Effect of Subassembly Clearance on Fast Reactor Performance Characteristics, *Trans. Amer. Nucl. Soc.*, **13:** 777 (1970).
100. P. R. Huebotter and T. R. Bump, The Cold-Wrapper Tube Approach for Accommodating Steel Swelling in LMFBRs, *Trans. Amer. Nucl. Soc.*, **13:** 788 (1970).
101. D. Okrent, Neutron Physics Considerations in Large Fast Reactors, *Power Reactor Technol.*, 7(2): 107 (Spring 1964).
102. D. A. Meneley, Reactor Development Program Progress Report, USAEC Report ANL-7595, pp. 8-12, Argonne National Laboratory, July 1969.
103. D. T. Eggen and P. R. Huebotter, Molybdenum to Mitigate Radiation Swelling Problems in LMFBR Fuel Assemblies, *Trans. Amer. Nucl. Soc.*, **14:** 169 (1971).
104. L. L. Bennett, W. E. Thomas, and F. J. Homan, Calculated Nuclear and Economic Performance of Niobium and Molybdenum in LMFBR Cores, USAEC Report ORNL-TM-3271, Oak Ridge National Laboratory, February 1971.
105. J. L. Brimhall and B. Mastel, Neutron Irradiated Molybdenum Relationship of Microstructure to Irradiation Temperature, *Radiat. Eff.*, **3:** 203 (1970).
106. P. J. Fulford and P. R. Huebotter, Periodic In-Situ Annealing to Reduce Stainless-Steel Swelling in the LMFBR, *Trans. Amer. Nucl. Soc.*, **13:** 559 (1970).
107. J. J. Holmes et al., Elevated Temperature Irradiation Hardening in Austenitic Stainless Steel, *Acta Met.*, **16:** 955 (1968).
108. T. R. Bump and W. Marr, An LMFBR Design to Accommodate Steel Swelling, *Trans. Amer. Nucl. Soc.*, **13:** 129 (1970).
109. D. T. Eggen, D. J. Stoker, and W. A. Flynn, Relative Economic Potential of Fast ^{233}U–Th Reactors, in Fast Reactor Symposium, Eighth Nuclear Congress, Rome, Italy, June 17–19, 1963.
110. The Use of Thorium in Nuclear Power Reactors, USAEC Report WASH-1097, Superintendent of Documents, U. S. Government Printing Office, Washington, June 1969.
111. General Electric Company, 1000 MW(e) LMFBR Follow-On Study, Task III and V Report, Methods, System Optimization, and Safety Studies for a 1000 MW(e) Sodium-Cooled Fast Reactor, USAEC Report GEAP-5710, February 1969.
112. B. J. Goulding, 1000 MW(e) LMFBR Accident Analysis and Safety System Design Study Topical Report—Effects of Irradiation-Induced Metal Swelling on Reference Design, USAEC Report BAW-1355, Babcock & Wilcox, Co., 1970.
113. Cost–Benefit Analysis of the U. S. Breeder Reactor Program, USAEC Report WASH-1126, April 1969.
114. H. H. Hummel and D. Okrent, *Reactivity Coefficients in Large Fast Power Reactors*, ANS Monograph on Nuclear Science and Technology, American Nuclear Society, 1970.

Selected Recent or Recently Released Publications*

Unless otherwise stated, the publications listed here are available from the National Technical Information Service (NTIS), U. S. Department of Commerce, Springfield, Va. 22151.

DESIGN AND PERFORMANCE EVALUATION OF THE ICE-CONDENSER REACTOR CONTAINMENT SYSTEM FOR THE DONALD C. COOK NUCLEAR PLANT

Authors: W. J. McCurdy, S. J. Weems, W. L. Boettinger, F. M. Bordelon, J. W. Dorrycott, N. P. Grimm, A. J. F. Iredale, W. G. Lyman, R. R. Oft, and R. van Seuren, Westinghouse Electric Corp., Pittsburgh, Pa.

Abstract: The design characteristics and performance analysis of the ice-condenser systems being applied to the reactor containments for the twin-unit Donald C. Cook nuclear plant are presented. Information covering the influence of the ice condenser on the reactor containment and engineered safeguards systems is included. (auth)

Available as WCAP-7833.

REACTOR FUEL-CYCLE COSTS FOR NUCLEAR POWER EVALUATION

Author: Oak Ridge National Laboratory, Oak Ridge, Tenn.

Abstract: As a part of an assessment of civilian nuclear power, a systems-analysis study of potential growth patterns of the U. S. central-station electric-power-generation system was conducted. In general terms, the main objective of the study was to estimate the relative extent to which existing and proposed types of nuclear power plants could be advantageously utilized in the total U. S. power-generating system over the next 50 years. From the analysis, it was hoped to establish the relative economic incentives for the development of the various nuclear reactor types. The systems-analysis study was based on a mathematical simulation model of the central-station power-generating system growth over the selected time period. A linear programming procedure was used to calculate the optimal combination of fossil-fired and nuclear power plants as a function of time that would meet a given set of criteria preselected to demonstrate the influence on total system costs of such factors as availability of reactor and fuel type, uranium-ore costs, total power growth rate, and the like. Comparisons of the total present-worthed costs of the various possible system growth patterns were used to indicate the potential economic benefits assignable to the different reactor types considered in the study. Among the costs that had to be included in the study were the fuel-cycle costs of the nuclear reactors. The estimation of these costs was the chief mission of the Fuel Recycle Task Force. The fuel-cycle cost data provided as input to the systems-analysis study, the methods developed for estimating prices for fuel-cycle services as a function of time, and the qualifications and limitations of the data and methods are presented. (auth)

Available as WASH-1099 from Superintendent of Documents, U. S. Government Printing Office, Washington, D. C. 20402.

DESIGN AND PERFORMANCE EVALUATION OF THE ICE-CONDENSER REACTOR CONTAINMENT SYSTEM FOR THE DONALD C. COOK NUCLEAR PLANT

Authors: W. J. McCurdy, S. J. Weems, W. L. Boettinger, J. W. Dorrycott, N. P. Grimm, A. J. F. Iredale, and W. G. Lyman, Westinghouse Electric Corp., Pittsburgh, Pa.

Abstract: Information concerning the mechanical design and performance analysis of the ice-condenser containment systems for the Donald C. Cook power reactors is presented. (D.C.C.)

Available as WCAP-7833(Suppl. 1).

DESIGN AND PERFORMANCE EVALUATION OF THE ICE-CONDENSER REACTOR CONTAINMENT SYSTEM

Authors: H. W. McCurdy, S. J. Weems, F. M. Bordelon, N. P. Grimm, E. J. Kilpela, and W. G. Lyman, Westinghouse Electric Corp., Pittsburgh, Pa.

Abstract: Information concerning analyses of performance and transient pressures of the ice-condenser containment systems for the Donald C. Cook power reactors is presented. 6 references. (D.C.C.)

Available as WCAP-7833(Suppl. 2).

*Compiled by the Reactor Technology Section of the AEC Technical Information Center, Oak Ridge, Tenn. 37830.

NUCLEAR SCIENCE ABSTRACTS

The U. S. Atomic Energy Commission publishes *Nuclear Science Abstracts (NSA)*, a semimonthly journal containing abstracts of the literature of nuclear science and engineering.

NSA covers (1) research reports of the U. S. Atomic Energy Commission and its contractors; (2) research reports of government agencies, universities, and industrial research organizations on a worldwide basis; and (3) translations, patents, books, and articles appearing in technical and scientific journals.

Complete indexes covering subject, author, source, and report number are included in each issue. These indexes are cumulated and sold separately.

Availability

SALE *NSA* is available on subscription from the Superintendent of Documents, U. S. Government Printing Office, Washington, D. C. 20402, at $42.00 per year for the semimonthly abstract issues and $34.50 per year for the cumulated-index issues. Subscriptions are postpaid within the United States, Canada, Mexico, and all Central and South American countries, except Argentina, Brazil, Guyana, French Guiana, Surinam, and British Honduras. Subscribers in these Central and South American countries, and in all other countries throughout the world, should remit $52.50 per year for subscriptions to semimonthly abstract issues and $43.00 per year for the cumulated-index issues. The single-copy price for the abstract issues is $1.75 postpaid, with this exception: Add one-fourth of $1.75 for mailing to the countries to which the $52.50 subscription rate applies.

EXCHANGE *NSA* is also available on an exchange basis to universities, research institutions, industrial firms, and publishers of scientific information. Inquiries should be directed to the USAEC Technical Information Center, P. O. Box 62, Oak Ridge, Tennessee 37830.

Subscription Information

Technical Progress Reviews may be purchased from Superintendent of Documents, U.S. Government Printing Office, Washington, D.C. 20402. *Nuclear Safety* at $3.50 per year (six issues) for each subscription or $0.60 per issue; *Reactor Technology* at $3.00 per year (four issues) for each subscription or $0.75 per issue.

Postage and Remittance

Postpaid within the United States, Canada, Mexico, and all Central and South American countries except Argentina, Brazil, Guyana, French Guiana, Surinam, and British Honduras. For these Central and South American countries and all other countries: add, for each annual subscription, $1.00 for *Nuclear Safety* and $0.75 for *Reactor Technology;* for single issues, add one-fourth of the single-issue price. Payment should be by check, money order, or document coupons, and MUST accompany order. Remittances from foreign countries should be made by international money order or draft on an American bank payable to the Superintendent of Documents or by UNESCO book coupons.